R.L. Myklebust

Electron Probe Analysis
Society of America

PROCEEDINGS
SIXTH NATIONAL CONFERENCE
ON
ELECTRON PROBE ANALYSIS

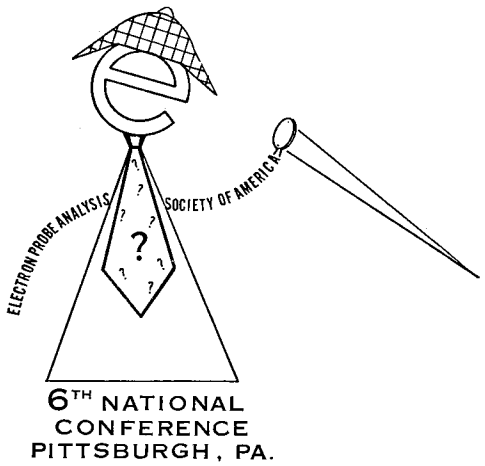

Pittsburgh, Pennsylvania

July 27-30, 1971

Additional copies of these Proceedings and for previous conferences may be obtained for $5.00 per copy, prepaid, from:

Dr. L. Vassamillet
Carnegie-Mellon University
4400 Fifth Avenue
Pittsburgh, Pennsylvania, 15213

Make checks payable to EPASA. Payment must accompany order, we will not invoice.

SIXTH NATIONAL CONFERENCE ON ELECTRON PROBE ANALYSIS

PRESENTED BY

THE ELECTRON PROBE ANALYSIS SOCIETY OF AMERICA

JULY 27-30, 1971

PITTSBURGH HILTON HOTEL
PITTSBURGH, PENNSYLVANIA

PREFACE

We in the Pittsburgh Section of the Electron Probe Analysis Society of America have had several factors working in our favor: the accumulated experience of past committees and especially that of last years committee and its Chairman, Paul Lublin, who initiated the Conference Manual, a most helpful guide to setting up committees, assigning duties and estimating costs; the generosity of the employers of all of the local committee members who permitted them to spend working hours on organizational matters and who in many instances provided secretarial help and postage; and ample manpower within the section so that no one person had to carry an unduly heavy burden. This last factor coupled with the willingness of all to carry out the responsibilities they accepted has been most especially appreciated by Joe Ryan- Arrangements Chairman, Gene White- Program Chairman, as well as myself.

No conference can succeed without a large measure of support from the associated industries. They have kept faith with us by signing up as exhibitors in even larger numbers then in previous years.

The Executive Committee has wisely insisted that more activities in behalf of members and attendees be arranged. The Tuesday Seminar is one result. Another is a meeting arranged for Sustaining members. Special thanks are due to John Bomback for his organization of the Tuesday Seminar, and to Don Beaman who has brought many new companies to our support as sustaining members.

On behalf of the local section and the national society may I extend our thanks to the authors of the papers to be given at this conference. We sincerely hope that the program will provide stimulation and excitement for all who attend.

Larry Vassamillet
General Chairman

THE ELECTRON PROBE ANALYSIS SOCIETY OF AMERICA

National Officers 1971

President	A. A. Chodos	California Institute of Technology
President Elect.	K. Keil	University of New Mexico
Secretary	J. D. Brown	University of Western Ontario
Treasurer	D. R. Beaman	Dow Chemical Company
Past-President	R. E. Ogilvie	Massachusetts Institute of Technology

Members-at-large:		Serves Until:
J. I. Goldstein	Lehigh University	1973
D. B. Wittry	Univ. of Southern California	1972
J. W. Colby	Bell Telephone Laboratories	1971

Standing Committee Chairmen:

Membership	J. Colby	Bell Telephone Laboratories
Users Groups	D. B. Wittry	Univ. of Southern California
Conference	L. F. Vassamillet	Carnegie-Mellon University
Legal	P. Lubin	General Tel. & Electronics Labs., Inc.
Sustaining Members	D. R. Beaman	Dow Chemical Company

ELECTRON PROBE ANALYSIS SOCIETY OF AMERICA

SUSTAINING MEMBERS

1971

AMR CORPORATION
Burlington, Massachusetts

APPLIED RESEARCH LABORATORIES
Glendale, California

CAMECA INSTRUMENTS INC.
Elmsford, New York

CANBERRA INDUSTRIES, INC.
Meriden, Connecticut

COATES AND WELTER INSTRUMENT CORPORATION
SUBSIDIARY OF AMERICAN OPTICAL CORPORATION
Sunnyvale, California

CORNING GLASS WORKS
Corning, New York

HI-REL LABORATORIES
San Marino, California

JEOL USA INCORPORATED
Medford, Massachusetts

ELECTRON PROBE ANALYSIS SOCIETY OF AMERICA

SUSTAINING MEMBERS

1971

KENT CAMBRIDGE SCIENTIFIC INC.
Morton Grove, Illinois

KEVEX CORPORATION
Burlingame, California

MATERIALS ANALYSIS COMPANY
Palo Alto, California

McCRONE ASSOCIATES
Chicago, Illinois

NUCLEAR DATA, INC.
Palatine, Illinois

NUCLEAR DIODES, INC.
Prairie View, Illinois

PERKIN-ELMER CORPORATION
Palo Alto, California

WEBB SCIENTIFIC COMPANY
ULTRASCAN COMPANY AND QUANTA/METRIX INC.
Cleveland, Ohio

SIXTH NATIONAL CONFERENCE COMMITTEE MEMBERSHIP

General Chairman	L. F. Vassamillet	Carnegie-Mellon University
Program	E. W. White	Pennsylvania State University
	J. L. Bomback	United States Steel Corp.
	C. J. Spengler	Westinghouse Electric Corp.
	P. DeNee	United States Bureau of Mines
	J. A. Zitterman	United States Steel Corp.
	P. H. Salmon-Cox	United States Steel Corp.
	J. H. Scott	United States Bureau of Mines
Arrangements	J. R. Ryan	Harbison-Walker Refractories Co.
	J. Makosey	Latrobe Steel Co.
	G. J. Wolfe	Kennametal Corp.
	P. T. Henderson	Jones & Laughlin Steel Corp.
Secretary	J. E. Shott	Gulf Research & Development Co.
Treasurer	H. Nikkel	Youngstown Sheet & Tube Co.
	L. K. Bench	United States Steel Corp.
Registration	R. Masse	Allegheny-Ludlum Industries
	J. J. Stepek	Allegheny-Ludlum Industries
Exhibits-Demonstration	C. E. Brickner	United States Steel Corp.
Publicity	J. Parsons	PPG Industries
	A. Maryland	PPG Industries
Hospitality	A. W. Danko	Westinghouse Electric Corp.
	W. D. Bingle	National Steel Co.
Ladies Program	Mrs. C. Spengler	
	Mrs. J. Bomback	
	Mrs. L. Vassamillet	

INVITED SPEAKERS

A. V. Crewe
Enrico Fermi Institute
Univ. of Chicago, Chicago, Illinois

P. Galle
Laboratorie de Biophysique
Faculté de Médecin, Université de Paris
Paris, France

J. M. Jaklevic
Lawrence Radiation Laboratories
Livermore, California

A. Lauchli
Texas A & M Univ.
College Station, Texas

D. J. Nagel
Naval Research Laboratory
Washington, D. C.

A. J. Tousimis
Biodynamics Research Corp.
Rockville, Maryland

STUDENT AWARD RECIPIENTS

M. R. Jackson
Lehigh University
Bethlehem, Pennsylvania

W. K. Jones
Massachusetts Institute of Technology
Cambridge, Massachusetts

J. Lebiedzik
Pennsylvania State University
University Park, Pennsylvania

J. C. Potosky
University of Southern California
Los Angeles, California

R. Warner
University of Rochester
Rochester, New York

A SHORT COURSE ON SCANNING ELECTRON MICROSCOPY AND X-RAY MICROANALYSIS

Held in conjunction with

SIXTH NATIONAL CONFERENCE ON ELECTRON PROBE ANALYSIS

ORGANIZED BY

Dr. John L. Bomback

JULY 27, 1971

PITTSBURGH HILTON HOTEL

LECTURES

Electron Beam/Solid Interactions.	Dr. John L. Bomback U. S. Steel
Instrumentation	Dr. John Russ EDAX Labs.
X-ray Detection	Dr. Donald Beaman Dow Chemical Co.
Quantitative X-ray Microanalysis.	Professor Joseph Goldstein Lehigh University
Computer Techniques	Dr. John Colby Bell Telephone Labs., Inc.
Practical Considerations.	Professor Eugene White Penn State University

The aim of this short course is to present material which will aid those using electron probe devices in getting the maximum amount of information from their instruments. These lectures will stress practical ("how to do it best") aspects. A few of the topics covered are: optimization of the electron optics and x-ray detection systems, tests to determine instrument performance, determination of detector dead times, how to measure x-ray background, statistical criteria for images and quantitative x-ray data, how to obtain and evaluate quantitative results, computational techniques, and specimen preparation. The course is open to all Conference registrants.

Schedule:

Registration	8:30 A.M. - 9:00 P.M.
Morning Session	10:00 A.M. -12:00 P.M.
Lunch	12:00 P.M. - 1:30 P.M.
Afternoon Session	1:30 P.M. - 5:30 P.M.

PROGRAM

SIXTH NATIONAL CONFERENCE ON ELECTRON PROBE ANALYSIS

TUESDAY JULY 27, 1971

8:30	Registration - Ballroom Foyer
10:00	Morning session short course - Ballroom 1
12:00	Lunch
1:30	Afternoon session short course - Ballroom 1
6:00	Executive Council of EPASA meeting, Black Diamond F

WEDNESDAY MORNING JULY 28, 1971

8:30	Registration - Ballroom Foyer
9:00	Exhibits open
9:00	Welcome by L. Vassamillet, Conference Chairman - Ballroom 1
9:05	Opening address by A. A. Chodos, EPASA President

ENERGY DISPERSIVE X-RAY ANALYSIS

JOHN BOMBACK, CHAIRMAN

1	9:15	INVITED PAPER. "Semiconductor X-ray Spectrometer and the Electron Microprobe"; J. M. Jaklevic, and F. S. Goulding - Lawrence Radiation Laboratory.
2	9:55	"The Accuracy of Quantitative Microanalysis Using Energy Dispersive Spectrometers"; D. R. Beaman - Dow Chemical Company.
3	10:15	"Energy Dispersive Trace Analysis - The X-ray Continuum as an Internal Standard"; J. L. Bomback - U.S. Steel Corporation.
4	10:35	"Storage and Treatment of Energy-Dispersive X-ray Data by Time-Shared Computer"; J. M. Short, and J. F. Stephany - Xerox Corporation.
5	10:55	"Limitations on Si(Li) X-ray Energy Analysis Systems at High Counting Rates"; D. A. Gedcke, E. Elad, and G. R. Dyer - ORETC, Inc.
6	11:05	"Comparison of Semi-quantitative Analyses Made with Energy and Wavelength Dispersive Analyzers of Extracted Intermetallic Particles"; G. Sabol, and C. J. Spengler - Westinghouse Electric Corporation.
7	11:25	KEYNOTE PAPER. "Production of Electron Probes a Few Å in Diameter"; A. V. Crewe - Enrico Fermi Institute.

WEDNESDAY AFTERNOON

RELATED PROBE TECHNIQUES

Ballroom 1

DAVID B. WITTRY, CHAIRMAN

8	2:00	"Quantitative Theory of Sputtered Ion Mass Analysis"; C. A. Anderson - Applied Research Laboratories.
9	2:20	"Surface Chemistry Characterization of Alumina Ceramic Substrates by Ion Microprobe Mass Analysis"; D. K. Conley - Western Electric Co.
10	2:40	"Ion Scattering Spectrometry - A New Technique for Surface Composition Analysis"; R. F. Goff - 3M Company.
11	3:00	"The Laser Mass Spectrometer Microprobe"; B. E. Knox - The Pennsylvania State University.
12	3:20	"The Field Ion Microscope Atom Probe; Imaging and Analysis on an Atomic Scale"; S. R. Goodman, J. T. McKinney, and S. S. Brenner - U.S. Steel Corporation.
13	3:40	"Auger and Characteristic Energy Loss Measurement as an Analytical Tool with the SEM"; E. Sternglass, and R. K. Matta - University of Pittsburgh.
	4:00	EPASA Business Meeting - Kings Plaza

WEDNESDAY EVENING

Ballroom 2

	6:30	Reception

THURSDAY MORNING JULY 29, 1971

AUTOMATION & COMPUTER PROGRAMS FOR MICROPROBE ANALYSIS

Ballroom 1

JOHN W. COLBY, CHAIRMAN

14	9:00	"LRL Computer Program: Microanalysis"; W. J. Steele - Lawrence Radiation Laboratory.
15	9:20	"Quantitative Microprobe Analysis and Data Reduction Using an On-Line Mini Computer"; A. A. Chodos, and A. L. Albee - California Institute of Technology.

16 9:40 "Computerized Microprobe Method for the Determination of the Thickness of Thin Films in Multilayered Integrated Circuits"; G. DiGiacomo - International Business Machines Corporation.

17 10:00 "MAGIC IV - A New Improved Version of MAGIC"; J. W. Colby - Bell Telephone Laboratories.

18 10:20 "Electron Microprobe Automation"; F. W. Kunz and E. Eichen - Ford Motor Company; and G. Matthews and S. Piner - Canberra Industries.

19 10:40 "An Automated Microprobe Under PDP-8 Control Using an IBM 360/65 for Program and Data Storage"; T. D. Kirkendall, and P. F. Varadi - Communications Satellite Corp.

20 11:00 "A Computerized Test for Homogeneity Characterization"; F. Kunz, E. Eichen, and A. Varshneya - Ford Motor Company.

21 11:20 "Computer Simulation of a Thin Film Metallurgy System"; B. I. Bertelsen, W. E. Veno, and D. H. Withers - International Business Machines Corporation.

22 11:40 "A Model for Analysis of Fine-Platelet Structures, Effect of Finite Beam Size"; M. R. Jackson, J. I. Goldstein, and R. W. Kraft - Lehigh University.

THURSDAY AFTERNOON SESSION A

MICROPROBE AND SEM APPLICATIONS

Ballroom 1

PHIL DENEE, CHAIRMAN

23 2:00 "Analytical Measurements on NBS Standard Reference Materials for Electron Probe Microanalysis"; R. L. Myklebust, and K. F. J. Heinrich - National Bureau of Standards.

24 2:20 "Microprobe Techniques for the Measurements of Oxygen and Xenon in Irradiated Mixed (Pu,U) Oxide Fuels"; T. E. Lannin, G. F. Melde, R. C. Wolf, and H. S. Rosenbaum - General Electric Co.

25 2:40 "Precision and Detection Limits of Certain Minor and Trace Elements in Silicates by Electron Microprobe Analysis"; R. H. Heidel, and G. A. Desborough - U. S. Geological Survey.

26 3:00 "The "a" Value Method Revisited"; R. B. Bolon, and E. Lifshin - General Electric Company.

27 3:20 "Solidification Structures and Phase Compositions in As-Cast High Speed Steels"; R. H. Barkalow, J. I. Goldstein, and R. W. Kraft - Lehigh University.

28 3:30 "Application of a Combination Scanning Electron Microscope-Microprobe to Forensic Analysis"; C. H. Anderson and J. W. Leitner - Applied Research Laboratories; R. Finn - Syracuse University Research Corp.; and Captain S. Ferriss - New York State Police Scientific Laboratories.

29 3:50 "Electron Probe Microanalysis of Trace Constituents"; K. F. J. Heinrich - National Bureau of Standards.

30 4:10 "Factors Affecting the Resolution of the Backscattered Electron Image in the Scanning Electron Microscope"; O. C. Wells - International Business Machines Corporation.

31 4:20 "Experimental Determination of the Absorption Correction by Use of a Solid State Detector"; W. K. Jones, and R. E. Ogilvie - Massachusetts Institute of Technology.

32 4:30 "Electron Probe Analysis of the Fiber-Resin Content of Graphite-Epoxy Composites"; R. E. Herfert - Northrop Corporation.

33 4:50 "Specimen Contamination During Electron Probe Analysis"; C. M. Taylor, A. J. Tousimis, and J. A. Nicolino - Biodynamics Research Corporation.

THURSDAY AFTERNOON SESSION B

BIOLOGICAL APPLICATIONS

Ballroom 2

A. J. TOUSIMIS, CHAIRMAN

34 2:00 INVITED PAPER. "The Application of Electron-Probe Micro-analysis in Medicine"; P. Galle - Laboratoire de Biophysique.

35 2:30 INVITED PAPER. "Applications of Electron Probe Analysis to Plant Sciences"; A. Lauchli - Texas A & M University.

36 3:00 INVITED PAPER. "Quantitative Electron Probe Analysis of Biological Tissue Sections"; A. J. Tousimis - Biodynamics Research Corporation.

37 3:30 "Calcium Measurements in Frog Skin"; E. Ingram, M. Ingram, and C. A. M. Hogben - University of Iowa.

38 3:40 "Extracellular and Intracellular Distribution of Electrolytes in Epithelia: Intestine and Skin"; A. J. Tousimis - Biodynamics Research Corporation.

39 4:00 "Zinc in Entamoeba Invadens"; R. S. Morgan, R. F. Sattilaro, and W. H. Zeigler - The Pennsylvania State University.

40 4:10 "Electron Microprobe Measurement of Fluorine Uptake in Human Teeth"; A. M. Sheble - Hi-Rel Laboratories, and D. Ocumpaugh - The Epoxylite Corporation.

41 4:30 "Sulfur and Copper in Tissues from Patients with Hepatolenticular Degeneration: Wilson's Disease"; A. J. Tousimis - Biodynamics Research Corporation.

42 4:40 "A Computer Program for the Analysis of Biological Material"; R. Warner - University of Rochester.

THURSDAY EVENING

6:00 CASH BAR - KINGS GARDEN

7:00 BANQUET - Ballroom 1

FRIDAY MORNING JULY 30, 1971

SOFT X-RAY SPECTROSCOPY

W. L. BAUN, CHAIRMAN

43 8:30 "Electron Microprobe Instrumentation for Soft X-ray Spectroscopy Applications"; J. S. Solomon - University of Dayton Research Institute, and W. L. Baun - Wright-Patterson AFB.

44 8:55 "Phosphorous Kβ and Kβ' Emission Spectra for Some Metaphosphates and Natural Apatite Minerals"; R. G. Hurley, and E. W. White - The Pennsylvania State University.

45 9:10 "Characterization of SiO Using Fine Features of X-ray K Emission Spectra"; W. L. Baun - Wright-Patterson AFB, and J. S. Solomon - University of Dayton Research Institute.

46 9:25 "The Distribution and Oxidation State of Sulfur in Structural Clay Products"; G. A. Savanick - Bureau of Mines, and E. W. White - The Pennsylvania State University.

47 9:40 "An Interpretation of the Chemical Effect in the Aluminum and Oxygen X-ray K-Emission Bands from Hydrated Aluminas"; G. A. Savanick - Bureau of Mines, and E. W. White - The Pennsylvania State University.

48 9:55 "Chemical Bonding Studies on Boron Interstitial Compounds"; W. L. Baun - Wright-Patterson AFB, and J. S. Solomon - University of Denver Research Institute.

49 10:15 "Rubidium Phthalate as X-ray Spectrometer Crystals in the Electron Microprobe, Together with Evidence on the Electron Bonding in the K-Spectra from Carbon and Carbon Compounds Using the Ohm Crystal"; A. A. McFarlane - United Kingdom Atomic Energy Authority.

50 10:35 "Bonding, Electronic Structure and Surface Oxide of Metals and Alloys by Soft X-ray Spectroscopy"; J. E. Holliday - U. S. Steel Corporation.

51 11:00 "Use of Soft X-ray Band Spectra for Determining Molecular Orbital Structures of Simple Compounds"; D. W. Fischer - Wright-Patterson AFB.

52 11:25 INVITED PAPER. "Total X-ray Characterization of Materials by Measurement of X-ray Spectral Details with the Electron Probe"; D. J. Nagel - Naval Research Laboratory.

FRIDAY AFTERNOON SESSION A

NEW PROBE TECHNIQUES & INSTRUMENTATION

Ballroom 1

CHARLES J. SPENGLER AND HENRY NIKKEL, CO-CHAIRMEN

53 2:00 "Pulse Height Stabilization in Gas Proportional X-ray Detector Systems"; C. J. Kelly and M. A. Short - Ford Motor Company; and C. A. Reynolds - Canberra Industries.

54 2:20 "Quantitative Analysis of Electron Probe Images"; C. Fisher, and D. W. Gibbard - Image Analyzing Computers Ltd.

55 2:40 "Simple Methods for Automatic Quantitative Analysis of SEM and Probe Images"; J. Lebiedzik, and E. W. White - The Pennsylvania State University.

56 3:00 "Detection of Backscattered Electrons with Silicon Solar Cells"; J. Potosky - University of Southern California.

57 3:10 "A Practical Convolution Technique for Interpreting Electron Probe Results"; J. B. Gilmour, G. R. Purdy, and J. S. Kirkaldy - McMaster University.

58 3:30 "The Location of Trapped Charge Introduced Into the Silicon Dioxide Passivation Layer of an Integrated Circuit During Electron Beam Microanalysis"; J. J. Bart, and J. R. Haberer - Rome Air Development Center.

59 3:45 "A Simplified Electron Microprobe"; M. Bayard - McCrone Associates.

60 3:55 "Universal X-ray Detector: A Flow Proportional Counter for Analysis of All Elements from Beryllium to Uranium"; A. J. Tousimis, and J. A. Nicolino - Biodynamics Research Corporation.

61 4:05 "A Novel Sample Spinner for Uniform Film Coating of Non-Conducting Samples for Electron Analysis and Scanning Electron Microscopy"; A. J. Tousimis, and J. A. Nicolino - Biodynamics Research Corporation.

FRIDAY AFTERNOON SESSION B

SESSION DEVOTED TO LATE-BREAKING DEVELOPMENTS AND SPECIAL INTEREST ITEMS

Ballroom 2

O. C. WELLS, CHAIRMAN

62	2:00	"Present Status of Microanalysis in Japan"; G. Shinoda - Japan Women's University.
63	2:20	"The Dependence of Analytical Accuracy Upon X-ray Spectrometer Geometry"; P. J. Killingworth - Cambridge Scientific Instruments, Ltd.
	2:40	OPEN - Consult with Chairman in advance to arrange for contributions at this time.

MEETING

SEVENTH NATIONAL CONFERENCE ON ELECTRON PROBE ANALYSIS

This meeting is to be held at the San Francisco Hilton Hotel, San Francisco, California (USA), July 18, 19, 20, 21, 1972.

The sponsor of the meeting will be the Electron Probe Analysis Society of America.

Attendance at the meeting is estimated to be between 400 and 500.

For general information pertaining to this meeting contact:

Dr. David F. Kyser K05-028
International Business Machines
Monterey & Cottle Roads
San Jose, California 94115

Mr. Bob Ruscica
Materials Analysis Co.
1060 E. Meadow Circle
Palo Alto, California 94303

The topics of the technical sessions will include:

Electron Microprobe X-Ray Analysis, Techniques and Instrumentation. Principles of Electron Scattering and X-Ray Generation, Quantitative Correction Procedures, Soft X-Ray Emission, Computer Control and Data Reduction, Energy Dispersion Analysis, Ion Microprobe Analysis, Scanning Electron Microscopy, New Methods and Instrumentation in Micro-Analysis, and Applications.

It is planned to offer a tutorial session and/or manufacturer's forum.

The number of papers to be presented is estimated to be between 75 and 125. Contributed papers will be considered and a "call for papers" will be issued through direct mailing and meeting announcements six or eight months in advance of the meeting. The deadline for papers will be April 1, 1972. Everyone is invited to contribute papers. Abstracts must be submitted in English and sent to:

Mr. Ted E. Lannin
General Electric Co.
Vallecitos Road
Pleasanton, California 94566

Exhibitors should contact:

Dr. H. F. Harnsberger
Chevron Research
Richmond, California 94802

SIXTH NATIONAL CONFERENCE OF THE ELECTRON PROBE ANALYSIS SOCIETY OF AMERICA (1971)

EXHIBITOR BOOTH ASSIGNMENTS

Company Name	Address	Booth Location
Ernest Fullman, Inc.	P. O. Box 444 Schenectady, New York 12301	1
Nuclear Diodes, Inc.	P. O. Box 135 Prairie View, Illinois 60069	2
Coates & Welter Instrument Corp.	2191 Ronald Street Santa Clara, California 95050	3
On-Line Systems, Inc.	4721 McKnight Road Pittsburgh, Pennsylvania 15237	4
Computer Power Systems, Inc.	722 E. Evelyn Avenue Sunnyvale, California 94086	5
Cameca Instruments, Inc.	101 Executive Blvd. Elmsford, New York 10523	6, 7, 8
Princeton Gamma Tech, Inc.	P. O. Box 641 Princeton, New Jersey 08540	9
Etec Corporation	2284 Old Middlefield Way Mountain View, California 94040	10, 11, 12
Bio-Dynamics Research Corp.	6010 Executive Blvd. Rockville, Maryland 20852	13
AMR Corporation	149 Middlesex Turnpike Burlington, Mass. 01803	14, 15
Kevex Corporation	898 Mahler Road Burlingame, California 94010	16
3M Company	3M Center 220-6E St. Paul, Minnesota 55101	17
Jeol USA, Inc.	477 Riverside Avenue Medford, Mass. 02155	18, 19
Quantex	Commercial Electronics Inc. 880 Maude Avenue Mountain View, California 94040	20

SIXTH NATIONAL CONFERENCE OF THE ELECTRON PROBE ANALYSIS SOCIETY OF AMERICA (1971)

EXHIBITOR BOOTH ASSIGNMENTS

Company Name	Address	Booth Location
Denton Vacuum, Inc.	Cherry Hill Industrial Center Cherry Hill, New Jersey 08034	21
Nuclear-Equip Corporation	931 Terminal Way San Carlos, California 94070	22
Canberra Industries	45 Gracey Avenue Meriden, Connecticut 06450	23, 24
Applied Research Laboratories	P. O. Box 129 Sunland, California 91040	25, 26, 27
Materials Analysis Co.	1060 East Meadow Circle Palo Alto, California 94303	28, 29, 30, 31
E. Leitz, Inc.	Rockleigh, New Jersey 07647	32
Nuclear Chicago	2000 Nuclear Drive Des Plaines, Illinois 60018	33
Quanta/Metrix Corp.	120 Industrial Way San Carlos, California 94070	34

SUMMARIES
OF
PAPERS

An Index of Authors and Their Affiliations Follows the Summaries.

SEMICONDUCTOR X-RAY SPECTROMETERS AND THE ELECTRON MICROPROBE

J. M. Jaklevic † and F. S. Goulding†

Lawrence Radiation Laboratory
University of California
Berkeley, California 94720

INTRODUCTION

Recent work on semiconductor X-ray spectrometers at the Lawrence Radiation Laboratory (Berkeley) and elsewhere has greatly benefited their application to electron probe microanalysis. This paper focuses attention on aspects of these developments of particular importance to the case of electron beam excitation. We will describe results bearing on extension of the method to analysis for light elements.

ENERGY RESOLUTION

The energy resolution of any X-ray fluorescence spectrometer primarily determines its ability to resolve adjacent elements in the periodic table--but also determines the minimum detectable quantity of an element in the presence of a general background. This is particularly important in electron-probe analysis where a Brehmstrahlung continuum is an inherent result using electron excitation.

The total energy resolution of a semiconductor detector spectrometer is the convolution of a contribution due to electronic noise in the detector-amplifier system, and one due to statistical fluctuations in the charge produced by the ionization process in the detector. The electronic noise is affected by such factors as detector leakage current, noise in the input amplifying element (always a field-effect transistor in modern spectrometers), and by the choice of pulse-shaping time constants in the amplifier. Recent years have witnessed a considerable decrease in this contribution, brought about by the isolation and elimination of various sources of noise. [1,2] Today it is not uncommon to realize electronic resolutions of less than 100 eV FWHM in carefully designed spectrometers. The second contribution due to charge-production statistics in the detector, is given by

$$\Delta E_{(FWHM)} = 2.35 \sqrt{FE\varepsilon}$$

where E is the energy of the radiation, ε is the average energy required to produce a hole-electron pair in the detector (3.81 eV in Si). F is the Fano factor, a parameter determined by statistics of sharing of energy losses between ionization and phonon (vibrational) excitation of the detector material. The value of F has been studied extensively, and a value of 0.06 is predicted.[3,4] However, silicon detectors normally exhibit effective values of F near 0.12--the discrepency is possibly due to microscopic defects in the material.

Figure 1 shows the variation in total resolution with energy for several assumed values of the electronic noise contribution. The dotted lines indicate an optimistic guess as to the ultimate performance of semiconductor detector spectrometers using silicon detectors--an electronic noise contribution of 50 eV representing an RMS deviation in charge of only ± 6 electrons per event) and a Fano factor of 0.06.

COUNTING RATE BEHAVIOR

All semiconductor detector spectrometers suffer degradation of resolution as the X-ray rate in the detector increases. This is particularly important in electron microprobe applications where the electron beam can provide intense excitation of fluorescent X-rays, and where high-counting rates are desired for scanning or imaging purposes. The pulse shaping times employed in the amplifier represent a compromise between small values, that reduce the degradation of resolution at high rates; and larger values that give the best resolution at low rates. This situation is illustrated in Fig. 2 which is data obtained with a pulsed-light feedback amplifier system.[5] The shaping times indicated refer to the peaking time of a Gaussian shaped amplifier pulse. This system includes circuitry to reject pulses where pile-up occurs, and also a baseline restorer to firmly clamp the baseline between pulses. It is much better in rate behavior than earlier systems. The variation of output rate as a function of input rate is also shown--the large losses at high rates are due to pile-up--the effect is reduced if short pulse-shaping times are used. It is expected that eventual improvements in field-effect transistors will permit equivalent energy resolutions for shorter pulses, thus improving rate performance.

DETECTION OF LOW-ENERGY X-RAYS

The energy resolution now available is illustrated by the data shown in Fig. 3. Resolutions less than 100 eV suggest the possibility of X-ray measurements below the energy limit established by absorption in the cryostat entrance window (about 1.5 keV). For example, carbon Kα (277 eV) and nitrogen Kα (392 eV) X-rays are separated by 115 eV while the resolution of the system of Fig. 3 should be 95 eV (FWHM) at these energies.

We have performed a series of measurements using a similar X-ray spectrometer assembled in a virtually "windowless" cryostat to evaluate low energy performance.[6] The possibility existed that problems due to X-ray attenuation in the detector entry window, and incomplete charge collection in any undepleted Si at the entry side of the detector would seriously degrade performance. Figure 4 shows a spectrum obtained for carbon Kα X-rays excited by 8 keV electrons striking a graphite block--an aluminum oxide spectrum is also shown for comparison. The system used a pulsed electron source and synchronously gated signal electronics to suppress the low-energy distribution of noise pulses. Results of the study indicate that there are no serious window problems although the resolution was slightly worse than expected. To avoid difficulties due to the sensitivity of the detector to surface contamination, and the effect of luminescence from the sample, a thin aluminum foil was used as a vacuum baffle and light barrier. The target was operated at + 8 keV to prevent backscatter electrons from reaching the detector.

We recognize that conventional microprobes would require modifications to permit pulsing and operation with the sample at positive voltage, but such changes may be essential for very low-energy X-ray work.

CONCLUSIONS

Recent work has resulted in substantial improvements both in energy resolution and counting-rate performance. These improvements are very important in existing microprobe elemental analysis systems, but extension of work to very low energies will require modifications of existing microprobes. Further improvements can be expected as new field-effect transistors become available, and possibly as the charge production process in the detector is studied further. However, these improvements will mainly reflect in improved rate behavior.

FOOTNOTE AND REFERENCES

† This work was carried out as part of the research program of the Nuclear Chemistry Division of the Lawrence Radiation Laboratory, which is supported by the U.S. Atomic Energy Commission Contract W-7405-eng-48.

1) F. S. Goulding, J. Walton, D. Malone, Nucl. Instr & Methods, 71, 273 (1969).

2) H. E. Kern, J. M. McKenzie, IEEE Trans. Nucl. Sci, NS-17, No. 1, 260 (1970).

3) C. A. Klein, IEEE Trans. Nucl. Sci., NS-15, No. 3, 214 (1968).

4) H. R. Zulliger and D. W. Aitken, IEEE Trans. Nucl. Sci., NS-17, No. 3, 187 (1970).

5) D A. Landis, F. S. Goulding, R. H. Pehl and J. T. Walton, IEEE Trans. Nucl. Sci., NS-18, No. 1, 115 (1971).

6) J. M. Jaklevic and F. S. Goulding, IEEE Trans. Nucl. Sci., NS-18, No. 1, 187 (1971).

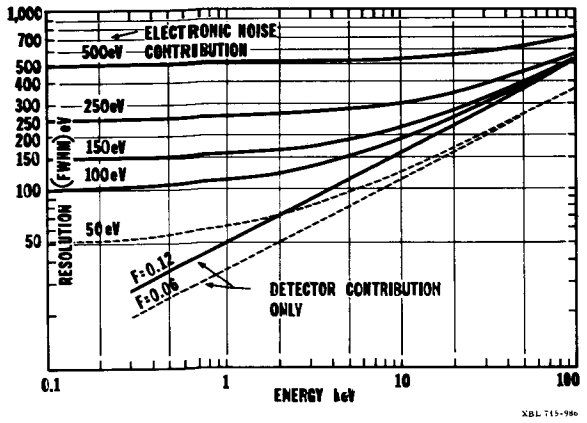

Fig. 1

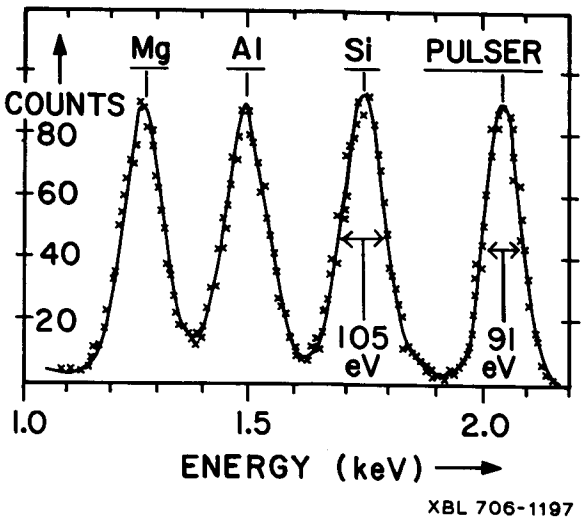

Fig. 3

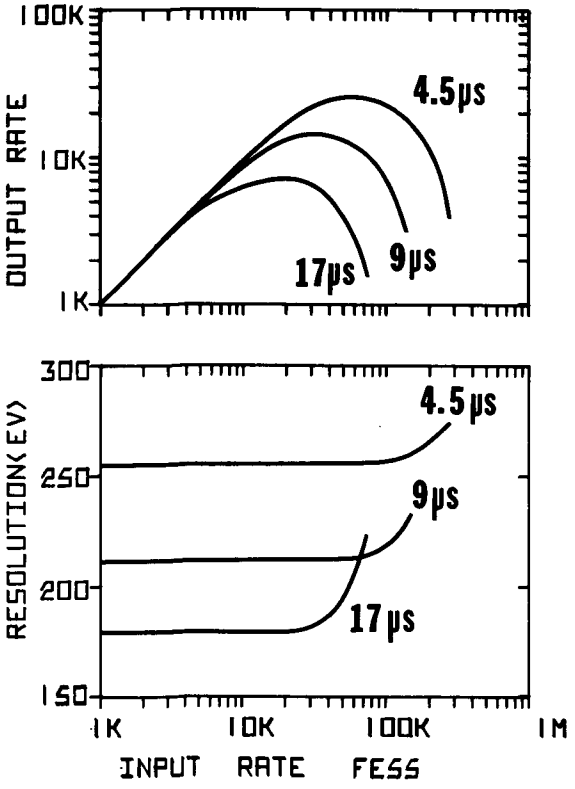

XBL 7010-6806

Fig. 2

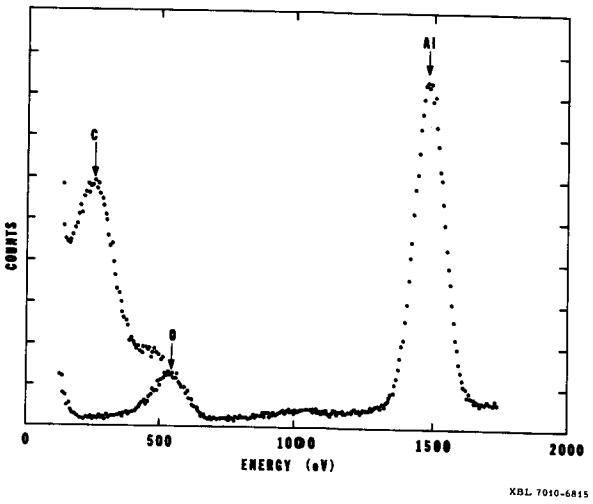

Fig. 4

THE ACCURACY OF QUANTITATIVE MICROANALYSIS USING ENERGY DISPERSIVE SPECTROMETERS

D. R. Beaman
The Dow Chemical Company, Midland, Michigan

The experimental accuracy and precision attainable in the determination of a x-ray intensity ratio, k, using an energy dispersive spectrometer (EDS) equipped with a Si detector have not yet been firmly established, notwithstanding the claims to the contrary. Attempts at quantitative analysis have been reported by Russ (1), Myklebust and Heinrich (2,3), Heinrich (4), Lifshin (5), Woodhouse (6), Tenny (7) and Beaman and Solosky (8). The results of these investigations will be discussed. The percentage of the analysis falling within specified limits for each investigator are listed in the table. The method of evaluation was to calculate a theoretical intensity ratio from the known alloy composition and compare this with the measured intensity ratio and report the relative error, 100 x $\Delta k/k$, where $\Delta k/k = \{k(expt)-k(calc)\}/k(calc)$. For investigators reporting compositions, the relative error was $\{C(calc)-C(chem)\} \times 100/C(chem)$ where C(calc) is obtained from k(expt). The histogram summarizes the relative error data.

There are several interesting aspects to this data which should help to establish expected accuracy values at the present time. When the analysis is restricted to compositions above 19.9% and integrated peak intensities are used, 37% of the relative errors are within ±2%, 53% are within ±4%, and the rms error is 8%. This compares to about 60% within ±2%, 80% within ±4%, and a rms error of about 6% when using an electron probe analyser (EPA) and a wavelength dispersive spectrometer (WDS). The EPA data were extracted from histograms published by Heinrich (9) and Duncumb, et al. (10). The alloys used in the EDS work were more carefully characterized with respect to homogeniety and composition than those used in the WDS work, e.g., in the analysis of 12 alloys (Cu-Zn, Ti-Nb and Cu-Au) all of the WDS analyses of Beaman and Solosky were within ±2% but only 42% were within the same limit with the EDS. Thus, the accuracy attainable with an EDS is not yet as good as with a WDS, but relative errors of better than ±6% should be generally expected at moderate concentration levels in simple alloy systems.

The mean of the distribution of 59 alloys with C>19.9% is +0.2% with 32 positive and 27 negative errors. While there is no significant bias in the distribution, there is definite bias within the individual sets of data. There is insufficient data to determine if the use of integrated intensities is superior to using spectral peak intensities less estimated spectral background (P-B). Beaman and Solosky obtain good results with (P-B) values in simple alloys when using relatively long counting periods (600 seconds).

There is a dramatic deterioration of the results obtained at low concentrations. The rms error for 16 analyses with C<19% is 138% and the mean is +71%. There is a large and positive bias evident which increases with decreasing concentration. This apparent enhancement makes quantitative analysis at low concentration questionable.

In view of the rapid analytical speed of an EDS and the reasonably good results obtained at moderate concentration levels, further work should be carried out aimed at accuracy improvement over a broad range of compositions. There is often a rapid degradation of accuracy when: 1) the complexity of the alloy system leads to spectral interferences; 2) the resolution is inadequate or degrades with counting rate; 3) the background intensity constitutes a significant portion of the peak; and 4) there is ambiguity in determining the effective x-ray take-off angle. These problems will be discussed.

1) J. C. Russ, in Energy Dispersion X-ray Analysis; X-ray and Electron Probe Analysis, ASTM STP 485, 1971, p. 154.
2) R. L. Myklebust and K. F. J. Heinrich, ibid, p. 232.
3) R. L. Myklebust and K. F. J. Heinrich, in Proceedings Fourth National Conference on Electron Microprobe Analysis, Pasadena, 1969, Paper No. 52.
4) K. F. J. Heinrich, in NBS Technical Note 502, 1969, p. 30.
5) E. Lifshin, private communication, G. E. Research Laboratory, Schenectady, New York, 1970.
6) J. Woodhouse, private communication, University of Illinois, Urbana, Illinois, 1970.
7) H. Tenny, Metallography, 1, 1968, p. 221.
8) D. R. Beaman and L. Solosky, to be published.
9) K. F. J. Heinrich, in Advances in X-ray Analysis, J. B. Newkirk, G. R. Mallett and H. G. Pfeiffer, Eds., Plenum Press, New York, 11, 1968, p. 40.
10) P. Duncumb, P. K. Shields-Mason and C daCasa, Tube Investments Research Laboratories Report, October, 1968.

TABLE: MAGNITUDE OF RELATIVE ERRORS IN SEVEN INVESTIGATIONS

Principal author and reference	No. of analyses	Method of analysis	Percentage of analyses within indicated % ±1	±2	±4	±6	±10	±20
Beaman(8)	12	integrated	17	42	58	83	100	
Myklebust(2-4)	32	integrated	22	47	59	69	84	97
Above 2	44	integrated	20	45	59	73	89	98
Lifshin(5)	14	integrated	8	8	36	36	71	86
Tenny(7)	15		33	33	33	47	60	73
Above 4(C>19%)	59		19	37	53	66	86	98
Russ(adjusted)	6	integrated	50	50	67	67	84	100
Russ(1)	64	integrated		72				
Beaman(8)	16	P-B	25	44	69	82	100	
Myklebust(2-4)	16	P-B	19	31	50	56	81	88
The results below were obtained with a WDS.								
Beaman(8)	12	P-B	75	100				
Duncumb(10)	333	P-B	45	60	80	87	93	99
Heinrich(9)	109	P-B	32	64	88	98	100	

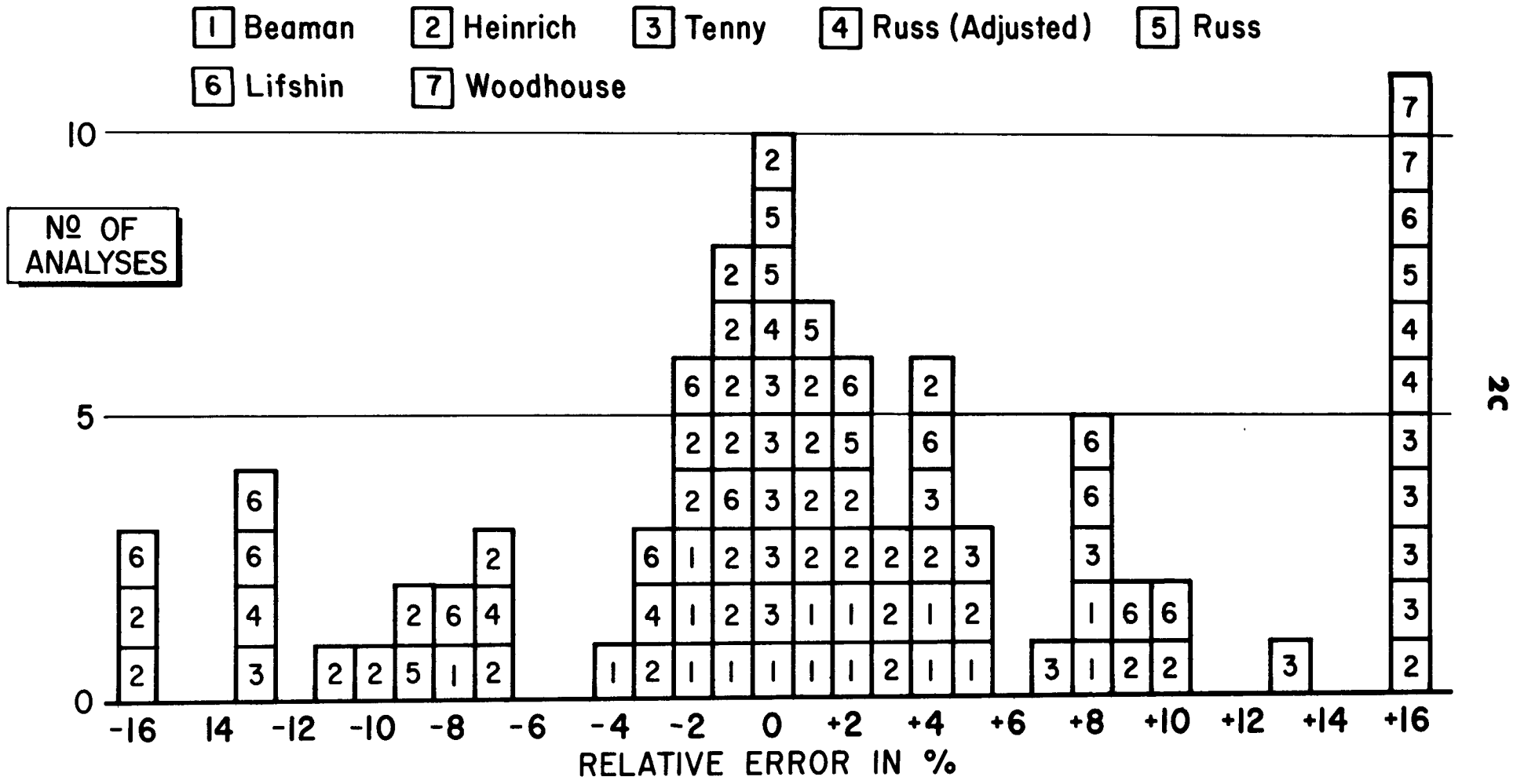
1 Beaman
2 Heinrich
3 Tenny
4 Russ (Adjusted)
5 Russ
6 Lifshin
7 Woodhouse
Nº OF ANALYSES
10
5
0
-16
14
-12
-10
-8
-6
-4
-2
0
+2
+4
+6
+8
+10
+12
+14
+16
RELATIVE ERROR IN %

ENERGY DISPERSIVE TRACE ANALYSIS-THE X-RAY CONTINUUM AS AN INTERNAL STANDARD

J. L. Bomback

Edgar C. Bain Laboratory
For Fundamental Research
United States Steel Corporation
Research Center
Monroeville, Pennsylvania

In the usual mode of electron probe analysis, the ratio of spectral line intensities emitted from unknown and standard materials is used to compute the concentration of the unknown. In the method described below, the ratio of spectral line and background intensities both emitted from the unknown is used. A similar method has been applied to x-ray fluorescence analysis [1] where the Compton scattered radiation was used as an internal standard.

Two assumptions are made in deriving an expression relating intensity and concentration: (1) at low concentrations, the emitted intensity of the trace component is proportional to its concentration; (2) the intensity of the x-ray continuum is independent of the concentration of the trace constituent. The concentration of the trace element is then given by

$$C_j = \beta(i,j)\ N_P/(N_B/eV) \qquad (1)$$

where N_P is the total integrated peak count above background for the spectral line of element j, (N_B/eV) is the background count at the peak wavelength per eV of spectrum and $\beta(i,j)$ a proportionality constant for element j in matrix i. $\beta(i,j)$, which is independent of spectrometer resolution and analyzer calibration, is determined empirically for a given accelerating potential, electron beam incidence angle, x-ray take-off angle, and matrix material.

The following advantages are gained with this internal calibration energy dispersive method over the conventional "external calibration" wavelength dispersive method.

1. Unknown, standard, and background intensities are measured separately in the latter method making the results sensitive to slight variations in electron beam current.

2. Errors due to uncertainty in the integration time are also eliminated.

3. The dead time correction is eliminated. This is important in wavelength dispersive systems when pure elemental standards are used with dilute unknowns.

4. Intensities from wavelength dispersive systems are sensitive to x-ray focussing geometry. Mechanical adjustment of the spectrometer or specimen stage necessary to obtain peak and background intensities can change the x-ray focus.

5. The related problem of spectral line wavelength difference between standard and unknown is also eliminated.

In order to test the validity of the technique, dilute alloys of Fe-Cu and Fe-V were analyzed. Data were taken with a ΔE = 250 eV(FWHM) spectrometer, normal electron incidence and 18° x-ray take-off angle. Figure 1 shows the superimposed spectra of the 1% alloys in the region of the K_α lines of the dilute constituent. Vanadium detectability in iron is limited by the Si escape peak from FeK_α. The background under each peak was determined by a least-squares linear fit to data-points well off the tails on either side of the peak. The number of background points used was limited by adjacent spectral lines and by curvature of the continuous spectrum. The summation for the integrated peak count was taken over $\pm$ 2 ΔE from the peak position. Figure 2 shows the ratio of the integrated peak count to the background count per eV for several iron copper alloys. The slope of the line is $(1/\beta)$. Figure 3 shows the dependence of β on overvoltage.

The detectability limit, C_{DL}, can be arbitrarily defined as that concentration which gives a maximum peak channel-count which is twice the standard deviation, σ_B, of the background count in that channel. For a Gaussian peak shape and constant background

$$C_{DL} \cong \frac{0.4\ \beta(i,j)}{\sqrt{N_{BT}}}\ \Delta E \qquad (2)$$

where ΔE is the spectrometer resolution (FWHM in eV) and N_{BT} is the total number of counts from each side of the peak used to determine (N_B/eV). Qualitatively, this expression shows that the sensitivity increases as the resolution of the spectrometer is improved, as counting time increases and as conditions are adjusted to minimize $\beta(i,j)$.

The method should be applicable for trace determination in multicomponent matrices when the concentrations of the major constituents do not vary appreciably. Furthermore, the presence of several trace constituents will not interfere with the analysis except when peaks overlap.

The author gratefully acknowledges the aid of William Gundaker of this laboratory for collecting the data used in this study.

---

[1] P. G. Burkhalter, Analytical Chemistry 43, 10 (1971).

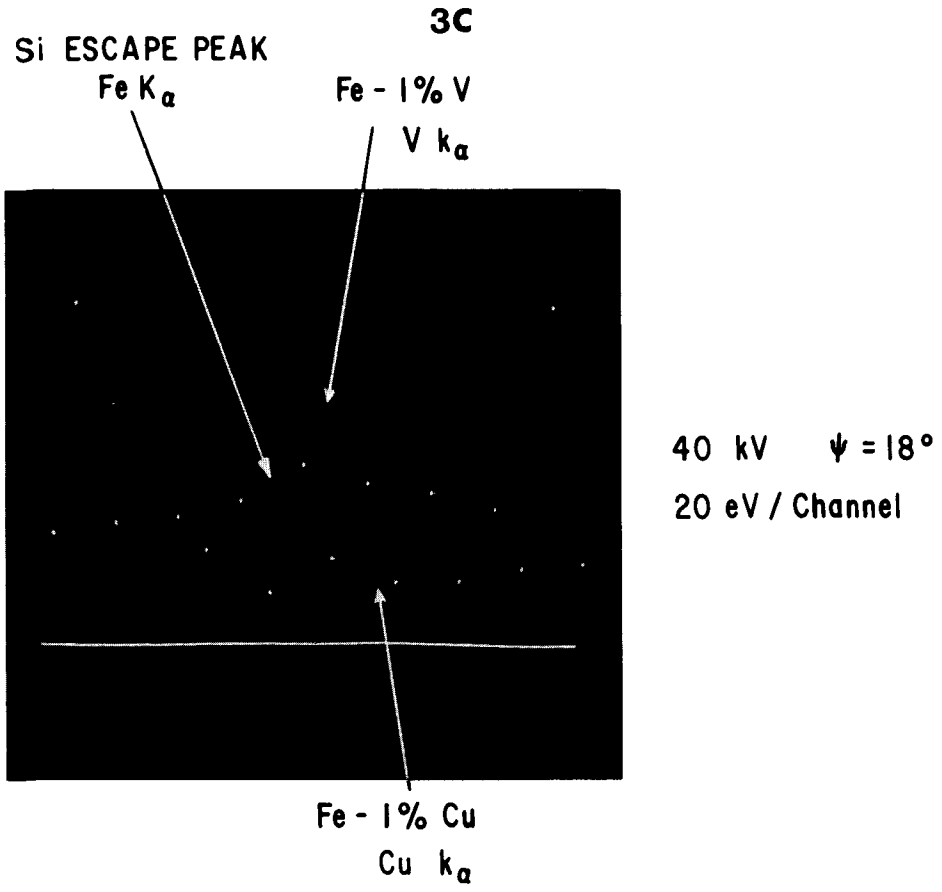

Fig. 1 - X-ray spectra for dilute Fe alloys.

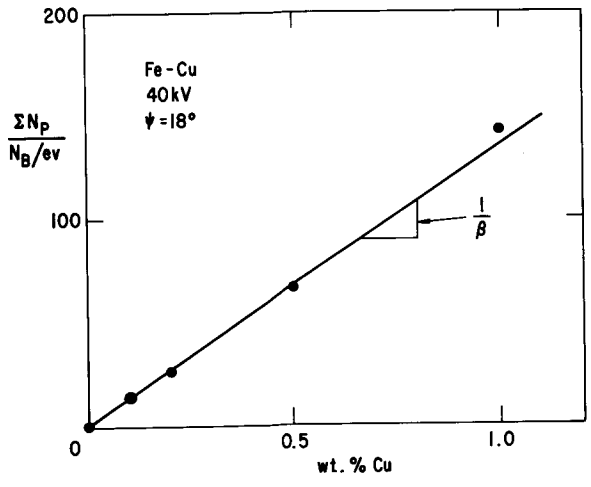

Fig. 2 - Calibration curve for Fe-Cu alloys.

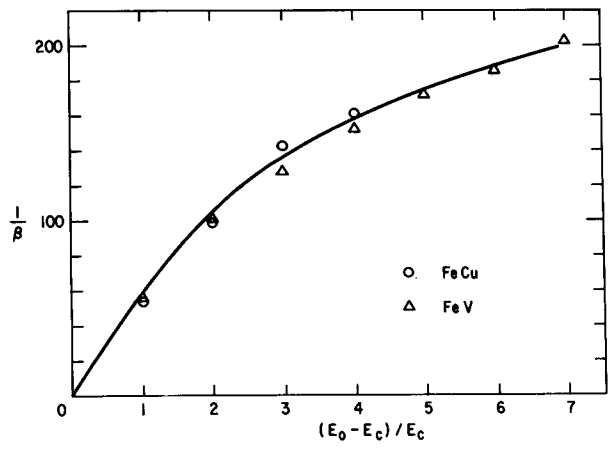

Fig. 3 - Dependence of empirically derived calibration coefficient on overvoltage.

operator initiates data output after specifying the options and programs he wishes to apply to the data. MCA output occurs one line at a time: the line-feed character generated by the input/output control inhibits the output until a computer-generated prompt symbol initiates output of the next line. This prevents data loss either by saturating the input buffer of the computer or by transmission while the computer is switched to other stations. Input into the MCA memory is controlled normally by the computer. The present system avoids expensive dedicated recording devices while adding the software advantages of time-sharing on a large computer.

The programs used to treat the X-ray data conform to conventional nuclear techniques, such as reported here last year by E. Lifshin, who also uses a time-shared transmission link. The spectrum is first smoothed with a moving average and the presence of peaks determined statistically. The peak positions are determined from the derivatives and converted to energy, and the X-ray lines are identified by a library search routine. Stripping and peak integration for quantitative analysis can be followed by application of standard microprobe techniques. Empirical methods are preferred for peak-fitting, since $L\alpha$ and especially $M\alpha$ lines often have non-Gaussian shapes.

The described combination of hardware and software, that we have developed, results in a rapid turn-around time for data processing and permits computer-operator interaction while the sample is still being observed in the instrument, thus allowing quick judgement of the quality of the data being taken.

LIMITATIONS ON Si(Li) X-RAY ENERGY ANALYSIS SYSTEMS AT HIGH COUNTING RATES

D. A. Gedcke, E. Elad, and G. R. Dyer
ORTEC, Incorporated
Oak Ridge, Tennessee 37830

In using the Si (Li) energy analysis systems on microprobes, fluorescence analyzers, and diffractometers, operation at high counting rates is often encountered. Unfortunately, the high counting rate limitations of these systems are not well publicized. These limitations are determined by the low noise preamplifier, the amplifier, and the multichannel pulse height analyzer (MCA).[1,2] However, in well-designed systems the amplifier provides the main limitation.

The preamplifier indirectly limits the high counting rate performance by requiring long amplifier shaping time constants, τ (wide pulses), in order to obtain optimum resolution. Optimum pulse widths in state-of-the-art systems are approximately 30 μsec for τ = 6 μsec (compared to 5 μsec for proportional counters). This long pulse duration constitutes the dominant deadtime of the system (assuming a 50-MHz MCA), typically causing 20% deadtime losses at 7,000 counts/sec. For higher counting rates, shorter pulse widths are necessary at the expense of energy resolution. Under these conditions the MCA processing time becomes the limiting deadtime. The average 500-channel MCA deadtime is 10 μsec for a 50-MHz ADC and 5 μsec memory cycle time.

Figure 1 shows the deadtime losses versus counting rate measured at the amplifier output. The deadtime losses for τ = 10 μsec and τ = 6 μsec are large even at low counting rates. The 2 μsec curve extends the 20% deadtime loss limit to 30,000 counts/sec. The deadtime losses are a strong function of counting rate above the 20% point. If no correction is applied, these losses become a limit of accuracy in quantitative analysis. The dashed curve in Fig. 1 shows the deadtime correction achievable with the livetime clock in the MCA. This curve clearly shows that to obtain 2% quantitative accuracy, the maximum counting rate is limited to 7,000 counts/sec (20% uncorrected deadtime losses). Similar results are obtained for other time constants, provided the uncorrected deadtime losses do not exceed 20%. To achieve this accuracy, the MCA must measure deadtime from the start of the amplifier pulse (not offered on all MCA's), and no biased amplifiers or stretchers can be introduced between the amplifier and the MCA.

The effect of counting rate on energy resolution is shown in Fig. 2. The best resolution (163 eV) is obtained at 10 μsec. For shorter time constants, poorer resolution results; but the flatness of the curve is preserved to higher counting rates. Special preamplifier feedback configurations are required to achieve flatness of the resolution curve below the 20% loss point. Above 20% deadtime losses, the resolution degrades rapidly with counting rate,

due to the amplifier baseline restorer losing control as the available baseline vanishes. Repeatability of performance at counting rates above 20% deadtime loss is unreliable and, therefore, operation at such counting rates is undesirable.

Figure 3 illustrates the counting rate limitations caused by the baseline restorer losing control. At high duty cycles, the baseline shifts to a negative value and causes a downward shift in the energy spectrum. In dynamic situations (i.e., distribution mapping on microprobes) this calibration shift may have the appearance of a gain shift. Both effects can introduce serious errors even into qualitative analysis. It is clear from Fig. 3 that the 20% deadtime loss points indicate the safe upper limit on the counting rate.

In conclusion, for qualitative analysis, lack of spectral distortion is important. The 20% deadtime loss points have been shown to represent the upper counting rate limit to avoid resolution broadening and energy calibration distortions. For quantitative analysis, deadtime losses are also important. In adequately designed systems the MCA can properly correct for losses up to the 20% point.

---

1. E. Elad, ASTM Technical Workshop on Energy Dispersion X-Ray Analysis, Toronto, June 24, 1970 (to be published).

2. F. J. Walter, ASTM Technical Workshop on Energy Dispersion X-Ray Analysis, Toronto, June 24, 1970 (to be published).

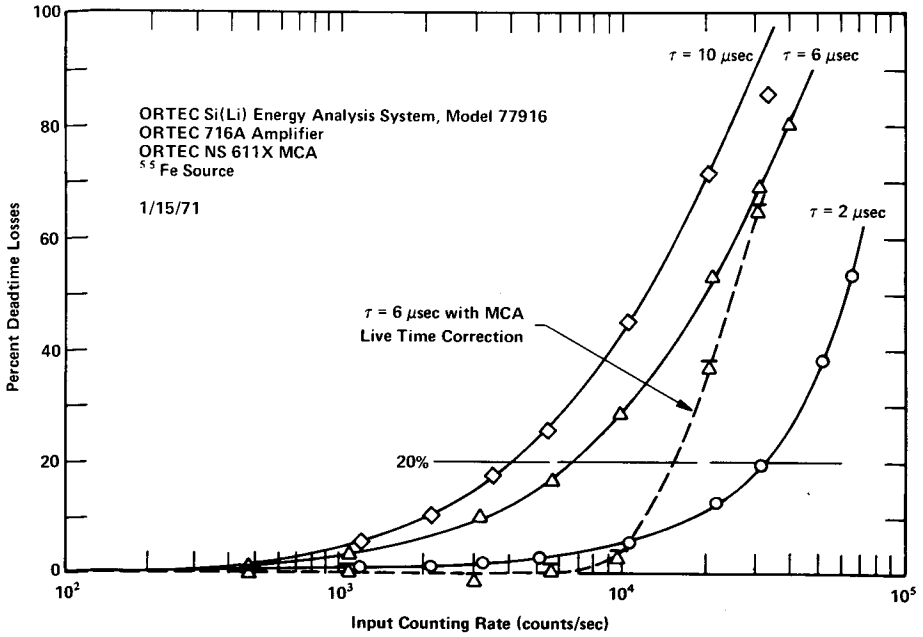

Figure 1. Deadtime Losses vs. Counting Rate for τ = 2, 6, and 10 μsec. The Dashed Curve Shows the Results of Deadtime Loss Corrections in the MCA.

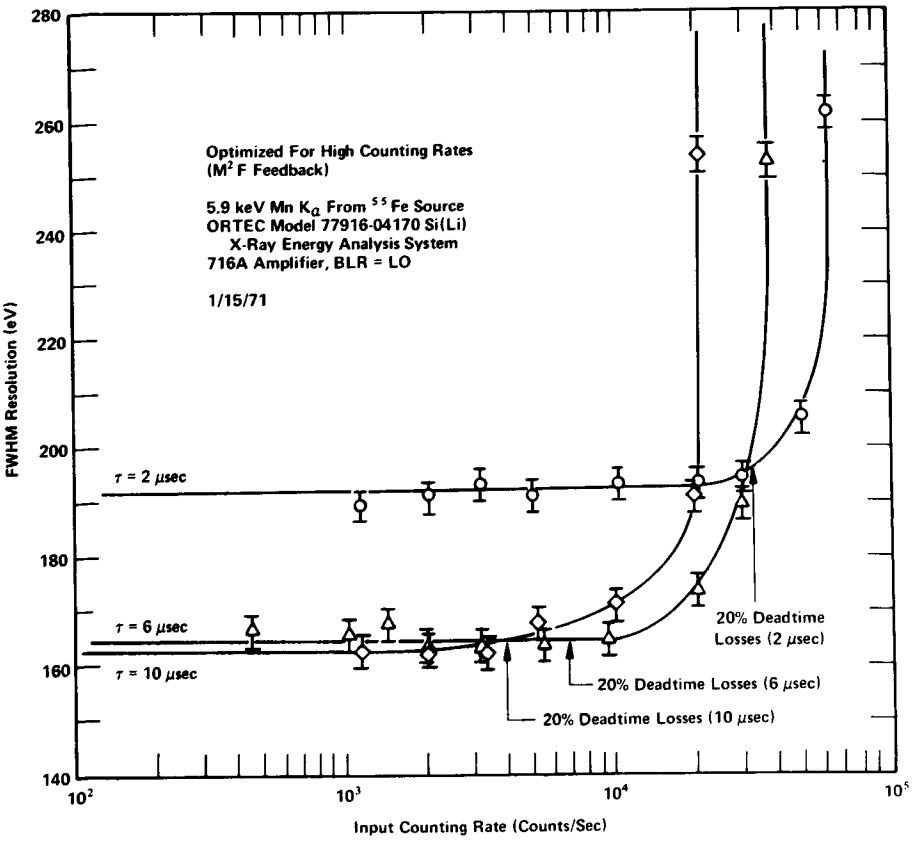

Figure 2. Resolution vs. Counting Rate for τ = 2, 6, and 10 μsec.

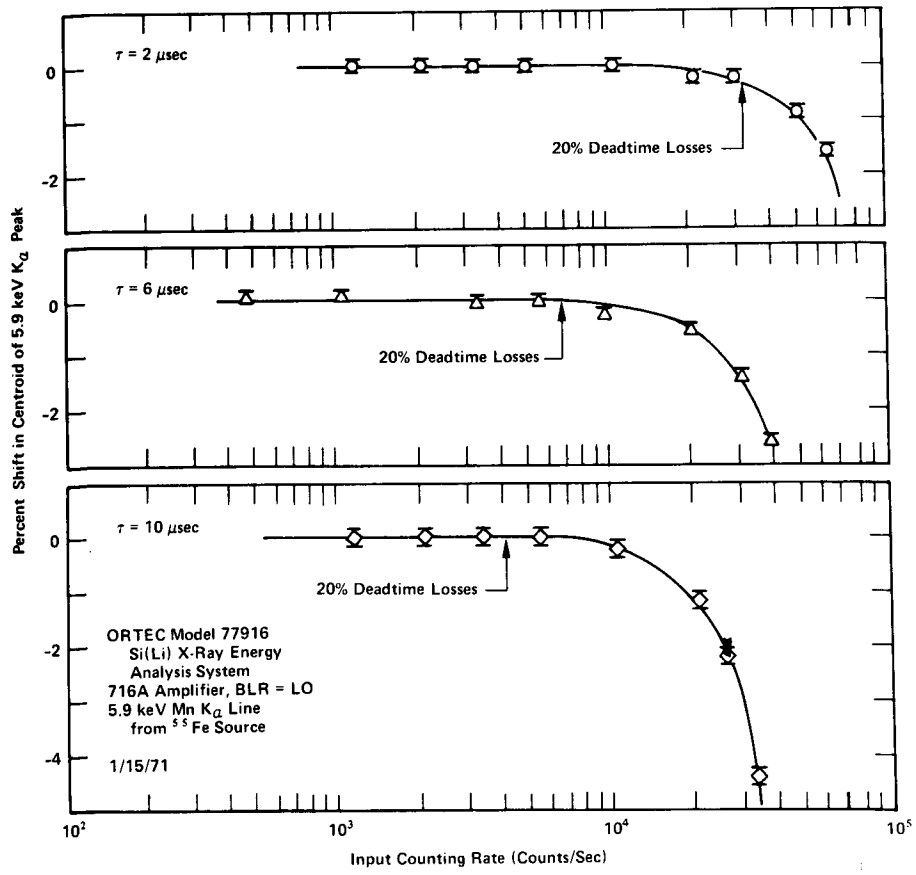

Figure 3. Baseline Stability vs. Counting Rate for τ = 2, 6, and 10 μsec.

COMPARISON OF SEMI-QUANTITATIVE ANALYSES MADE WITH ENERGY AND WAVELENGTH DISPERSIVE ANALYZERS OF EXTRACTED INTERMETALLIC PARTICLES

G.P. Sabol and C.J. Spengler
Westinghouse Research Laboratories

The use of wavelength dispersive (WD) and energy dispersive (ED) x-ray spectrometers for quantitative analysis of bulk samples has been well documented[1]. However, in some metallurgical investigations chemical analysis is often required of discrete micron or sub-micron sized precipitate particles. To perform an accurate analysis of such particles, extraction replica techniques have been utilized[2,3] to isolate the particles from the matrix for a direct analysis in the electron-beam microanalyzer (EBM). It is advantageous because of the better imaging capability of the scanning electron microscope (SEM) to use this instrument, in conjunction with an ED x-ray spectrometer, for the chemical analysis. Therefore, it was the objective of this investigation to compare results obtained on comparable specimens, both bulk and particulate, with use of both the WD-EMB and ED-SEM systems.

The specimens were bulk $ZrCr_2$ and extracted particles of $ZrCr_2$. The particles contained 3 w/o iron in solid solution with the chromium and ranged in size from 0.5 to 10 μm in diameter, with most particulates 2-3 μm.

The WD-EBM system used was a MAC-400 model, take-off angle 38.5°, with LiF crystal/sealed proportional counter and PET crystal/flow proportional counter spectrometers. The operational parameters were 20 keV and 0.03×10^{-6} amperes target current (on pure Zr). The ED-SEM system used was a Cambridge Steroscan Mark IIA with Nuclear Diodes ED x-ray analysis system (20 ev/channel). The working distance, beam current, and acceleration voltage were held constant at 10 mm, 9.6×10^{-10} amperes, and 20 keV, respectively.

Analyses with the ED-SEM system were made at different take-off angles by changing the tilt of the specimen stage. The geometrical relationship of the electron beam, x-ray detector collector, and axis of specimen stage tilt are not known with sufficient accuracy to state the effective x-ray take-off angle. Therefore, the data are referenced to the specimen stage tilt. The effect of stage tilt, and hence take-off angle, was determined for the pure metals and bulk $ZrCr_2$ at tilts between 5° and 80°. The particulates were analyzed at tilts of 30, 40, and 50°.

The bulk $ZrCr_2$ was analyzed with the ED-EBM system as an unknown against pure standards. The k-values were corrected for absorption[4] and atomic number effect[5]; the fluorescence correction[6] was negligible. The corrected analysis Zr-0.463, Cr-0.532 agrees well with the theoretical composition (Zr-0.467 and Cr-0.533, weight fraction). Six particulates were analyzed, also against pure standards. The x-ray intensities were corrected only for background and dead time and the k-values were normalized to total 1.00 wt fraction. Table I shows the normalized k-values.

In the analysis of the bulk $ZrCr_2$ against pure standards with the ED-SEM system the respective x-ray intensities varied with changing tilt as shown in Fig. 1. The effect of the take-off angle on the x-ray absorption is more apparent on the 6.07Å ZrLα than the 2.29Å CrKα or 1.94Å FeKα x-rays. Also from Fig. 1 it is seen that the Zr and Cr k-values will vary with tilt. At low tilts, 0-10°, the Cr k-value varies from 0.15 to .43. From 10-40° the Cr k-value increases gradually from 0.43 to 0.50; above 40° tilt it is constant at 0.50 to 80° tilt. The Zr k-value, at tilts over 10°, increases gradually from 0.37 to 0.48 up to 80° tilt. No corrections were applied to the k-values because of the uncertainty of the effective x-ray take-off angle. Seven particulates (including the six analyzed with the WD-EBM system) were analyzed against pure standards at tilts of 30, 40, and 50°. Table I shows the normalized k-values. The variation of the respective k-values with tilt is due partially to the variation of the x-ray intensity from the bulk standards, and predominantly to changes in surface scattering unique to the geometry of each particle as it is rotated under the electron beam.

The respective k-values for each individual particulate determined at 40 and 50° tilt with the ED-SEM system bracket the comparable k-values determined with the WD-EBM system.

Inspection of the analytical results for both the bulk $ZrCr_2$ and the particulates indicates that at a stage tilt of 45° the effective x-ray take-off angles are comparable for both systems. The k-values of the particulates, adjusted to total 1.00, indicate that the particulates are small enough to ignore the absorption and atomic number corrections. This is consistant with the findings of others[7]. The WD-EBM system gave better analytical results only because the geometrical aspects of the x-ray generation are better understood. The ED-SEM should produce comparable results when quantitative data are known for take-off angles, beam incidence, and working distance.

References

1. Proceedings of the 5th National Conference on Electron Microprobe Analysis, (1970).
2. M.J. Fleetwood, G.M. Higginson, and G.P. Miller, Brit. J. Appl. Phys., 16 (1965) p. 645.
3. M.J. Fleetwood, Electron Microscopy and Microanalysis of Metals, J.A. Belk and A.L. Davies, ed., Elsevier Publishing Company (1968) p. 225.
4. P. Duncumb and P.K. Shields, The Electron Microprobe, John Wiley and Sons (1966) p. 284.
5. P. Duncumb and S.J.B. Reed, Quantitative Electron Probe Analysis, NBS Special Publication 298 (1968) p. 133.
6. S.J.B. Reed, Brit. Jour. Appl. Phys., 16, (1965) p. 913.
7. B.R. Banerjee and W. D. Bingle, The Electron Microprobe, John Wiley and Sons (1966) p. 653.

TABLE I

k-VALUES OF ANALYZED $ZrCr_2$ PARTICULATES

Specimen	WD-EBM			ED-SEM								
				30°			40°			50°		
	Zr	Cr	Fe	Zr	Cr	Fe	Zr	Cr	Fe	Zr	Cr	Fe
A	.475	.483	.042	.491	.473	.036	.486	.484	.030	.451	.518	.031
B	.485	.490	.025	.499	.468	.033	.477	.489	.034	.458	.504	.038
C	.478	.496	.026	.499	.472	.029	.476	.490	.034	.467	.502	.031
D	.456	.508	.035	.516	.455	.029	.498	.468	.034	.468	.503	.029
E	.477	.495	.028	.487	.485	.028	.452	.513	.035	.428	.540	.032
F	.468	.491	.041	.475	.491	.034	.464	.499	.037	.450	.519	.031
G	-	-	-	.503	.469	.028	.520	.444	.036	.528	.442	.030
Avg.	.473	.494	.033	.496	.473	.031	.482	.484	.034	.464	.504	.032
Theoretical	.466	.503	.031									

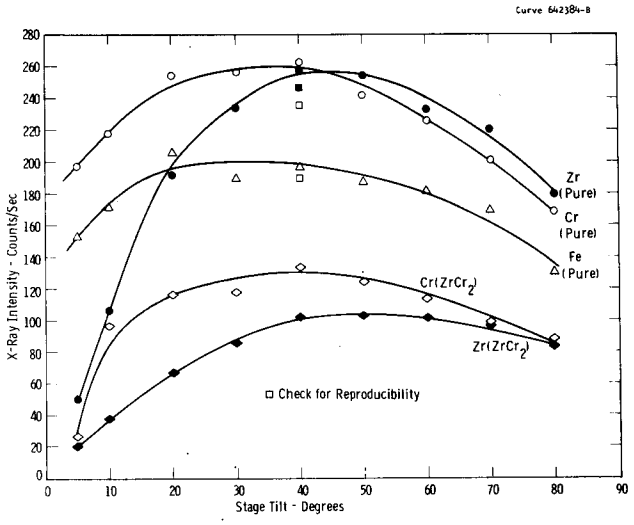

Fig. 1—Variation of X-ray intensity with tilt of specimen stage for pure standards and bulk $ZrCr_2$

PRODUCTION OF ELECTRON PROBES A FEW Å IN DIAMETER*

Albert V. Crewe
Departments of Physics and Biophysics and Enrico Fermi Institute
The University of Chicago, Chicago, Illinois 60637

During the past several years we have undertaken a program to improve the resolution of the scanning microscope. The aim of this program was to produce electron probes a few angstroms in diameter containing an adequate electron current to produce a micrograph in a few seconds. The competitive instrument for producing micrographs with a few Å resolution is the conventional transmission electron microscope, which has a point resolution in the neighborhood of 4 Å. The aim of our program was to produce a scanning microscope having comparable resolution.

If we assume that an acceptable electron micrograph contains approximately one million resolution elements and that an acceptable electron intensity would be 1000 incident electrons per resolution element, we see that it takes 10^9 electrons to form a micrograph. The micrograph can be formed in 10 seconds, and we therefore need an electron current of a few times 10^{-10} amps.

This requirement of the size of the focused spot and the beam current places a severe restriction upon the kinds of electron source which can be used in such a microscope, and in particular it means that a hot tungsten filament cannot be used because the inherent brightness is much too low. A field emission source appears to be the only one capable of being used.

Much of our work, therefore, has consisted of the engineering development of field emission sources, together with a suitable electron gun for subsequent acceleration. We have found that our design of source and gun is capable of producing a current of about 10^{-10} amps in a 100 Å diameter focused spot without the aid of any other focusing elements. This device alone can be made into a very simple but effective scanning microscope.

In order to reduce the spot size, we have constructed a second instrument which consists of the field emission source, the electron gun, and one short focal length magnetic lens. This machine focuses a beam of 30 kv electrons into a spot of 5 Å diameter which can contain up to 5×10^{-10} amps. With this machine we have been able to demonstrate that single heavy atoms can be seen in the microscope.

There are two ways in which the performance of our current instrument can be improved. The first of these is by increasing the voltage of the microscope. This reduces the electron wavelength. We have designed a 100 kv machine which uses two magnetic lenses and which should be able to produce a focused spot of electrons smaller than 3 Å in diameter and containing a current of more than 10^{-10} amps, which is adequate for microscopy.

*Work supported by the U. S. Atomic Energy Commission.

The other way to improve the performance of this machine is to attempt to eliminate the effect of the spherical aberration of the magnetic lenses, for it is the spherical aberration which limits the spot size at the moment. A spherical aberration corrector consisting of four quadrupole lenses and three octupole lenses is now under construction. In theory it would allow us to correct the spherical aberration of the final focusing element in the microscope. If this can be achieved in practice, the resolution--that is, the spot size--should be reduced considerably below 3 Å, while at the same time the current in the focused spot should remain constant.

brightness $B = \frac{N}{\pi \delta^2} = \frac{N}{\pi \lambda^2}$ diffraction limited.

Vacuum must be around 2×10^{-10} Torr. - optimum.

QUANTITATIVE THEORY OF SPUTTERED ION MASS ANALYSIS

C. A. Andersen

Hasler Research Center
Applied Research Laboratories
Goleta, California

An analytic model has been developed (1) for the interpretation of sputtered ion emission from samples bombarded with high energy beams of reactive gases. It has been demonstrated that both positive and negative sputtered ion emission can be enhanced and controlled by the proper chemical selection of the primary bombarding ion beam. The analytic model proposed that sputtered atoms and ions created in the atomic collisions initiated by the bombardment process are subject to electron attachment from the surface of the sample. Electron attachment in the majority of cases is proposed to be a thermionic process governed by the Fermi-Dirac distribution of electrons and the effective electron temperature of the bombarded surface. The proposed model states that ions of different chemical elements from a single matrix undergo the same degree of electron attachment because of the common surface potentials affecting them. Quantitative interpretation of the sputtered ion yields from a single matrix, therefore, reduces to understanding the initial ion generation process.

In the present theory it is assumed that the excitation states of the atoms at the surface of the bombarded sample can be described as if the sputtered ion source were a plasma in partial thermal equilibrium. Under these conditions the Saha-Eggert ionization equations (2) can be used to predict the ratio of the number of atoms in one charge state to the number of atoms of the same chemical element in the succeeding charge state. The product of the number of atoms in two successive stages of ionization and the electron concentration in the excited sputtered plasma is given in terms of the atomic partition functions of the two ionization stages, the ionization potential of the lower state, and the kinetic ion temperature. The experimental determination of the number of ions in two successive stages of ionization and a knowledge of the atomic partition functions permits the calculation of the electron concentration and the kinetic ion temperature of the sputtered plasma.

Figure 1 shows the ratio of the number of sputtered positive single charged ions to the number of neutral atoms as that ratio is modified by the atomic partition functions of the two ionization stages plotted as a function of the ionization potential for several elements from a well characterized mineral standard. The electron concentration and the kinetic ion temperature of the sputtered plasma were obtained by solving a pair of simultaneous ionization equations in which the observed ratios of the number of doubly charged to singly charged ions for two different elements were used. These data are directly observable in the mass spectra taken from the sample. The fit of the data to a straight line on such a graph supports the assumption that the sputtered plasma is in partial thermal equilibrium (3).

Sputtered ion intensities from metals can be described with the same ionization equations. In these cases the kinetic ion temperatures are observed to be

lower. Sputtered negative ion intensities and molecular ion intensities can be interpreted with the same model.

It is possible to relate the kinetic ion temperatures obtained from the ionization equations, using the observed ratios of doubly to singly charged ions, to the inelastic energy losses of the primary bombarding ion in the sample. The temperatures calculated from experimental data taken at different accelerating potentials of the bombarding ion beam correlate well with the inelastic stopping power calculated using the model developed by Lindhard and Scharff (4). For a given sample, increasing the accelerating potential of the bombarding beam increases the kinetic ion temperature attained in the sputtered plasma.

The quantitative method proposed is to assume the sputtered plasma to be in partial thermal equilibrium and to apply the Saha-Eggert ionization equations to the ion intensities observed in the sputtered mass spectrum. The kinetic ion temperature and the electron concentration of the sputtered plasma are used in these ionization equations to predict the degree of ionization of all the elements observed in the mass spectrum of the sample. The observed ion intensities are corrected for this degree of ionization to yield the total number of atoms of that element in the sputtered plasma. These totals, for all the elements in the mass spectrum, give the atomic composition of the sputtered plasma which has been shown to be representative of the solid sample under bombardment.

It should be noted that the kinetic ion temperature and electron concentration of the sputtered plasma can often be obtained from ratio of doubly to singly charged ions in the mass spectrum. This ratio is independent of the concentration of the element contributing the ions and opens the possibility for standardless analysis of unknown compounds. Such standardless analyses of mineral specimens have been accomplished with relative errors in the determination of major elements of less than 5%. The quantitative method proposed has been incorporated in a general computer program entitled CARISMA, (Corrections to Applied Research laboratories Ion Sputtering Mass Analyzers), (5).

REFERENCES

1. C. A Andersen, Third, Fourth and Fifth Natl. Electron Microprobe Conf., Chicago, 1968; Pasadena, 1969; New York, 1970; J. Mass Spect. and Ion Physics, 2 (1969) 61; 3 (1970) 413.

2. M. N. Saha, Phil. Mag., 40 (1920) 472,809; Z. Physik 6 (1921) 40: J. Eggert, Z. Physik 20 (1919) 570.

3. C. H. Corliss, J. Res. Nat. Bur. Std. A. Phys. and Chem. 66A (1962) 169.

4. J. Lindhard and M. Scharff, Phys. Rev. 124 (1961) 128.

5. J. R. Hinthorne and C. A. Andersen, Appl. Res. Labs. Internal Rept. (in preparation).

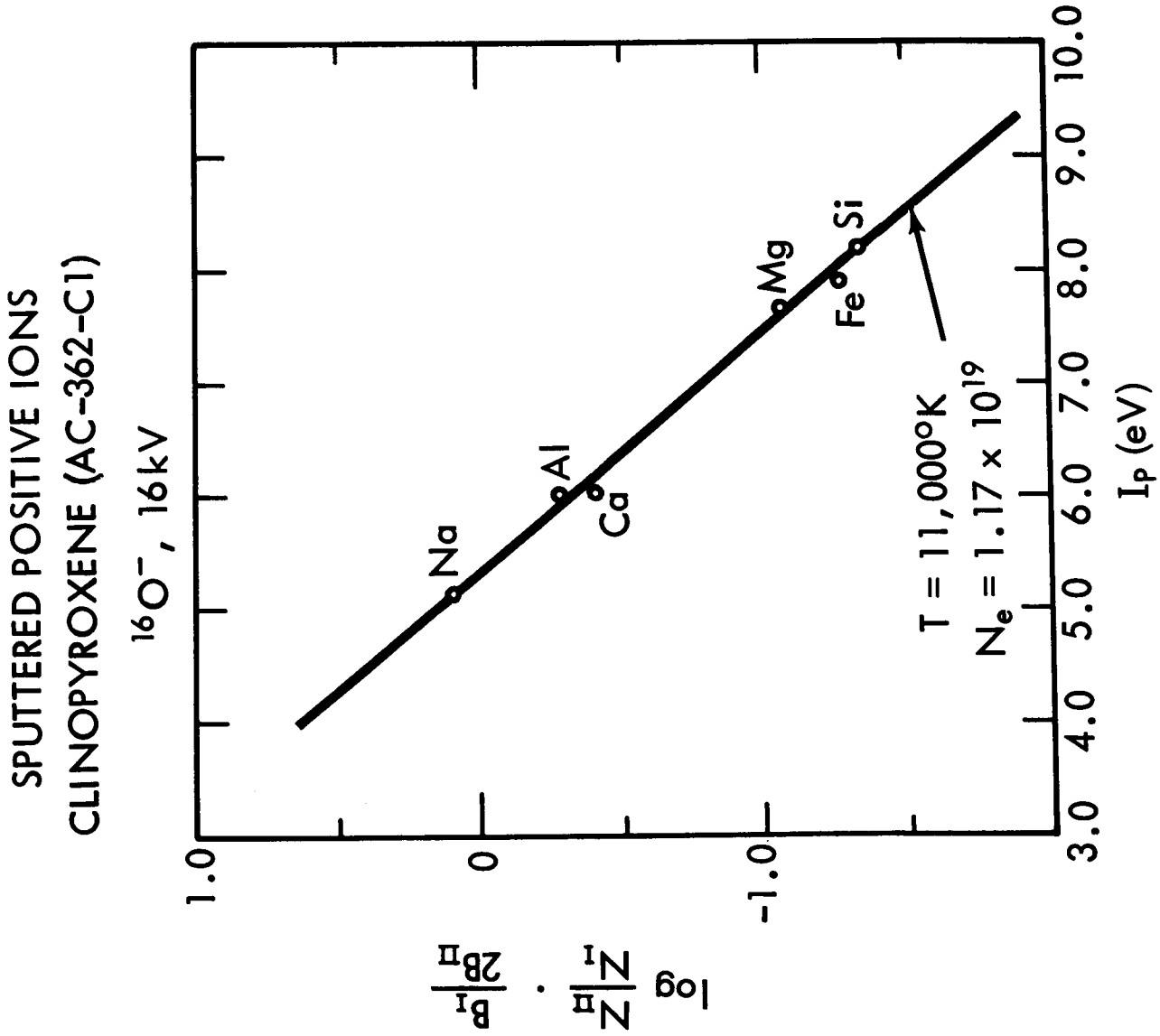
SPUTTERED POSITIVE IONS
CLINOPYROXENE (AC-362-C1)
$^{16}O^-$, 16kV
Na
Al
Ca
Mg
Fe
Si
T = 11,000°K
$N_e = 1.17 \times 10^{19}$
$\log \frac{N_i}{N_n} \cdot \frac{B_i}{2B_n}$
I_p (eV)
1.0
0
-1.0
3.0
4.0
5.0
6.0
7.0
8.0
9.0
10.0

SURFACE CHEMISTRY CHARACTERIZATION OF ALUMINA CERAMIC SUBSTRATES BY ION MICROPROBE MASS ANALYSIS

Donald K. Conley
Western Electric Co.

The surface chemistry of alumina ceramic substrates was determined in an effort to relate it to the adherence characteristics of sputtered tantalum nitride thin films. This was accomplished by obtaining concentration depth-profiles for the impurity elements with the Applied Research Laboratories ion Microprobe Mass Analyzer.

When thin films of tantalum nitride are sputtered onto ceramic substrates, various substrate lots exhibit varying degrees of sputtered tantalum film adherence. The impurities contained in the ceramic evidently play a major role in the bonding mechanism since tantalum nitride adhesion to a sapphire surface (pure alumina) is poor. It has been observed that alumina substrates, with good adherence characteristics, which then have their surfaces either mechanically ground or acid etched exhibit poor adherence. If the lot which has been acid etched is then refired, it regains its good adherence characteristics. It has been assumed that these effects are partially due to the removal of impurities concentrated on the surface which evidently enter into the bonding mechanism.

A good adherence lot of ceramic substrates (as received) was divided into three portions. The first portion was left in the "as received" condition, the second and third portions were acid etched with one of these portions receiving a refiring treatment. Impurity concentration-depth profiles were obtained for Si, Mg, Ca, Sr, Ba, Na, K and B of samples from the three aforementioned portions. This was done in an attempt to qualitatively determine if a specific ion or ionic species accounts for the difference in good and bad adherence characteristics.

Raw data was reduced to chemical composition using C. A. Anderson's (Applied Research Laboratories) quantitative model and computer programs developed by John Colby of Bell Telephone Laboratories. The corrected digital data was converted to analog form through use of a Cal-Comp plotter to obtain the concentration depth curves.

Data will be shown which represents the super-imposition of the "as received," acid etched and acid etched then refired concentration-depth curves for each of the following elements: magnesium, silicon, potassium, sodium and calcium. From these curves it is seen that the refiring cycle brings the impurity concentrations back up to the original levels or in two cases, magnesium and sodium, to even higher levels. This is economically important since it allows one to reclaim ceramic substrates which have become surface contaminated or have had errors occur in metallization processing by acid etching and subsequent refiring at 1500° C.

In the typical concentration depth curves, one observes that most of the impurity above the background concentration or bulk level is contained in the first 4000 A of the surface. These minor quantities (up to one weight percent) concentrated over a relatively great distance into the ceramic surface could possibly be indicative of solute surface segregation by the vacancy drag mechanism.

The eight curves which deviated from the 88 "typical" distribution curves were those of magnesium and barium. Magnesium and barium oxides evidently play an important role in whatever processes are occurring at the surface and appear to be related to adherence characteristics.

The most significant difference in the distribution with depth of the various impurity elements when comparing the as received, the refired and the acid etched samples is the surface depletion of magnesium in the acid etched sample. It is possible that this phenomenon is related to the bad adherence characteristics of the acid etched alumina surface due to a lack of magnesium to enter into the bonding mechanism. Bulk analyses performed between one and two microns from the surface showed that all the impurities are more concentrated in a known (bad adherence) alumina lot as compared to a known (good adherence) alumina lot.

Table I shows that although the bulk analysis of the bad lot (Column 6) contains more impurities than the good lot (Column 3), the good lot has higher surface concentrations of magnesium, silicon and barium (Column 1) than the bad lot. In Table I for the bad lot, we also observe a sub-surface depletion effect as we go from surface to bulk for magnesium, silicon and barium. However in the good lot this sub-surface depletion effect for these elements is absent.

Scanning electron micro-graphs taken by our laboratory of the alumina substrate has shown the presence of a glassy appearing, smooth textured second phase in increasing amounts as the tantalum film adherence has degraded. It is suspected that this phase has been formed by magnesium and barium oxides acting as a flux in conjunction with SiO_2 and Al_2O_3 to lower the melting point within the localized region. It is theorized on cooling that a phase change in the surface layer occurs that may effect the availability of Mg^{+2} ion for bonding reactions with Ta_2N.

It is theorized that the other phase contains the Mg^{+2} ion which is available to enter into the bonding mechanism. It is, however, recognized that under prolonged annealing or under reducing conditions MgO can escape from the theorized good surface phase.

Table I

Ion Microprobe Analyses (PPM Weight)
Good and Bad Adherence Lots

	(1)	(2)	(3)	(4)	(5)	(6)
	Good			Bad		
Element	Surface	Sub-Surface	Bulk	Surface	Sub-Surface	Bulk
Boron	8.	0.8	--	4.0	0.9	--
Sodium	9100.	1000.	683.	9100.	2800.	1359.
Magnesium	1733.	800.	845.	1080.	585.	929.
Silicon	3300.	1033.	946.	1300.	400.	2156.
Potassium	9500.	1000.	305.	11000.	1250.	767.
Calcium	1550.	350.	266.	3250.	1000.	1259.
Titanium	32.	21.	27.	71.	22.	23.
Barium	170.	40.	35.	68.	36.	46.

"ION SCATTERING SPECTROMETRY - A NEW TECHNIQUE FOR SURFACE COMPOSITION ANALYSIS"

By R. F. Goff
Central Research Laboratories
3M Company
St. Paul, Minnesota 55101

A sensitive method of surface composition analysis is obtained through monitoring the binary scattering of low energy noble gas ions from surface atoms. Such analyses have been shown to be accomplished with simplified instrumentation and to be sensitive primarily to the average first surface monolayer. (1) Identification of surface atoms is accomplished by measurement of the energy spectra of the scattered binary ions at a given scattering angle. These energy spectra consist of a number of peaks at various energies; the number of peaks corresponds to the number of constituents present, and the energy corresponds uniquely to the mass of each constituent through the following relation:

$$\frac{E_1}{E_o} = \frac{M_s - M_o}{M_s + M_o}$$

where: E_1 = Energy of scattered noble gas ion
E_o = Energy of probe noble gas ion
M_s = Mass of surface atom
M_o = Mass of noble gas ion

Thus, by selection of the probe ion M_o and measuring the scattered ion energy ratio E_1/E_o, the mass of the unknown surface atom is uniquely determined. Furthermore, the height of each peak gives a relative measure of the quantity of each constituent present. Elements throughout the periodic table can be identified in multi-component surfaces with no extra signal processing. Since the binary scattering process is mass sensitive, either high atomic weight materials (e.g. Au or Pb) or light elements (e.g. O or Al) are identified respectively by a single scattering peak. Further controlled ion bombardment etching of a sample yields a depth profile analysis - the elemental composition of successive atomic sublayers.

The instrument produces a nominal 1 mm diam. He^+ beam throughout an operating range of 300-3000 eV; by additional focusing adjustments beam diameters from 0.5 mm to several mm diam. may be achieved yielding current densities of from 1 - 50 uA/cm^2. Through adjustment of both ion beam focusing and static gas pressure, the current densities may be widely varied yielding average monolayer removal times as long as an hour.

A spectra obtained with 1500 eV He^+ ions scattered from an alloy surface is shown in Figure 1. ②

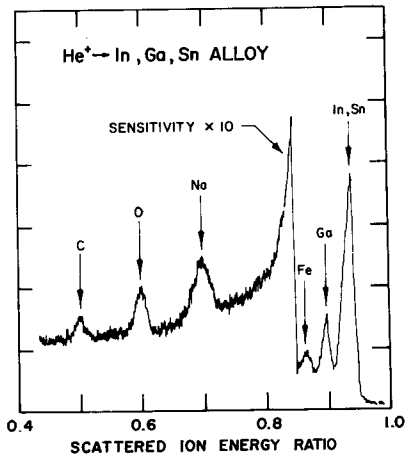

Figure 1

The ordinate is a plot of the number of ions scattered and the abscissa is a plot of the scattered ion energy ratio. One energy ratio (E_1/E_0) directly gives one mass (M_s) within the resolving power of the instrument. In actual instrument operation, this energy ratio is slowly scanned from 0 to 1 yielding a mass range from M_0 to ∞. The alloy examined consists of a terinary compound of In, Ga, Sn on a stainless steel substrate. In addition to peaks due to Sn, In and Ga, a peak resulting from He^+ scattered from Fe is noted, a result of incomplete coverage of the stainless steel substrate. Note that In(115) and Sn(119) are not resolvable with He^+ probe ions but yield a single scattering peak. Ar^+ ions could be utilized to resolve these two peaks. C, O, and Na are surface contaminants observed in the first few spectra taken on the surface.

The unique ability of Ion Scattering Spectrometry to measure the composition of the first monolayer of atoms has had wide application in areas such as complex alloy studies, thin films, surface contamination monitor, oxidation-corrosion studies, determination of surface to bulk compositional gradients, and semi-conductor surface preparations. The analytical technique has been extended to include the direct examination of electrically insulating surfaces without the need for a conductive overcoat being applied. With this capability, surface composition analyses are directly obtained from ceramic, glass and plastic surfaces.

Examination of thin films and multi-layer thin film structures is a prime example of the dual utilization of the probe ion beam both to simultaneously analyze and controllably remove surface atoms. Such a composition depth profile is obtained for a thin film sandwich structure composed of 200Å of TiO_2 on 175Å of Au on a glass substrate. An initial spectrum from the TiO_2 film is

shown in Figure 2 with peaks resulting from Ti and O surface atoms present in addition to minor impurity peaks from F and Al.

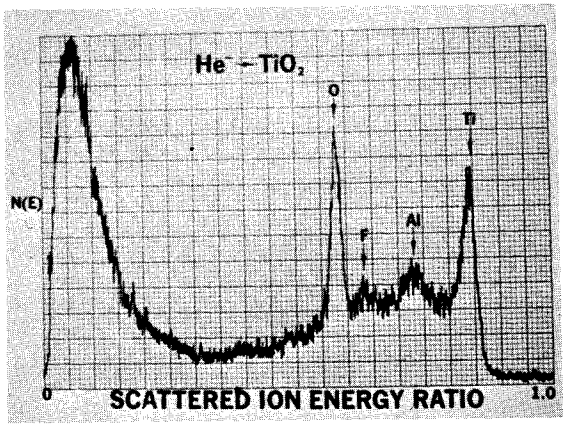

Figure 2

Repeated measurement of the spectra using controlled probe beam conditions yields a depth profile analysis of the thin film structure as shown in Figure 3.

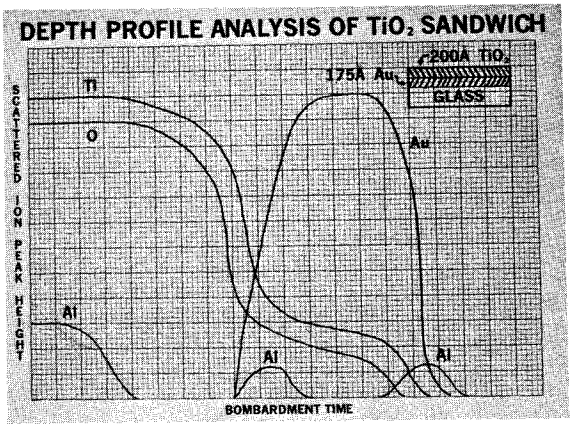

Figure 3

It is apparent from this normalized plot of scattering peak heights with bombardment time that: the various interfaces have Al as a contaminant; that the Au is not in a simple planar film but probably is nucleated (due to the coexistence of TiO_2 and Au); and that the thin film thicknesses are approximately accurate.

Other examples of composition depth-profiles of technological surfaces include that of polyvinylchloride where it was found through such a profile that chlorine was not present in the outermost

monolayers, apparently the result of the outward diffusion of the plasticizer.

The inherent ability of ISS to yield quantitative results after calibration is demonstrated in the Si and SiO_2 system. Since the scattered ion peak heights are proportional to the number of surface atoms present in the outer monolayer, one merely need establish the value of the single element clean surface peak height (in this case Si) and also the ratio of peak heights of the two elements in a stoichiometric compound (in this case SiO_2). Then judgments as to the approximate stoichiometry can be made such as in the case of the unknown system (SiO_x).

---

① R. F. Goff and D. P. Smith, J. Vac. Sci. Technol. 7, 72 (1970).

② R. F. Goff, Pittsburgh Conference on Analytical Chemistry and Applied Spectroscopy, March 4, 1971.

THE LASER MASS SPECTROMETER MICROPROBE

Bruce E. Knox
Materials Research Laboratory
and
Department of Materials Sciences
The Pennsylvania State University

The advent of the laser in the early 1960's provided a new energy source for experimentalists in many fields, including mass spectrometry. The possibility of heating a solid material in or near the ionization source of a mass spectrometer without heating the source components, a crucible, or anything other than the sample itself became apparent to many who were able to comprehend the energy that could be conveyed in a coherent light beam. Giant pulse lasers and normal pulse lasers with large energy flux outputs were used by many of the early investigators with anything but encouraging results. Often as not they were discouraged by the large kinetic energy spreads of the fragments produced. More satisfactory results were obtained in other laboratories where lasers with small power outputs were used. However, the fragments often were very unusual, bearing little resemblance to those produced in mass spectrometers with conventional vaporization sources. Only recently have laser solid interaction phenomena been understood well enough to begin to explain the results produced in the laser mass spectrometer microprobe.

The choice of laser to be used with a mass spectrometer depends primarily on the material to be vaporized for study. The most important aspect affecting laser vaporization is the coupling of the energy in the photon beam to the solid. Thus, a number of factors must be considered: the wavelength of the laser radiation; various absorption frequencies of the solid; the reflectivity of the solid surface; and the thermal properties of the solid. The focused flux from the laser is also important and is determined by the power output of the laser, the duration of the laser pulse, and the parameters of the optical system used for focusing. Both Q-switched and normal pulsed lasers have been used with mass spectrometers, but the effects produced by the normal pulsed lasers are much easier to reproduce and explain. Mechanisms of interaction, vaporization and ionization vary, depending on the nature of the solid, i.e., whether it is metallic or dielectric, etc. No general theory of laser-solid interaction can explain all of the different situations satisfactorily.

Many different commercial lasers can be utilized with mass spectrometers. Pulsed lasers are most desirable for many reasons. Electronic pulsing of gas lasers has opened up new wavelengths for use. Theoretically, any type of mass analyzer can be used with a laser; practically, the time-of-flight mass spectrometer is the most suitable. Figure 1 shows a typical coupling scheme between a pulsed ruby laser and a time-of-flight mass spectrometer. The laser beam strikes the sample surface approximately normal to its surface. No special sample preparation is necessary for bulk solids; powders can be pelletized, and internal standards added with ease.

The laser-solid interaction produces two distinctly different sets of vapor species. During the peak intensity of the laser output, ionic species are formed directly by the laser. For inorganic materials the process is undoubtedly thermal in nature, while for organic materials a chemical ionization process predominates. During the

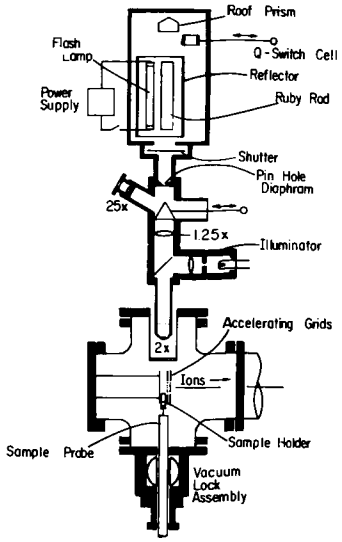

Figure 1. Source for laser mass spectrometer microprobe.

peak of the laser pulse, very unusual species are observed in the vapor, some as ions and others as neutral species. Recoil pressures from the expanding plasmas can easily reach several thousand atmospheres, sufficient to superheat many materials to their critical points or higher. Coupled with laser-produced surface temperatures of several thousand degrees, these pressures can cause many materials to vaporize at or near their critical region: transition from the condensed to the vapor phase occurs with little bond-breaking, thus preserving the short-range-order of the condensed phase. After the laser pulse has ceased to interact with the solid, only neutral species appear in the vapor. These must be ionized before mass analysis can be performed; since these species are often in some excited state, low energy electrons can produce reasonable ionization with little, if any, fragmentation.

Recording the vast amount of information produced by the laser mass spectrometer in the times involved is one of the problems of the technique. At the present time, only photographic recording of an oscilloscope trace provides the speed necessary to capture the information as it is presented. Another limitation of the technique is the difficulty in making the analyses quantitative. Calibration is rather difficult, and the laser is rather selective in vaporizing mixtures. In addition, the quantities of some ions, such as the alkali metal ions, produced by laser-solid interaction and detected by mass spectrometry are well below the detection limits of any other technique. Although the basic principles of laser-solid interaction are reasonably well understood, a number of details have not been explained. This includes the partitioning of energy between increasing the temperature of the condensed phase and providing heats of melting and vaporization. With inorganics most of the energy seems to go to increasing the temperature, while in the case of organic materials, ΔH seems to be favored.

Because the laser beam can be focused on the surface of a solid, spots as small as about 10 μm can be vaporized and analyzed by the mass spectrometer. Depending on the spot size and the energy flux produced by the laser, anywhere from a few nanograms to a microgram of material is vaporized with each laser pulse. However, one pulse gives a complete mass spectral analysis, as well as the time variation of species produced. In addition, some structural information may also be produced. Thus, the laser mass spectrometer can be considered a true microprobe with some unique properties as well as some deficiencies. Quantitative analysis is difficult, at best. Probing must be done on a point-by-point basis, although raster-mapping is a possibility when information can be recorded fast enough. The inherent sensitivity of the mass spectrometer for ultratrace amounts of various elements has not been sacrificed by coupling with a laser. Isotope ratios can also be measured from a single laser pulse interacting with a micro-inclusion or with the bulk material itself. Thus, the laser mass spectrometer microprobe must be viewed with an open mind as a new technique with valuable contributions to be made to the field of compositional characterization, not as the savior of the analytical world, but as a complementary technique to those now in service.

THE FIELD ION MICROSCOPE ATOM PROBE; IMAGING AND ANALYSIS ON AN ATOMIC SCALE

S. S. Brenner, J. T. McKinney and S. R. Goodman
E. C. Bain Laboratory for Fundamental Research, United States Steel Corp., Monroeville, Pennsylvania 15146

The field ion microscope is known to have atomic resolution. However, in the past, two problems have hindered its development into a widely-used analytical tool. First was the stringent restrictions on imaging; the high fields required for helium ionization made it difficult to image anything except the refractory metals, and the operator was required to be totally dark adapted to view the dim image. Second, work with alloys was always open to question, since it was impossible to distinguish which constituent was being imaged. Experimental advances have been made that overcome these difficulties, and we are now using the instrument to study early phases of precipitation in ferrous alloys. An example is shown in Figure 1, which shows the micro-sectioning through a small copper precipitate in an iron lattice. Chemical analysis of the particle shows it to be nearly 100 percent copper, and the concentration drops to the average matrix value in the alloy within one or two lattice spacings.

Improved imaging conditions are made possible by the use of a micro-channel plate, which is an imaging ion converter and electron multiplier. Very many small (40 μm diameter) channel electron multipliers are put together in an array; the ion image is projected onto the front face of this array and a multiplied electron image is available at the back face. Acceleration of the electrons onto a phosphor screen placed in close proximity produces an image that can easily be seen and photographed in reduced room illumination. Since the image brightness is not a function of the mass of the incident ions, heavier ions with lower ionization energies can be used, and the lower fields required for imaging permit the use of ferrous alloys in the instrument. Chemical analysis is made possible by a technique first proposed and demonstrated by E. W. Mueller, the original inventor of the Field Ion Microscope. It makes use of a process called field-evaporation in which the surface layer of atoms can be removed from the specimen as ions by raising the field above that required for imaging. The field-evaporated metal ions follow the same trajectory as the imaging ions. To analyze an atom or a group of atoms located at a certain region, the image of that region is placed over a probe hole in the screen by manipulating the position of the sample. When a short voltage pulse is applied to the specimen to field-evaporate the surface atoms only those atoms imaged over the probe hole are able to enter the drift tube at the end of which is located an ion detector. By measuring the time between the application of the field-evaporation pulse and the generation of the detector output signal the ratio of the mass to electronic charge of the field-evaporated particle can be determined. A schematic of the apparatus is shown in Fig. 2.

An example of the type of experiment performed in the atom probe is shown in Figures 3 and 4. An iron-3 atomic percent molybdenum alloy that is aged in nitrogen at constant activity has been shown to have desirable hardness properties, but no precipitates can be resolved in electron micrographs. Figure 3 shows a field ion micrograph of a specimen under conditions where the matrix

shows little contrast but the edges of the thin precipitate platelets are bright; the overlay shows the intersection of the specimen surface with three sets of {100} planes. By evaporation through the specimen, the morphology of the small precipitates can be followed, and it is shown that they are platelets about 2 atom layers thick that lie on {100} planes in the matrix. Figure 4 shows how the chemical analysis is performed; a particular precipitate is placed over the probe hole, and analysis of the area imaged inside the probe hole is carried out. The histogram in figure 4 shows the results of the analysis of a precipitate platelet, along with the suggested composition of the particle as $Fe_3Mo_3N_2$.

Figure 1. Microsectioning through copper-rich precipitate particle in Fe-1.4 Cu alloy.

Figure 2. Schematic of Field Ion Microscope Atom Probe, showing sample chamber with H_2 liquefiers for specimen cooling (specimen manipulator is omitted), movable micro-channel plate internal image converter and intensifier (for variable magnification), electrostatic lens for focusing field-evaporated ions, drift tube for time of flight spectroscopy, and detector for focused ions.

Figure 3. Precipitate platelets in Fe-3% Mo aged in NH_3/H_2 at 480°C. Net of white lines shows intersection of 3 families of {100} planes with specimen surface; each precipitate is about 2 atom layers thick, and is seen to lie in a {100} plane. Image conditions are selected to reduce the contrast in the matrix which can be faintly resolved near the top of the picture.

Figure 4. Analysis of platelet precipitates shown in Figure 3. Platelet is placed over probe hole (black spot in center of picture) and analysis begun. Neon ions are detected because neon is used for imaging. Ratio of detected Fe, Mo, and N suggests composition of platelet may be $Fe_3Mo_3N_2$.

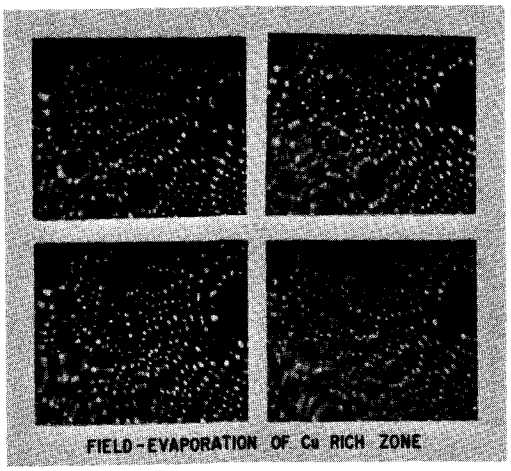

Fig. 1

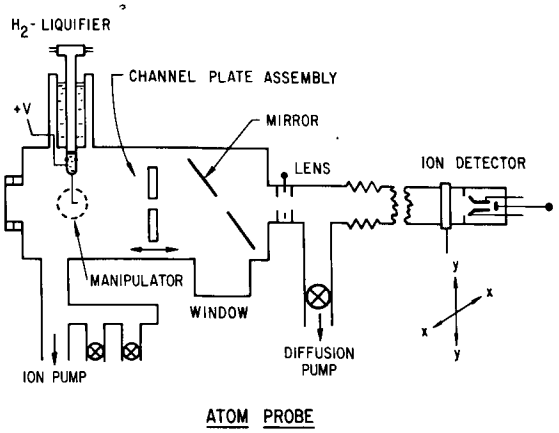

Fig. 2

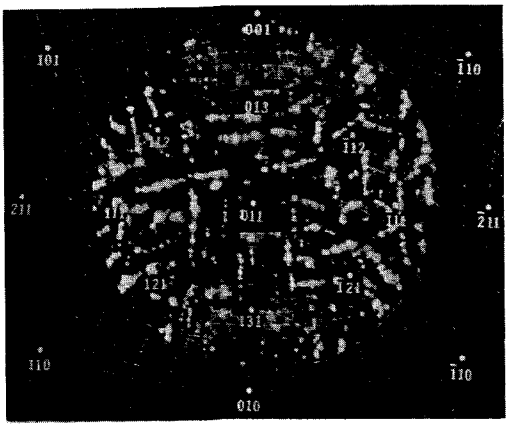

Fig. 3

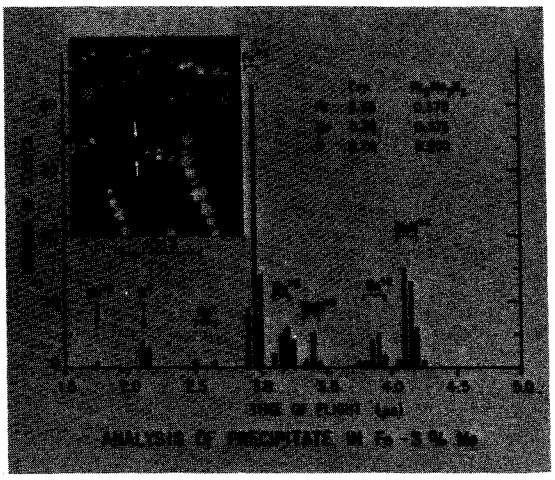

Fig. 4

AUGER AND CHARACTERISTIC ENERGY LOSS MEASUREMENT AS AN ANALYTICAL TOOL WITH THE SEM

E. J. Sternglass and R. K. Matta
University of Pittsburgh
Pittsburgh, Pennsylvania 15213

The feasibility of combining qualitative Auger spectroscopy with scanning electron microscopy has been shown by various investigators[1,2,]; the major advantages of this combination are greater spatial resolution and the ability to visualize the area being analyzed. This, combined with the possibility of simultaneous x-ray analysis and characteristic energy loss analysis, makes this technique appear quite attractive. In this paper we describe recent results obtained from studies being carried out in an attempt to (a) develop an electron velocity analyzer suitable to permit quantitative analysis of surfaces in the scanning electron microscope, and (b) to elucidate more clearly the various physical mechanisms responsible for the different types of energy losses which occur when electrons are incident on a sample. A study of these losses is made both in reflection and transmission through thin film.

A comparison has been made of three commonly available analyzers, specifically the retarding field, the 127° sector and the cylindrical mirror type. Each of these has both advantages and disadvantages. For example, the retarding field analyzer has a high collection efficiency but because it collects all electrons with energies greater than the applied retarding field, a high background, or shot, noise results. The 127° sector analyzer, utilizing narrow entrance and exit slits, has a resolution of about 0.5% with a significant decrease in shot noise but suffers from its extremely low electron transmission. The cylindrical mirror analyzer described by Hafner[3] has a collection efficiency about the same as the retarding field but without the associated shot noise. However, sample positioning is critical and secondary electrons needed for obtaining image information are difficult to collect. A prototype retarding field and the cylindrical mirror are discussed in detail.

In addition to our work on the development of a suitable analyzer, we have studied the various characteristic energy losses in an effort to identify the physical processes involved. A close correlation of the most prominent characteristic energy loss values of the elements with their ionization potentials and position in the atomic table strongly suggests that these losses result from individual ionization processes or the formation of secondary electrons[4]. A study of the binding energies of the outer four atomic shells shows that whenever these are known, characteristic losses are found to occur having an energy some 1 to 3 ev higher, corresponding to the most probable energy given to the secondary electrons formed.

If such correlations are further confirmed in experiments presently being carried out on vapors and solids, it would lead to a simple theoretical understanding of

most characteristic energy losses in terms of individual ionization and excitation processes rather than the excitation of collective plasma oscillations, which appear to involve mainly the low-lying losses in metals.

Data will be presented which shows how the studies of electronic velocity spectra in free and bound atoms can lead to a deeper understanding of chemical bonding and the structure of the outer electronic shells in solids.

References

1. E. J. Sternglass and R. K. Matta, Conference on Photoelectric and Secondary Electron Emission, University of Minnesota, 1969.

2. N. C. McDonald, H. L. Marcus and P. W. Palmberg, 3rd Annual Scanning Electron Microscope Symposium, IITRI, 1970.

3. H. Hafner, J. Arol Simpson and C. E. Kuyatt, Rev. Sci. Inst., Vol. 39, No. 1, 1968.

4. E. J. Sternglass, Nature, 178, 1387, 1956.

LRL COMPUTER PROGRAM: MICROANALYSIS†

Wayne J. Steele
Lawrence Radiation Laboratory, University of California
Livermore, California

March 17, 1971

SUMMARY

A Fortran 4 computer program, which has been written at LRL for our electron-beam microprobe analyzer,* provides a readout in weight and atomic concentrations and requires a minimum of program instructions per problem. The program corrects for dead time, drift, continuum background, absorption, secondary fluorescence, and atomic number. For samples having concentration gradients (maximum of 150 data points), the atomic and weight percentages are plotted as functions of distance from a fiducial mark. If plots are not required, weight and atomic concentrations are printed with a sum of all the analyzed areas.

The microanalysis computer program was written at LRL for converting raw data from our Model 400S microprobe analyzer to weight and atomic concentrations, using CDC 6600 and 7600 computers.

A review of the literature revealed that some existing programs eliminate the need for a drift correction by alternately taking a few readings between elemental standards and the sample. Other programs call for a hand-calculated drift percentage to be included as part of the computer input. The author found that the analysis time for a diffusion-couple concentration gradient is too long to ignore the drift correction, and that it is also impractical to take alternate readings on a sample and elemental standards. Hence, a drift correction was included in the LRL computerized microanalysis program.

To correct for drift, the raw data must include the relative time of each event. A timer-coder, designed and built at LRL, records the relative time and the appropriate identification code for each data scan. This device includes 14 manually set number coders, in addition to the relative timer, that are used to identify the data from each spectrometer, the counting time, the distance between counting points, and the number of counting events to be averaged per point. As a bonus, each data scan is identified with a different relative time, facilitating the editing of the data.

The program also provides for (1) compensation for K and L fluorescence, (2) the Philibert-Tixier atomic-number correction[1], (3) the use of either α or β spectral lines, and (4) a spectral background correction. This program,

---

†Work done under the auspices of the U.S. Atomic Energy Commission.

*Materials Analysis Corp., Model 400S.

however, does not correct for continuum fluorescence or fluorescence involving M and N spectral lines.

Instead of using the mass-absorption coefficient as input for each analysis, we append a library of coefficients to the program. For a nine-element system, 81 mass-absorption coefficients are needed for the absorption correction, together with several additional ones for the fluorescence correction, if required. Except for cases near absorption edges, Heinrich's mass-absorption coefficients are used.[2] For those exceptions, we apply J. Frazer's computerized values.[3] When better values become available, we will update our library.

In the course of the program, the computer seeks out, selects, and reads out all of the parameters required for the correctional formulas for each problem. The computer also checks and corrects the data for fluorescences, such as K excites K, K excites L, L excites K, and L excites L. The program is written to use binary-compound standards when the elemental ones (e.g., P, S, and Cl) are not available. With the coders set at the appropriate number, the computer back-calculates and reenters the correct number of counts/sec, as though the pure element were the standard.

Analyses obtained by the use of this program on NBS gold-copper standards agree to within 2% relative of the values reported with the standards.

REFERENCES

1. J. Philibert and R. Tixier, "Electron Penetration and the Atomic Number Correction in Electron Probe Microanalysis," Brit. J. Appl. Phys. 1, 685-694 (1968).

2. T.D. McKinley, K.F.J. Heinrich, and D.B. Wittry, Eds., X-Ray Absorption Uncertainty, The Electron Microprobe (John Wiley and Sons, Inc., New York, 1966).

3. J. Frazer, A Computer Fit to Mass Absorption Coefficient Data, Institute for the Study of Matter, University of California, La Jolla, SIO Ref. No. 67-29 (1967).

QUANTITATIVE MICROPROBE ANALYSIS AND DATA REDUCTION USING AN ON-LINE MINI COMPUTER

Arthur A. Chodos and Arden L. Albee
Division of Geological and Planetary Sciences, California Institute of Technology, Pasadena, California 91109

The invited paper by Duncumb (1970) at last year's National Conference raised the question of whether a small computer dedicated to on-line control of a microprobe could additionally be used for processing the final results and questioned whether the various corrections might be calculated and combined into a single coefficient with little loss in accuracy and a substantial saving in core storage. The answer to both questions is yes.

Such correction factors have been used and tested in our laboratory for several years for the analysis of silicates, oxides, carbonates, phosphates, and sulphates (Bence and Albee, 1968; Knowles, et al., 1969; Albee and Ray, 1970) and are now used by a large number of other laboratories. The system was originally developed and tested on large computers, but has been successfully transferred to small computer usage.

In the authors' laboratory a PDP-8L computer with 8192 words of memory and no peripheral devices, has been used, in conjunction with a MAC-5 microprobe, to gather and reduce the data for 14 elements in complex phosphates and silicates. Programs are written in FOCAL, a high level conversational language, to which has been added a series of command strings which control the microprobe operation and which are implemented by simply formulated instructions. This resident system takes about 4200 words of memory; the rest is available for analytical programs and calculations.

A typical quantitative analysis program directs the spectrometers to predetermined peak and background positions for 14 elements, counts for a preset time while sampling the beam current, normalizes to constant beam current flux, corrects for background and dead time, compares to standards and prints out "K-values" (the ratio of the intensity of the element to that of the oxide), calculates weight percent of constituent oxides with 4 iterations, attributes deficiency in total to OH^-, computes 3 more iterations and prints weight percent, computes and prints catatom percent, and normalizes to give formula proportions. The total program is about 2100 words; running time for this operation is approximately 9 minutes for the data collection and two minutes for data reduction.

A peak-seek program (~500 words) is used, when necessary, to determine peak locations on standards at the initiation of a series of analyses. Time to locate and set a peak is 1 minute and this program can reside in memory at the same time as the quantitative analysis program.

A qualitative analysis program (~2300 words) counts for 2 seconds at predetermined peak and background locations for 44 elements, applies a significance test, and prints peak and background intensities for the elements present. The running time for this program is 8-10 minutes so that it may be used in lieu of wavelengths scans with a pronounced saving in both running and interpretation time.

We cannot overemphasize the importance of using a high-level, highly interactive language like FOCAL in a general purpose laboratory with a number of operators. Students and staff members with little or no programming experience can control the operation of the microprobe and format the output. Existing programs can be readily modified or new ones written for special purposes.

References

Albee, A. L. and Ray, L. A., 1970, Correction factors for electron probe microanalysis of silicates, oxides, carbonates, phosphates, and sulphates: Anal. Chem. v. 42, p. 1408-1414.

Bence, A. E. and Albee, A. L., 1968, Empirical correction factors for the electron microanalysis of silicates and oxides: J. Geol., v. 76, p. 382-403.

Duncumb, P., 1970, Quantitative microprobe analysis: Proc. 5th National Conference on Electron Probe Analysis, N. Y., N. Y.

Knowles, C. R., et al., 1969, X-ray emission microanalysis of rock forming minerals. VII Garnets: J. Geol., v. 77, p. 439-451.

COMPUTERIZED MICROPROBE METHOD FOR THE DETERMINATION OF THE THICKNESS OF THIN FILMS IN MULTILAYERED INTEGRATED CIRCUITS

G. DiGiacomo

IBM Components Division
East Fishkill Facility
Hopewell Junction, New York 12533

Electron microprobe analysis is based on the measurement of the X-ray intensity generated in a specimen by electron excitation and then detected by a counter after the radiation has emerged from the sample surface. The radiation is generated within a specimen whose thickness is considered infinite in comparison to electron penetration.

For a layer of infinite thickness, the X-ray intensity reaching the counter is the integral from zero to infinity of all intensities expressed by the excitation function $\phi(\rho z)$ and attenuated through their distance from the surface of the specimen.

To analyze a layer of less than infinite thickness which lies on a substrate or is at a given depth from the surface, one must integrate the function $\phi(\rho z)$between the limits and then account for the energy absorbed throughout the layer above it before it emerges to the surface. This suggests that, when dealing with thin films which are part of a layer system, the electron excitation and detected intensity can be calculated on a layer basis. However, the analytical approach to the film system in terms of electron penetration and X-ray absorption must be kept the same as with infinite thickness, except that each material is dealt with individually. The analysis of thin films is two-fold: (1) measurement of thickness and depth of film and (2) determination of composition; one is required to determine the other. With integrated circuits, the determination of the thicknesses and depths of the metallurgical film components is easily achieved because the components have a known composition. To accomplish such an analysis in situs, one could use metal tracer standards of known thicknesses buried at different depths within a matrix as in the samples to be analyzed, and determine the X-ray intensity of the tracer and matrix elements at a fixed voltage for both standards and samples. The thickness of each sample layer and its depth from the surface is then determined from the X-ray intensitites obtained under the same conditions as the standards.

This procedure is expensive, laborious, and practically unfeasible even if one single acceleration voltage could be used to cover all thicknesses and depths involved in the analysis. The use of more than one accelerating voltage when analyzing a number of samples is necessary for reasons of detectability and electron beam penetration. To be suitable and satisfactory, an analytical method must be flexible enough to be able to translate or equate

X-ray intensities obtained at different accelerating voltages for different specimens, and must be fast enough and economically feasible for every-day applications.

The microprobe technique presented here was designed to take care of the analytical difficulty as well as the laboriousness and inefficiency. All this is accomplished by a computer program based on the electron excitation function which is based on the density-depth as well as acceleration voltage. It was derived on the basis of known published $\phi(\rho z)$ curves for various voltages. It was found that, to a good approximation, each electron excitation normalized curve is approximately a parabola whose apex shifts to the right and the latus rectum increases as the accelerating voltage is increased. The fit is good if the accelerating voltage is at least $20 kV/mg/cm^2$.

The excitation function $\phi(\rho z, V)$ thus determined was subsequently checked experimentally with X-ray intensity values obtained from a copper tracer of 2500Å on a silicon substrate and covered in a stepwise fashion by nickel layers ranging from 500Å to 5000Å in steps of 500Å. An uncovered copper layer was also included for the purpose of X-ray intensity normalization. The metal pattern was achieved by depositing the copper layer over the silicon wafer followed immediately by the vaporization of nickel whose stepwise deposition on the copper was controlled by a rotating disc interposed between the source and silicon substrate. The disc had concentric slots of different length such that the amount of nickel deposited on the copper was proportional to the length of the slot. The copper and nickel were analyzed by probe at ten accelerating voltages ranging from 10 to 30kV and the X-ray intensity values plotted versus ρz for each voltage. The intensity distribution agreed well with the calculated or predicted distribution.

The derived electron excitation function is written as:

$$\phi(\rho z, V) = \phi_{max} - 2 \times 3^{(4 - \frac{V}{10})} \left[\rho z - \frac{1}{8} \phi_{max}^{(\frac{V}{10} - 1)} \right]^2 \qquad (1)$$

where $\phi_{max} \cong 1.6$ is the maximum normalized intensity independent of accelerating voltage corresponding to the apex of each parabola, see Fig. 1.

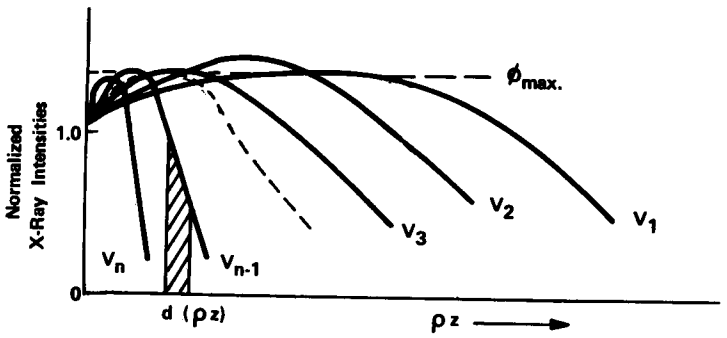

Fig. 1. Electron excitation function $\phi\rho z$ for various accelerating voltages.

When this function is integrated between the depth limits of the tracer and the X-ray attenuation through the upper layers is considered, the resulting expression represents the detected intensity which is a function of ρz, V and the absorption properties of the materials through which the X-ray is attenuated.

The normalized detected intensity is:

$$\phi^1(\rho z, V) = \frac{A\alpha\delta^2}{x_N}\left\{(\alpha\beta^2 - \phi_{max})\left(e^{-x_N\rho_N z_n} - e^{-x_N\rho_N z_{n-1}}\right)\frac{1}{\alpha\delta^2} + \right.$$

$$\left[(\rho_N z_n)^2 + 2\left(\frac{1}{x_N} - \frac{\beta}{\delta}\right)(\rho_N z_n + \frac{1}{x_N})\right] e^{-x_N\rho_N z_n} +$$

$$\left.\left[(\rho_N z_{n-1})^2 + 2\left(\frac{1}{x_N} - \frac{\beta}{\delta}\right)(\rho_N z_{n-1} + \frac{1}{x_N})\right] e^{-x_N\rho_N z_{n-1}}\right\}$$

$$e^{-x_1\rho_1(z_1 - z_0)}\, e^{-x_2\rho_2 z_2 - z_1} \ldots . e^{-x_{N-1}\rho_{N-1}(z_{n-1} - z_{n-2})} \qquad (2)$$

where: $x_N = \left(\frac{\mu}{\rho}\right)_N \operatorname{cosec}\theta$,

$\alpha = 2.3\,(4 - \frac{V}{10})$,

$\beta = \frac{1}{8}\,\phi_{max}^{(\frac{V}{10} - 1)}$,

$\delta = 10^3$ mg/g, and

P_N = density.

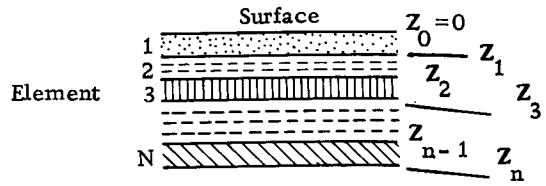

The constant, A, is determined by measuring the X-ray intensity of a standard of known thickness and depth and using the measurement in Eq. 2; this is a calibration step. Once A is determined, Eq. 2 is employed to determine unknown thickness and depths in samples. This is done by measuring the X-ray intensity of each layer above that of interest and using these intensities to determine the thicknesses of such layers, one at a time, from the surface down. In other words, Eq. 2 is applied to the surface layer ($N=1$, $n=0$ 1) to obtain its thickness ($z_1 - z_0$). Equation 2 is then applied to the second layer using the first as an absorption layer. This yields the thickness of the second layer which, together with the first, are used as absorption layers for the determination of the third, and so on. However, one must have one standard available for each element, preferably on a substrate of the same material as in the specimen. The standards are used to calibrate Eq. 2 for each element. The standard film need not have the same thickness as the sample or be at the same depth. One could use different potentials if necessary because the function $\phi(\rho z, V)$ takes care of this.

A computer program was written based on Eq. 2 so that X-ray intensities from layers of a sample plus X-ray intensities from layers of a sample plus X-ray intensities from one standard of each element are sufficient to determine the thickness and depth of each layer. Equation 2 is practically independent of material and checks well with the Cu-Ni system. Other systems involving metals with much different atomic numbers as well as metals and silicon oxide are being studied to test the adequacy of Eq. 2.

References

1. L. S. Birks, "Electron Probe Microanalysis", Interscience, 1963.
2. W. E. Sweeney, Jr., et al, "Electron Probe Measurements of Evaporated Metals Films", Journal of Applied Physics, Vol. 3, No. 6, June 1960, page 1061.
3. J. W. Colby, "Quantitative Microprobe Analysis of Thin Dielectric Films", Proceedings of 1969 Electrochemical Society conference on Thin Films and Dielectrics, pages 491-519.

MAGIC IV - A NEW IMPROVED VERSION OF MAGIC

J. W. Colby
Bell Telephone Laboratories, Incorporated
555 Union Boulevard
Allentown, Pennsylvania 18103

Since its creation in 1966, MAGIC has achieved a rather wide acceptance by other microprobe users. Where necessary, it has been converted to run on IBM, Honeywell, GE, Burroughs, RCA, CDC, and PDP computers. At least three different time share companies have made it available to their customers. Probably the most significant factor which contributed to its popularity, is its simplicity in usage. As a consequence of its usage by so many other laboratories, a fair amount of feedback has been obtained, prompting version IV of MAGIC.

One of the main objections to the use of MAGIC was the large amount of core ($\sim$ 100K bytes) required. A second objection, or shortcoming according to the recent survey by Beaman and Issasi was its inability to utilize standards having more than two elements. A third objection received from some users, was due to the restricted form of input intensities. These objections or shortcomings have all been removed in the current version, MAGIC IV.

Whereas, earlier versions of MAGIC required storage of 3600 constants, which in turn were used to calculate other constants, the present version calculates all constants, from relatively small subroutines. All edges, useful emission lines, coefficients and exponents for the absorption coefficients, fluorescence yields, absorption jump ratios, critical excitation potentials, and backscatter loss factors have been fit to polynomials, as a function of atomic number. The mean relative error on the curve fits, is less than 0.1%, and the maximum relative error is $\sim$1%, for some of the longer wavelength lines which are not likely to be used for analytical purposes. Subroutines have also been written for the calculation of the absorption coefficients, and for the fluorescence and absorption correction, making subsequent programming, considerably simpler, and less redundant. Recent tabulation of the K-beta and K-alpha intensity ratios were also curve-fitted, along with the beta-to-alpha ratios for other lines, and were written into a subroutine. This subroutine makes fluorescence corrections due to beta lines practical.

Multiple element standards (up to 9 elements) may also be employed quite simply. MAGIC IV also looks for other lines which though not being used for analysis, are excited and in turn cause fluorescence. For example, in analyzing the copper-gold system at 20 kev, and using the copper K line, and gold M line for analysis, the gold L line is excited, and in turn causes a large fluorescence of the copper K line. This is properly taken into account in MAGIC IV. Separate backgrounds and counting times may be employed for standard and unknown.

There are several other useful features of MAGIC IV which will be discussed in more detail. The input has not changed appreciably, i.e., it is as simple as the earlier version. The input and output formats, as well as results obtained will also be discussed.

ELECTRON MICROPROBE AUTOMATION

by

F. Kunz and E. Eichen
Ford Motor Company, Dearborn, Michigan

G. Matthews and S. Piner
Canberra Industries, Meriden, Connecticut

Electron microprobe automation has been the subject of much work[1-3]. In nearly all instances the automation has consisted of using an on-line minicomputer to provide control of the spectrometers, sample stage and electron beam. This paper describes the methods which we have used to obtain automated quantitative analysis using a minicomputer to locate X-ray peaks, collect data from standards and specimen, calculate statistics, calculate probe ratios and apply corrections for fluorescence, absorption, and atomic number effects. In addition, a program used to calculate probe ratios from true concentrations is described.

The hardware necessary to provide the desired degree of automation has been previously reported[1], however, the minicomputer now being used is a PDP-11/20 8,000 word computer. This computer provides increased versatility for time sharing the electron micorprobe with other analytical instruments as well as offering extended programming through byte addressing and peripheral data interchange.

The software necessary to operate the electron microprobe and other time shared instruments has been written in CLASS* language which was designed specifically for operating and controlling analytical instruments. The CLASS language can be viewed as a conversational and control language which is a cross between FORTRAN and FOCAL. However, the most important feature of the language is the ability to chain large programs together. Without this chaining feature, quantitative analysis combined with equipment control would be virtually impossible to accomplish in an 8,000 word minicomputer. The three commands which make quantitative analysis possible in a system of this kind are DELETE (function name), CHAIN, and ERASE (variable name). The DELETE (function name) command permits the deletion of a named function, whereas the CHAIN command deletes all functions in core memory yet the variables are retained. The ERASE (variable name) command is used to delete variables after they are no longer needed. It is these commands which permit sections of programs (or corrections) to be brought into memory, processed, erased and subsequent sections brought in. The variables are passed from one section to the other until they are erased.

* Canberra Laboratory Automation Software System

Figure 1 shows the results of an automated analysis of National Bureau of Standards SRM 482, Copper-Gold electron microprobe standards. The analysis consisted of an initial dialogue entry from the teletype, the moving of the standards under the electron beam, and X-ray peak location by stepping across the standard peak. The location of each peak was stored in core memory and used to calculate the high and low background wavelengths. A total of five counts were accumulated for high background, low background, and peak wavelength and then the peak counts were subjected to counting statistics[4] to determine statistical significance. Each of the four NBS standard reference materials were brought under the electron beam and counts from four different areas on the specimens were accumulated. The electron beam was moved to the different areas by computer addressing a dual digital to analog converter. The probe ratios, corrected for deadtime and background were then calculated and entered into a chained version of MAGIC[5] which corrects these ratios for fluorescence, absorption and atomic number effects.

Also shown in Figure 1 are the results of entering the true concentrations into a ZAF[6] computer program which is used to calculate probe ratios. It is evident that the exact probe ratios cannot be calculated, however, the results do indicate the direction in which the measured ratios are to be corrected.

---

1. Eichen, E., Kunz, F., and Matthews, G., 5th National Conf. on Microprobe Analysis, New York, N. Y.

2. Wolf, R. and Saffir, A. J., 5th National Conf. on Microprobe Analysis, New York, N. Y.

3. Chambers, W. F., 5th National Conf. on Microprobe Analysis, New York, N. Y.

4. Evans, R. D., The Atomic Nucleus, McGraw-Hill Book Company, New York, N. Y., 1955.

5. Colby, J. W., MAGIC: Version III, personal communication.

6. Philibert, J. and Tixier, R. in Quantitative Electron Probe Micro-Analysis, K.F.J. Heinrich, Ed., NBS Special Pub. 298, 1968.

ELECTRON MICROPROBE
AUTOMATED ANALYSIS OF NBS SRM 482
Au – Cu

	SRM 482 TRUE CONCENTRATION	CALCULATED (ZAF) PROBE RATIO, k	AUTOMATED* PROBE RATIO, k	CORRECTED** WEIGHT FRACTION
GOLD	0.801	0.749	0.751	0.801
COPPER	0.198	0.229	0.219	0.194
GOLD	0.603	0.531	0.525	0.594
COPPER	0.396	0.430	0.420	0.386
GOLD	0.401	0.333	0.331	0.399
COPPER	0.599	0.630	0.633	0.602
GOLD	0.201	0.158	0.147	0.187
COPPER	0.798	0.816	0.819	0.802

* Corrected for Deadtime and Background

** Corrected for Fluorescence, Absorption and Atomic Number Effect

Figure 1

AN AUTOMATED MICROPROBE UNDER PDP-8 CONTROL USING AN IBM 360/65 FOR PROGRAM AND DATA STORAGE *

T. D. Kirkendall and P. F. Varadi
COMMUNICATIONS SATELLITE CORPORATION
COMSAT Laboratories
Clarksburg, Maryland

There are now several successful applications of computer automation of electron microprobes. The popular means of achieving computer control of the various microprobe functions appears to be the use of individually addressable NIM modules in the probe readout console commanded by a mini-computer via a parallel data bus.(1) However, there is little agreement among the present users of automated probes on the question of how the data from the microprobe are to be handled and stored, how the ZAF and other correction programs are to be applied and how the corrected data should be retrieved. The small dedicated computer such as the PDP-8(2) with 4K, or, more typically, 8K, words of core memory is adequate for on-line control and monitoring of the numerous needs of the probe. However, data handling, because of the large quantity one is able to collect under automation and the application of correction programs because of their very large size, press the need for a high capacity, high speed data and program storage facility such as magnetic tape or disc.

At the COMSAT Laboratories where we already have an IBM 360/65 computer we believe we have found a functionally and economically attractive solution to the question of the distribution of job functions of a dedicated mini-computer, the handling and storage of data and programs and the means of data correction and retrieval. As shown in the attached figure, the system consists of a PDP-8/I computer with 8K words of core but no additional storage capacity. The operating programs for the PDP-8 and the data gathered by the PDP-8 from the probe are stored on disc in the IBM 360/65. There is a hardwire telephone line, about 500 feet long, connected via data sets, or modems, between the I/O bus of the PDP-8 and an IBM 2703 Telecommunications Processing Unit, a peripheral of the 360/65. Using this interface, EIA standard ASCII characters are presently transmitted at the rate of 120 characters/sec or 10 times the standard teletype speed. Typically, it takes less than 30 seconds to "GET" a PDP-8 program from the 360 disc into the PDP-8 core or to "PUT" onto the 360 disc a block of data accumulated in the PDP-8.

Under this arrangement, the PDP-8 is used only for controlling the probe and gathering data from the instrument which are labeled and transmitted in blocks to the IBM facility for disc storage. The PDP-8 is therefore essentially subservient to the needs of the microprobe at all times. Upon command from the probe operator via batch or remote job entry, the disc filed data are made available to any one of a large number of Fortran programs in the 360 for correction, analysis and presentation. In this approach, not only is the PDP-8 free to perform as an instrument controller, but also because all major calculations are performed in the 360, the requirements of writing new software or converting existing programs to operate in the limited core

of the PDP-8 are greatly minimized. Only two new programs had to be written to permit "hand shaking" between the PDP-8 and the 360 and the passive transfer of data and programs between the two. The communications program for the PDP-8 occupies about 2,000 words and is permanently resident in the upper 4K of core. The 360 program of 60K words includes a file search routine, READ and WRITE routines as well as line test and other housekeeping functions. PDP-8 programs and data are stored by name on the same disc file in the 360. The present reserved on-line disc storage capacity is 350,000 words but may be expanded as needed.

In order to further simplify the job of operating the automated microprobe, we are writing a comprehensive new control program for probe control based on the conversational approach. The operator is relieved of the former task of assembling his specific probe instructions and needs only a minimal knowledge of computer hardware and software.

Another feature the authors believe to be unique with this system is the means we now have to use the PDP-8 as a multichannel pulse height analyzer to accumulate an X-Ray spectrum using the Si(Li) detector on the probe and to transfer this complete spectrum to the 360 for quantitative analyses. Also, matrix mapping of elemental concentrations can be computer programed with full ZAF corrections at each point. Future plans include 360 analysis of SE, BSE and SI images transmitted via a proposed high speed interface to the IBM computer.

---

(1) Manufactured by Canberra Industries, Meriden, Connecticut

(2) Manufactured by Digital Equipment Corporation, Maynard, Massachusetts

* This paper is based upon work performed in COMSAT Labs under corporate sponsorship.

COMPUTERIZED ELECTRON MICROPROBE/SEM

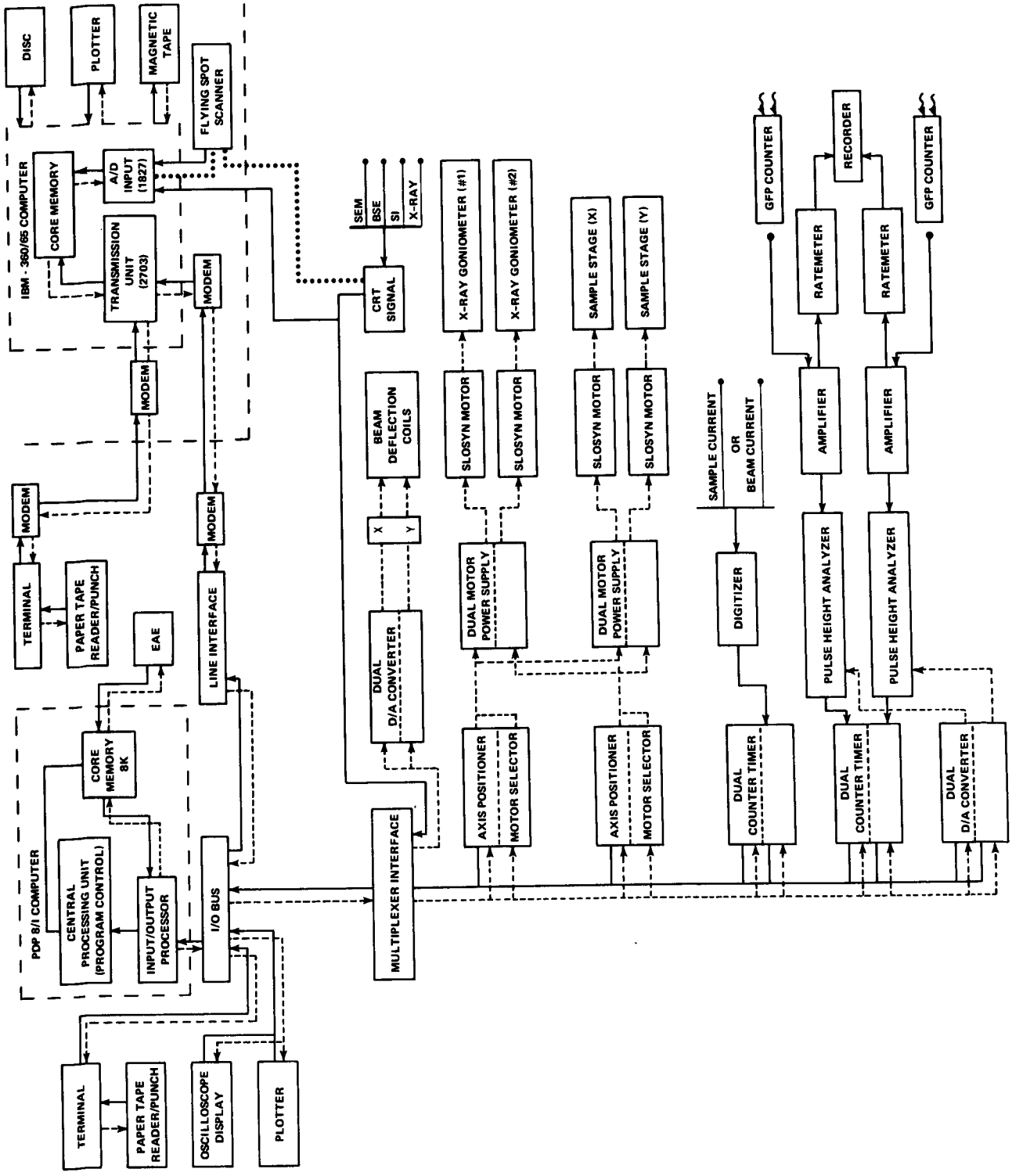

A COMPUTERIZED TEST FOR HOMOGENEITY CHARACTERIZATION

by

Frank Kunz, Erwin Eichen, and Arun Varshneya
Scientific Research Staff, Ford Motor Company, Dearborn, Michigan

Homogeneity characterization of material by electron microprobe techniques has been the subject of much work[1-4] and most recently by Varshneya and Cooper[5]. Each of the reported methods require large data sets (normally X-ray intensities) to be accumulated and subjected to statistical tests for the final homogeneity characterization. The National Bureau of Standards method is to acquire X-ray data from each point in a 100 x 100 matrix from several areas on a specimen[3]. The Midwest Probe Users Group method[4] is to acquire 20 X-ray intensities from one area on the specimen and then from 20 random areas, refocusing the specimen after each translation. The method that we report is basically that of Varshneya and Cooper[5] which has been altered to include beam deflection rather than specimen translation. Also, the beam deflection, data collection and data reduction has been automated by using an on-line computer system.

As shown in Figure 1, the system includes an 8,000 word computer, magnetic tape drives, high speed paper tape reader/punch and a teletype. The electron beam is controlled by a dual digital to analog converter which positions the beam to any point in a 1000 x 1000 matrix. The software necessary to control the system is written in CLASS language.

The method consists of automatically stepping the electron beam over the specimen surface and accumulating X-ray data at each point of dwell. As shown in Figure 2, the data is collected from each point on a line in one direction and then from the same points in the opposite direction. Normally, a total of 10 intensities are recorded from each point and used to construct a 10 x 10 matrix. On application of the two variables of classification, analysis of variance[6] to this data, the F-ratio for the column means reflects the variation due to inhomogeneity and Rowland circle effects, whereas, the F-ratio for the row means reflects the variation due to time dependent drift[5], i.e. filament drift. The variation due to Rowland circle effects is shown in Figure 3 which plots the magnification of X-ray image versus the F-ratio for the column means. Experimental data indicates that if the magnification is maintained at 500X or greater the F (column) ratio will reflect the inhomogeneity contribution to the ratio, that is, the contribution from Rowland circle effects are negligible. The method is then usable to characterize material for its homogeneity. An alternate approach is to obtain the ratio of X-ray intensities from two elements before constructing the matrix for the F-test which also reduces the Rowland circle effect.

A typical output from the computerized system is shown in Figure 4, which is the analysis applied to a pure silicon disc used to determine Rowland circle contributions.

1. H. Yakowitz, D. L. Veith, and R. E. Michaelis, "Homogeneity Characterization of NBS Spectrometric Standards III: White Cast Iron and Stainless Steel Powder Compact", NBS Misc. Publ. 260-12, 13 pp. (1966).

2. H. Yakowitz, D. L. Veith, K. F. J. Heinrich and R. E. Michaelis, "Homogeneity Characterization of NBS Spectrometric Standards II: Cartridge Brass and Low-Alloy Steel", NBS Misc. Publ. 260-10, 28 pp. (1965).

3. H. Yakowitz, R. E. Michaelis and D. L. Veith, "Homogeneity Characterization of NBS Spectrometric Standards IV: Preparation and Microprobe Characterization of W-20% Mo Alloy Fabricated by Powder Metallurgical Methods", Advances in X-ray Analysis, 12, Plenum Press, New York, 1969, p. 418.

4. Minutes of Midwest Probe Users Group, dated March 14, 1968.

5. A. K. Varshneya and A. R. Cooper, "Inhomogeneities and Iron Diffusion in a Thailand Tekite", J. Geophys. Res., 1969 (27), p. 6845.

6. W. J. Dixon and F. J. Massey, Introduction to Statistical Analysis, (second ed.), McGraw-Hill Book Co., New York 1957, p. 155.

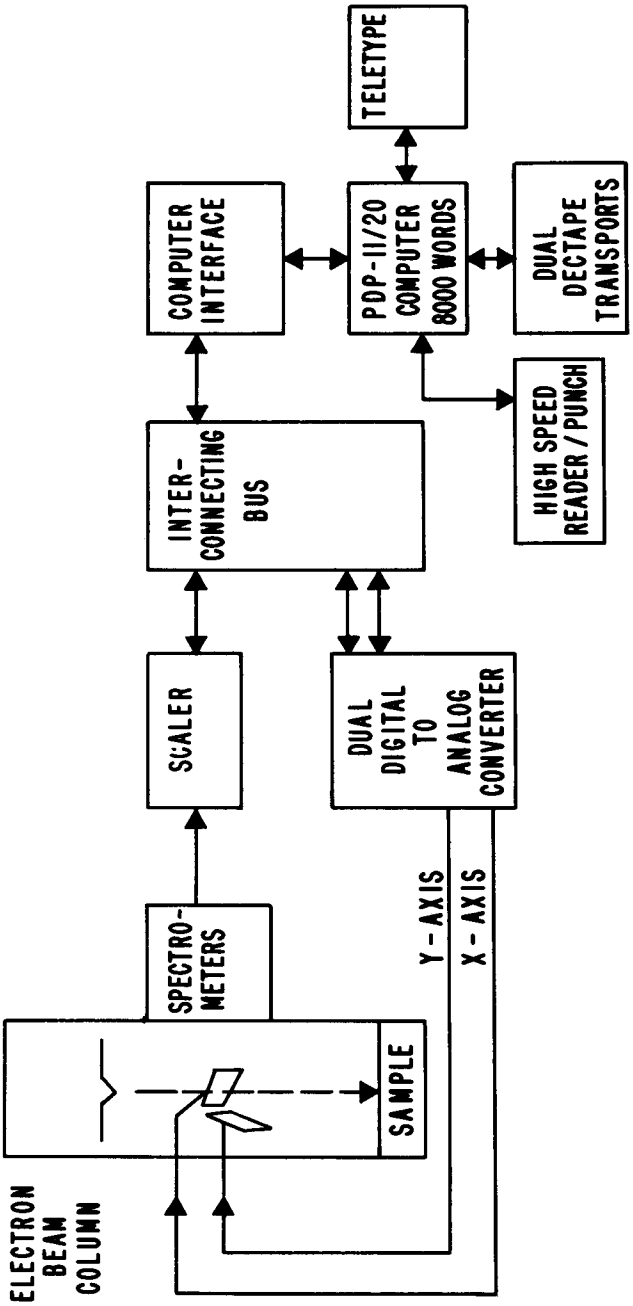
TELETYPE
COMPUTER INTERFACE
PDP-11/20 COMPUTER 8000 WORDS
DUAL DECTAPE TRANSPORTS
HIGH SPEED READER / PUNCH
INTER-CONNECTING BUS
SCALER
DUAL DIGITAL TO ANALOG CONVERTER
SPECTRO-METERS
Y-AXIS
X-AXIS
SAMPLE
ELECTRON BEAM COLUMN

Figure 1

No. OF COLUMNS = No. OF POSITIONS = K

No. OF ROWS = No. OF REPETITIONS AT THE SAME POSITION = n

	X_{11}	X_{12}	X_{13} -------	X_{1K}	$\bar{X}_{1j}$
	X_{21}	X_{22}	X_{23} -------	X_{2K}	$\bar{X}_{2j}$
	X_{31}	X_{32}	X_{33} -------	X_{3K}	$\bar{X}_{3j}$
	—	—	— ---------	—	— —
	—	—	— ---------	—	— —
	X_{n1}	X_{n2}	X_{n3} -------	X_{nK}	$\bar{X}_{nj}$
MEAN	$\bar{X}_{i1}$	$\bar{X}_{i2}$	$\bar{X}_{i3}$ -------	$\bar{X}_{iK}$	$\bar{X}_{ij}$

THE SEQUENCE OF DATA COLLECTION IS:

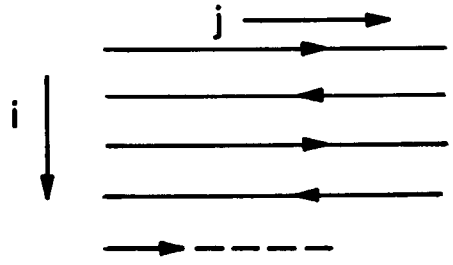

Figure 2

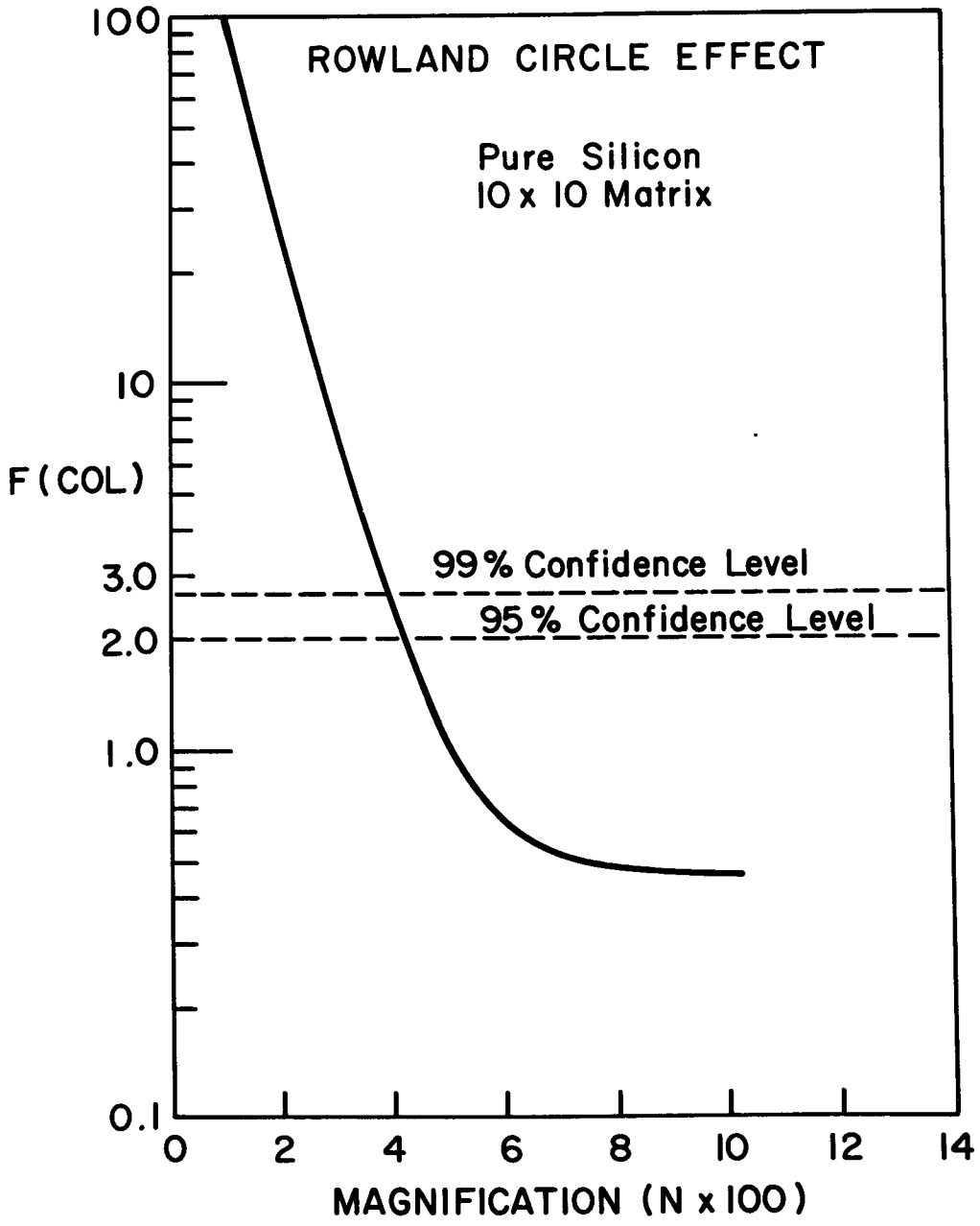
ROWLAND CIRCLE EFFECT
Pure Silicon
10 x 10 Matrix
100
10
1.0
0.1
F(COL)
3.0
2.0
99% Confidence Level
95% Confidence Level
0
2
4
6
8
10
12
14
MAGNIFICATION (N x 100)

Figure 3

ELEMENT: SILICON
MAGNIFICATION: 500X
SCALER: 46

5045	4949	5064	4957	5038	4983	4869	5079	5079	4852
5015	4962	4969	4997	4906	5035	4997	4894	5088	4934
4979	5025	5036	4901	5066	4960	4964	4826	5086	5054
5104	5045	4900	5020	5064	4923	4950	4901	4944	4822
4994	4879	5014	4957	4962	4847	4839	5004	4944	4973
4954	4864	4943	4908	5047	5010	4897	4983	5050	4969
4987	4983	5072	4961	4951	4958	5026	4906	4921	4989
4952	4849	5087	4975	4938	5065	5003	5019	4999	5031
5084	5022	4923	5039	5019	4898	4912	5019	5020	5008
4984	4986	5013	4833	5115	4888	4933	4869	4942	5006

	SUM OF SQUARES	DF	MEAN SQUARE
COL MEANS	73912	9	8212
ROW MEANS	28478	9	3164
REMAINDER	379564	81	4685
TOTAL	481954	99	

F(ROW)= .675
F(COL)= 1.75
SAMPLE IS RATED HOMOGENEOUS

END OF FTEST

Figure 4

COMPUTER SIMULATION OF A THIN FILM METALLURGY SYSTEM

B. I. Bertelsen, W. E. Veno, and D. H. Withers
IBM Corporation
Essex Junction, Vermont 05452

INTRODUCTION

A new method is proposed to determine the copper concentration vs. thickness in a thin film, where the Al_2Cu precipitate is uniformly distributed around aluminum grains. These results provide a base line to determine the actual distribution of copper in the film due to causes external to the model. For the mathematical model, a digital computer program was formulated that performs simulation of the film formation. An efficient means for determining the most probable distribution of percent copper by weight as a function of distance from a smooth, nonreactive substrate-film interface is presented.

Film formation hypothesis is briefly described. Atoms of aluminum and copper are evaporated onto a smooth, nonreactive substrate. During the process, some aluminum atoms tend to form aggregate grains. Other aluminum atoms combine with copper atoms and form Al_2Cu molecules residing on the surfaces of the aluminum grains. The number of Al_2Cu particles that becomes associated with a given aluminum grain depends on the size of the particular aluminum grain and the size of the individual particles. However, the total weight of the copper in all the Al_2Cu particles around an aluminum grain is known to be a fixed percentage of the weight of that particular grain.

The grain size is a normal variate since the number of aluminum molecules that unite to form the grain is a random variable. When the radius of a particular grain is known, the mass of the grain is easily computed. The total mass of the particles was estimated to be the product of the mass of the copper and the ratio of the densities of copper and aluminum.

The radius of an individual Al_2Cu particle is also a normal random variate. For a given particle radius, the mass may be calculated. By dividing the mass of Al_2Cu associated with an aluminum grain by the mass of an individual Al_2Cu particle, the number of Al_2Cu particles associated with an aluminum grain is determined. These particles are then "placed" around the aluminum grain.

SIMULATION MODEL ASSUMPTIONS

1. Radii of Al and Al_2Cu: Radii were assumed to have averages of 3500 Å and 500 Å, respectively. The standard deviations of the grains' radii were 1167 Å and 500 Å. The standard deviation of the radius of Al_2Cu particles was 2 Å.

2. Distribution of Al_2Cu particles on grain: Two methods were used to position the Al_2Cu particles around the circumference of the grain.

   a. Random Uniform Distribution
   A random starting point on the circumference (the circle in a two-

dimensional simulation) of the grain was generated. This point was generated in the range of 0-2 π with a uniform distribution. The first particle was placed at this point. Succeeding random angular displacements, $\bar{\theta}$, were generated with $\bar{\theta} = 2\pi/\#$ of grains. This method was discarded in favor of the following method, which more closely follows the intent of the analysis.

b. Uniformly Distributed
As in the previous method, a random-starting point on the circumference of the grain was generated. However, the displacement between particles was fixed at $\frac{2\pi}{\text{no. of } Al_2Cu \text{ particles.}}$

3. Grain spherically shaped: Due to the extreme complexity of a three-dimensional simulation, the model was restricted to only two dimensions.

   The two dimensional spheres were overlapped thereby providing reasonably close approximation to the actual physical system.

4. Reaction precipitate point mass: The Al_2Cu particles were approximated by point masses.

5. A small percentage of copper in solution in the aluminum was neglected.

SUMMARY

The results of the work described in this paper are essentially the following: The simulation lends credibility to the initial hypothesis that the distribution of copper concentration through the thin film can arise from a random fallout of Al_2Cu around grains of relatively pure aluminum content.

An equation was generated which permits easy subtraction of the uniform fallout contribution to the concentration distribution from the sum of other effects (e.g., preferential nucleation at the substrate interface and others). Tests with the equation prove that the distance from the substrate at which minimum copper concentration occurs is equal to $\bar{R}_{grain}$ for any $\bar{R}_{grain}$. This unexpected result indicates that the electron microprobe analysis of beveled sections of Al-Al_2Cu films may provide one of the best (and simplest) methods of grain-size determination. Since the model only approximates the real film structure, this indication must be tested further. The model does not account for varying $\bar{R}_{grain}$ with x, as may intentionally be generated in real films. The $\bar{R}_{grain}$ at minimum copper concentration is, however, representative of grain size in the first layer of grains on the substrate.

CONCLUSION

The results obtained from the simulation model of the film formation compare quite closely to the observed laboratory results. The authors are confident that the model may be refined to any required accuracy to parallel the physical process. The ability to determine a functional relationship for copper concentration has also been demonstrated.

Finally, the authors are confident enough in the model to state that the copper distribution (by weight) is not uniform over the film thickness, but is maximum at the interface and minimum at a distance of approximately one grain radius from the interface.

A MODEL FOR ANALYSIS OF FINE-PLATELET STRUCTURES, EFFECT OF FINITE BEAM SIZE

M. R. Jackson, J. I. Goldstein, and R. W. Kraft
Department of Metallurgy and Materials Science
Lehigh University, Bethlehem, Pennsylvania

We are continually seeking to analyze smaller volumes with the EPMA. Recently, deconvolution techniques (1,2) have been used to increase probe resolution for analysis on a scale finer than V_B, the x-ray generation volume. For analysis of small particles (where one or more of the particle dimensions is smaller than dimensions of V_B), deconvolution cannot be used. To study such a geometry it appears necessary first to calculate the fraction of V_B (the x-ray generation volume) that is in the particle and the fraction that is in the matrix, and then to apply the usual ZAF (3) corrections to the various volumes.

To this end a study has been made of measured intensity ratios from lamellar Al-$CuAl_2$ eutectic plates of varying sizes. The eutectic consists of equal volumes of alternating plates of α-Al (0.4w/o Cu) and Θ-$CuAl_2$ (53.5w/o Cu). Using single-plate widths of 3.5μm to 0.13μm, either phase may be considered as a particle in a matrix of the second phase. The lengths and depths of the plates are large, but the widths are nearly the same as or smaller than the dimensions of the x-ray generation volume. The measured intensity ratios were compared to ratios calculated from a simplified x-ray generation volume model.

As a first approximation, the model assumes that the lateral x-ray distribution at any depth is a two-dimensional Gaussian, the same as is generally assumed for electrons (4,5). The x-ray distribution in depth is assumed to follow a truncated Gaussian. The function chosen is an approximate fit to depth distributions for Al K_α in α and Θ predicted by Shimizu (6). The model is applied to a eutectic of any platelet size. The fraction of VB occupied by each phase is determined as a function of B/λ (B is the lateral Gaussian half-peak width and λ is the platelet-pair width), as is shown schematically in Figure 1.

Since x-rays generated below the surface may pass through a second phase before exiting, it is necessary to consider absorption effects. If Φ_1 is the phase in which the electron beam is centered, several volume fractions can be defined:

V_{11} - x-rays are generated in and exit through Φ_1,
V_{12} - x-rays are generated in Φ_1 and exit through Φ_1 and Φ_2,
V_{21} - x-rays are generated in Φ_2 and exit through Φ_2 and Φ_1,
V_{22} - x-rays are generated in and exit through Φ_2.

These volumes were calculated as a function of B/λ. The results for a take-off angle of 52.5° are shown in Figure 2. For small B/λ the

x-ray volume is completely within ϕ_1. For large B/λ V11and V_{22} should approach zero while V_{12} and V_{21} should each approach 0.5 (the eutectic is 50%α and 50% θ).

Composite absorption corrections and atomic number corrections were calculated from the weight fractions of each of the four volume fractions. The predicted curve of I/I_o as a function of B/λ is given in Figure 3. The upper curve is for Al K_α radiation generated by centering the beam in α, while the lower curve is for the beam centered in θ. For small B/λ both curves show intensity ratios that would be measured in the bulk phases. For large B/λ both curves converge to the ratio expected from a homogeneous alloy of eutectic composition.

Experimentally measured intensity ratios were compared to the predicted curves. Matching ratios yield a value of B/λ. Values of B for several plate sizes at the same operating voltage agree to within 10%. The following are results of the comparison of measured intensity ratios to predicted ratios:

1. B for Cu K_α is smaller than B for Al K_α in both α and θ.
2. B for either radiation is smaller in the higher atomic number θ than in α.
3. B decreases with decreasing operating voltage.

The model can be modified to treat cases where the volume fractions of the two phases are vastly different, i.e., when one phase is a true particle. Furthermore, the program can be modified to treat any particle geometry in length and width, provided the geometry is constant with depth and that the particle depth is greater than x-ray volume depth. Thus, the model proposed should greatly reduce the minimum particle size that can be analyzed with the electron probe.

REFERENCES

1. Gupta, P. K., "Finite Beam Diameter Effect in Microprobe Analysis," 1970, J. Phys. D: Appl. Phys., 3, 1919-1924.
2. Rapperport, E. J., "Deconvolution: A Technique to Increase Electron Probe Resolution," 1969, Electron Probe Microanalysis, (Academic Press, New York), 117-136.
3. Goldstein, J. I., and Comella, P. A., "A Computer Program for Electron Probe Analysis in the Fields of Metallurgy and Geology," 1969, (Goddard Space Flight Center, Greenbelt, Md., X-642-69-115).
4. Wittry, D. B., "Resolution of Electron Probe Microanalyzers," 1958, J.A.P., 29, 1543-1548.
5. Shinoda, G., Murata, K., and Shimizu, R., "Scattering of Electrons in Metallic Targets," 1968, Quantitative Electron Probe Microanalysis, (N.B.S. Special Publication 298, Washington, D.C.), 155-187.
6. Shimizu, R., Ikuta, T., Nishigori, N., and Murata, K., "Calculation of X-Ray Production in Alloy Targets by New Approach Using Monte Carlo Method," 1970, Jap. J.A.P., 9, 1429-1430.

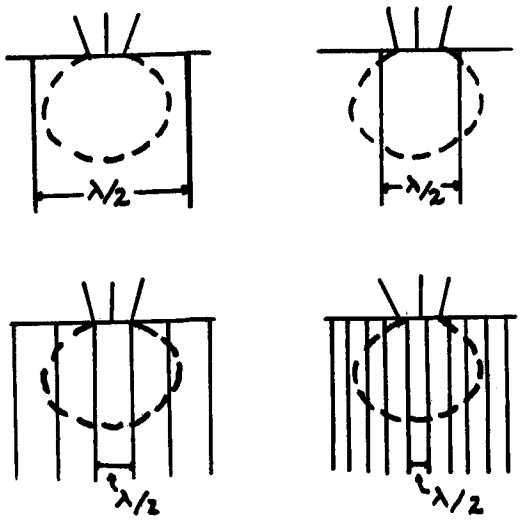

Figure 1 - Schematic representation of variation of B/λ.

Figure 2 - Variation of the four regions of the x-ray generation volume with B/λ.

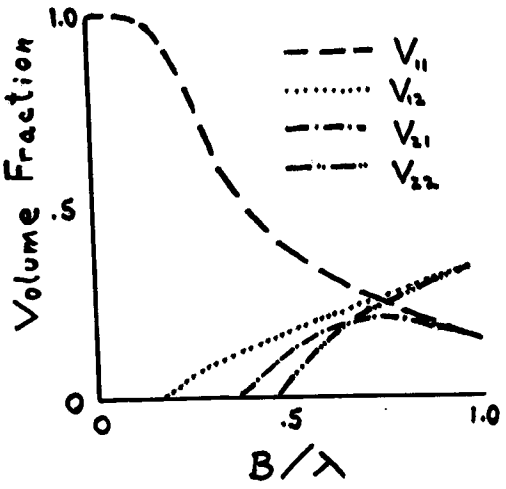

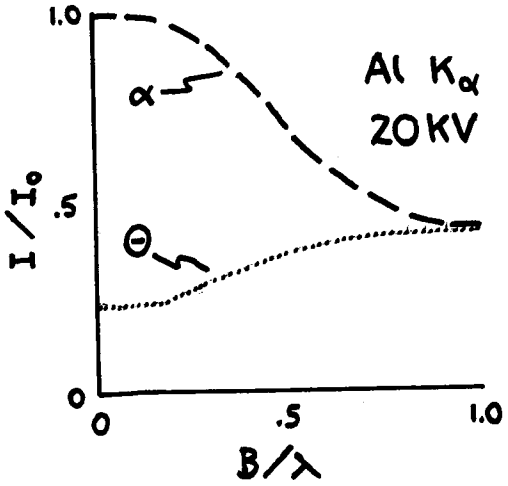

Figure 3 - Predicted intensity ratios for Al K_α. Beam centered in 1) α, and 2) Θ.

ANALYTICAL MEASUREMENTS ON NBS STANDARD REFERENCE MATERIALS FOR ELECTRON PROBE MICROANALYSIS

R. L. Myklebust and K. F. J. Heinrich
National Bureau of Standards
Washington, D. C. 20234

Abstract

Although the foundations for a theoretical method of calculating correction factors for quantitative electron probe microanalysis were established in 1949 [1], tests of this method, performed a few years ago on specimens of known composition, raised considerable question concerning capabilities of the electron probe microanalyzer as a quantitative tool [2-4]. It became quite evident that various practical techniques proposed for calculating the corrections [5-10] were in considerable disagreement and that in many cases all proposed procedures failed to properly correct the experimental data obtained by experienced investigators. The resulting analytical errors frequently exceeded 10% relative. A detailed analysis of these tests [3] suggested that the following potential sources of error may be responsible for these failures.

1. Some of the test specimens of presumably well known composition may have been poorly characterized on a macroscopic scale or be microscopically inhomogeneous.
2. Although the fundamentals of the generation of x-rays by electron excitation are well known, there are uncertainties in parameters and constants - such as the x-ray absorption coefficients - which adversely affect the accuracy of the method. The resulting uncertainties may be particularly large if the instrument conditions have been choosen injudiciously [3, 11-14].
3. Lack of adequate computational facilities has frequently prompted the investigator to use simplified calculation procedures which may also introduce error.

In order to improve the accuracy of the correction procedures for electron probe microanalysis, it is thus necessary to obtain carefully prepared, microscopically homogeneous, and chemically analyzed standard materials. The measurement under carefully controlled conditions of x-ray emission intensities from these standards, including all necessary correction calculations [15], will permit empirical adjustment within the precision of the measurement of those factors which are affected presently by uncertainty. Once these factors have been established, the standard reference materials will enable the analyst to test the accuracy of his measurement technique by comparing the relative x-ray intensities he obtains from such materials with those obtained by other operators under carefully defined operating conditions.

We have extensively analyzed the binary alloy systems gold-copper (Standard Reference Material 482) and gold-silver (Standard Reference Material 481) using a variety of x-ray lines, operating voltages, and correction procedures. The k values predicted by various theoretical procedures are plotted together with the experimentally obtained k values in Figure 1 for one case.

The results indicate that in general the existing theory can predict with reasonable accuracy the relative x-ray intensities observed experimentally. There is, however, some residual uncertainty in the generation equation (atomic number correction), where neither of the proposed mean excitation potentials seems to lead to negligible error [16, 17].

In accordance with previous predictions [11], excessive absorption corrections (low $f(\chi)$ values) may lead to substantial errors.

As will be discussed, further systems must be investigated in order to produce a significant improvement of the existing theory of corrections for quantitative analysis.

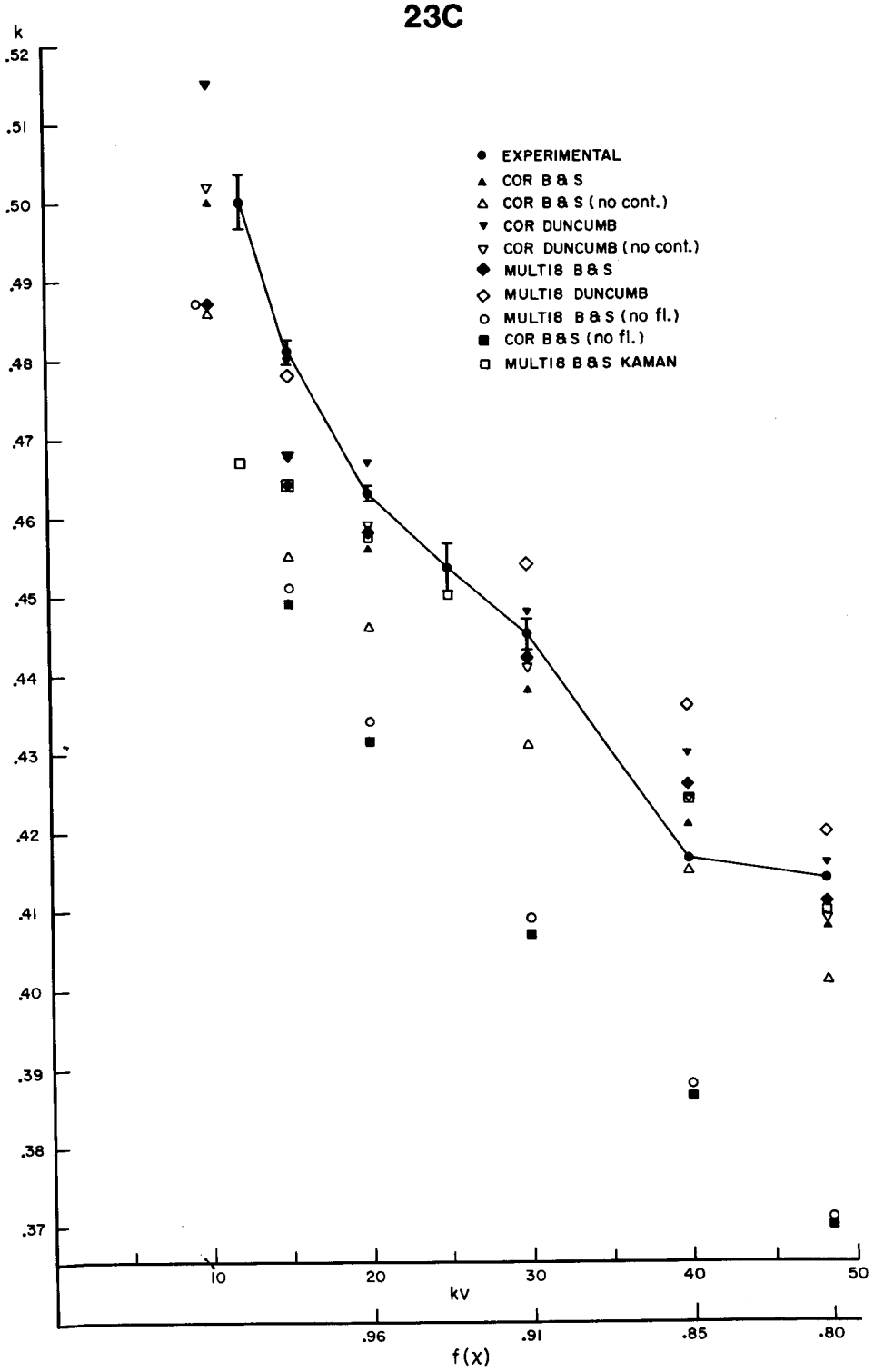

Figure 1. Experimental and theoretical intensity ratios of copper Kα for a nominally Au60-Cu40 alloy.

LIST OF REFERENCES

[1] Castaing, R., Doctoral Thesis, U. Paris, 1951.

[2] Thomas, P. M., At. Energy Res. Estab. (Gt. Brit.) Rept. 4593 (1964).

[3] Heinrich, K. F. J., Adv. in X-ray Analysis 11, (Plenum Press, New York, 1968) p. 40.

[4] Poole, D. M., in NBS Special Publ. 298, 93 (1968).

[5] Thomas, P. M., Brit. J. Appl. Phys. 14, 397 (1963).

[6] Duncumb, P. and Shields, P. K., in The Electron Microprobe, T. D. McKinley, K. F. J. Heinrich, and D. B. Wittry, Eds. (J. Wiley and Sons, Inc., New York, 1966) p. 284.

[7] Belk, J. A., Birmingham C.A.T. Tech. Note, MET/26/1964 (1964).

[8] Ziebold, T. O. and Ogilvie, R. E., Anal. Chem. 35, 621 (1963).

[9] Archard, G. D. and Mulvey, T., X-Ray Optics and X-Ray Microanalysis (Academ. Press, New York, 1962) p. 393.

[10] Theisen, R., Quantitative Electron Microprobe Analysis (Springer-Verlag, New York, 1965).

[11] Yakowitz, H. and Heinrich, K. F. J., Mikrochim. Acta 1968, 182.

[12] Heinrich, K. F. J. and Yakowitz, H., Mikrochim. Acta 1968, 905.

[13] Heinrich, K. F. J. and Yakowitz, H., Mikrochim. Acta 1970, 123.

[14] Heinrich, K. F. J. and Yakowitz, H., Proc. Vth Internat. Congress on X-ray Optics and Microanalysis, Tübingen, 1968, G. Möllenstedt and K. H. Gaukler, Eds. (Springer-Verlag, Berlin, 1969) p. 151.

[15] Heinrich, K. F. J., NBS Tech. Note 521 (1970).

[16] Duncumb, P. and Reed, S. J. B., in NBS Special Publ. 298, 133 (1968).

[17] Berger, M. J. and Seltzer, S. R., Tables of Energy Losses and Ranges of Electrons and Positrons, Natl. Acad. Sci., Nat. Res. Council Publ. 1133, 205 (1964).

MICROPROBE TECHNIQUES FOR THE MEASUREMENTS OF OXYGEN AND XENON IN IRRADIATED MIXED (Pu,U) OXIDE FUELS*

T.E. Lannin, R.C. Wolf, and H.S. Rosenbaum

General Electric Company, Vallecitos Nuclear Center
Pleasanton, California

G.F. Melde

General Electric Company, Breeder Reactor Development
Operation, Sunnyvale, California

Preliminary results on the location and distribution of xenon and oxygen in irradiated mixed (Pu,U) oxide fuels are presented and the techniques used to obtain these results are reviewed. Zelezny, et al (1) have discussed the retention of the fission product gas, xenon, in fuel plates containing a mixture of UAl_4 and U_3O_8 dispersed in the same aluminum matrix. These fuel plates were irradiated to 17.7 a/o burnup of the fissionable material at a temperature of 125°C and the residual xenon determined by microprobe techniques. The authors are not aware of any previous microprobe results for oxygen in heavy element matricies. The samples examined were irradiated for 24 hours in a thermal flux at a linear power level in excess of 23 $kW\text{-}Ft^{-1}$. This power level created a thermal gradient > $5000°C\text{-}Cm^{-1}$. Microprobe analyses of mixed oxide fuels have indicated that the thermal gradient (linear power) and burnup have a direct relation to the distribution of oxygen and retained xenon in irradiated fuels. The understanding of the location and redistribution of these elements are important to predicting the irradiation behavior of mixed oxide fuels. This paper presents early results from these investigations and techniques utilized in the measurements.

Quantitative oxygen analysis in heavy element matricies is difficult for several reasons:

1. High current densities are required to achieve an adequate x-ray intensity.

2. High specimen currents required (0.5-1.5 μ amps) cause sufficient carbon buildup to observe a noticeable intensity decrease.

3. Standards near the composition of the material being analyzed are required because of the peak shift from compound to compound.

4. Superficial reduction of some compounds under the stationary beam can occur at the high specimen currents required.(2)

Shirawa and Fujino(3) have examined the problem of quantitative oxygen analysis of several metal oxides through Cu (Z=29). These data were corrected using the Philibert absorption correction, the Poole-Thomas atomic number correction, and emperical mass absorption coefficients where applicable. The results of that study show a dependence of x-ray intensity with accelerating potential before correction of the data with the $O\text{-}K_\alpha$ intensity decreasing with increasing Z. Results on mixed oxides are in general agreement with Shirawa's data except that for U(Z=92) and Pu(Z=94) the corrected intensity (background correction only) was still increasing at 20 kV. This is in contrast to

*Work performed under the auspicies of the United States Atomic Energy Commission on Contract AT(04-3)-189, PA-10.

the general trend of decreasing O-K_α intensity with increasing Z and accelerating potential. This difference will be discussed.

Based on the work of Aitken[4] a computer program was developed to calculate the oxygen distribution as a function of the radius of the mixed (Pu,U) oxide nuclear fuel. Measured O-K_α intensity was found to be in good agreement with the calculated oxygen redistribution (Figure 1). In addition to the oxygen measurements in mixed oxides, a limited amount of work has been completed on oxygen in stainless steel cladding of the mixed (Pu,U) oxide (Figure 2). This work and the work in progress will be discussed.

The results of these investigations are presently being utilized to further evaluate the effect and magnitude of fission gas induced swelling and the effect of oxygen distribution on cladding attack by fission products.

References

1. Zelezny, W.F., Gibson, G.W., Grabce, M.T., "A Microprobe Study of the Retention of the Fission Gas Xenon in Irradiated Uranium Fuels Dispersed in Aluminum Clad Nuclear Reactor Fuel Plates", Conf. 690910, Presented at "The National Symposium on Developments in Irradiation Testing Technology", Sandusky, Ohio, Sept. 9-11, 1969, Sponsored by the USAEC.

2. Private Communication, Dr. Ahmed El Coresey, Max-Plank-Institut Für Kernphysik, 69 Heidelburg 1, Germany.

3. Shirawa, T., and Fujino, N., "Quantative Electron Probe Microanalysis of Oxygen", Japanese Journal of Applied Physics, V9, #8, August, 1970.

4. Aitken, E.A., "Thermodynamic Analysis of Possible Chemical Interactions in the System: UO_2-PuO_2, Fuel-Sodium-Stainless Steel", GEAP-5683, July, 1968.

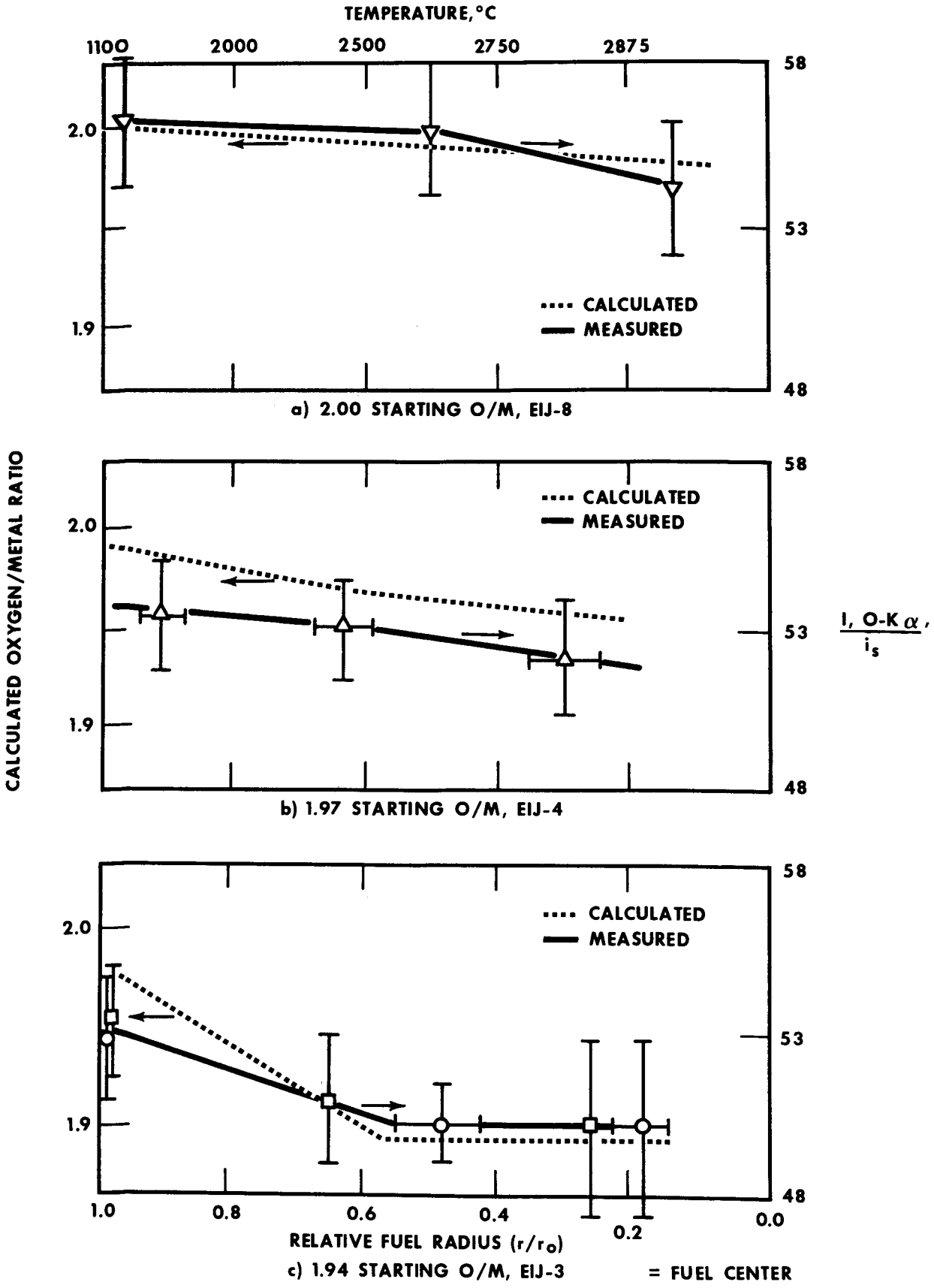

FIGURE 1. COMPARISON OF CALCULATED TO MEASURED OXYGEN LEVELS IN EIJ-3, EIJ-4, AND EIJ-8 (MEASURED VALUES ARE RELATIVE WITHIN THE THREE SAMPLES EXAMINED).

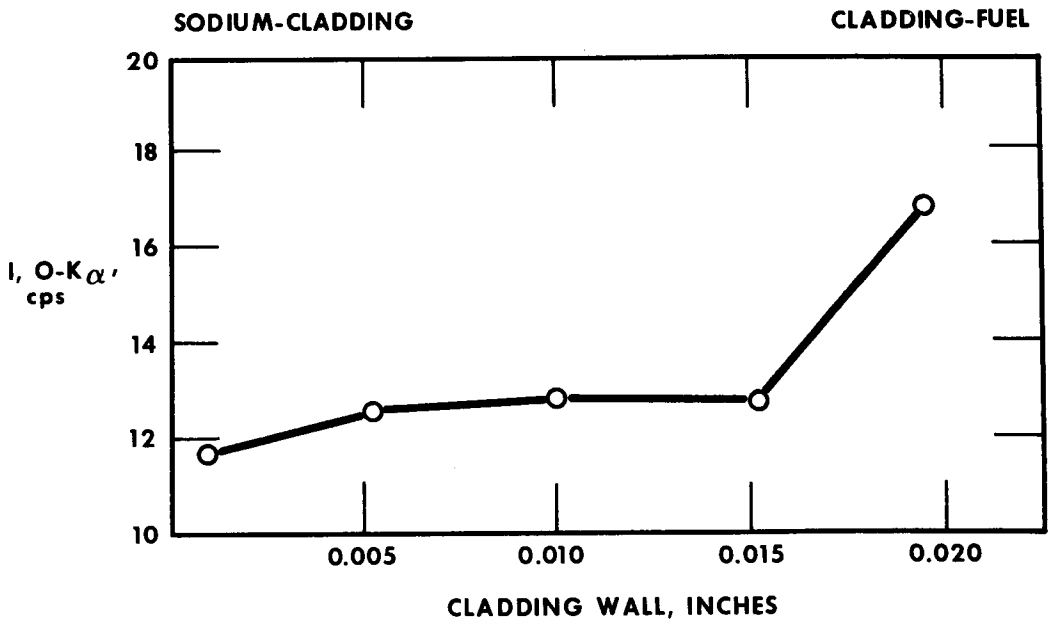

FIGURE 2. RELATIVE INTENSITY, OKα, VERSUS CLADDING THICKNESS

PRECISION AND DETECTION LIMITS OF CERTAIN MINOR AND TRACE ELEMENTS IN SILICATES BY ELECTRON MICROPROBE ANALYSIS

Robert H. Heidel and George A. Desborough
U.S. Geological Survey
Denver, Colorado 80225

Titanium, vanadium, chromium, manganese, cobalt, copper, nickel, and zinc in concentrations as low as 200 to 500 ppm in silicates are commonly of geologic significance. To study the amount of these elements present in silicates we used an ARL-EMX-SM microprobe, operated at 15 and 20 kV and specimen current at 2×10^{-8} amperes, on benitoite ($BaTiSi_3O_9$). The beam diameter was set at 5 microns. X-ray intensities of the K_α lines of the above elements were obtained on the spectrometers having LiF crystals. Fixed beam current termination, set to a counting time of approximately 10 seconds for each observation, was used. Ten observations were made on random areas of the sample.

Three U.S. Geological Survey synthetic glass standards (USGS standards) prepared by Corning Glass Works contain about 500, 50, and 10 ppm each of the elements of interest. These standards also contain about 30 additional elements in minor or trace quantities. They were initially procured for quantitative and semiquantitative spectrochemical analysis (1), but have been found useful also as probe standards. The standards have concentrations of major elements similar to those in common silicate rocks containing the following in weight percent as oxides: Si ~ 61-62, Al ~ 14-15, Fe (as FeO) ~ 6, Mg ~ 4, Ca ~ 5, Na ~ 4.5, and K ~ 3.5. National Bureau of Standards (NBS) Standard Reference Materials (SRM 610 and 612 Trace Elements in a Glass Matrix) were analyzed to compare USGS standards with NBS materials (both of which were prepared by Corning Glass Works) with respect to trace element content and homogeneity.

Values for background intensities for each element were estimated (a) from on-peak readings of pure SiO_2, (b) graphically, by extrapolation of the calibration-curve to zero concentration, and (c) from off-peak readings on the high and low wavelength sides of the peak. Background readings at the peak were also taken on pure MgO (periclase) and Al_2O_3 (corundum) as well as SiO_2 (quartz) because any one of these in some form of an oxide may be present separately or in combination and may contribute significantly to background. Intensities of these three compounds in most instances are less than those obtained from off-peak intensity measurements. X-ray intensities obtained on the two lowest concentration standards, i.e., at the ~ 50 and ~ 10 ppm levels, are slightly higher than the on-peak intensity for SiO_2.

For 15 kV operation the minimum detectability limits (C_{DL}) at 3σ (99 percent confidence level) above background (2) range from 200 ± 100 ppm for titanium to 450 ± 200 ppm for zinc. At 20 kV the range is from approximately 150 ± 75 ppm for titanium to 400 ± 200 ppm for zinc. The values obtained by electron probe analysis of the NBS Standard SRM-610 (~ 500 ppm level) fall within one standard deviation of the calibration-curves from the USGS standards. The results reported are based on 10 observations with total counts of 1000 to 2000, depending on concentration, and show the degree of reliability in a rapid, routine trace element determination.

References

(1) A. T. Myers, U.S. Geological Survey, Denver, Colorado, personal communication, 1969.

(2) L. S. Birks, "X-ray Spectrochemical Analysis," Interscience Publishers, Inc., New York, 1959.

THE "a" VALUE METHOD REVISITED

R. B. Bolon and E. Lifshin
General Electric Corporate Research and Development

The recent application of small computers with limited storage and computational capability to quantitative electron microprobe analysis has resulted in renewed interest in the "a" value method. This method first proposed by Ziebold and Ogilvie[1] in 1964 showed that for many binary systems K_A, the corrected relative intensity of element A, could be simply related to C_A, the composition of element A by an equation of the form:

$$\frac{1-K_A}{K_A} = {}^{a}_{AB}\frac{1-C_A}{C_A}$$

where the constant ${}^{a}_{AB}$ can be determined at a given voltage and take-off angle either from empirical calibration measurements or calculated directly from a greatly simplified version of the ZAF method. It was also shown that an extension of this procedure could be applied to multicomponent samples using a calculation requiring a set of binary "a" values for all of the elements taken two at a time. Since the needed binary standards are not always available, and the simplified ZAF method not always sufficiently accurate, Lifshin and Hanneman[2] determined "a" values by least squares fitting the Ziebold-Ogilvie equation to full ZAF calculations. They found that recalculated compositions rarely differed by more than 1% of the amount present for compositions greater than 10 w/o .

In the present study we are again applying the least squares fitting method, this time to the most recent ZAF corrections using a modified version of Colby's MAGIC[3] computer program and determining not only "a" values, but also the dependence of "a" values on voltage and take-off angle as shown for the chromium-silicon system in Figures 1 and 2. Since large deviations of "a" values are associated with undesirably large correction factors, examination of curves of this type combined with peak intensity data and peak to background ratios has proved useful in determining operating conditions for optimizing sensitivity and accuracy. Our findings also show that separate "a" values determined for the 0 to 10 w/o region can be used to approximate the ZAF method by better than 1% of the amount present. This suggests that a slightly more refined curve fitting expression can give better than a 1% fit for the overall ZAF calibration curve.

Figure 1.

Effect of beam voltage on "a" values for selected take off angles - Si-Cr system.

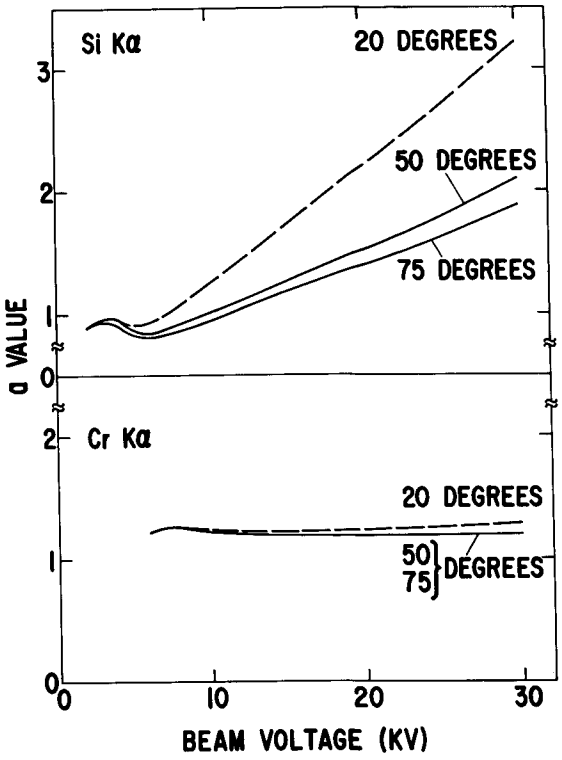

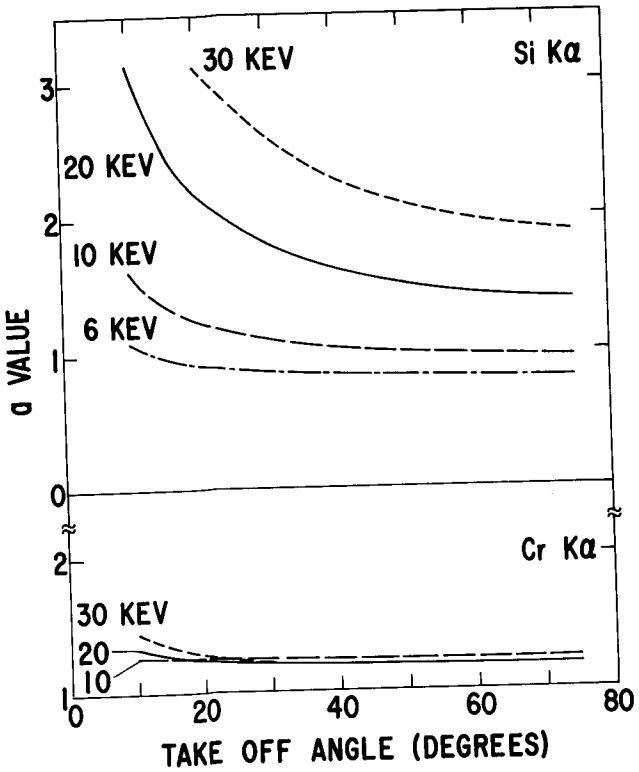

Figure 2.

Effect of take off angle on "a" values for selected beam energies - Si-Cr system

1. T. O. Ziebold and R. E. Ogilvie, "An Emperical Method for Electron Microanalysis" Analytical Chemistry, 36, No. 2, p. 322-327, 1964.

2. E. Lifshin and R. E. Hanneman, "An Automated Method for the Collection and Analysis of Microprobe Data," paper presented to the first National Conference on Electron Microprobe Analysis, College Park, Md., May 1966.

3. J. Colby, Advances in X-ray Analysis, G. Mallett, M. Fay and M. Mueller, Eds., Plenum Press, New York, 11 (1968), p. 287.

SOLIDIFICATION STRUCTURES AND PHASE COMPOSITIONS IN AS-CAST HIGH SPEED STEELS

R. H. Barkalow, J. I. Goldstein, and R. W. Kraft
Department of Metallurgy and Materials Science
Lehigh University
Bethlehem, Pennsylvania 18015

Scanning electron microscopy and quantitative electron probe microanalysis were employed in a study of solidification structures and phase relationships in AISI type M2 high speed tool steel (nominal composition: 6%W, 5%Mo, 4%Cr, 2%V, 0.85%C). Dendritic and eutectic morphologies and qualitative carbide compositions were examined by scanning techniques, and the compositions of the matrix solid solution and intermediate phases were later determined quantitatively. The commercial alloy and a series of high carbon and high vanadium modifications were studied to define the influence of these elements on the composition and uniformity of the matrix and the chemistry and morphology of the interdendritic eutectic carbides.

Essentially the solidification of high carbon alloy steels begins with primary crystallization of a relatively pure solid solution and ends with eutectic decomposition of severely enriched interdendritic liquid. In most commercial high speed steels the balance between carbon and ferrite stabilizing elements is such that the primary dendrites are ferrite, and austenite begins to form in a subsequent peritectic type reaction between the original ferrite and the solute enriched interdendritic liquid. This sequence of freezing steps gives rise to an unusual solidification structure consisting of ferrite-cored austenite dendrites and a continuous network of alloy rich eutectic carbides crystallized from the last-remaining interdendritic liquid.

The microstructural constituents just described are illustrated in the sample current image of Fig. 1, which includes a primary dendrite axis intersecting the plane of the specimen. The central cross or "plus sign" is a decomposition product of the high temperature ferrite, and the eutectic carbides approximately bisect the four right angles of the dendrite cross. Note also the two morphologically and chemically distinguishable forms of interdendritic carbides; i.e. three of the eutectic arms contrast sharply with the iron-base matrix, while the fourth arm at the lower left has an average atomic number much less than that of the other eutectic structures.

Fig. 1. Dendrite axis in as-cast high speed steel. Sweep length: 25 μm/cm.

The composition of these various types of eutectic carbides and the nature of the solute distribution across the primary dendrite axis (e.g. along the dotted lines in the photograph) were determined quantitatively in the commercial M2 steel and the high carbon and high vanadium modifications. For analysis of the carbide phases pure element or iron-base binary standards were used to determine the metal content, and a slowly cooled meteorite with large cementite (Fe_3C) particles was used as a carbon standard. Other than polishing and cleaning of the samples and standards immediately before use, no precautions were taken to avoid carbon contamination, it being assumed that equivalent contamination of the sample and standard would cancel each other. From this procedure reasonable carbide compositions were obtained. In the case of eutectic structures consisting of the stoichiometric carbide phases M_6C and MC, the measured atomic percent of carbon was 15% and 48% respectively. More complex eutectic structures, probably multiphase mixtures, gave carbon analyses inconsistent with any simple stoichiometric ratio. These carbides are currently being examined by scanning electron microscopy to attempt resolution of their proposed multiphase structure.

For determination of the concentration profiles across the bulk of the dendrite, a simplified procedure was employed to convert raw intensity ratios to weight percent of solute. A base composition of 3.5%W, 3.0%Mo, 3.5%Cr, 1.0%V, 0.5%C, balance Fe was assumed to approximate that of a typical point in the matrix solid solution, and a program permitting the calculation of expected intensity ratios from an input of chemical composition[1] was used to compute I/I_o for each of the metallic elements in the base composition. The computed intensity ratios for each solute were then divided by the input concentration of that solute to determine a set of conversion factors between I/I_o and weight fraction. Although these conversion factors are strictly valid only for the base composition, further calculations showed the analysis for a given element is only slightly affected by the concentration of the other solutes in the specimens analyzed. The simplified procedure for treatment of a six component system was therefore used to determine the concentration of the dissolved alloying elements in the matrix solid solution.

---

1. J. I. Goldstein and P. A. Comella: A Computer Program for Electron Probe Microanalysis in the Fields of Metallurgy and Geology. Report No. X-642-69-115, Goddard Space Flight Center, April 1969.

APPLICATION OF A COMBINATION SCANNING ELECTRON MICROSCOPE-MICROPROBE TO FORENSIC ANALYSIS

C. H. Anderson & J. W. Leitner, Applied Research Laboratories
R. Finn, Syracuse University Research Corporation
Captain S. Ferriss, New York State Police Scientific Laboratories

INTRODUCTION

Forensic science is a field that embraces a broad spectrum of analytical techniques. Until recently the optical microscope has been used almost exclusively for examining and comparing the external features of a wide variety of materials for use as evidence in courts of law. Similarly, chemical analysis, either by classical wet methods or instrumental methods such as optical emission spectroscopy are commonly used where elemental analysis is advantageous or required. With the development of the scanning electron microscope, and particularly with the development of the combined SEM and microprobe, it would appear that the criminologist has an additional potentially powerful tool for conducting his investigations. The SEM, with its remarkable depth of focus and high magnifications, is capable of bringing out details in a specimen not detected in the optical microscope; the microprobe allows a quantitative elemental analysis to be conducted on the identical area examined by the SEM. In order to show the utility of a combination scanning electron microscope and microprobe to forensic work, a variety of samples of interest to a crime laboratory--hair, paint, cloth, etc. were analyzed and the results are discussed briefly below.

AUTOMOBILE PAINTS

Two sets of automobile paints were examined from the point of view of determining whether, within each set, each specimen originated from the same source. In the first set, shown in Figure 1, there were differences in surface characteristics (weathering cracks, surface oxidation). Confirming evidence that the paints were different was obtained from an elemental analysis showing the presence of barium in Sample A, but absent in Sample B. In this case it should be noted that titanium was present in both samples and a high resolution wavelength dispersion system was required to resolve the BaL_{α} from TiK_{α} radiation.

A second set showed almost identical surface characteristics and elemental analysis, strong evidence that the paints were from the same source.

HAIR

Two sets of hair samples were examined in the SEM mode and analyzed by x-ray microanalysis. Figure 2 shows SEM pictures of the two specimens in the first set. The first set showed the same sulfur and chlorine content, but one hair was 50% larger in diameter. In the second set one hair was much different in diameter and surface characteristics from the other. Furthermore, there was a significant difference in sulfur and chlorine content.

TEXTILE FIBERS

Two textile fibers were compared, found to possess different surface characteristics, and also contained significantly different amounts of chlorine and titanium.

CARTRIDGE CASINGS

Two cartridge casings were examined at the firing pin impact area to determine whether both cartridges had been fired from the same gun. General similarities of the surface of this area were apparent but no definite conclusions could be drawn.

ALUMINUM SIDING

Three similar holes in aluminum siding were examined to determine whether they had been made by bullets. Lead residues were found on two of the impact areas and were considered strong evidence that these holes were the result of bullet penetration.

MISCELLANEOUS INORGANIC MATERIAL

Three safe-insulating materials from three manufacturers were examined to determine whether the analysis of each was sufficiently unique for the identification of each manufacturer's product. Two were clearly distinguishable, but only subtle differences were found in the third.

Samples of a red powder from two different sources were shown to be identical and, as indicated from the presence of CoK_α and OK_α, to be cobalt oxide.

SUMMARY AND CONCLUSION

It was concluded that the additional and complementary information obtainable by a combination microprobe and scanning electron microscope can be a valuable aid in the examination of forensic samples.

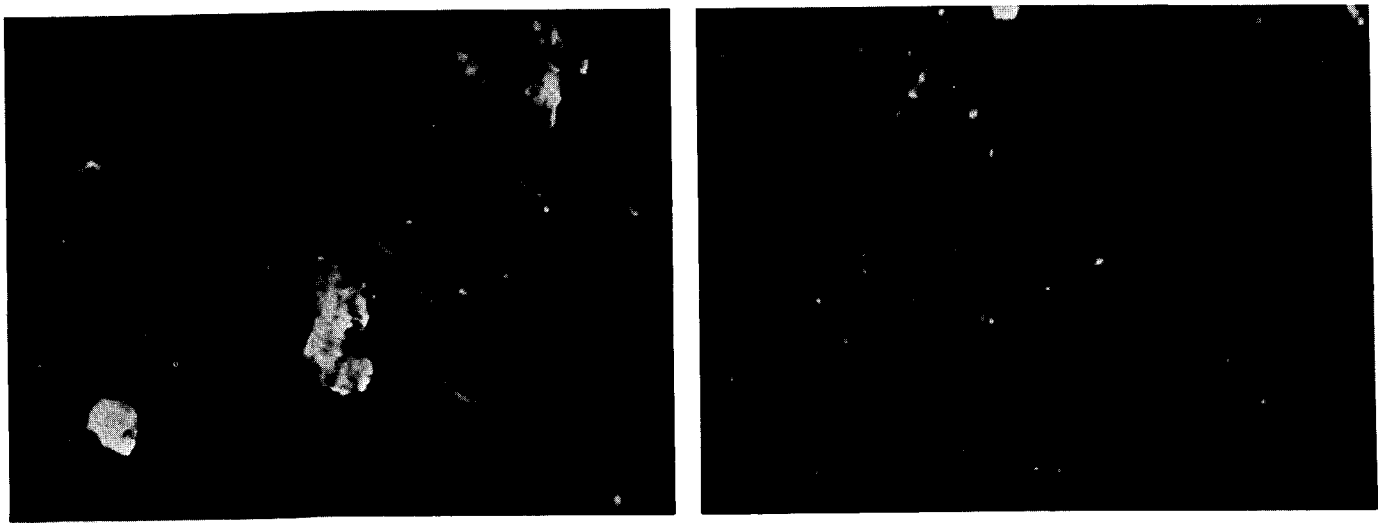

3300x Sample 1A 3μm 3300x Sample 1B 3μm

AUTOMOBILE PAINT
FIGURE 1

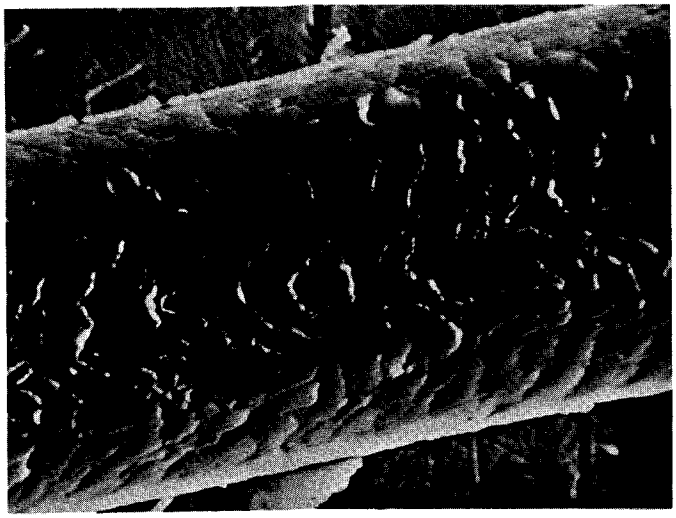

800x Sample 7A 12.5μm

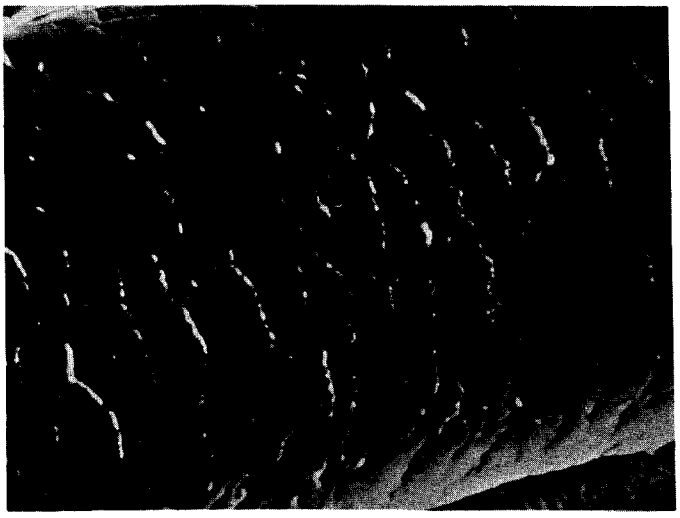

800x Sample 7B 12.5μm

HAIR SAMPLES

FIGURE 2

ELECTRON PROBE MICROANALYSIS OF TRACE CONSTITUENTS

K. F. J. Heinrich
National Bureau of Standards
Washington, D. C. 20234

Abstract

Electron probe microanalysis permits the detection and measurement of quantities of elements as small as 10^{-15}g. However, it cannot be used to detect very low concentrations of elements. Hence, electron probe microanalysis is typically a micro-analytical, but not a trace analytical technique.

The determination of the lower limit at which elements can be detected with the electron probe requires a number of decisions. In the first place, the limit of detection must be defined. There are several proposed definitions for the limit of detection; some of these are objectionable on theoretical grounds. Most proposed limits of detection are, in fact, based on the assumption that no errors other than those inherent in the Poissonian counting statistics are present. However, as the operator increases his efforts to lower the limit of detection, non-Poissonian errors become more prevalent. Hence, the definitions of limit of detection based on the Poissonian model are optimistic estimates rather than a measure of real sensitivity.

As shown by Currie [1], the range of limits of detection obtained according to diverse proposed definitions covers three orders of magnitude. One must conclude that the intuitive notion of a defined limit of detection has no unique accurate definition. It is proposed that an estimate of the standard deviation of the background - from which the diverse expressions of limit of detection can be derived - is the most appropriate expression of statistical precision at the trace level.

However, there are two further difficulties with the definition of sensitivity. First, there is no unique sensitivity for an instrument, rather, different procedures (line scan, fixed time count, etc.) differ in sensitivity. Secondly, the possibility of significant systematic errors (mainly in the background level) makes it impossible to realistically estimate the limit of detection on the sole basis of statistical signal fluctuations.

This further implies that the sensitivity depends on the technique of background estimation, the availability of appropriately characterized standards at the zero concentration level, and on the complexity of the spectrum in the region of the measured line.

A comparison of results obtained by various authors on low-alloy steels under realistic operating conditions indicates that concentrations in the order of 0.01% ($k = 10^{-4}$) are detectable. This barely qualifies electron probe analysis as a trace analysis method, according to the definition of trace level by Morrison and Skogerboe [2]. Indications of detection at considerably lower levels are either unrealistically optimistic, or correspond to extremely tedious operating conditions which are not met in typical situations of routine analysis.

LIST OF REFERENCES

[1] Currie, L. A., Anal. Chem. 40, 586-593 (1968).

[2] Morrison, G. H., ed., Trace Analysis: Physical Methods, Interscience Publishers, New York, 1965, p. 1.

FACTORS AFFECTING THE RESOLUTION OF THE BACKSCATTERED ELECTRON IMAGE IN THE SCANNING ELECTRON MICROSCOPE

Oliver C. Wells

IBM Corporation
Thomas J. Watson Research Center
Yorktown Heights, New York 10598

The resolution of the backscattered electron image can be improved by operating with oblique incidence and by collecting electrons that have suffered the smallest possible deflection in the specimen. These electrons have a higher mean energy than those that have suffered the larger deflections, and so in general have emerged after a short penetration path in the target. Some practical aspects of high energy electron detection will be discussed.

EXPERIMENTAL DETERMINATION OF THE ABSORPTION CORRECTION BY USE OF A SOLID STATE DETECTOR

W. Kinzy Jones and Robert E. Ogilvie

Massachusetts Institute of Technology
Cambridge, Massachusetts

The absorption correction term, $f(\chi)$, given by the expression

$$f(\chi) = \frac{\int_0^\infty \phi_A(\rho z) \exp \chi\rho z \, d\rho z}{\int_0^\infty \phi_A(\rho z) \, d\rho z}$$

where $\chi = (\mu/\rho) \csc \theta$, can be determined experimentally by two methods. The first method, the tracer technique[1], is used to determine $\phi_A(\rho z)$, which then allows the evaluation of $f(\chi)$. This technique, however, requires extensive sample preparation and therefore has not found wide experimental evaluation. In the second method, $f(\chi)$ is determined by varying χ through changing the take-off angle. This can be accomplished in two manners: (1) by moving the spectrometer with respect to the specimen, keeping the incident angle of the electron beam normal to the specimen surface[2] or; (2) by rotating an inclined specimen, keeping the spectrometer in a fixed position[3]. However, when using the rotating specimen technique, additional corrections to the data are needed since the incident angle of the electrons is not normal to the surface, which is undesirable. In this work, $f(\chi)$ was determined for Cu at 20 keV by use of the variable χ method, utilizing a normal angle of incident of the electron beam. The complications of spectrometer alignment was removed by using a Si(Li) solid state detector for the X-ray analysis.

The work was done using a Cambridge Stereoscan scanning electron microscope employing an Ortec solid state detector (resolution of 213 ev FWHM at 6.4 keV) with a 10 cm active diameter. The detector was positioned at 4 1/4" from the electron optical axis. The accelerating potential was fixed at 20 keV and the electron spot size was maintained less than 10 μm. To obtain the variable take-off angle, a specimen stage was constructed which had two primary functions (see Fig. 1): (1) to move the specimen in a vertical motion and (2) to position a collimator at a constant radius from the specimen at the desired take-off angle. The stage allowed for a continuous take-off setting from 0 to 30 degrees. The collimator had a divergence of .08 degrees and since the collimator was always positioned at a constant radius, the solid angle of transmitted X-rays was a constant. The detector was shielded to allow only radiation passing through the collimator to be measured. The zero alignment of the stage, which was obtained by

use of a mechanical jig, was better than 9 minutes of arc.

Data was collected in a multichannel analyzer which had been calibrated to 25 ev/channel. The specimen current, which was in the nanoamp range, was monitored and kept constant during the entire run. Since X-ray generation is proportional to the beam current, the current range was selected to optimize the X-ray signal while minimizing the dead time of the system (which was always less than 3%). Data was taken five times for each take-off angle (to increase the confidence level of the data according to the Student t test) and the sample was rotated between each measurement to minimize (1) any contamination and (2) any inhomogeneties in the sample. The intrgrated intensities of the copper spectrum was obtained by integrating the spectrum over 3σ of the peak width. For counting times of 3 minutes, the total counts between these limits were between 10 and 20 thousand. To obtain the $f(\chi)$ curve from the raw data one must find the intensity at zero χ. This is obtained by plotting ln I versus χ and extrapolating to $\chi = 0$, giving greatest weight to those values with low χ. Once $I\ (\chi = 0)$ is known, the $f(\chi)$, uncorrected for fluorescence effect from the continuum is readily obtained from

$$f(\chi) = \frac{I(\chi)}{I(\chi = 0)}$$

The effect of secondary fluorescence from the continuum must be taken into account to be in accord with the definition of $f(\chi)$, which is for primary excitation. The $f(\chi)$ primary can be calculated from

$$f(\chi)_{total} = S\ f(\chi)_{secondary} + (1-S)\ f(\chi)_{primary}$$

where S = fraction of characteristic radiation due to secondary ionization and

$$f(\chi)\ \text{secondary} = \frac{N_{ks}\ (\chi)}{N_{ks}\ (\chi = 0)}$$

where N_{ks} is the contribution due to secondary ionization. Obtaining S from the work of Green and Cosslett[4] and evaluating $f(\chi)$ secondary allows one to determine $f(\chi)$ primary from the measured $f(\chi)$ total. The resultant $f(\chi)$ primary is given in Fig. 2.

The results of this work are compared to the experimental work of Green and the calculation of the Philibert equation utilizing the σ_c of Duncumb and Shields[5]. The agreement between this work and the work of Green and Philibert is excellent.

This paper has been limited to the determination of the $f(\chi)$ of copper at 20 keV. The primary purpose of this paper was to define an experimental method for a more rapid evaluation of $f(\chi)$. The results of this method are being extended to various elements and alloy systems at different accelerating voltages.

The total results from this research will allow for a greater understanding of the effects on the absorption correction and will allow for (1) the definition of limiting curves for $f(\chi)$ in alloy systems and (2) a reevaluation of the parameters in the Philibert equation, if needed, to better fit the data. The experimental method is rapid and more error free than the previous methods.

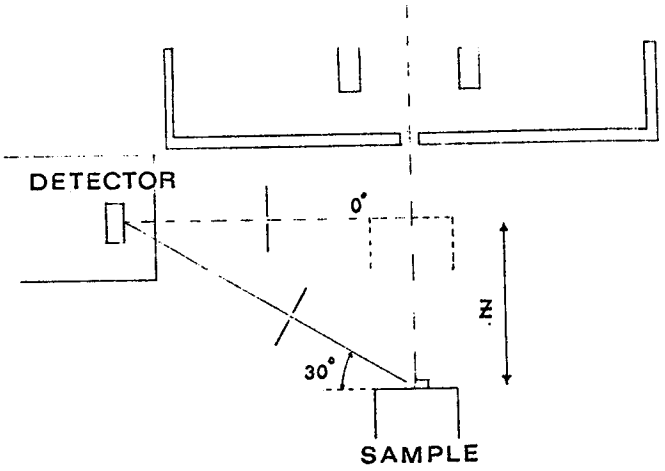

Figure 1

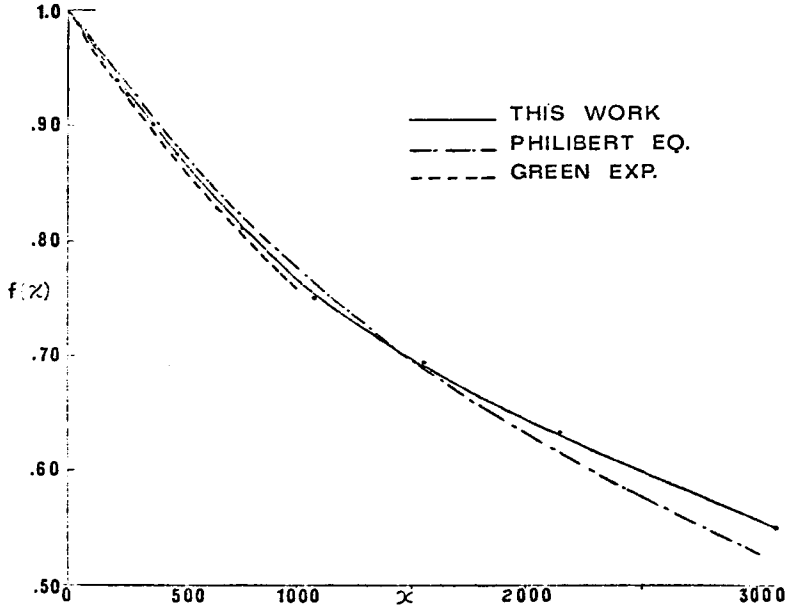

Figure 2

Bibliography

1. R. Castaing and J. Descamp, J. Phys. Radium, 16, 304 (1955).

2. M. Green, Proc. Phys., Soc. (London) 82, 204 (1963)

3. D. Brown, Ph.D. Thesis, M.I.T.

4. M. Green and V. E. Cosslett, Proc. Phys. Soc. (London) 78, 1206 (1961).

5. P. Duncumb and P. K. Shields, Brit. J. Appl. Physics, 14, 617 (1963)

ELECTRON PROBE ANALYSIS OF THE FIBER-RESIN CONTENT OF GRAPHITE-EPOXY COMPOSITES

R. E. Herfert
Northrop Corporation
3901 W. Broadway
Hawthorne, California 90250

The electron probe analyzer was developed as a "Quantimet" type instrument for the analysis of fiber volume, resin content, and void content of various graphite-epoxy composites. The normal method for obtaining the fiber/resin content is one of a wet chemical technique. Here one would take a predetermined volume of material and obtain an average of the fiber/resin ratio. However, in a graphite-epoxy composite, the relative variation in distribution of the fiber/resin content is a more critical value than the average analysis. The mechanical properties of the composite are related to the distribution of the fibers in the matrix and the uniformity therein. A method was established whereby the carbon content and the oxygen content was used to determine the percent analysis of the fibers (carbon) and resin (oxygen). Analytical curves were established for variations in the carbon and oxygen content as a function of the wet chemical analysis of the composite (see Figures 1 and 2). The relative sensitivity of the analytical tool was determined and graphical representations of blocks of analysis across the composite surface were determined. A series of control specimens, where variations in fiber content existed, were tested to determine the ultimate strength. These strengths showed a definite relationship to the gaussian spread of the fiber/resin analysis for the graphite-epoxy composite. This is shown in Figure 3. The main disadvantage was found in that an increased amount of contamination within the microprobe was obtained by vaporization of the surface of the composite.

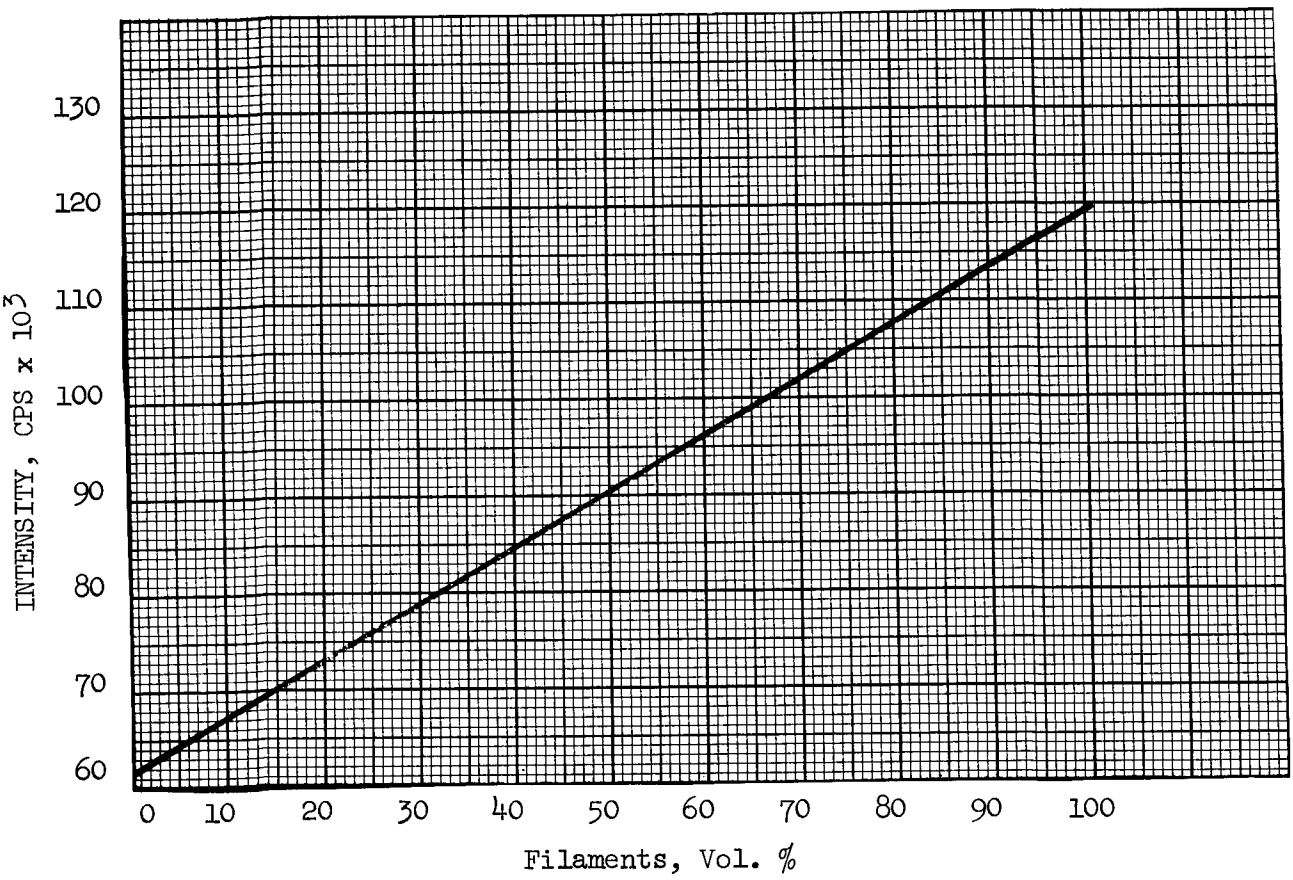

Figure 1. Analytical Curve of Filament Content Based on Carbon Analysis.

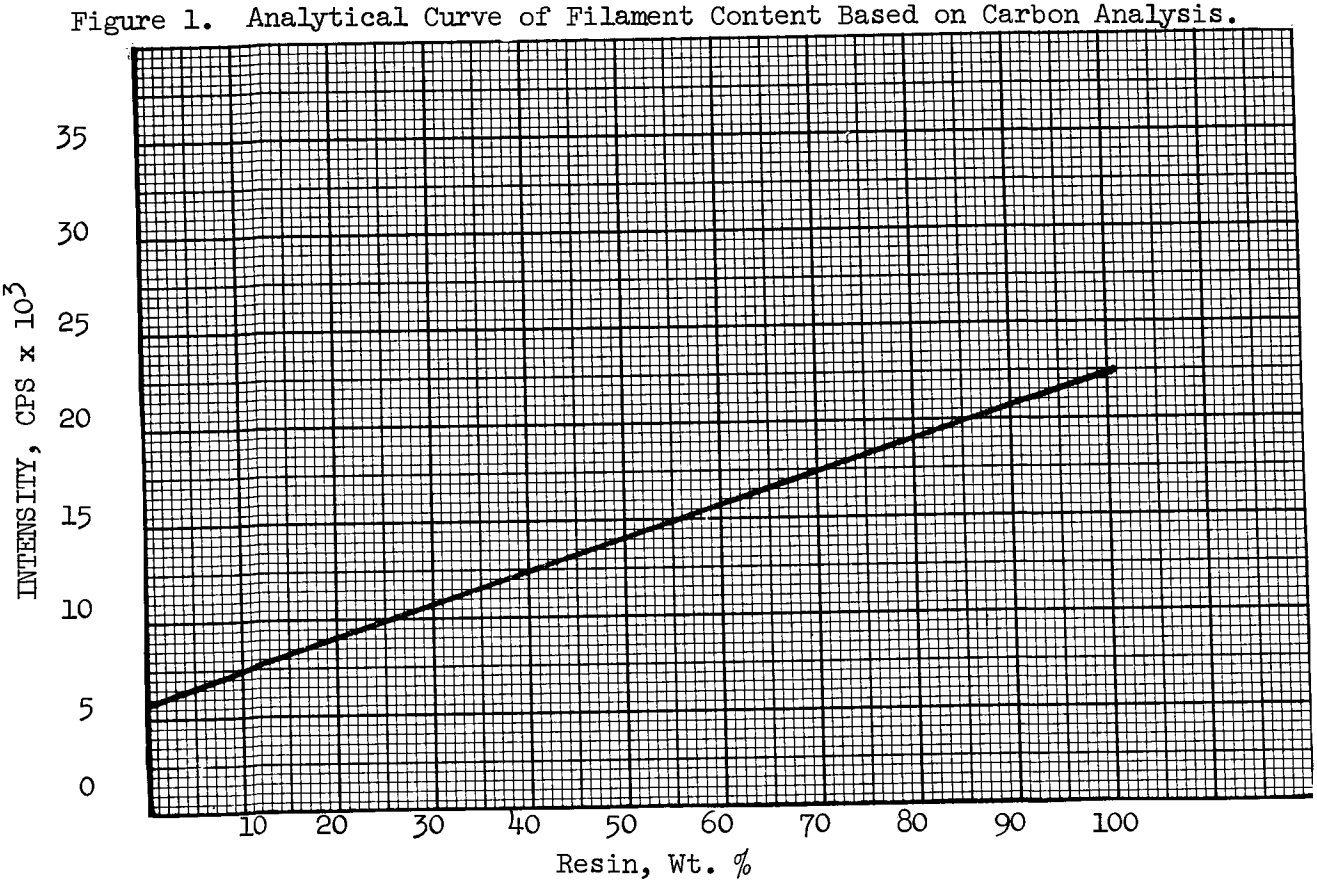

Figure 2. Analytical Curve of Resin Content Based on Oxygen Analysis.

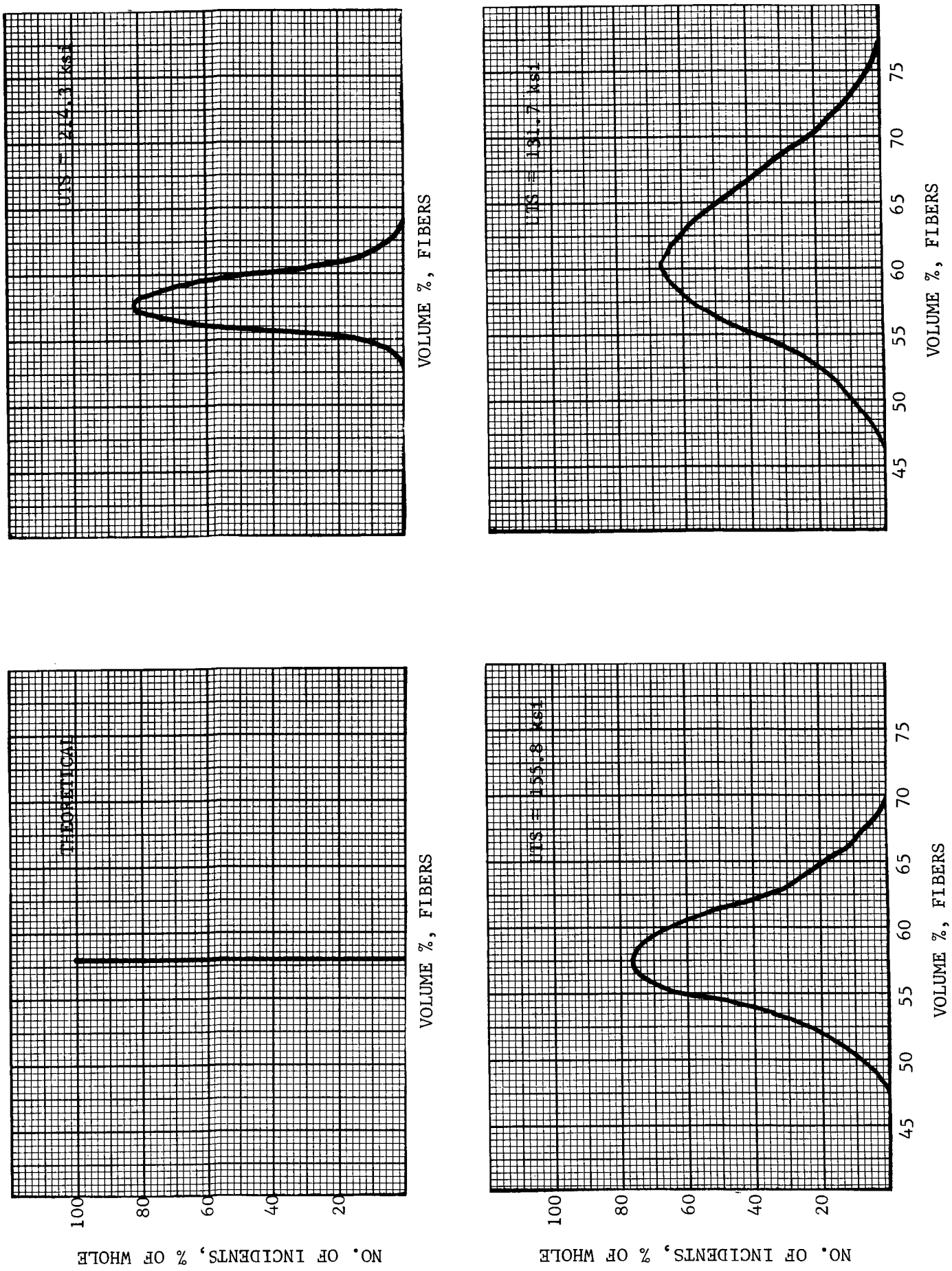

FIGURE 3. DISTRIBUTION OF VARIATIONS IN FIBER CONTENT WITH RESPECT TO ULTIMATE TENSILE STRENGTH OF MORGANITE II/4617 GRAPHITE COMPOSITE

SPECIMEN CONTAMINATION DURING ELECTRON PROBE ANALYSIS*

by

C.M. Taylor,** A.J. Tousimis and J.A. Nicolino
brc-Laboratories
Biodynamics Research Corporation
Rockville, MD. 20852

Figure 1 is a transmission light micrograph of a biological tissue section after it has been exposed to a 20KV electron probe of 0.04 uAmpere specimen current from right to left. The contamination left on the tissue section is approximately three times wider than that on the support substrate surface of quartz glass. This widening could be due to the differences in the two surfaces. Figure 2 shows contamination areas left on the surface of a metallographic specimen after two different magnification scanning electron micrographs were made with a 20KV electron probe and 10^{-12}Ampere specimen current. This contamination results from the interaction of the electrons with the specimen surface which is constantly exposed to molecules from various sources from within the vacuum system (1). The chemical nature of this contamination layer could have serious effects not only on the ultrastructure of the specimen but also on the elemental analyses both for low atomic number elements and trace analysis for the heavier elements (2, 3, 4). Several methods to decrease this contamination have been proposed and successfully applied. These range from heating the sample (1) to cooling the specimen surrounding (5) and from ion or gas bombardment (6) to the use of dry vacuum systems. Very few laboratories employ these methods.

The detectable elements present in the contamination layer have been measured using high purity germanium as target material. Extreme care was taken to keep the Ge surface clean from any contaminants before exposure to a 25KV electron beam with specimen currents up to 0.4uAmperes in a MAC-400S electron probe equipped with three X-ray spectrometers. Contamination spots 150um in diameter were produced. At different time intervals spectral analysis (semi-quantitative) was performed. The goniometers were equipped with LOD (Lead Octadecanate) and thin window X-ray detector for the low atomic number elements and KAP, PET and LiF for the higher atomic numbers. The

---

* We are indebted to Dr. V.G. Macres, MAC, for his cooperation during the initial stages of this project.

** Present address: Stanford University, Stanford, CA.

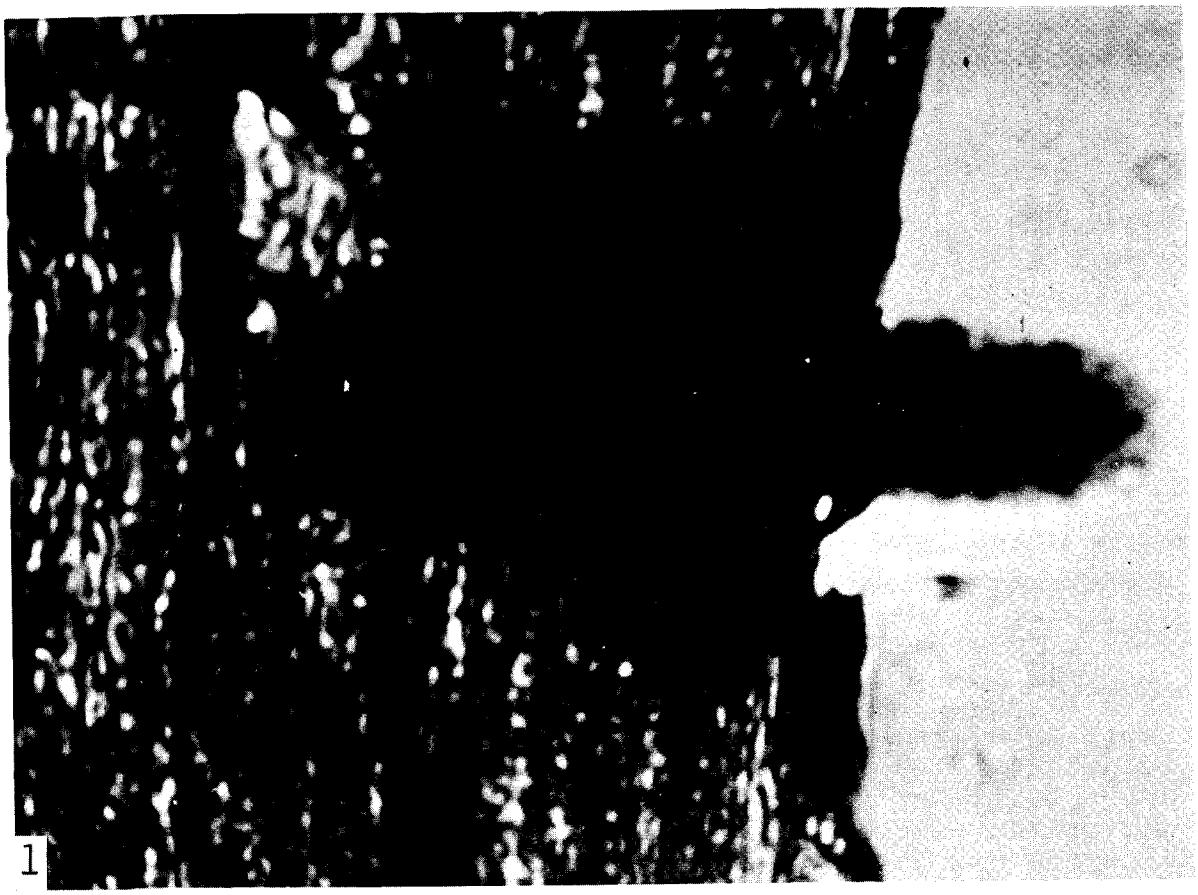

Figure 1. Light micrograph of a biological tissue section on quartz surface (to the right), traversed with an electron probe. Note the heavier contamination on the section.

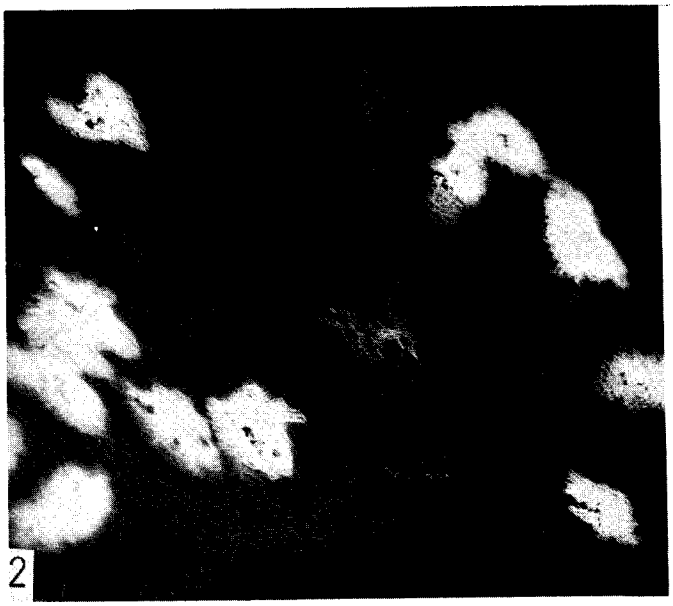

Figure 2. Scanning electron micrograph of two raster scans made at higher magnification and longer exposures each.

results of a typical long exposure contamination spot (the contamination thickness absorbed the GeK when produced by 15KV electron excitation below the contamination surface) are shown below:

Spectral Analysis of Contamination Spot

Element	Estimated Weight Percent
C	94
O	3 - 4
Sn	0.7 - 0.8
Si	0.5 - 0.6
S	0.3 - 0.4
P	0.1
Cl	0.05

Each of the elements measured in the contamination layer reach their detectability limits at different rates. Carbon and Silicon are the first to be detected while oxygen and sulfur are detected prior to tin, phosphorus and chlorine. The main contributors to the elemental composition of the contamination spot are: carbon from the oil vapors back-streaming from the forepump, oxygen from either adherent gas molecules or thin oxide film on the specimen surface, tin from soldered internal vacuum components, silicon from oils and greases used to lubricate vacuum moving parts and/or in some cases diffusion pump oils and sulfur probably from the o-rings, lubricating or pump oils. Phosphorus and chlorine are deposited very slowly, and since they require longer time than most routine analyses, they present no problem in quantitative analyses unless the specimen is left in the electron probe vacuum system for several days. Probable sources for these elements could be o-rings, lubricating oils and the samples themselves.

REFERENCES

(1) ENNOS, A.E., Brit. J. Appl. Phys. 4, 101 (1953) and 5, 27 (1954).

(2) MOLL, S.H., First Nat. Conf. Electron Probe Microanalysis 27, (1966).

(3) MOLL, S.H. and G.W. BRUNO, Second Nat. Conf. Electron Probe Microanalysis #57 (1967).

(4) ONG, P.S. in "Electron Probe Microanalysis" p. 144, A.J. Tousimis and L. Marton, Ed., Academic Press, NY(1969).

(5) HEIDE, H.G., Fifth Intern. Conf. Electron Microscopy, Philadelphia, PA. Acad. Press, NY(1962).

(6) CASTAING, R. and J. DESCAMPS, Comptes Rendus, 238, 1506 (1954).

THE APPLICATION OF ELECTRON-PROBE MICRO-ANALYSIS IN MEDICINE*

by

P. Galle
Laboratoire de Biophysique
de la Faculte de Medecine de Creteil, France

Electron-probe micro-analysis was first applied in pathology in 1963: Tousimis and Adler (1), studying the Descemet's membrane of Wilson disease, showed how important this method could be in medicine.

Since, the techniques have been improved. Construction of new instruments combining an electron-probe micro-analyzer and an electron microscope (2) have made possible an extension of this method to the study of ultrathin tissue sections, which is of great interest in cellular pathology.

In medicine, electron-probe micro-analyzer is particularly useful in the study of two organs, lung and kidney: the pulmonary epithelium, which is directly exposed to atmospheric dusts, and the renal epithelium, the function of which is to eliminate foreign substances after their concentration in specialized organelles.

PULMONARY PATHOLOGY

1. The study of occupational pneumoconiosis presents in itself a vast field of application. Here, we will simply say that the pathological changes in these diseases merit a study of ultra-thin tissue sections with a micro-probe combined with an electron microscope. Only this technique can precisely identify the intracellular location of these absorbed dust particles.

2. The study of intrapulmonary black pigment was performed on fifteen patients most of whom had died from renal failure and none of whom had been submitted to any occupational exposure to dust. Microanalysis revealed that these pigments, called Anthracosis Pigments, contain only very little carbon, contrary to what was previously thought, but consist of a large number of highly concentrated mineral compounds. Silicon, calcium, aluminium, magnesium, titanium and iron compounds were found in these fifteen patients, all living in the Paris area. Analysis of atmospheric dust from the same area revealed that it contains these same elements in high concentration in the form of inframicroscopic microdusts.

---

* Travail effectue dans le cadre de la R. C. P. No. 162 du C N R S.

3. An unusual lesion was observed in two patients over 50 years old. It presented dense macrofibrillar deposits in the interstitial tissue of the pulmonary parenchyma.

Microanalysis showed that they contained a large proportion of silicon. These were probably elastic fibers impregnated by this element. These fibers are always surrounded by a large number of collagen fibrils. Whether or not this lesion is responsible for the genesis of pulmonary sclerosis is open to discussion.

4. A very unusual type of pneumoconiosis was studied. In a three-month old child with an obstructive lobar emphysema which had necessitated surgical ablation of the corresponding lobe, microanalysis revealed very numerous microscopic deposits of barium. The cause responsible for this lobar emphysema could thus be determined: this child had a barium X-ray of the stomach at the age of 10 days, and had probably inhaled some barium at that time. The pulmonary emphysema did not occur until three months later.

RENAL PATHOLOGY

1. Microanalysis has uncovered the kidney mechanism for concentration and elimination of a number of mineral elements. Gold, injected in the form of gold salts used in human therapy, concentrates in the mitochondria of the kidney proximal tubular cell (3). Uranium, however, concentrates in the lysosomes where it crystallizes with phosphorus in the form of needle-like microcrystals. Iron is concentrated in intracellular organelles which are neither mitochondria nor lysosomes. Silver is found in the glomerular basement membrane where it crystallizes with sulfur and calcium.

2. The study of nephrocalcinoses allowed us to classify them into six individual types, differing from each other by both ultrastructure and chemical composition. Most interesting medically is the nephrocalcinosis secondary to hyperparathyroidism. It is known that diagnosis of this condition is quite important since it necessitates surgical treatment, but this diagnosis is sometimes very difficult. Microanalysis combined with electron microscopy is helpful in finding the cause of a nephrocalcinosis of undetermined origin.

REFERENCES

1. TOUSIMIS, A.J. and ADLER, I.: Journal Histochem. Cytochem., 11, 40, (1963).

2. GALLE, P.: Sixth Intern. Cong. Electron Microscopy, 2, 79, Kyoto (1966).

3. STUVE, J. and GALLE, P.: J. Cell Biol., 44, 667 (1970).

APPLICATIONS OF ELECTRON PROBE ANALYSIS TO PLANT SCIENCES

André Läuchli
Department of Plant Sciences
Texas A&M University
College Station, Texas 77843

Investigators, who study the physiology of plants, often utilize two entirely different tools, that is transmission electron microscopy to acquire knowledge of the ultrastructures and microanalytical methods to measure physiological and biochemical processes. There is an increasing desire to combine these two kinds of methods by performing analyses at the cellular and subcellular level. Electron probe analysis offers unique possibilities in that it permits an essentially complete analysis of chemical elements in cells and cell compartments of plants (1).

Läuchli and Schwander (2) were the first to apply electron probe analysis to plant materials. In their report data were presented on the cellular localization of the elements potassium and phosphorus in fresh, frozen sections of corn leaves. Thereafter, several other laboratories used this method for studying the transport of inorganic solutes and mineral metabolism in plants. Yet, electron probe analysis is not as widely utilized by plant scientists as by researchers from the medical and animal sciences. Apart from the fact that the instrument is very expensive, difficulties in the preparation of specimens seems to limit the application of electron probe analysis to plant materials. Mineral elements in the plant occur in part as solutes. It is essential to minimize the displacement of inorganic solutes in the tissue during specimen preparation. Sectioning of unfixed, frozen sections in a cryostat is believed to allow solutes to be retained at the original sites. Hence, it has been employed to prepare plant material for electron probe analysis (3,4,5,6). Routine cryostat sectioning of plant material, however, yields relatively thick sections on the order of 16-20 μm, and the preservation of cellular structures is poor. To overcome these difficulties, Läuchli et al. (7) developed a freeze-substitution, epoxy resin embedding technique involving ether as the substituting fluid. This new preparation technique permits sections of 1-2 μm thickness and assures an improved spatial resolution in electron probe analysis.

The majority of applications of the electron probe was on the detection of mineral deposits *in situ*. For example, it was found that the strikingly low concentration of calcium in seeds is due partly to the deposition of calcium-containing microcrystals in tissues outside of the seeds (8). Microcrystals and amorphous deposits of minerals in plants appear to be characterized chemically by electron probe analysis with more efficiency than by crystallographic methods. The translocation of inorganic solutes in plants also can be investigated effectively with this method, particularly by employing the line scan technique. Thus, results from studies using electron probe analysis led to the proposal of a new mechanism by which inorganic nutrients may be translocated in roots (9).

The absolute standardization of electron probe analyses of plant material poses a serious problem because it is difficult to prepare adequate standards.

Little information is available regarding standards that were used successfully with plant specimens. As yet, the most feasible approach to the preparation of standards was undertaken by Humble and Raschke (10) for measuring absolute amounts of potassium in stomata of leaves. Calibration of the relative data of potassium was achieved by means of microcrystals of potassium oxalate and potassium chloride, the volumes of which had been determined microscopically. The use of crystals might be criticized because of differences in chemical composition and physical properties between the standards and the plant specimens. However, no major error in standardization was made since the beam integrated totally for potassium in both the crystals and plant specimens.

Not only has electron probe analysis proved itself to be applicable to plant physiology, but it may also have a great impact upon ecological research. Tolerance of certain plant species to high concentrations of metals in the substrate is not well understood physiologically. Studies with the electron probe yields new insights into this phenomenon (11), and may widen our knowledge of such important problems as metal toxicity (6,12) and salt tolerance (13) of economically important plants. In addition, the concentration in the biosphere of environmental pollutants like arsenic, mercury and lead appears to be rising at an alarming rate. This rise in concentration could be monitored by measuring the levels of the respective metals in certain test species of plants.

---

1. Läuchli, A. Electron probe analysis. In: Methods of Microautoradiography and Electron Probe Analysis, U. Lüttge, ed. Springer, Berlin (in press).

2. Läuchli, A. and H. Schwander. Experientia 22, 503 (1966).

3. Läuchli, A. Histochemie 11, 286 (1967).

4. Rasmussen, H. P., V. E. Shull and H. T. Dryer. Develop. Appl. Spectrosc. 6, 29 (1968).

5. Satter, R. L., P. Marinoff and A. W. Galston. Amer. J. Bot. 57, 916 (1970).

6. Waisel, Y., A. Hoffen and A. Eshel. Physiol. Plant. 23, 75 (1970).

7. Läuchli, A., A. R. Spurr and R. W. Wittkopp. Planta 95, 341 (1970).

8. Läuchli, A. Planta 73, 221 (1967).

9. Läuchli, A., A. R. Spurr and E. Epstein. Plant Physiol. (in press).

10. Humble, G. D. and K. Raschke. Plant Physiol. (submitted).

11. Noeske, O., A. Läuchli, O. L. Lange, G. H. Vieweg and H. Ziegler. Dtsch. Bot. Ges. N. F., Nr. 4, 67 (1970).

12. Rasmussen, H. P. Planta 81, 28 (1968).

13. Waisel, Y. and A. Eshel. Experientia 27, 230 (1971).

QUANTITATIVE ELECTRON PROBE ANALYSIS OF BIOLOGICAL TISSUE SECTIONS*

by

A.J. Tousimis
brc-Laboratories
Biodynamics Research Corporation
Rockville, MD. 20852

Quantitative electron probe analysis of biological tissue thin sections requires special considerations which are not necessary with specimens infinitely thick with respect to the penetration of the electron beam. In the case of the "infinitely" thick biological specimen, one can proceed with analyses similar to those carried out on metallurgical samples yet they must sacrifice both chemical and morphological resolution due to considerations involving range of electrons in organic matricles. In order to improve morphological resolution, we turn to thin tissue sections and sacrifice, in the process, X-ray intensities from the sample and introduce factors of non-infinite thickness to the correction procedures necessary to render the X-ray information from the specimen quantitative. Yet, in biological studies the value of relating the physical with chemical information available through electron probe analysis is of prime importance. The elements of general interest in analyses of biological samples are: P, N, O, C, Ca, Na, K, Cl, S, Mg, F, Fe and a few others in specific cases. In our laboratories specimens commonly used for the analysis of these elements are taken from bulk pieces of tissue which have been rapidly frozen in isopentane cooled to $\sim$ -155°C. Frozen thin sections 2 to 10 microns thick are then lyophilized and mounted on quartz discs. According to this technique to be described elsewhere not only the microstructure is maintained but also an absolute minimum of migration of diffusable cellular constituents is insured. The mounted sections are then uniformly coated with a layer of $\sim$ 50Å of carbon with the SAMSPIN to render the specimen electroconductive for use in the electron probe.

Quantitative electron probe analysis has, for the most part, been developed for specimens that are "infinitely" thick with respect to the penetration of the electron beam. By this we mean that an electron striking the specimen, if not elastically back-scattered, will travel in the specimen and produce X-rays until its energy is

* Supported in part by Contract Nos. PH-43-66-10 and PH-44-67-104. The cooperation of J.C. Hagerty, T.R. Padden and V.G. Scotti during these studies is gratefully acknowledged.

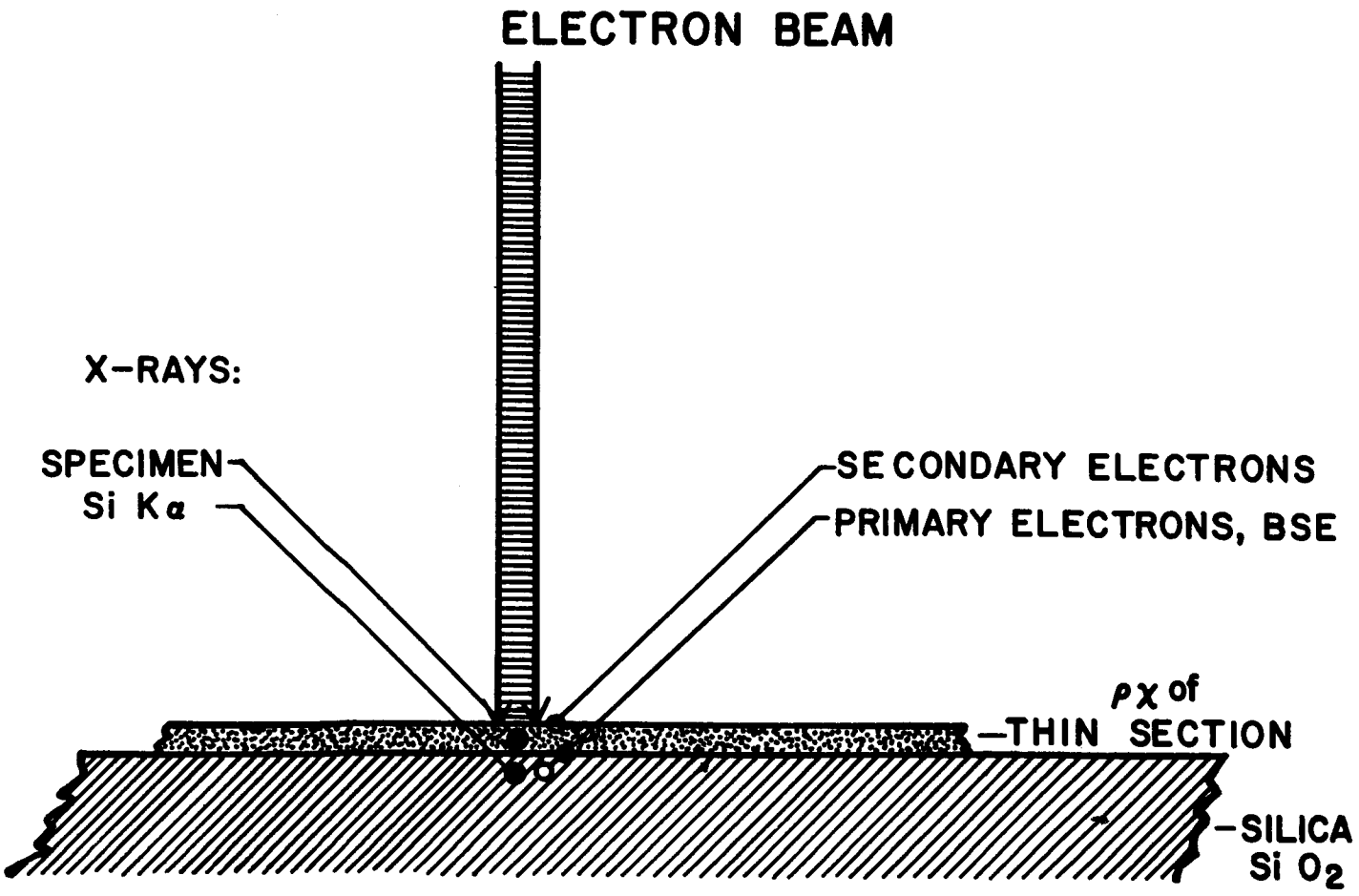

Figure 1. The X-ray intensities of both the SiK and elements from the specimen are recorded for each point (see text).

less than the critical excitation energy necessary to produce the radiation being measured. The concentration C_A of an element A in a specimen is determined by considering the ratio of the measured intensity I_A from the specimen, with the spectrometer set for a particular radiation of element A, to the measured intensity I(A) of that radiation on a standard of pure A. The correction expression can be written incorporating the theoretically calculated atomic number, absorption and fluorescence correction factors. These are based on the assumption that the specimen is infinitely thick. Since this often is not the case in a thin film, where the mass thickness ρx is on the order of .01mg/cm^2, a similar expression cannot be meaningfully applied. The situation is made more complex by specimens where the mass thickness ρx is not known or by inhomogeneous specimens, as is often the case in biological work, where the ρx varies from point to point as a result of variations both in thickness x and elemental composition.

The basic problem then is to determine the concentration of the elements in a thin film when the mass thickness ρx is not necessarily known. There are two apparent approaches to take. The first would be to develop a method to determine the ρx of the film or thin section and then derive an expression to calculate the concentration. The second would be to determine the concentrations by a method that does not require knowing or calculating ρx.

Hutchins (1) developed a method to determine ρx while Colby (2) has an expression to calculate the concentration given the mass thickness ρx. Hall (3) calculated the elemental composition by considering the ratio of the characteristic intensity to the background for the specimen and the standard, and thus does not require determining ρx. Tousimis (4) has introduced a method for determining ρx for each point of the thin section analyzed with the electron probe using the substrate excitation as a basis. The work presented is an attempt to place substrate intensity vs ρx measurements on a quantitative basis and to relate this to the analysis of biological samples.

Figure 1 shows schematically the arrangement of the specimen when exposed to the electron probe. The thin section or film, with thickness 0.1 μm to 5 μm is irradiated with an electron beam (1.5 to 25 KV and 0.01 μA) varying in diameter from 0.05 μm to 2 μm depending on the electron intensity and voltage. Both the X-rays from the specimen and the supporting silica substrate (SiKα) are measured. In addition the secondary or primary backscattered electrons are detected and used to modulate the oscilloscope electron beam intensity to form an image. The absorption of electrons by the specimen or substrate depends on the density ρ, atomic number $\underline{Z}$ and atomic weight $\underline{A}$ and is directly proportional to (Z/A). The $\underline{Z}/A$ is between 0.4 and 0.5 for most elements, therefore the density ρ is or importance for both the electrons and X-rays. Biological samples, as prepared for electron probe microanalysis, may vary spatially both in density ρ and thickness $\underline{x}$. The need, therefore,

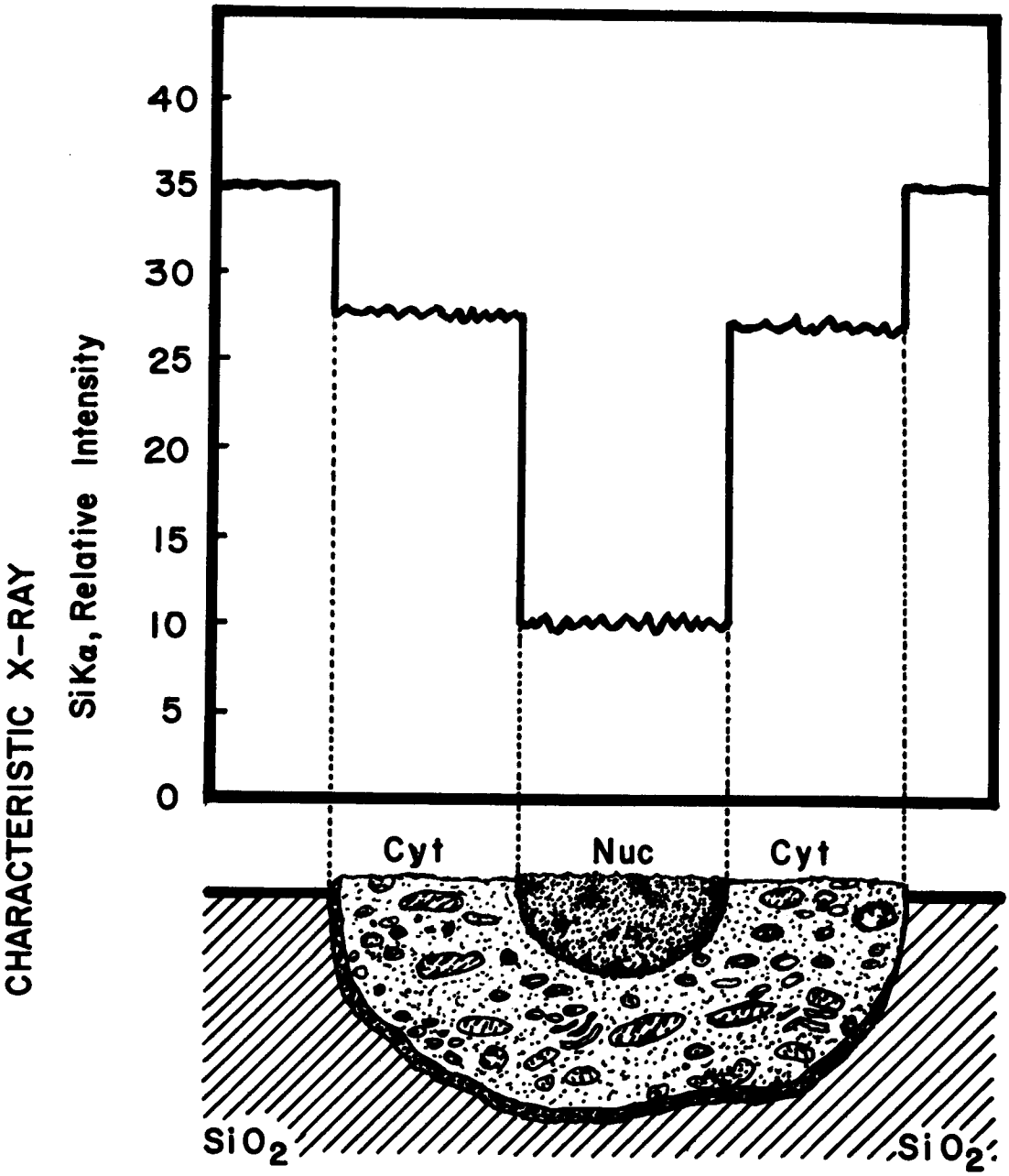

Cyt-cytoplasm; nuc-nucleus; SiO_2-silicon dioxide glass; SiKα-silicon K-alpha characteristic X-ray.

Figure 2. Variation of the SiK intensity from the supporting SiO_2 as the electron beam passes across the cell center of the 3u section of the amphibian red blood cell. Note the sharp changes from maximum SiK intensity from the quartz (SiO_2) to that from the cytoplasm (cyt.), the nucleus (nuc.) again increased at the cytoplasm and reaching the same initial maximum from the quartz.

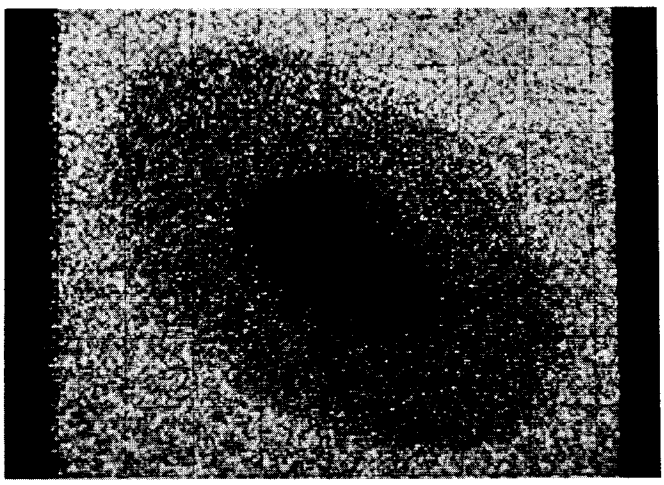

Figure 3. SiK intensity measured through a nucleated red blood cell. The nuclear (center of micrograph) absorbs completely the SiK radiation from the substrate.

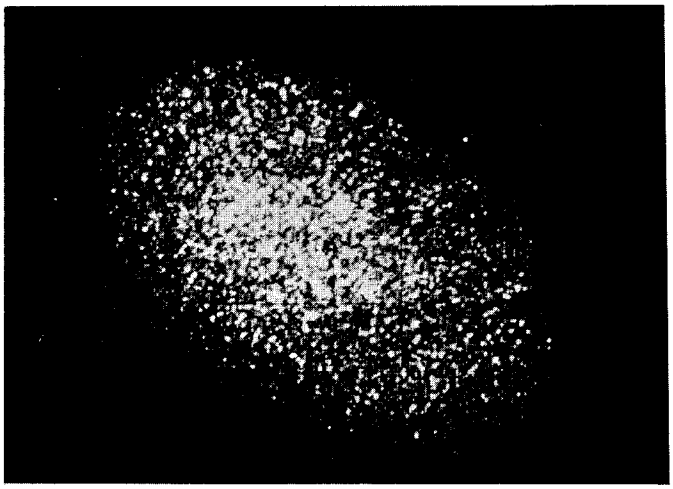

Figure 4. Sulfur distribution in the same cell shown in figure 3.

of determining the mass-thickness (ρx) of the biological sample simultaneously with the X-ray intensity of the element (s) analyzed is imperative if we are to render the data quantitative. To accomplish this we have chosen to measure the transmitted X-ray intensity of a suitable substrate on which the standard film or tissue section is placed. For the studies thus far we have employed pure silica (SiO_2) and measured the SiKα (7.126 Å) intensity transmitted through the sample.

The variation of the relative SiKα intensity from the quartz substrate, measured in the electron probe spectrometer as the electron beam (20KV, 0.04 microamperes) traversed across a three (3) micron thick specimen (amphibian nucleated erythrocyte) is shown in figure 2. The sharp changes in the SiK X-ray intensity observed between Silica (without tissue on its surface), to that measured from the cell cytoplasm and nucleus, indicate the effect of the mass-thickness (ρx) and not the thickness alone. Furthermore it is the chemical composition of the tissue section that effects primarily the silicon X-ray intensity. X-ray raster micrographs in terms of the silicon X-ray intensity from the supporting quartz glass and that for sulfur from the single cell-section is shown in figures 3 and 4. The highest silicon concentration is seen around the cell, less from the cytoplasm and none (in this semiquantitative type of display) in the nucleus. This result is in agreement with that seen in figure 2. Thus far, there is no other approach subject to both theoretical and experimental approaches. By measuring the transmission of the silicon X-ray (generated below the tissue section) through any point of the cell, reference to the universal thickness curves (based on measurements from thin film standards) is made, then taking into account all the elements present in the analyzed point the precise amount(s) of one or all elements can be determined.

REFERENCES

(1) HUTCHINS, G.A., in "The Electron Microprobe", John Wiley and Sons, New York p. 390, T.P. McKinley et al, Editors (1966).
(2) COLBY, J.W., in "Advances in X-ray Analysis", Plenum Press, New York p. 287, J.B. Newkirk et al, Editors (1968).
(3) HALL, T., in NBS publication No. 298, p. 269, "Quantitative Electron Probe Microanalysis" K.F.J. Heinrich, Editor (1968).
(4) TOUSIMIS, A.J. in X-ray Optics and Microanalysis, Academy Press, New York p. 550, H.H. Pattee et al, Editors (1963).

CALCIUM MEASUREMENTS IN FROG SKIN

by

F. Duane Ingram, Mary Jo Ingram and C. Adrian M. Hogben
Department of Physiology and Biophysics
University of Iowa
Iowa City, Iowa 52240

The frog skin is characterized as a rather complicated organ functioning as a thermal regulator, respiratory aid and a form of kidney. Not only are the body salts maintained by the Na^+ pump, but the acid-base balance is also apparently regulated in some species through the action of the Na^+ - H^+ exchange pump.[1]

Audoradiographic studies of frog skin had demonstrated a pooling of Na^+ and Ca^{++} between the papillary and reticular layers (stratum laxum and stratum compactum) of the corium.[2] Subsequent analysis with wet chemical techniques revealed the calcium content of this pool to be in excess of 100 mM/Kg w.w. in some species.[3]

The finding of large Ca^{++} concentrations in the skin led to speculation that it had a role in the operation of these cation transport systems. It would be even more interesting if indeed Na^+ and Ca^{++} are both pooled in the same structure of the skin.[2] The present study was undertaken to locate precisely and characterize the Ca^{++} deposits in the abdominal skin on the Rana pipiens.

A section of skin was quick frozen with supercooled liquid propane, freeze dried, fixed with osmium tetroxide and embedded in plastic.[4] The embedded tissue blocks were faced on a microtome with a steel knife, shadow casted with carbon and analyzed with our ARL-EMX electron microprobe.[5]

Figure 1 is an optical micrograph of a section of the frog skin adjacent to the section analyzed with the electron microprobe. Figure 2 is the oscillographic representation of the backscattered electron signal covering the 250 μ square area depicted in Figure 1. Figure 3 is the oscillographic representation of the Ca^{++} signal for the same area showing that the high concentration of calcium is indeed seen to lie in an amorphous layer between the stratum laxum and the stratum compactum of the corium. This amorphous layer is not present in all species of frog which may explain the low Ca^{++} levels found in skin of frogs from some species.[3]

The calcium levels through the rest of the skin appears normal except for isolated places in the stratum laxum where the Ca^{++} concentration may be as high as 50 to 100 mM/Kg. As the complicated nature of the skin requires additional histological work to correlate these locations of higher Ca^{++} with known features of the skin, we are not in a

position at this time to comment on these isolated pockets.

Using a hydroxyapatite standard, it was determined that the Ca^{++} concentration in the amorphous layer is as high as 4 M/Kg. The ratio of counts of calcium to phosphorus in the amorphous layer was 1.57 while the ratio was 1.60 in hydroxyapatite. As we do not consider the difference significant, the calcium is most probably present in the form of hydroxyapatite.

Line scan profiles taken across the skin for Na^+ and Cl^- reveal a gradual rise in concentration of these ions across a distance of 5 to 10 μ in the lowermost or basal layer of the stratum germinativum. This is precisely the location of the Na^+ pump as presented in[6] the Koefoed-Johnsen-Ussing model of the frog skin Na^+ pump system. We find no evidence of increased Na^+ concentration in the amorphous layer between the stratum laxum and stratum compactum that one might expect from the autoradiographic data.[2]

The large calcium pool in the abdominal skin of the Rana pipiens is located in an amorphous layer between the stratum laxum and stratum compactum of the corium. This calcium is in a mineralized form, most probably hydroxyapatite, which because of its form and remoteness from the sight of the Na^+ pump, plays no direct role in the active transport of Na^+.

REFERENCES

1. Romeu, F. G., A. Salibián, and S. Pezzani-Hernández, The Nature of the In Vivo Sodium and Chloride Uptake Mechanisms through the Epithelium of the Chilean Frog, J. of Gen. Physiol., 53:816-835, 1969.

2. Imamura, A. H. Takeda, and N. Sasaki, The Accumulation of Sodium and Calcium in a Specific Layer of Frog Skin, J. Cell. and Comp. Physiol., 66:221-226, 1965.

3. Zadunaisky, J. A. and M. A. Lande, Calcium Content and Exchange in Frog Skin, Fed. Proc. 29:724, 1970.

4. M. J. Ingram and C. A. M. Hogben, Procedures for the Study of Biological Soft Tissue with the Electron Microprobe, Developments in Applied Spectroscopy, 6:43-64, 1968.

5. Applied Research Laboratories, Glendale, California.

6. Koefoed-Johnsen, V., and H. H. Ussing, The Nature of the Frog Skin Potential, Acta Physiol. Scand., 42:298-308, 1958.

LIMITATIONS ON Si(Li) X-RAY ENERGY ANALYSIS SYSTEMS AT HIGH COUNTING RATES

D. A. Gedcke, E. Elad, and G. R. Dyer
ORTEC, Incorporated
Oak Ridge, Tennessee 37830

In using the Si (Li) energy analysis systems on microprobes, fluorescence analyzers, and diffractometers, operation at high counting rates is often encountered. Unfortunately, the high counting rate limitations of these systems are not well publicized. These limitations are determined by the low noise preamplifier, the amplifier, and the multichannel pulse height analyzer (MCA).[1,2] However, in well-designed systems the amplifier provides the main limitation.

The preamplifier indirectly limits the high counting rate performance by requiring long amplifier shaping time constants, τ (wide pulses), in order to obtain optimum resolution. Optimum pulse widths in state-of-the-art systems are approximately 30 μsec for τ = 6 μsec (compared to 5 μsec for proportional counters). This long pulse duration constitutes the dominant deadtime of the system (assuming a 50-MHz MCA), typically causing 20% deadtime losses at 7,000 counts/sec. For higher counting rates, shorter pulse widths are necessary at the expense of energy resolution. Under these conditions the MCA processing time becomes the limiting deadtime. The average 500-channel MCA deadtime is 10 μsec for a 50-MHz ADC and 5 μsec memory cycle time.

Figure 1 shows the deadtime losses versus counting rate measured at the amplifier output. The deadtime losses for τ = 10 μsec and τ = 6 μsec are large even at low counting rates. The 2 μsec curve extends the 20% deadtime loss limit to 30,000 counts/sec. The deadtime losses are a strong function of counting rate above the 20% point. If no correction is applied, these losses become a limit of accuracy in quantitative analysis. The dashed curve in Fig. 1 shows the deadtime correction achievable with the livetime clock in the MCA. This curve clearly shows that to obtain 2% quantitative accuracy, the maximum counting rate is limited to 7,000 counts/sec (20% uncorrected deadtime losses). Similar results are obtained for other time constants, provided the uncorrected deadtime losses do not exceed 20%. To achieve this accuracy, the MCA must measure deadtime from the start of the amplifier pulse (not offered on all MCA's), and no biased amplifiers or stretchers can be introduced between the amplifier and the MCA.

The effect of counting rate on energy resolution is shown in Fig. 2. The best resolution (163 eV) is obtained at 10 μsec. For shorter time constants, poorer resolution results; but the flatness of the curve is preserved to higher counting rates. Special preamplifier feedback configurations are required to achieve flatness of the resolution curve below the 20% loss point. Above 20% deadtime losses, the resolution degrades rapidly with counting rate,

due to the amplifier baseline restorer losing control as the available baseline vanishes. Repeatability of performance at counting rates above 20% deadtime loss is unreliable and, therefore, operation at such counting rates is undesirable.

Figure 3 illustrates the counting rate limitations caused by the baseline restorer losing control. At high duty cycles, the baseline shifts to a negative value and causes a downward shift in the energy spectrum. In dynamic situations (i.e., distribution mapping on microprobes) this calibration shift may have the appearance of a gain shift. Both effects can introduce serious errors even into qualitative analysis. It is clear from Fig. 3 that the 20% deadtime loss points indicate the safe upper limit on the counting rate.

In conclusion, for qualitative analysis, lack of spectral distortion is important. The 20% deadtime loss points have been shown to represent the upper counting rate limit to avoid resolution broadening and energy calibration distortions. For quantitative analysis, deadtime losses are also important. In adequately designed systems the MCA can properly correct for losses up to the 20% point.

---

1. E. Elad, ASTM Technical Workshop on Energy Dispersion X-Ray Analysis, Toronto, June 24, 1970 (to be published).

2. F. J. Walter, ASTM Technical Workshop on Energy Dispersion X-Ray Analysis, Toronto, June 24, 1970 (to be published).

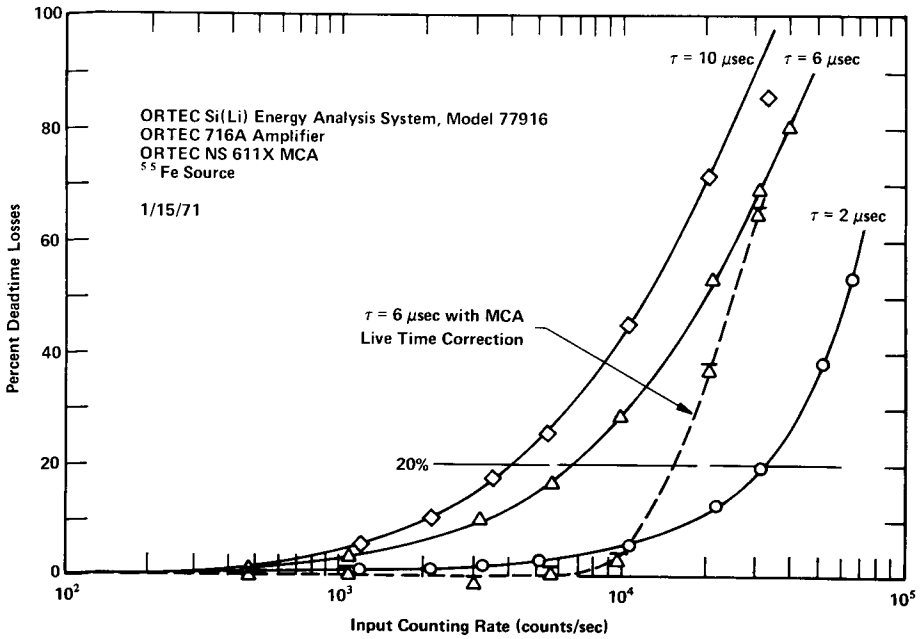

Figure 1. Deadtime Losses vs. Counting Rate for τ = 2, 6, and 10 μsec. The Dashed Curve Shows the Results of Deadtime Loss Corrections in the MCA.

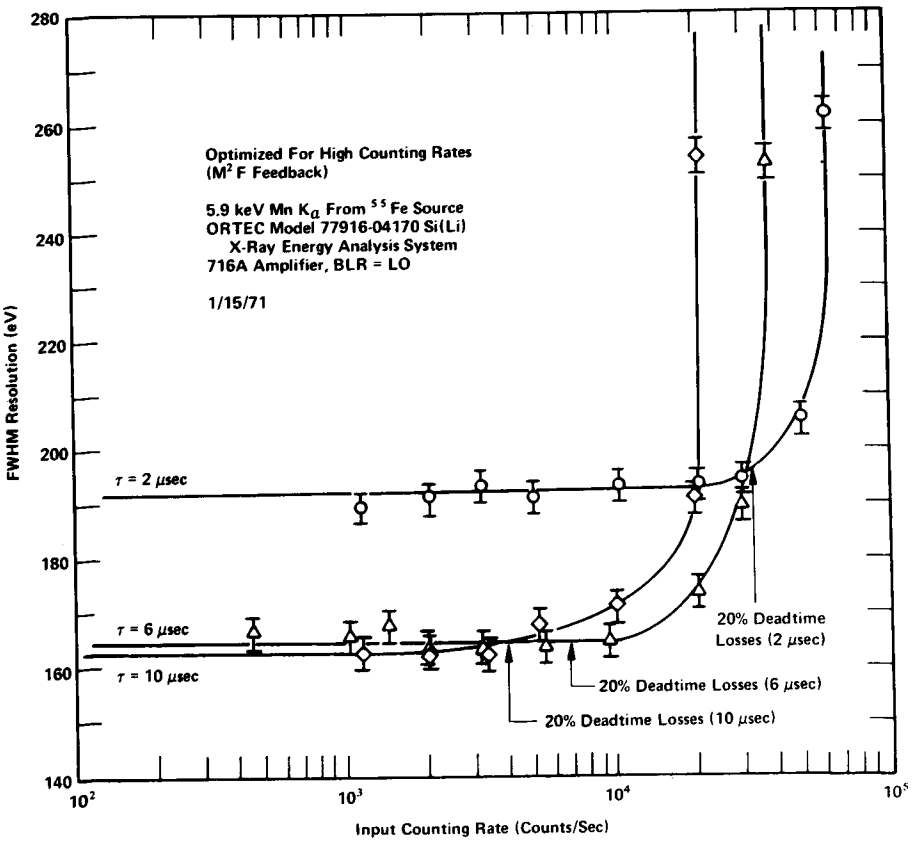

Figure 2. Resolution vs. Counting Rate for τ = 2, 6, and 10 μsec.

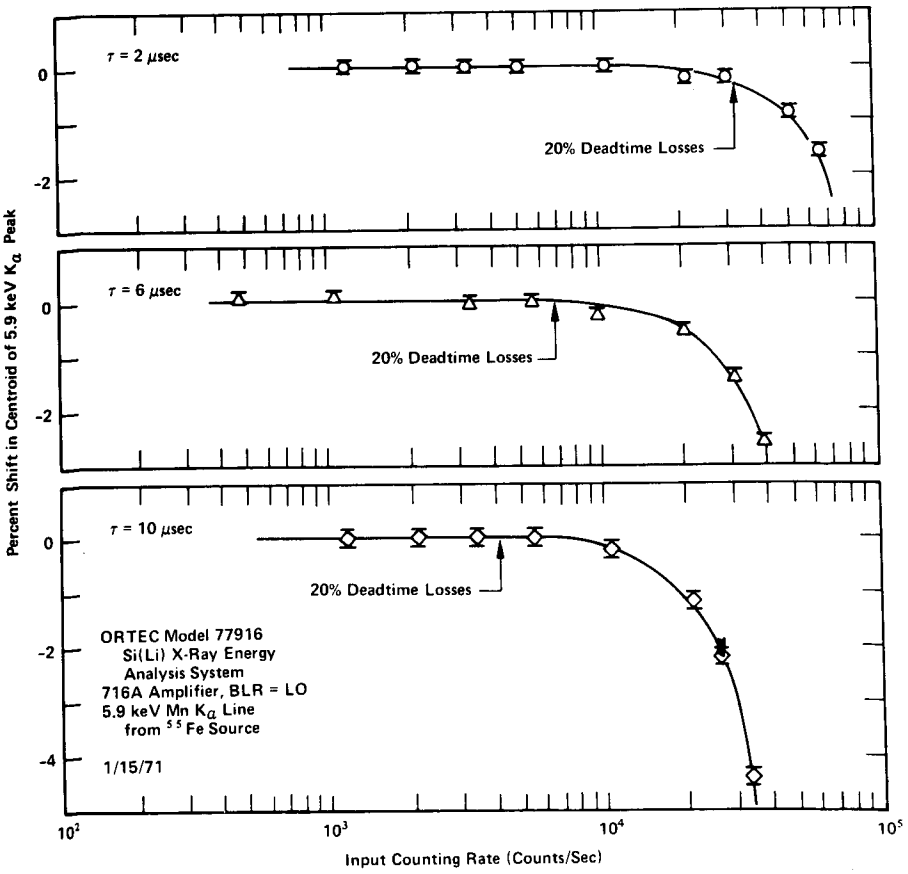

Figure 3. Baseline Stability vs. Counting Rate for τ = 2, 6, and 10 μsec.

COMPARISON OF SEMI-QUANTITATIVE ANALYSES MADE WITH ENERGY AND WAVELENGTH DISPERSIVE ANALYZERS OF EXTRACTED INTERMETALLIC PARTICLES

G.P. Sabol and C.J. Spengler
Westinghouse Research Laboratories

The use of wavelength dispersive (WD) and energy dispersive (ED) x-ray spectrometers for quantitative analysis of bulk samples has been well documented[1]. However, in some metallurgical investigations chemical analysis is often required of discrete micron or sub-micron sized precipitate particles. To perform an accurate analysis of such particles, extraction replica techniques have been utilized[2,3] to isolate the particles from the matrix for a direct analysis in the electron-beam microanalyzer (EBM). It is advantageous because of the better imaging capability of the scanning electron microscope (SEM) to use this instrument, in conjunction with an ED x-ray spectrometer, for the chemical analysis. Therefore, it was the objective of this investigation to compare results obtained on comparable specimens, both bulk and particulate, with use of both the WD-EMB and ED-SEM systems.

The specimens were bulk $ZrCr_2$ and extracted particles of $ZrCr_2$. The particles contained 3 w/o iron in solid solution with the chromium and ranged in size from 0.5 to 10 μm in diameter, with most particulates 2-3 μm.

The WD-EBM system used was a MAC-400 model, take-off angle 38.5°, with LiF crystal/sealed proportional counter and PET crystal/flow proportional counter spectrometers. The operational parameters were 20 keV and 0.03×10^{-6} amperes target current (on pure Zr). The ED-SEM system used was a Cambridge Steroscan Mark IIA with Nuclear Diodes ED x-ray analysis system (20 ev/channel). The working distance, beam current, and acceleration voltage were held constant at 10 mm, 9.6×10^{-10} amperes, and 20 keV, respectively.

Analyses with the ED-SEM system were made at different take-off angles by changing the tilt of the specimen stage. The geometrical relationship of the electron beam, x-ray detector collector, and axis of specimen stage tilt are not known with sufficient accuracy to state the effective x-ray take-off angle. Therefore, the data are referenced to the specimen stage tilt. The effect of stage tilt, and hence take-off angle, was determined for the pure metals and bulk $ZrCr_2$ at tilts between 5° and 80°. The particulates were analyzed at tilts of 30, 40, and 50°.

The bulk $ZrCr_2$ was analyzed with the ED-EBM system as an unknown against pure standards. The k-values were corrected for absorption[4] and atomic number effect[5]; the fluorescence correction[6] was negligible. The corrected analysis Zr-0.463, Cr-0.532 agrees well with the theoretical composition (Zr-0.467 and Cr-0.533, weight fraction). Six particulates were analyzed, also against pure standards. The x-ray intensities were corrected only for background and dead time and the k-values were normalized to total 1.00 wt fraction. Table I shows the normalized k-values.

In the analysis of the bulk $ZrCr_2$ against pure standards with the ED-SEM system the respective x-ray intensities varied with changing tilt as shown in Fig. 1. The effect of the take-off angle on the x-ray absorption is more apparent on the 6.07Å ZrLα than the 2.29Å CrKα or 1.94Å FeKα x-rays. Also from Fig. 1 it is seen that the Zr and Cr k-values will vary with tilt. At low tilts, 0-10°, the Cr k-value varies from 0.15 to .43. From 10-40° the Cr k-value increases gradually from 0.43 to 0.50; above 40° tilt it is constant at 0.50 to 80° tilt. The Zr k-value, at tilts over 10°, increases gradually from 0.37 to 0.48 up to 80° tilt. No corrections were applied to the k-values because of the uncertainty of the effective x-ray take-off angle. Seven particulates (including the six analyzed with the WD-EBM system) were analyzed against pure standards at tilts of 30, 40, and 50°. Table I shows the normalized k-values. The variation of the respective k-values with tilt is due partially to the variation of the x-ray intensity from the bulk standards, and predominantly to changes in surface scattering unique to the geometry of each particle as it is rotated under the electron beam.

The respective k-values for each individual particulate determined at 40 and 50° tilt with the ED-SEM system bracket the comparable k-values determined with the WD-EBM system.

Inspection of the analytical results for both the bulk $ZrCr_2$ and the particulates indicates that at a stage tilt of 45° the effective x-ray take-off angles are comparable for both systems. The k-values of the particulates, adjusted to total 1.00, indicate that the particulates are small enough to ignore the absorption and atomic number corrections. This is consistant with the findings of others[7]. The WD-EBM system gave better analytical results only because the geometrical aspects of the x-ray generation are better understood. The ED-SEM should produce comparable results when quantitative data are known for take-off angles, beam incidence, and working distance.

References

1. Proceedings of the 5th National Conference on Electron Microprobe Analysis, (1970).
2. M.J. Fleetwood, G.M. Higginson, and G.P. Miller, Brit. J. Appl. Phys., 16 (1965) p. 645.
3. M.J. Fleetwood, Electron Microscopy and Microanalysis of Metals, J.A. Belk and A.L. Davies, ed., Elsevier Publishing Company (1968) p. 225.
4. P. Duncumb and P.K. Shields, The Electron Microprobe, John Wiley and Sons (1966) p. 284.
5. P. Duncumb and S.J.B. Reed, Quantitative Electron Probe Analysis, NBS Special Publication 298 (1968) p. 133.
6. S.J.B. Reed, Brit. Jour. Appl. Phys., 16, (1965) p. 913.
7. B.R. Banerjee and W. D. Bingle, The Electron Microprobe, John Wiley and Sons (1966) p. 653.

TABLE I

k-VALUES OF ANALYZED $ZrCr_2$ PARTICULATES

Specimen	WD-EBM			ED-SEM								
				30°			40°			50°		
	Zr	Cr	Fe	Zr	Cr	Fe	Zr	Cr	Fe	Zr	Cr	Fe
A	.475	.483	.042	.491	.473	.036	.486	.484	.030	.451	.518	.031
B	.485	.490	.025	.499	.468	.033	.477	.489	.034	.458	.504	.038
C	.478	.496	.026	.499	.472	.029	.476	.490	.034	.467	.502	.031
D	.456	.508	.035	.516	.455	.029	.498	.468	.034	.468	.503	.029
E	.477	.495	.028	.487	.485	.028	.452	.513	.035	.428	.540	.032
F	.468	.491	.041	.475	.491	.034	.464	.499	.037	.450	.519	.031
G	-	-	-	.503	.469	.028	.520	.444	.036	.528	.442	.030
Avg.	.473	.494	.033	.496	.473	.031	.482	.484	.034	.464	.504	.032
Theoretical	.466	.503	.031									

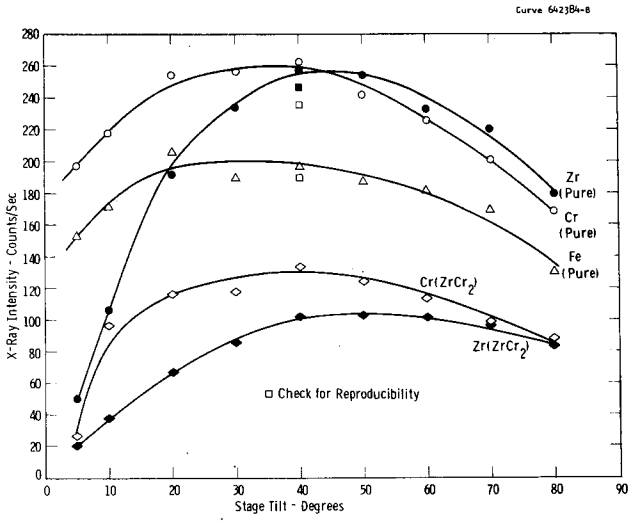

Fig. 1—Variation of X-ray intensity with tilt of specimen stage for pure standards and bulk $ZrCr_2$

PRODUCTION OF ELECTRON PROBES A FEW Å IN DIAMETER*

Albert V. Crewe
Departments of Physics and Biophysics and Enrico Fermi Institute
The University of Chicago, Chicago, Illinois 60637

During the past several years we have undertaken a program to improve the resolution of the scanning microscope. The aim of this program was to produce electron probes a few angstroms in diameter containing an adequate electron current to produce a micrograph in a few seconds. The competitive instrument for producing micrographs with a few Å resolution is the conventional transmission electron microscope, which has a point resolution in the neighborhood of 4 Å. The aim of our program was to produce a scanning microscope having comparable resolution.

If we assume that an acceptable electron micrograph contains approximately one million resolution elements and that an acceptable electron intensity would be 1000 incident electrons per resolution element, we see that it takes 10^9 electrons to form a micrograph. The micrograph can be formed in 10 seconds, and we therefore need an electron current of a few times 10^{-10} amps.

This requirement of the size of the focused spot and the beam current places a severe restriction upon the kinds of electron source which can be used in such a microscope, and in particular it means that a hot tungsten filament cannot be used because the inherent brightness is much too low. A field emission source appears to be the only one capable of being used.

Much of our work, therefore, has consisted of the engineering development of field emission sources, together with a suitable electron gun for subsequent acceleration. We have found that our design of source and gun is capable of producing a current of about 10^{-10} amps in a 100 Å diameter focused spot without the aid of any other focusing elements. This device alone can be made into a very simple but effective scanning microscope.

In order to reduce the spot size, we have constructed a second instrument which consists of the field emission source, the electron gun, and one short focal length magnetic lens. This machine focuses a beam of 30 kv electrons into a spot of 5 Å diameter which can contain up to 5×10^{-10} amps. With this machine we have been able to demonstrate that single heavy atoms can be seen in the microscope.

There are two ways in which the performance of our current instrument can be improved. The first of these is by increasing the voltage of the microscope. This reduces the electron wavelength. We have designed a 100 kv machine which uses two magnetic lenses and which should be able to produce a focused spot of electrons smaller than 3 Å in diameter and containing a current of more than 10^{-10} amps, which is adequate for microscopy.

*Work supported by the U. S. Atomic Energy Commission.

The other way to improve the performance of this machine is to attempt to eliminate the effect of the spherical aberration of the magnetic lenses, for it is the spherical aberration which limits the spot size at the moment. A spherical aberration corrector consisting of four quadrupole lenses and three octupole lenses is now under construction. In theory it would allow us to correct the spherical aberration of the final focusing element in the microscope. If this can be achieved in practice, the resolution--that is, the spot size--should be reduced considerably below 3 Å, while at the same time the current in the focused spot should remain constant.

QUANTITATIVE THEORY OF SPUTTERED ION MASS ANALYSIS

C. A. Andersen

Hasler Research Center
Applied Research Laboratories
Goleta, California

An analytic model has been developed (1) for the interpretation of sputtered ion emission from samples bombarded with high energy beams of reactive gases. It has been demonstrated that both positive and negative sputtered ion emission can be enhanced and controlled by the proper chemical selection of the primary bombarding ion beam. The analytic model proposed that sputtered atoms and ions created in the atomic collisions initiated by the bombardment process are subject to electron attachment from the surface of the sample. Electron attachment in the majority of cases is proposed to be a thermionic process governed by the Fermi-Dirac distribution of electrons and the effective electron temperature of the bombarded surface. The proposed model states that ions of different chemical elements from a single matrix undergo the same degree of electron attachment because of the common surface potentials affecting them. Quantitative interpretation of the sputtered ion yields from a single matrix, therefore, reduces to understanding the initial ion generation process.

In the present theory it is assumed that the excitation states of the atoms at the surface of the bombarded sample can be described as if the sputtered ion source were a plasma in partial thermal equilibrium. Under these conditions the Saha-Eggert ionization equations (2) can be used to predict the ratio of the number of atoms in one charge state to the number of atoms of the same chemical element in the succeeding charge state. The product of the number of atoms in two successive stages of ionization and the electron concentration in the excited sputtered plasma is given in terms of the atomic partition functions of the two ionization stages, the ionization potential of the lower state, and the kinetic ion temperature. The experimental determination of the number of ions in two successive stages of ionization and a knowledge of the atomic partition functions permits the calculation of the electron concentration and the kinetic ion temperature of the sputtered plasma.

Figure 1 shows the ratio of the number of sputtered positive single charged ions to the number of neutral atoms as that ratio is modified by the atomic partition functions of the two ionization stages plotted as a function of the ionization potential for several elements from a well characterized mineral standard. The electron concentration and the kinetic ion temperature of the sputtered plasma were obtained by solving a pair of simultaneous ionization equations in which the observed ratios of the number of doubly charged to singly charged ions for two different elements were used. These data are directly observable in the mass spectra taken from the sample. The fit of the data to a straight line on such a graph supports the assumption that the sputtered plasma is in partial thermal equilibrium (3).

Sputtered ion intensities from metals can be described with the same ionization equations. In these cases the kinetic ion temperatures are observed to be

lower. Sputtered negative ion intensities and molecular ion intensities can be interpreted with the same model.

It is possible to relate the kinetic ion temperatures obtained from the ionization equations, using the observed ratios of doubly to singly charged ions, to the inelastic energy losses of the primary bombarding ion in the sample. The temperatures calculated from experimental data taken at different accelerating potentials of the bombarding ion beam correlate well with the inelastic stopping power calculated using the model developed by Lindhard and Scharff (4). For a given sample, increasing the accelerating potential of the bombarding beam increases the kinetic ion temperature attained in the sputtered plasma.

The quantitative method proposed is to assume the sputtered plasma to be in partial thermal equilibrium and to apply the Saha-Eggert ionization equations to the ion intensities observed in the sputtered mass spectrum. The kinetic ion temperature and the electron concentration of the sputtered plasma are used in these ionization equations to predict the degree of ionization of all the elements observed in the mass spectrum of the sample. The observed ion intensities are corrected for this degree of ionization to yield the total number of atoms of that element in the sputtered plasma. These totals, for all the elements in the mass spectrum, give the atomic composition of the sputtered plasma which has been shown to be representative of the solid sample under bombardment.

It should be noted that the kinetic ion temperature and electron concentration of the sputtered plasma can often be obtained from ratio of doubly to singly charged ions in the mass spectrum. This ratio is independent of the concentration of the element contributing the ions and opens the possibility for standardless analysis of unknown compounds. Such standardless analyses of mineral specimens have been accomplished with relative errors in the determination of major elements of less than 5%. The quantitative method proposed has been incorporated in a general computer program entitled CARISMA, (Corrections to Applied Research laboratories Ion Sputtering Mass Analyzers), (5).

REFERENCES

1. C. A Andersen, Third, Fourth and Fifth Natl. Electron Microprobe Conf., Chicago, 1968; Pasadena, 1969; New York, 1970; J. Mass Spect. and Ion Physics, 2 (1969) 61; 3 (1970) 413.

2. M. N. Saha, Phil. Mag., 40 (1920) 472,809; Z. Physik 6 (1921) 40: J. Eggert, Z. Physik 20 (1919) 570.

3. C. H. Corliss, J. Res. Nat. Bur. Std. A. Phys. and Chem. 66A (1962) 169.

4. J. Lindhard and M. Scharff, Phys. Rev. 124 (1961) 128.

5. J. R. Hinthorne and C. A. Andersen, Appl. Res. Labs. Internal Rept. (in preparation).

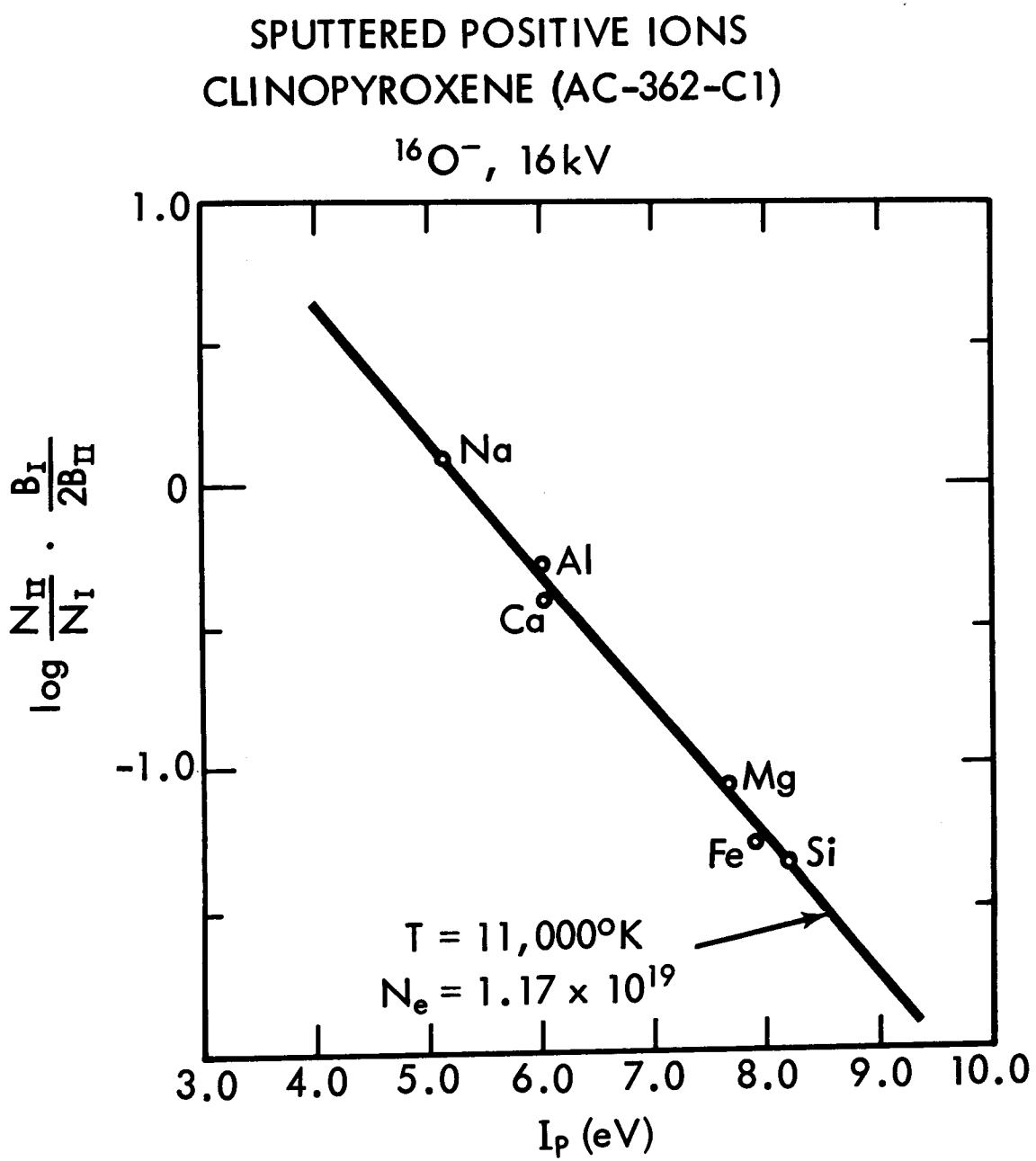
SPUTTERED POSITIVE IONS
CLINOPYROXENE (AC-362-C1)
$^{16}O^-$, 16kV
1.0
0
-1.0
$\log \frac{N_{II}}{N_I} \cdot \frac{B_I}{2B_{II}}$
Na
Al
Ca
Mg
Fe
Si
T = 11,000°K
$N_e = 1.17 \times 10^{19}$
3.0
4.0
5.0
6.0
7.0
8.0
9.0
10.0
I_p (eV)

SURFACE CHEMISTRY CHARACTERIZATION OF ALUMINA CERAMIC SUBSTRATES BY ION MICROPROBE MASS ANALYSIS

Donald K. Conley
Western Electric Co.

The surface chemistry of alumina ceramic substrates was determined in an effort to relate it to the adherence characteristics of sputtered tantalum nitride thin films. This was accomplished by obtaining concentration depth-profiles for the impurity elements with the Applied Research Laboratories ion Microprobe Mass Analyzer.

When thin films of tantalum nitride are sputtered onto ceramic substrates, various substrate lots exhibit varying degrees of sputtered tantalum film adherence. The impurities contained in the ceramic evidently play a major role in the bonding mechanism since tantalum nitride adhesion to a sapphire surface (pure alumina) is poor. It has been observed that alumina substrates, with good adherence characteristics, which then have their surfaces either mechanically ground or acid etched exhibit poor adherence. If the lot which has been acid etched is then refired, it regains its good adherence characteristics. It has been assumed that these effects are partially due to the removal of impurities concentrated on the surface which evidently enter into the bonding mechanism.

A good adherence lot of ceramic substrates (as received) was divided into three portions. The first portion was left in the "as received" condition, the second and third portions were acid etched with one of these portions receiving a refiring treatment. Impurity concentration-depth profiles were obtained for Si, Mg, Ca, Sr, Ba, Na, K and B of samples from the three aforementioned portions. This was done in an attempt to qualitatively determine if a specific ion or ionic species accounts for the difference in good and bad adherence characteristics.

Raw data was reduced to chemical composition using C. A. Anderson's (Applied Research Laboratories) quantitative model and computer programs developed by John Colby of Bell Telephone Laboratories. The corrected digital data was converted to analog form through use of a Cal-Comp plotter to obtain the concentration depth curves.

Data will be shown which represents the super-imposition of the "as received," acid etched and acid etched then refired concentration-depth curves for each of the following elements: magnesium, silicon, potassium, sodium and calcium. From these curves it is seen that the refiring cycle brings the impurity concentrations back up to the original levels or in two cases, magnesium and sodium, to even higher levels. This is economically important since it allows one to reclaim ceramic substrates which have become surface contaminated or have had errors occur in metallization processing by acid etching and subsequent refiring at 1500° C.

In the typical concentration depth curves, one observes that most of the impurity above the background concentration or bulk level is contained in the first 4000 A of the surface. These minor quantities (up to one weight percent) concentrated over a relatively great distance into the ceramic surface could possibly be indicative of solute surface segregation by the vacancy drag mechanism.

The eight curves which deviated from the 88 "typical" distribution curves were those of magnesium and barium. Magnesium and barium oxides evidently play an important role in whatever processes are occurring at the surface and appear to be related to adherence characteristics.

The most significant difference in the distribution with depth of the various impurity elements when comparing the as received, the refired and the acid etched samples is the surface depletion of magnesium in the acid etched sample. It is possible that this phenomenon is related to the bad adherence characteristics of the acid etched alumina surface due to a lack of magnesium to enter into the bonding mechanism. Bulk analyses performed between one and two microns from the surface showed that all the impurities are more concentrated in a known (bad adherence) alumina lot as compared to a known (good adherence) alumina lot.

Table I shows that although the bulk analysis of the bad lot (Column 6) contains more impurities than the good lot (Column 3), the good lot has higher surface concentrations of magnesium, silicon and barium (Column 1) than the bad lot. In Table I for the bad lot, we also observe a sub-surface depletion effect as we go from surface to bulk for magnesium, silicon and barium. However in the good lot this sub-surface depletion effect for these elements is absent.

Scanning electron micro-graphs taken by our laboratory of the alumina substrate has shown the presence of a glassy appearing, smooth textured second phase in increasing amounts as the tantalum film adherence has degraded. It is suspected that this phase has been formed by magnesium and barium oxides acting as a flux in conjunction with SiO_2 and Al_2O_3 to lower the melting point within the localized region. It is theorized on cooling that a phase change in the surface layer occurs that may effect the availability of Mg^{+2} ion for bonding reactions with Ta_2N.

It is theorized that the other phase contains the Mg^{+2} ion which is available to enter into the bonding mechanism. It is, however, recognized that under prolonged annealing or under reducing conditions MgO can escape from the theorized good surface phase.

Table I

Ion Microprobe Analyses (PPM Weight)
Good and Bad Adherence Lots

	(1)	(2)	(3)	(4)	(5)	(6)
	Good			Bad		
Element	Surface	Sub-Surface	Bulk	Surface	Sub-Surface	Bulk
Boron	8.	0.8	--	4.0	0.9	--
Sodium	9100.	1000.	683.	9100.	2800.	1359.
Magnesium	1733.	800.	845.	1080.	585.	929.
Silicon	3300.	1033.	946.	1300.	400.	2156.
Potassium	9500.	1000.	305.	11000.	1250.	767.
Calcium	1550.	350.	266.	3250.	1000.	1259.
Titanium	32.	21.	27.	71.	22.	23.
Barium	170.	40.	35.	68.	36.	46.

"ION SCATTERING SPECTROMETRY - A NEW TECHNIQUE FOR SURFACE COMPOSITION ANALYSIS"

By R. F. Goff
Central Research Laboratories
3M Company
St. Paul, Minnesota 55101

A sensitive method of surface composition analysis is obtained through monitoring the binary scattering of low energy noble gas ions from surface atoms. Such analyses have been shown to be accomplished with simplified instrumentation and to be sensitive primarily to the average first surface monolayer. (1) Identification of surface atoms is accomplished by measurement of the energy spectra of the scattered binary ions at a given scattering angle. These energy spectra consist of a number of peaks at various energies; the number of peaks corresponds to the number of constituents present, and the energy corresponds uniquely to the mass of each constituent through the following relation:

$$\frac{E_1}{E_o} = \frac{M_s - M_o}{M_s + M_o}$$

where: E_1 = Energy of scattered noble gas ion
E_o = Energy of probe noble gas ion
M_s = Mass of surface atom
M_o = Mass of noble gas ion

Thus, by selection of the probe ion M_o and measuring the scattered ion energy ratio E_1/E_o, the mass of the unknown surface atom is uniquely determined. Furthermore, the height of each peak gives a relative measure of the quantity of each constituent present. Elements throughout the periodic table can be identified in multi-component surfaces with no extra signal processing. Since the binary scattering process is mass sensitive, either high atomic weight materials (e.g. Au or Pb) or light elements (e.g. O or Al) are identified respectively by a single scattering peak. Further controlled ion bombardment etching of a sample yields a depth profile analysis - the elemental composition of successive atomic sublayers.

The instrument produces a nominal 1 mm diam. He^+ beam throughout an operating range of 300-3000 eV; by additional focusing adjustments beam diameters from 0.5 mm to several mm diam. may be achieved yielding current densities of from 1 - 50 uA/cm^2. Through adjustment of both ion beam focusing and static gas pressure, the current densities may be widely varied yielding average monolayer removal times as long as an hour.

A spectra obtained with 1500 eV He^+ ions scattered from an alloy surface is shown in Figure 1. ②

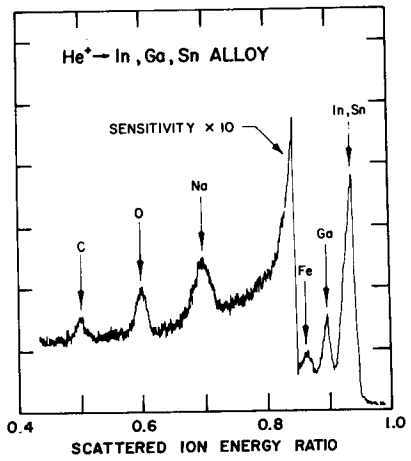

Figure 1

The ordinate is a plot of the number of ions scattered and the abscissa is a plot of the scattered ion energy ratio. One energy ratio (E_1/E_O) directly gives one mass (M_S) within the resolving power of the instrument. In actual instrument operation, this energy ratio is slowly scanned from 0 to 1 yielding a mass range from M_O to ∞. The alloy examined consists of a terinary compound of In, Ga, Sn on a stainless steel substrate. In addition to peaks due to Sn, In and Ga, a peak resulting from He^+ scattered from Fe is noted, a result of incomplete coverage of the stainless steel substrate. Note that In(115) and Sn(119) are not resolvable with He^+ probe ions but yield a single scattering peak. Ar^+ ions could be utilized to resolve these two peaks. C, O, and Na are surface contaminants observed in the first few spectra taken on the surface.

The unique ability of Ion Scattering Spectrometry to measure the composition of the first monolayer of atoms has had wide application in areas such as complex alloy studies, thin films, surface contamination monitor, oxidation-corrosion studies, determination of surface to bulk compositional gradients, and semi-conductor surface preparations. The analytical technique has been extended to include the direct examination of electrically insulating surfaces without the need for a conductive overcoat being applied. With this capability, surface composition analyses are directly obtained from ceramic, glass and plastic surfaces.

Examination of thin films and multi-layer thin film structures is a prime example of the dual utilization of the probe ion beam both to simultaneously analyze and controllably remove surface atoms. Such a composition depth profile is obtained for a thin film sandwich structure composed of 200Å of TiO_2 on 175Å of Au on a glass substrate. An initial spectrum from the TiO_2 film is

ELECTRON MICROPROBE INSTRUMENTATION FOR SOFT X-RAY SPECTROSCOPY APPLICATIONS

James S. Solomon
University of Dayton Research Institute, Dayton, O. 45409
and
William L. Baun
Air Force Materials Laboratory (LPA), W-PAFB, O. 45433

The quantitative and qualitative value of changes in fine features of soft X-ray spectra due to the chemical state of the analyzed specimen has been well documented in the literature. Electron microprobes are excellent soft X-ray sources with direct electron excitation and large take-off angles. The flow proportional detectors and curved crystal optics require little or no modifications for the detection and recording of finely resolved soft X-ray spectra. One such modification is reduced pressure detector operation, which results in very narrow pulse widths and improved signal to background ratios[1,2]. However, there are certain precautions that must be taken when operating detectors at reduced pressures[3].

Measuring spectral changes from recorded soft X-ray spectra with precision can be difficult and time consuming if data is extracted from analog strip chart recordings. To further complicate matters, low intensities are often encountered resulting in large statistical fluctuations in the data. This means a greater probability for measurement errors and misinterpretations. Therefore, the routine use of soft X-ray spectra for analytical applications is really only possible if fast, accurate, reliable, and reproducible automatic data acquisition and handling systems are used.

A typical automatic data acquisition system, outlined by the block diagram in Figure 1, incorporates a digital drive stepping motor to advance the spectrometer and digitizes the output data.

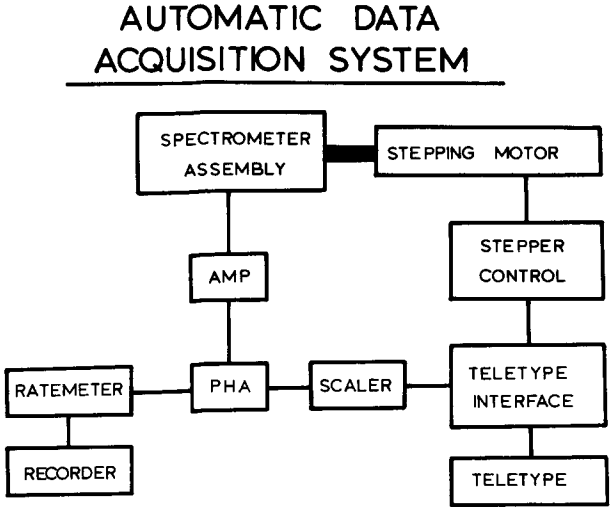

Fig 1 - Block Diagram of Automatic Data Acquisition System

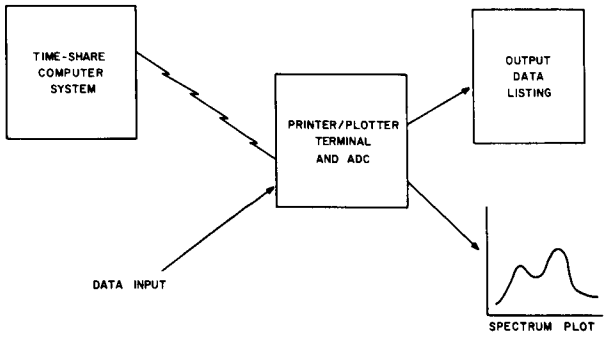

Fig 2 - Flow Diagram of Data Processing Steps

As seen in Figure 1, the signal from an X-ray detector in a spectrometer is amplified and passed on to a pulse height analyzer (PHA). There the signal is split going to a ratemeter and strip chart recorder output and to a printing scaler for digital output on a computer compatible papertape through a teletypewriter with papertape output. The scaler, with built-in timer, is connected to the teletypewriter and stepper control with a teletype interface.

The data collection sequence is initiated with the scaler which is preset for a specific counting time. When this preset time has elapsed the scaler stops counting and this information is printed out and punched on paper tape. When printout is completed the stepping motor advances the spectrometer the preset increment size and the scaler again starts counting data. This sequence automatically recycles until a preset number of steps is reached or the system is manually stopped. To achieve better data statistics the entire scan can be recycled several times, the counting time per step can be lengthened, or the scaler counting and printout can be recycled several times per step.

When data collection is completed the data can be rapidly processed and plotted by a commercial time-sharing computer system through a terminal and computer controlled digital plotter conveniently located to the microprobe laboratory. Figure 2 is a pictorial flow diagram showing the general steps involved to obtain a data listing and computer plotted X-ray spectrum from the experimental data. First a terminal is linked to a time-sharing computer system through a standard telephone with an acoustic data coupler (ADC). Then the data processing program is called and the experimental data, on papertape, is fed to the computer through the papertape reader of the terminal. Finally the processed data is made available for printout and plotting the spectrum.

The data processing program outputs a smoothed and normalized version of the original data. This, coupled with the plotting options of various plotting programs, enables the analyst to plot spectrum of any convenient size for comparison and spectral measurements. In addition, certain measurements can be taken directly from the data output listings without the necessity of making a plot. These include maximum positions, edge positions, intensity relationships, and band half widths.

References

1. N. Spielberg, in Adv in X-Ray Analysis, 10, p 534 (Plenum Press, New York, 1966).

2. B. Henke, in Adv in X-Ray Analysis, 12, p 480 (Plenum Press, New York, 1969).

3. L. S. Birks, Electron Probe Microanalysis, p 105 (Interscience Publishers, New York, 1963).

PHOSPHOROUS Kβ AND Kβ' EMISSION SPECTRA FOR SOME METAPHOSPHATES AND NATURAL APATITE MINERALS

R. G. Hurley and E. W. White
Materials Research Laboratory
The Pennsylvania State University
University Park, Pennsylvania 16802

Recent work in this laboratory has been directed toward the measurement of x-ray emission spectra with a microprobe and interpreting these shifts in relation to various crystal chemical parameters. Measurements of the Si Kβ and the Al Kβ x-ray emission band shifts for a large number of silicates, aluminosilicates and oxides using an electron microprobe have been reported by White and Gibbs[1,2]. More recently Gigl, Savanick and White[3] have applied the measurement of x-ray wavelength shifts to the characterization of thin Al-O-OH layers on an aluminum substrate. While Krause et al.,[4] have applied oxygen x-ray emission band shifts to the characterization of transition metal oxide surface layers.

The purpose of this investigation is to extend this work to the measurement and interpretation of phosphorous Kβ and Kβ' x-ray emission spectra for several metaphosphates and apatites.

An ARL model EMX electron microprobe operated at 25 keV and 1.5 x 10^{-7} amps was used to excite and analyze the phosphorous x-ray spectra. An electron beam diameter of about 100 μm was used in order to minimize specimen damage. A 4-inch radius curved crystal spectrometer equipped with an ADP x-ray analyzing crystal was used in conjunction with a thin window flow proportional detector.

The majority of the metaphosphates used in this study were in the form of powders pressed in a 1/4" diameter die to form a solid pellet. These then were coated with a thin layer of carbon to provide a conductive surface. The apatite mineral specimens were mounted in an epoxy resin, polished, and also coated with carbon.

Measurements of the phosphorous Kβ and Kβ' were made for the metaphosphates and apatite minerals with respect to an arbitrarily selected, but well characterized, aluminum orthophosphate.

Typical spectra recorded for the apatites in this investigation are reproduced in Figure 1. These spectra show that the Kβ and Kβ' for the hydroxyapatite is shifted to a higher energy than the cholorapatite. Although not shown the Kβ and β' of the fluorapatite falls between these two spectra. Data on changes in peak position and line widths are shown in Table I. The values are recorded as changes in peak position as measured at two-thirds height and referenced to the peak of aluminum orthophosphate.

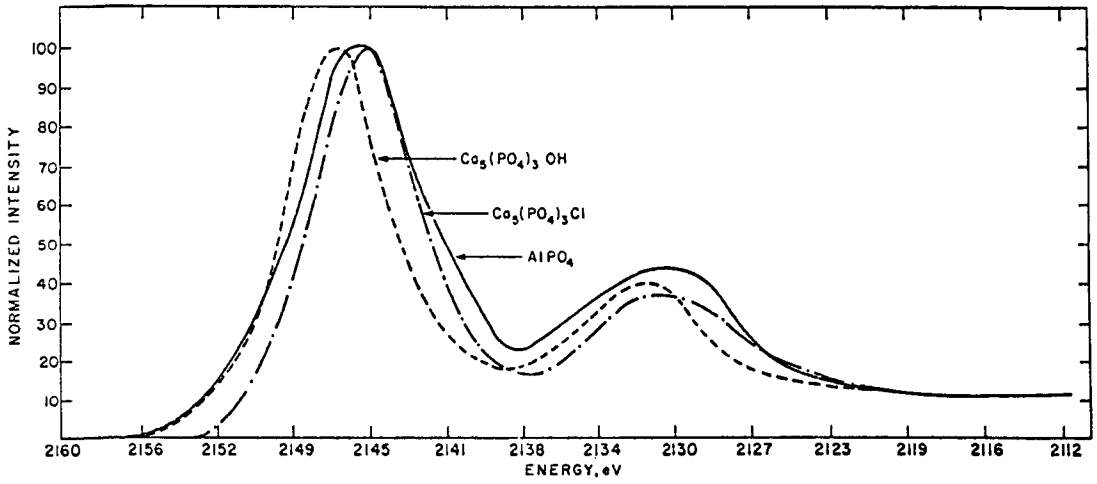

Figure 1. P Kβ and Kβ' Emission Spectra of Aluminum Orthophosphate, Cholorapatite, and Hydroxyapatite.

Some spectra have also been run using a flat germanium crystal in our soft x-ray spectrometer[5]. The highly perfect crystal and fine slits yield higher resolution spectra than from the probe. In spite of having used a phosphorous-containing analyzing crystal (ADP) in this investigation there appears to be no significant distortion in the phosphorous Kβ spectra.

REFERENCES

1. White, E. W. and Gibbs, G. V. (1969), "Structural and Chemical Effects on the Al Kβ X-Ray Emission Band Among Al Containing Silicates and Al Oxides," Am. Mineral., 54, 931.

2. White, E. W. and Gibbs, G. V. (1967), "Structural and Chemical Effects on the Si Kβ X-Ray Line for Silicates," Am. Mineral., 52, 985.

3. Gigl, P. D., Savanick, G. A., and White, E. W. (1970), "Characterization of Corrosion Layers on Aluminum by Shifts in Aluminum and Oxygen X-Ray Emission Bands," J. Electrochem. Soc., 117, 15-17.

4. Krause, H. B., Savanick, G. A., and White, E. W. (1970), "Oxygen X-Ray Emission Band Shifts Applied to the Characterization of Transition Metal Oxide Surface Layers," J. Electrochem. Soc., 117, 557.

5. Baun, W. L. and White, E. W. (1969), "A Vacuum Spectrometer for Studying The Chemical Effect on Soft X-Ray Spectra," Advances in X-Ray Analysis, 13, Plenum Press, New York, 237.

TABLE I

P Kβ and Kβ' wavelength shifts for some metaphosphates and natural apatites. The wavelength of the band from aluminum orthophosphate was used as the reference position.

Standard	Formula	Δ P Kβ (eV)	P Kβ width 2/3 ht. (eV)	Δ P Kβ' (eV)	P Kβ' width 2/3 ht. (eV)
Aluminum Orthophosphate	$AlPO_4$	0	5.6	0	5.5
Potassium Metaphosphate	$(KPO_3)_x$	0.9	6.5	0.7	6.6
Magnesium Metaphosphate	$Mg(PO_3)_2$	0.4	6.5	0.2	4.6
Zinc Metaphosphate	$Zn(PO_3)_2$	0.3	7.0	-0.2	6.4
Sodium Metaphosphate	$(NaPO_3)_x$	-0.5	7.0	-0.8	5.1
Chlorapatite	$Ca_5(PO_4)_3Cl$	-0.3	3.7	-0.3	3.9
Fluorapatite	$Ca_5(PO_4)_3F$	0.4	3.7	-0.4	3.9
Hydroxyapatite	$Ca_5(PO_4)_3OH$	-0.5	4.3	-0.1	4.1

CHARACTERIZATION OF SiO USING FINE FEATURES OF X-RAY K EMISSION SPECTRA

William L. Baun
Air Force Materials Laboratory (LPA)
Wright-Patterson Air Force Base, Ohio 45433

and

James S. Solomon
University of Dayton Research Institute
Dayton, Ohio 45409

The author of the recent review "Silicon Monoxide: Fact or Fiction"[1] failed to present results of X-ray emission analysis of SiO films. X-ray emission spectra provide convincing evidence that SiO in a condensed state consists of an intimate mixture of elemental silicon and silicon dioxide.

Si K emission spectra in the 7Å region are easily obtainable using electron microbeam probe analyzers such as the Hitachi XMA-S used in this work. In addition, commercial X-ray fluorescence equipment is capable of sufficient resolution to use some[2] of the spectral features to deduce the composition of SiO films. White and Roy used an electron microbeam probe to analyze SiO films and concluded from the splitting of the K band that the films were mixtures of Si and SiO_2.

The K band splitting may be used semiquantitatively to analyze SiO films. It is difficult to obtain quantitative results because the curves overlap and one component is asymmetrical and the other is symmetrical. With the commercial curve plotter used in this work (E. I. DuPont de Nemours and Company Model 310) it is not possible to skew only one curve in an overlapping mixture of curves. The data could be processed by computer, however, where synthetic curves of any shape could be programmed.

Further evidence that SiO is a mixture may be found in the position and intensity of Kβ', where the same relationships exist as in SiO_2. These results are in agreement with Mendel[3] who found using a commercial vacuum spectrograph and secondary excitation that the Kβ - Kβ' spacing in SiO remained approximately the same as in SiO_2 and the integrated intensity of Kβ' in SiO was about one-half that of SiO_2. With an electronic curve analyzer or with computer curve unfolding techniques, it would be possible to quantitatively analyze thin SiO films by obtaining integrated intensity from Kβ' and Kβ and relating the Kβ'/Kβ ratio to composition.

Another feature of the SiK spectrum which may be used to characterize SiO films is the Kα satellite pair $K\alpha_{3,4}$ which involve transitions from multiply ionized levels. These lines are several times as strong as Kβ and an order of magnitude stronger than Kβ', making measurements easier and statistics better. The satellite lines are very sensitive to chemical combination with $K\alpha_4/K\alpha_3$ about 0.60 in pure Si and nearly unity in SiO_2. Many different line profiles in the $K\alpha_{3,4}$ region are obtained for SiO films depending on vaporization conditions. Nevertheless, it has been possible in this work to match each contour by synthesizing curves for SiO_2 and Si and then adding these curves on the curve resolver. It is possible to obtain a calibration curve relating the composition of films with the area or peak heights in the

individual curves. Analyzed thick films and bulk specimens may be used as secondary standards. Figure 1 shows a typical $K\alpha_{3,4}$ spectrum from an SiO film along with curve (III) obtained by adding curves from Si(I) and SiO_2(II). Curve III was synthesized on the DuPont Curve Resolver by (1) matching curves from pure Si and SiO_2, (2) placing the curve from SiO_2(II) on the screen, and (3) gradually adding the curve from Si(I)until a match was achieved with the experimental SiO which had been placed on the resolver table. The area under each curve may be read directly from the instrument and related to composition of chemically analyzed samples and a calibration curve may then be prepared.

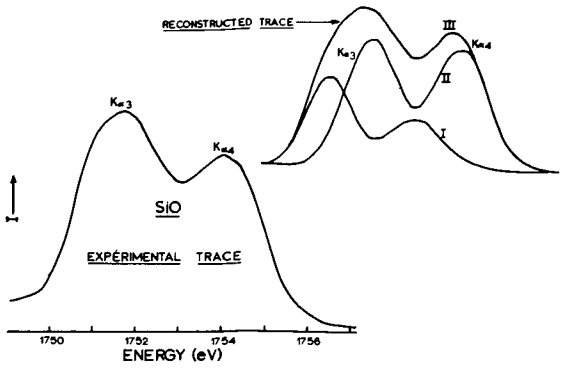

Fig 1 - Si $K\alpha_{3,4}$ Experimental Curve From SiO, Si(I), SiO_2(II) and Addition of I and II to Form Synthesized SiO Curve III.

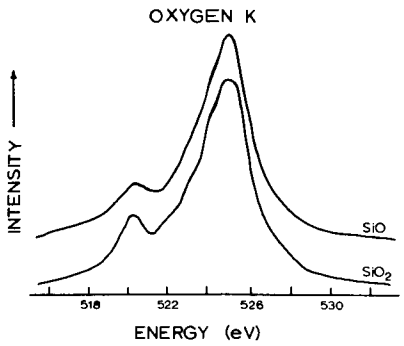

Fig 2 - Oxygen K Band for SiO and SiO_2 (α-quartz).

The oxygen K spectrum from SiO films is virtually identical to the spectrum obtained from SiO_2 (α-quartz) as seen in Figure 2. The oxygen K band requires at least four main gaussian components to match the curve shown in Figure 2. A small change in intensity of one of these components accounts for the slight difference noted on the low energy portion of the SiO curve. This may be interpreted as a change in population of a molecular orbital and could be an indication that the SiO_2 phase in SiO (1) is one of the high temperature phases, (2) contains stresses which have distorted the typical SiO_4 tetrahedral structure or (3) is slightly changed in Si - O stoichiometry. In addition, it is possible that the addition of impurities has disturbed one or more of the molecular orbitals compared to α-quartz.

Each of the lines and bands investigated in this work provides further proof that in the condensed phase SiO consists of a variable mixture of Si and SiO_2.

References

1. J. Beynon, Vacuum, 20, 293 (1970).
2. E. W. White and R. Roy, Solid State Communications, 2, 151 (1964).
3. H. Mendel, Koninkl. Ned. Akad. Van Wettenshappen B., 70, 276 (1967).

THE DISTRIBUTION AND OXIDATION STATE OF SULFUR IN STRUCTURAL CLAY PRODUCTS

By

George A. Savanick, Twin Cities Mining Research Center, Bureau of Mines, U. S. Department of Interior, Minneapolis, Minnesota
and
Eugene W. White, Materials Research Laboratory, The Pennsylvania State University, University Park, Pennsylvania

This paper examines the stages of sulfur burnoff that occur in a clay body during manufacture. The concentration, spatial distribution, and especially the oxidation state of the sulfur were determined as a function of kiln temperature. X-ray emission peak shifts are used for the oxidation state determinations.

A series of extruded bars of Clarion clay representing sequential stages in the kiln heating cycle were studied with an X-ray fluorescence spectrometer to determine the concentration and oxidation state of the sulfur in bulk, whereas an electron probe microanalyzer was used to determine the sulfur distribution and oxidation state on a microscale.

Oxidation state studies were carried out by comparing the SKα peak positions of the samples to similar measurements obtained from pyrite and gypsum. By assuming a linear relationship between peak position and sulfide/sulfate ratio, the extent of sulfate formation as a function of firing temperature was determined.

The sulfur concentration of the brick (table 1) remains practically constant up to 600° F, increases between 600° F and 1000° F as a result of dehydration, then decreases sharply until it practically vanishes at 2000° F. Wavelength shift data from bulk samples (table 2) indicates that very little oxidation occurs below 800° F, but that the proportion of sulfate sulfur in the brick increases progressively at higher temperatures.

A survey of the spatial distribution of the sulfur over the sample surface revealed that sulfur is concentrated either in recognizable pyrite grains or in iron oxide nodules which presumably are the oxidation products of pyrite. Only trace amounts of sulfur were detected outside these areas.

Wavelength shift measurements taken with the electron microprobe (table 3) indicate that the sulfides are oxidated to sulfates as the temperature is increased. The data from nodules that have lost most of their sulfur is somewhat imprecise because of the low signal to background ratio.

X-ray fluorescence of the grey "heart" of a nonuniformly oxidized brick

shows that it contained 0.032 percent sulfur (calculated as SO_3) while a completely oxidized area contained 0.004 percent SO_3. The nonuniformly oxidized brick exhibited three color zones: a grey center, a white periphery, and an intermediate area colored orange. Peak shift data (table 4) indicates that the sulfur contained in the nodules in the grey and orange areas exists in the sulfide state while the iron oxide nodules in the white portion of the brick contains predominately sulfate sulfur.

The results outlined above illustrate how chemical shift data gathered from the electron microprobe differs from measurements taken on an X-ray fluorescence spectrometer. The large area under primary X-ray excitation and the absence of the Bremsstrahlung with the consequent higher peak to background ratio dictates that X-ray fluorescence is suited for measuring peak shifts from low elemental concentrations in bulk. The elctron probe yields otherwise unavailable chemical state data from isolated microscopic areas because it permits the precise positioning of a selected spot under a finely focused static elctron beam.

The significance of this study is that it demonstrates the feasibility of performing peak shift measurements from low elemental concentrations and on isolated microscopic areas.

Table 1 - Description and Sulfur Content of Draw Sample

Code	Temperature at Draw	% SO_3	Comment
A-1	Raw Blend Sample	0.092	85% (-14 Mesh Clay)
			15% (-40 Mesh Clay)
B-1	Room Temp -80°F	0.085	Clay Mix-Air Dried
C-1	Dried to 350°F	0.089	
D-1	500°F	0.071	From Gas Fired Test Kiln
E-1	600°F	0.077	From Gas Fired Test Kiln
F-1	700°F	0.082	From Gas Fired Test Kiln
G-1	800°F	0.081	From Production Kiln
H-1	1000°F	0.1176	From Production Kiln
I-1	1200°F	0.084	From Production Kiln
J-1	1400°F	0.034	From Production Kiln
K-1	1600°F	0.009	From Production Kiln
L-1	1800°F	0.028	From Production Kiln
M-1	2000°F	0.005	From Production Kiln
N-1	2050°F	0.001	From Production Kiln
O-1	350°F	0.001	After Cooling at End of Kiln

Table 2 - SK_{α} Peak Shifts from Bulk Samples

as Determined by X-ray Fluorescence

Sample	Firing Temperature °F	$\Delta\lambda$*(Angstroms)	% Sulfide
B-1	80	0.0002	94
C-1	350	0.0008	74
D-1	500	0.0007	77
E-1	600	0.0006	80
F-1	700	0.0008	74
G-1	800	0.0024	20
H-1	1000	0.0024	20
I-1	1200	0.0021	30
J-1	1400	0.0028	7
K-1	1600	0.0023	24
L-1	1800	0.0025	17
M-1	2000	0.0029	7
N-1	2050	0.0030	0
O-1	2050	0.0024	20
Pyrite		0.0000	
Gypsum		0.0030	

* $\Delta\lambda = \lambda$ (Pyrite) - λ (Sample)

Table 3 - Peak Shifts in Nodules

Sample	Firing Temperature °F	Δλ*(Angstroms)	% Sulfide
A-1	80	0.0000	100
C-1	350	0.0004	88
E-1	600	-0.0008	100
F-1	700	0.0005	84
G-1	800	0.0016	50
H-1	1000	0.0024	25
I-1	1200	0.0030	6
J-1	1400	0.0018	44
K-1	1600	0.0023	28
L-1	1800	0.0014	56
M-1	2000	0.0023	28
N-1	2050	0.0022	31
O-1	2050	0.0022	31
Pyrite		0.0000	
Gypsum		0.0032	

*$\Delta\lambda = \lambda$ (Pyrite) - λ (Sample)

Table 4

Sulfur Kα Peak Shifts from Nodules in

Brick with a Severe "Heart" Development

	$\Delta\lambda$*
Nodules from Grey Area of Brick	-0.0001
Nodules from Orange Area	-0.0005
Nodules from White Area	0.0019
Pyrite	0.0000
Gypsum	0.0029

*$\Delta\lambda$ = λ (Pyrite) - λ (Sample); Mean of 10 Determinations

AN INTERPRETATION OF THE CHEMICAL EFFECT IN THE ALUMINUM AND OXYGEN X-RAY K-EMISSION BANDS FROM HYDRATED ALUMINAS

by

George A. Savanick, Twin Cities Mining Research Center
Bureau of Mines, U. S. Department of Interior, Minneapolis, Minnesota

and

Eugene W. White, Materials Research Laboratory
The Pennsylvania State University, University Park, Pennsylvania

The purpose of this paper is to present an interpretation of slight wavelength differences observed in the AlKβ and OKα x-ray emission bands from corundum (αAl_2O_3), γ-Al_2O_3, boehmite (AlOOH), diaspore ($AlHO_2$), bayerite ($Al(OH)_3$) and gibbsite ($Al(OH)_3$) in terms of the degree of ionicity of the bonding and the role played by hydrogen in these compounds.

X-ray emission from powdered reference standards of these compounds was excited and analyzed by an ARL model EMX electron microprobe operated at 1.0 to 3.7 x 10^{-8} amp specimen current with a 100 μm electron beam diameter. The aluminum band was dispersed with an ADP crystal while a clinochlore crystal was used to diffract the oxygen band.

The measured chemical shifts in the AlKβ and OKα bands are presented in Table 1 along with refractive index data and infrared absorbtion data for these AlOOH compounds. The peak shift data represent changes in the wavelength (measured at 2/3 height) of these bands referenced to the AlKβ and OKα bands from αAl_2O_3.

To a first approximation chemical shifts in soft x-ray emission spectra can be explained in terms of variation of the coulombic attraction between the nucleus of the emitting ion and the surrounding valence electrons. This results in a differential displacement of energy levels and causes a given x-ray line to shift to shorter wavelengths with increasing effective nuclear charge.

Table 1

Standard	Formula	$\Delta OK\alpha$ (Å x 10^4)	$\Delta AlK\beta$ Å x 10^4	Refractive Indices	OH Stretching Frequencies cm^{-1}***
Corundum	Al_2O_3	0	0	n_e 1.76 n_o = 1.77	
γ-Alumina	Al_2O_3*	+45	+1	n = 1.70	
Diaspore	$AlHO_2$ OOH**	+67	-11	n_α = 1.70 n_β = 1.72 n_γ = 1.75	2900
Boehmite	AlO(OH)	-16	-7	n_α = 1.65 n_β = 1.65 n_γ = 1.66	3079 3262
Gibbsite	$Al(OH)_3$	-99	-14	n_α = 1.55 n_β = 1.55 n_γ = 1.57	3361 3378 3428 3518 3616
Bayerite	$Al(OH)_3$	-120	-23	n = 1.55	3401 3454 3518 3533

* in defect spinel structure

** probably more accurately written as $AlHO_2$

*** from L. D. Frederickson, Anal. Chem., 26, 1883 (1954)

An ideal ionic bond involves ions with charges equivalent to their valence while members of an ideally covalent bond are neutral. The disparity of the actual charge on the ions and their valence is a measure of the degree of ionicity of a chemical bond.

The extent of polarization of the anions in a crystal by the cations is another measure of the degree of ionicity. This is directly related to the refractivity of the anion and hence to the refractive indices of the crystal. The anions in crystals with high refractive indices are more highly polarized than anions in compounds with lower refractive indices. Thus highly refractive substances can be considered less ionic than crystals with lower refractive indices.

The AlKβ line (Table 1) undergoes a progressive shift to shorter wavelength as the proportion of hydroxide ions in the crystal increases. The refractive indices of this series of compounds (Table 1) decreases progressively with the shift to shorter wavelength. Thus there is a progressive increase in the degree of ionicity or effective charge which accounts for the progressive shift to shorter wavelengths in the series Al_2O_3 - AlO(OH) - $Al(OH)_3$. An anamoly in this trend is that γ-Al_2O_3 has a somewhat longer AlKβ wavelength then would be predicted from its refractive index. This may be explained by the mixed octahedral and tetrahedral coordination number of aluminum in γ-Al_2O_3.

There is no simple progressive OKα wavelength shift with refractive index, thus the degree of ionicity of the Al-O bond does not appear to be the prime factor determining the OKα wavelength.

In a hydroxide ion a proton is embedded inside an oxygen ion where it enhances the coulombic attraction of the nucleus for the electrons by neutralizing some of the excess negative charge. It seems reasonable to assume that the OKα band should shift to shorter wavelengths as the proportion of hydroxide ions increase.

The data (Table 1) for five of the six compounds are consistent with this model. However, the OKα band of diaspore occurs at a much longer wavelength than that of boehmite and in fact, it has the longest wavelength band of the six compounds. The anomalous behavior of diaspore can be explained with reference to the differing strength of hydrogen bonding found in these structures. The relative strength of the hydrogen bonding in these structures can be deduced with reference to infrared absorbtion data. The OH stretching frequency from boehmite (Table 1) although somewhat lower than those of bayerite and gibbsite,

was significantly higher than that of diaspore. These data indicate that hydrogen bonding is dominent in diaspore, of intermediate strength in boehmite, and very weak in gibbsite and bayerite where the proton is tied into strong OH complexes. The ranking of these compounds with respect to the strength of hydrogen bonding is consistent with the oxygen shift data (Table 1) which shows that boehmite has an OKα wavelength intermediate between that of diaspore and the hydroxides.

As argued above, the existence of hydroxide ions tends to shift the OKα band to shorter wavelengths. This should not be true for hydrogen bonded oxygens because the proton is not preferentially associated with either oxygen and should therefore influence each less. Hence it is not surprising in view of the relative strength of the hydrogen bonding, that boehmite emits a shorter OKα wavelength than diaspore.

The OKα band from diaspore not only occurs at longer wavelengths than for boehmite, but is also longer than that from α-Al_2O_3 and γAl_2O_3. A possible explanation for this is the presence of residual OH substituting for oxygen in these structures.

The significance of this paper is that it demonstrates that chemical shifts in soft x-ray emission spectra can reflect subtle changes in the role played by hydrogen and the degree of ionicity of chemical bonds.

CHEMICAL BONDING STUDIES ON BORON INTERSTITIAL COMPOUNDS

William L. Baun
Air Force Materials Laboratory (LPA), W-PAFB, O. 45433
and
James S. Solomon
University of Dayton Research Institute, Dayton, O. 45409

Pure alpha boron forms a structure of three dimensional frameworks containing linked boron icosahedra. These three dimensional "cage" structures contain large regularly disposed vacancies which can accommodate foreign atoms. The occupation of these interstitial sites in the alpha boron structure is the basis for the formation of boron carbide, boron suboxide, subphosphide, and many metal borides.

The soft X-ray emission band structure for some interstitial boron compounds, as well as for conventional compounds such as B_2O_3 and BN, has been studied from spectra obtained from the electron microbeam probe. The spectra from the interstitial compounds are very similar to pure boron while spectra from conventionally bonded compounds show large differences in shape, band position and number of components in the spectrum.

The B_xO (suboxide) series, in which x varied from 3.5 to 8 in the starting material, gave spectra which are very similar to the boron spectrum, but showing a measurable shift in the emission edge position and a slightly broadened emission band. These spectra give an indication of the type or types of bonding present and the degree of atomic orbital overlap to form molecular orbitals. The spectra of the interstitial compounds show an enhancement of the low energy hump which has also been observed in spectra from impure boron. It is seen in Figure 1 that this low energy feature becomes more prominent as more oxygen is added.

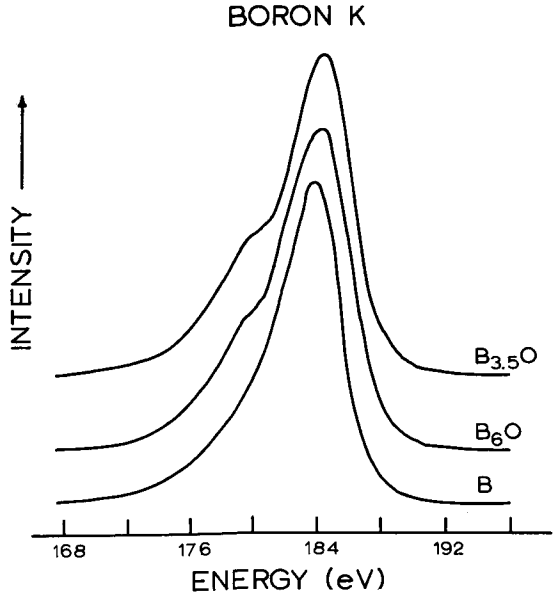

Fig 1 - Boron K Band from Two Nominal Suboxide Compositions and from Pure Boron

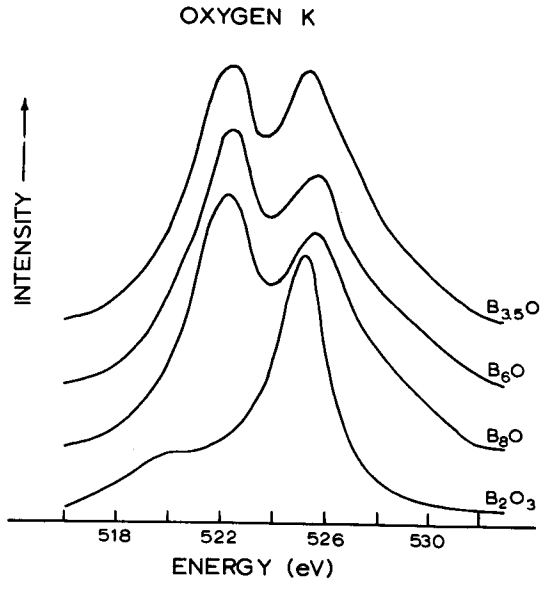

Fig 2 - Oxygen K Spectra from Three Nominal Suboxide Compositions and from B_2O_3.

The oxygen K spectrum obtained from boron suboxides is significantly different from the O K spectrum obtained from B_2O_3 as seen in Figure 2. The O K spectra from suboxides always show two distinct maxima separated by about 3 eV, compared to B_2O_3 where one main peak is observed with a much weaker component appearing on the low energy side. The relative intensities of the two components appear to vary with oxygen content. This could be a very sensitive method for determining suboxide stoichiometry once some well characterized standards were available for reference. The compositions shown in Figure 2 are nominal based on the original starting composition of the raw materials. We do not infer that the numbers shown are the true stoichiometry of the fully reacted suboxides. Assuming the numbers shown are close to the composition of the suboxides, this would infer that in "B_8O", some of the interstitial sites are filled with oxygen while others are vacant or are filled with boron atoms. "B_6O" would theoretically have oxygen at X sites and Y sites would be vacant. The composition "$B_{3.5}O$" has an oxygen excess and all sites, X and Y, would be filled with oxygen in a scheme similar to the B_4C interstitial structure where the carbons are arranged in strings of 3 carbon atoms at the vertices of the icosahedra.

The appearance of two components in the suboxides must indicate formation of split molecular orbitals. If the transitions are considered in terms of the simple (but apparently only approximate) crossover theory in which transitions from boron outer levels to oxygen inner levels (B2p - O1s) are allowed in addition to O2p - O1s, then based on published values of the energy levels the two bands should be separated by 2.5 to 3 eV. This is approximately the separation that is experimentally observed. It should be emphasized that the published energy level values are "atomic" and do not take orbital overlap into consideration. A complete molecular orbital treatment for suboxides, as described by Fischer[1] for transition element compounds, would be necessary to entirely explain the spectra.

References

1. D. W. Fischer, "Use of Soft X-Ray Band Spectra for Determining Molecular Orbital Structures of Simple Compounds," Sixth National Conference on Electron Probe Analysis, Pittsburgh, Pa., 28-30 July 1971.

THE USE OF OCTADECYL HYDROGEN MALEATE AND RUBIDIUM HYDROGEN PHTHALATE AS X-RAY SPECTROMETER CRYSTALS IN THE ELECTRON MICROPROBE, TOGETHER WITH EVIDENCE ON THE ELECTRON BONDING IN THE K-SPECTRA FROM CARBON AND CARBON COMPOUNDS USING THE OHM CRYSTAL

by

Angus A. McFarlane

(Risley Engineering & Materials Laboratory, U.K.A.E.A. Risley, Warrington, Lancashire, England)

SUMMARY

The first order K-bands of the light elements are normally utilised in electron probe microanalysis in order to obtain adequate sensitivity together with minimum beam diameter and specimen damage. In the case of the lead octadecanoate crystal,[1,2] (2d = 100.6 Å) the first order spectra do not give an entirely satisfactory performance. At low Bragg angles specular reflection of ultra soft X-rays prevents a really low background level being obtained even when pulse height analysis is used, and poor wavelength resolution may allow adjacent line interference. The foregoing considerations suggest that alternative crystal analysers are desirable to complement lead octadecanoate. The assessment of two such alternative materials, octadecyl hydrogen maleate,[3] (2d=63.35Å) and rubidium hydrogen phthalate,[4] (2d=26.12Å) for use in light element microprobe analysis, is the subject of this paper.

Comparisons between the OHM, LOD, KAP and RAP crystals are drawn for wavelength resolution, count-rates at the K-band peaks of the light elements, and peak-to-background ratios. Adjacent line interference is considered in terms of the known K-bandwidths relative to actual resolution. The effect on analysis of the differences in the anomalous reflection at 23.3Å by KAP and RAP crystals is considered. An outline of OHM performance is given in an appended table.

Comments on the OHM Performance

The result for carbon is a great improvement over the already acceptable performance by the lead octadecanoate crystal at this wavelength. With the use of a thin (2μ) film of polypropylene over the counter window, the very good peak-to-background ratio can be even further improved.

The carbon results are also remarkable for their wavelength resolution, as demonstrated in the attached figure, showing comparative spectra of diamond, pyrolytic graphite, and several metallic carbides, in each case derived from single crystal specimens. The differences are sufficiently marked to be usable as evidence of lattice structure or chemical bonding. Comparison with results obtained by J E Holliday[5] using a grating spectrometer show peak widths at half-height are similar (within 1 ev) for both grating and crystal spectrometers, although the background level is an order lower in the OHM results.

The intensities for sodium and fluorine are much greater than those achieved with potassium hydrogen phthalate (KAP) at the same excitation although the background is higher for sodium. The use of P10 gas for Na_K would probably improve intensity even further.

The nitrogen performance represents a very useful decrease in background level, (now symmetrical on either side of the peak) and the reduction in the line width will remove some adjacent line interference, previously unavoidable using the LOD crystal. Scanning X-ray photographs of N_K with OHM show a greater benefit from the change in

the N_K band shape (from LOD) than numerical comparison of the peak widths at half-height would anticipate. Although disappointing from the immediate analytical viewpoint, the very low oxygen result from OHM is not surprising in view of the low mass absorption coefficient difference between carbon and oxygen for oxygen K-radiation. A fuller understanding of the reflection mechanism, and a useful final performance may be achieved by substitution of heavier atoms in the OHM lattice.

Rubidium Hydrogen Phthalate

The report by I W Ruderman and B Michelman[4] that the substitution of rubidium for potassium in potassium acid phthalate improved the reflectivity for $CU_{K\alpha}$ radiation, suggested the possibility that RAP might be superior to KAP in the long wavelength range also.

The sample of RAP prepared for the spectrometer described (see table) did not give a performance significantly different from the two KAP crystals already in use, in terms of count-rate and peak-to-background ratio, over the range Si_K to O_K, except in one particular respect. The intensity of the subsidiary peak at 23.3Å, relative to the main peak in the oxygen K-band, (out of MgO) dropped from 65% for KAP to 15% for RAP, giving a result similar to that reported by Mattson and Ehlert[6] in 1965 (75% for KAP, 19% for RAP). It has been shown recently[7,8,9] for KAP that the subsidiary peak is due to an anomalous reflectivity 'spike'. This 'spike' was observed (but not explained) as unidentified peaks in the spectra of Cr and V L-lines obtained with a KAP crystal two years ago in this laboratory. It is shown that less adjacent line interference from Cr, V, etc., would occur using RAP for oxygen analysis, since the reflectivity 'spike' is less pronounced.

Conclusions

(1) That the OHM crystal gives a large improvement in carbon analysis, over the LOD crystal, particularly in peak-to-background ratio, and wavelength resolution, to the extent that it can demonstrate changes due to chemical bonding or lattice structure.

(2) That the OHM crystal gives an improved performance for nitrogen analysis, in better peak-to-background ratio and wavelength resolution, over the LOD crystal.

(3) That the OHM crystal gives a large intensity increase for Na_K and F_K radiation over the KAP crystal, while retaining very useful peak-to-background ratios and wavelength resolution.

(4) That the OHM crystal is not useful for oxygen analysis, but a useful performance might be obtained by crystal modification.

(5) That the RAP crystal will reduce adjacent line interference in oxygen analysis in certain circumstances, while maintaining a performance similar to KAP for the light elements.

References

(1) B L Henke, R White and B Lundberg. J. Appl. Phys. 28:98 (1956).

(2) P S Ong, "Technique for Electron Microprobe Analysis of the Light Elements" Pittsburgh Conference of Analytical Chemistry & Applied Spectroscopy (March, 1964).

(3) I W Ruderman and K J Ness, "Analyser crystals for X-ray Spectroscopy in the region 25-100 Å. Appl. Phys. Letters, Volume 7, Number 1, pp.17-19, 1st July, 1965.

(4) I W Ruderman and B Michelman. 5th International Congress on X-ray Optics and Microanalysis. Tubingen, 1968.

(5) J E Holliday, J. Appl. Physics, Volume 38 No. 12, p.4722, 1967.

(6) R A Mattson and R C Ehlert, "The application of a soft X-ray spectrometer to study the oxygen and fluorine emission lines from oxides and fluorides." Advances in X-ray Analysis, Volume 9, p.478.

(7) B L Henke and Robert E Lent "Some recent work in low energy X-ray and electron analysis", Advances in X-ray Analysis, Vol. 12, p.482.

(8) R L Blake, "X-ray interaction coefficients: effect on interpretation of solar X-ray data". Advances in X-ray Analysis, Volume 13, p.365-368.

(9) R J Liefeld, S Hanzély, T B Kirby and D Mott, "X-ray spectrometric properties of potassium acid phthalate crystals". Advances in X-ray Analysis, Volume 13, p.378-380.

TABLE

Performance of Octadecyl Hydrogen Maleate Analyser

Conditions throughout: 20KV, 10^{-7}A, Counter: 120 torr, P75

X-ray line and nominal wavelength for peak & background measurement	Material used for peak measurement	Peak intensity (cps)	Material used for background measurement	Peak-to-back ground ratio	Special conditions
Na_K 11.91 Å	NaCl	4400	Diamond	50:1	No slit
Na_K 11.91 Å	NaCl	3600	Diamond	100:1	0.030" slit
F_K 18.31 Å	LiF	9100	Diamond	450:1	No slit
F_K 18.31 Å	LiF	5400	Diamond	1000:1	0.030" slit
O_K 23.7 Å	Al_2O_3	3	LiF	2:1	No slit
N_K 31.6 Å	BN (cubic)	38	LiF	30:1	No slit
C_K 44.5 Å	Diamond	4900	Be	1200:1	No slit
C_K 44.5 Å	Diamond	1600	Be	2000:1	~ 2μ poly-propylene filter on counter

Experimental Conditions. Crystals of OHM and RAP were used in a linear Johansson spectrometer of Rowland circle radius 13.5 cm. The crystals were 2.5 x 1 cm in area, bent and ground to the appropriate radii. The gas counter was used with 75% CH_4, 25% A at 120 torr, and a polypropylene window of approximately 0.2 μm thickness.

CARBON 'K' SPECTRA FROM VARIOUS MATERIALS USING
A CRYSTAL OF OCTADECYL HYDROGEN MALEATE IN A
LINEAR JOHANSSON SPECTROMETER (AUTHOR'S RESULTS)

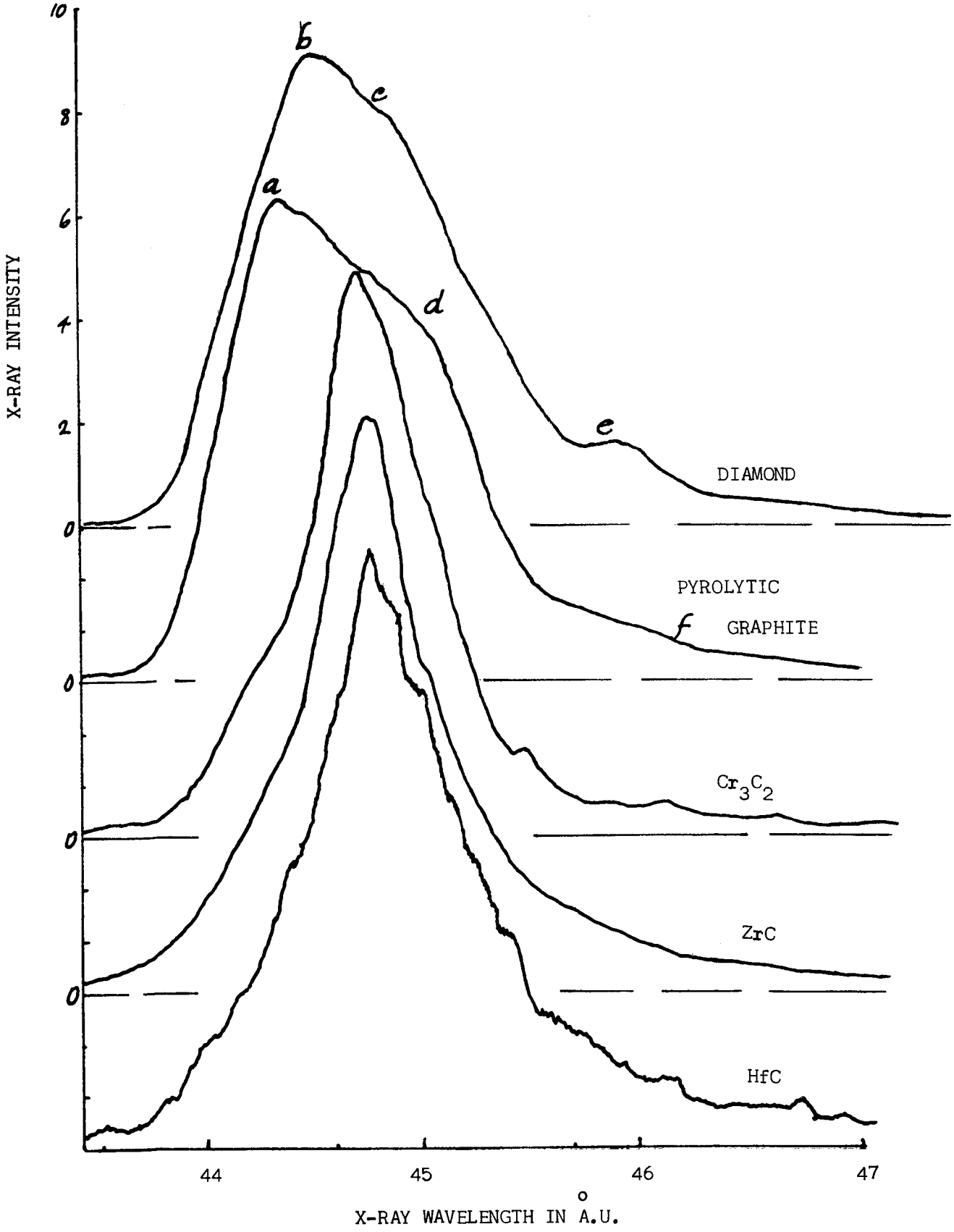

ANALYSIS OF BONDING, ELECTRONIC STRUCTURE AND SURFACE OXIDES OF METALS AND ALLOYS BY SOFT X-RAY SPECTROSCOPY

J. E. Holliday
Fundamental Research Laboratory
U. S. Steel Corp. Research Center
Monroeville, Pennsylvania

Soft x-ray spectroscopy has proven to be an effective tool for studying the electronic structure of metals and bonding in alloys and metallic compounds. Changes in the peak wavelength of the band from the element in the metal compound relative to its uncombined state can give information on its valence and coordination number. Intensity distribution changes in the band can give a qualitative indication of the degree of ionicity in the alloy, and the change can be related to the heat of formation when the bond is predominantly an electrostatic type. Peaks observed in the spectra of the element in the alloy not present when the element is uncombined, due to cross electron transitions between the combining elements, provide information about the degree of localization and the relative locations of s, p and d bands in metallic compounds. Examples will be given of analyses of the above bonding and electronic structure factors from soft x-ray spectra of transition metals, intermetallic compounds and transition metal carbides and nitrides.

In addition, it has been found that soft x-ray spectroscopy can provide information about the nature of surface oxides on alloys. The spectra shown in Fig. 1 illustrate the differences in Cr $L_{II,III}$ emission bands from oxide films on chromium and several Fe-Cr alloys. The Cr $L_{II,III}$ bands from chromium and chromium oxide were resolved by utilizing a DuPont curve analyzer and it may be seen that the intensity of the Cr L_{III} band from Cr_2O_3 decreases relative to Cr L_{III} band from chromium with increasing concentration of chromium. This indicates a change in oxide composition with chromium content since it is generally considered that the oxide thickness of the Fe-Cr alloys remains relatively constant except between 10 and 14% chromium. The spectra were all measured at 3 kv accelerating voltage so that the x-rays came from a depth of about 200 Å in each case. The above results show the importance of considering surface oxides when analyzing changes in emission bands. Examples from the literature will be cited where changes in the emission band spectra on alloying can be attributed to variations in oxide film composition rather than in electronic structure.

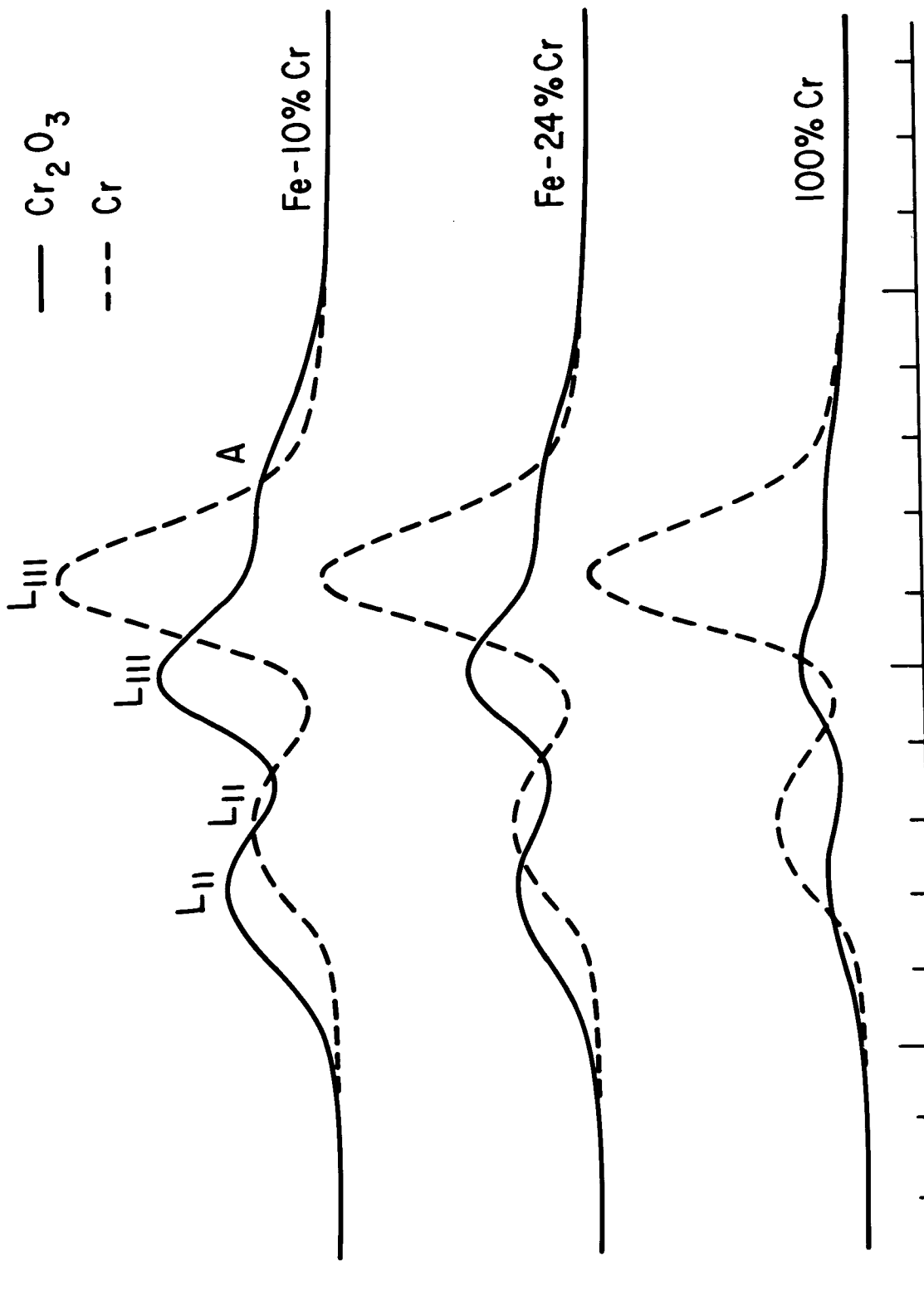

Cr L_{II}, L_{III} EMISSION BAND FROM Cr AND Fe-Cr ALLOYS AT V_T = 3 kV

FIGURE 1

USE OF SOFT X-RAY BAND SPECTRA FOR DETERMINING MOLECULAR ORBITAL STRUCTURES OF SIMPLE COMPOUNDS

David W. Fischer
Air Force Materials Laboratory (LPA)
Wright-Patterson Air Force Base, Ohio 45433

It has been known for quite some time that soft X-ray band spectra have considerable potential for determining the electronic structure of a material. Many investigators, however, are presently using the soft X-ray emission bands from the light elements for qualitative and semi-quantitative analysis without recognizing that these very spectra contain much more useful information than this about certain physical and chemical characteristics of the material. Such characteristics include valence state, bonding character, coordination symmetry, bonding distances, electrical conductivity, heats of formation, and so on, all of which are dependent on the electronic structure. It is the purpose of this paper to show why such characteristics are reflected in the band spectra and to demonstrate how this information can be extracted by using a molecular orbital (MO) model to interpret the spectra.

In forming a simple transition metal compound, such as an oxide, it must be recognized that the outer orbitals of both the metal ion and non-metal ion interact to form chemical bonds. There are several ways of attempting to predict the results of such an interaction but the only model considered here is the familiar (to most chemists) molecular orbital method using the linear combination of atomic orbital (LCAO) approximation. The resultant energy level diagram for transition metal compounds is to be found in many textbooks. An example is shown here in Figure 1 for TiO. In this compound the titanium atom is surrounded by an octahedral arrangement of oxygen atoms. The titanium 3d, 4s and 4p atomic orbitals will therefore interact with the oxygen 2s and 2p orbitals to form a set of molecular orbitals as shown in the figure. When the material is bombarded by an X-ray or electron beam which is energetic enough to create an inner level vacancy an electron from one of the outer orbitals can fall in, giving rise to an X-ray emission band. In TiO, the TiL_{III}, $TiK\beta_5$ and OK bands are produced in this manner. In the past, when performing an X-ray band study of material, it has been the usual practice to take a single spectral series, such as $TiK\beta_5$, and attempt to deduce the electronic structure. An important point of this paper is that such a practice is of questionable importance and certainly gives a very incomplete picture of the electronic structure. The reason is rooted in the dipole selection rules which govern X-ray transitions. Notice in Figure 1 that the molecular orbitals consist of intimate admixtures of s, p and d wave symmetries. According to the selection rules the K band will reflect only the distribution of p symmetry in the outer levels and tell us nothing about the distribution of s and d symmetry. Conversely, the L band will reflect the distribution of s and d symmetry but not of p symmetry. Obviously, then, if we expect to obtain a complete picture of the outer electronic structure it will be necessary to combine the information present in both the K and L band spectra.

This has now been done for a number of transition metal compounds[1,2] and an example of the results is shown in Figure 2 for Cr_2O_3. The CrL_{III}, CrK and OK emission and absorption bands are all combined on a common energy scale and unfolded into their individual components. Each component is then assigned, on the basis of the dipole

selection rules, as arising from an electron transition to or from a specific bonding, antibonding or nonbonding molecular orbital. In this manner a complete MO diagram is empirically deduced for the compound. The resultant MO diagrams for several compounds will be compared with other types of experimental data and with theoretical calculations. It will also be pointed out why the X-ray band spectra undergo certain changes in appearance with different coordination symmetries, different valence states of the metal ion, different ligands, etc.

It is concluded that X-ray band spectra have a great advantage over all other experimental techniques in determining the molecular orbital structure. No other technique can even approach the X-ray method in its overall simplicity, completeness and flexibility. This is the first time that complete MO diagrams have been experimentally determined and also the first time that all the components of the X-ray emission and absorption band spectra could be logically explained in terms of bonding between the two components of the compound.

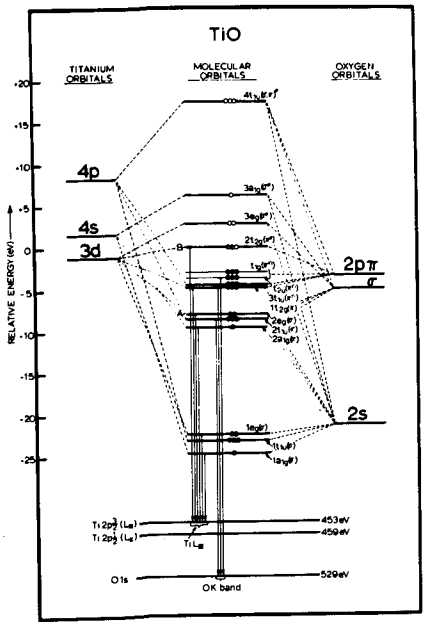

Fig 1 - Atom-MO-Atom Diagram for Octahedrally Coordinated Transition Metal Oxides.

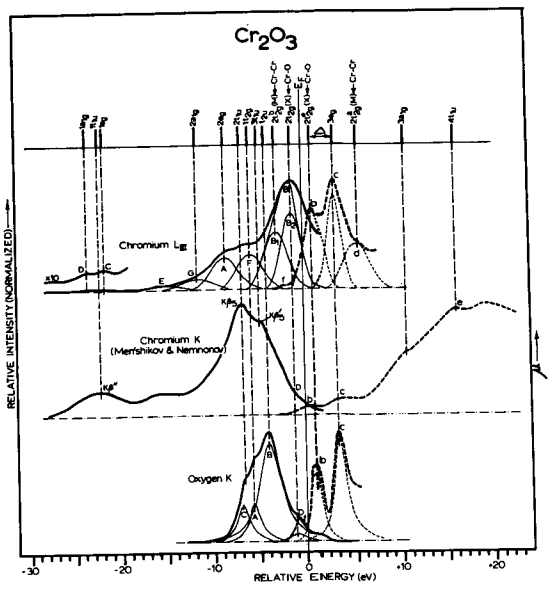

Fig 2 - Empirical Deduction of MO Structure of Cr_2O_3 by Combining the CrL_3, CrK and Oxygen K X-Ray Band Spectra.

References

1. D. W. Fischer, J. Appl. Phys., 41, 3561 (1970).
2. D. W. Fischer, J. Phys. Chem. Solids, to be published (1971).

TOTAL X-RAY CHARACTERIZATION OF MATERIALS BY MEASUREMENT OF X-RAY SPECTRAL DETAILS WITH THE ELECTRON PROBE

David J. Nagel

Naval Research Laboratory, Washington, D. C. 20390

The goal of electron probe measurements is determination of some characteristic of the sample. Most often elemental composition is desired, but total characterization of an unknown also requires determination of the atomic arrangement and bonding. X-ray spectroscopy is one of the few experimental tools which can provide information on all three of these general characteristics of a material.

The electron probe has two advantages, in addition to the small sample size, for total x-ray characterization of materials. First, several types of x-ray spectra may be measured with a microprobe. These include the usual diagram lines, the non-diagram satellite lines, valence band spectra, and even absorption spectra. All of these spectra are useful for determination of atomic structure and bonding. Second, the curved-single-crystal spectrometers on most microprobes offer high resolution and good efficiency for the measurement of spectral details. For microprobe work aimed at quantitative analysis, the intensity of an x-ray line is of prime interest, and resolution is important only because of line/background considerations. In contrast to this, information on atomic structure and bonding is gotten from line shifts, the relative intensity of closely spaced satellite features and valence band spectra shapes and widths, all of which require high resolution measurements.

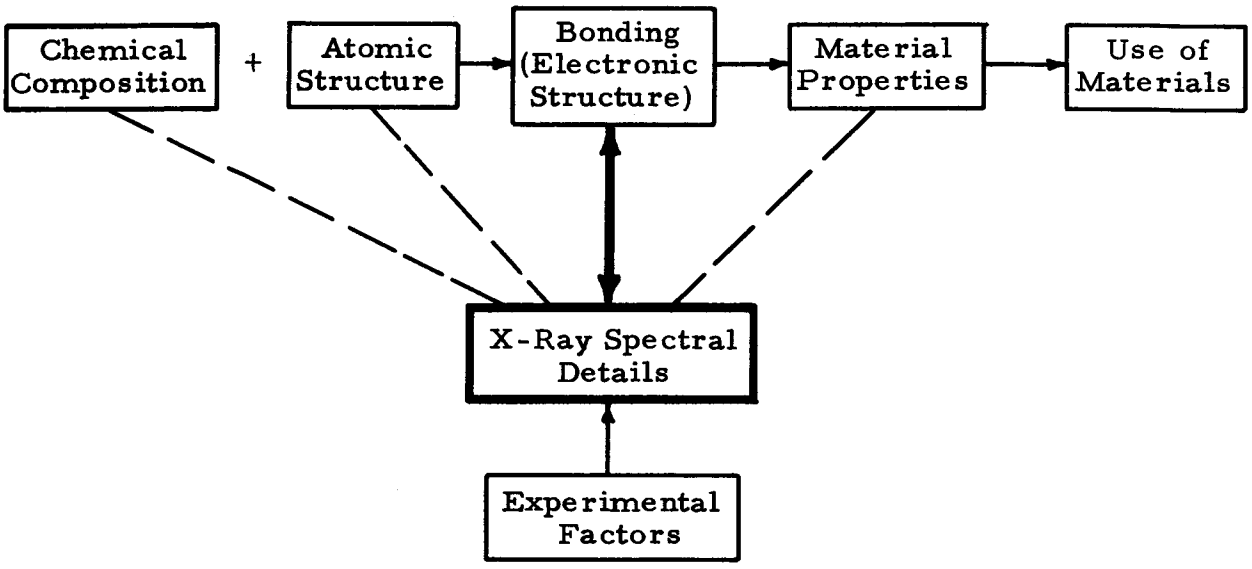

The figure shows the relation between the materials characteristics, properties and use across the top and the x-ray spectral details available from microprobe measurements. Two kinds of connections shown in this diagram are important. First, there are correlations between composition, atomic structure, and properties on one hand and details of valence band spectra on the other. Correlations, shown by dashed lines, can be found empirically and used even without understanding of the bonding in a sample. For example, the chemical compounds present in an unknown can be determined from the location and separation of peaks in valence band x-ray spectra. Correlations of structural factors, such as bond length and coordination, with x-ray energies and spectral shapes have also been exhibited. In several cases, correlations have been made between various valence band spectral details and electronic, magnetic and thermodynamic properties. Examples of these relations between materials and spectra will be given. Most of the correlations are not based on microprobe data, but the microprobe offers the possibility of more of this kind of work.

The second important relationship shown in the figure by the heavy line is that between the details of bonding (electronic structure) and spectral fine structure. The distributions of bonding electrons in energy and space are the most important aspects of electronic structure. Various x-ray spectra yield different kinds of information concerning electron energies and densities. For example, small shifts in x-ray line energies depend on the potential energy of the inner shell electrons, which depends in turn on the spatial distribution of bonding electrons. Hence, the effective charges on atoms in a molecule or solid can be determined from line shifts. Also, the relative intensity of x-ray satellite peaks depends on the energy separation of the multiplet lines within the satellite spectrum. The component line spacing is sensitive to the bonding electron distribution so that relative x-ray satellite intensities provide another means to study electronic structure in materials.

Valence band emission and absorption spectra depend directly on the bonding electron energies and provide the most powerful x-ray method for determination of electron structure. There are two approaches to the use of band spectra for bonding studies. First, for compounds, it has been shown recently that the separation of electron energy levels can be gotten by matching the predictions of Molecular Orbital Theory to experimental spectra. Details of the bonding electron spatial distribution can then be calculated from the empirical level separations. In the second approach, emission and absorption spectra are calculated in detail from the results of Band Theory. A few such calculations for metals and ordered alloys have appeared in the recent past. Calculations of x-ray spectra and comparison with experiment has the double payoff of yielding an understanding of the spectral details while at the same time providing a check on the computed band structure. Examples of spectra compared with Molecular Orbital Theory and calculated from Band Theory will be given. The use of bonding information, obtained in part by x-ray spectroscopy, to understand and calculate material properties will also be outlined.

PULSE HEIGHT STABILIZATION IN GAS PROPORTIONAL X-RAY DETECTOR SYSTEMS

Carol J. Kelly and M. A. Short
Scientific Research Staff, Ford Motor Company, Dearborn, Michigan

and

C. A. Reynolds
Canberra Industries, Meriden, Connecticut

A self-contained electronic stabilizer has been designed to provide automatic compensation for the decrease in pulse amplitude output which occurs in both flow and sealed gas proportional detectors at high counting rates. The unit, which is inserted in the counting electronics between the linear amplifier and the pulse height analyzer, consists essentially of a variable gain amplifier controlled internally so as to maintain the amplitude of the input pulses at some preset level. This level is determined by the setting of the pulse height analyzer. The stabilizer is rapid in action, has no moving parts, has no feedback to other system components, and does not degrade the pulse pair resolution of the system. It will also compensate for changes in pulse amplitude due to amplifier and pre-amplifier gain drifts, detector power supply fluctuations, temperature and pressure changes in detectors, and so on. The unit may, consequently, be used not only in X-ray counting systems employing gas proportional detectors, but also in systems using other types of detectors where changes or drifts in gain may occur. The stabilizer is compatible with most transistorized linear amplifiers giving a positive output pulse.

The principle of operation of the stabilizer is shown schematically in Figure 1. Pulses from the linear amplifier are fed into the stabilizer, pass through an internally controlled variable attenuator, through a fixed gain amplifier, and continue on to the stabilizer output. These stabilizer output pulses are also fed

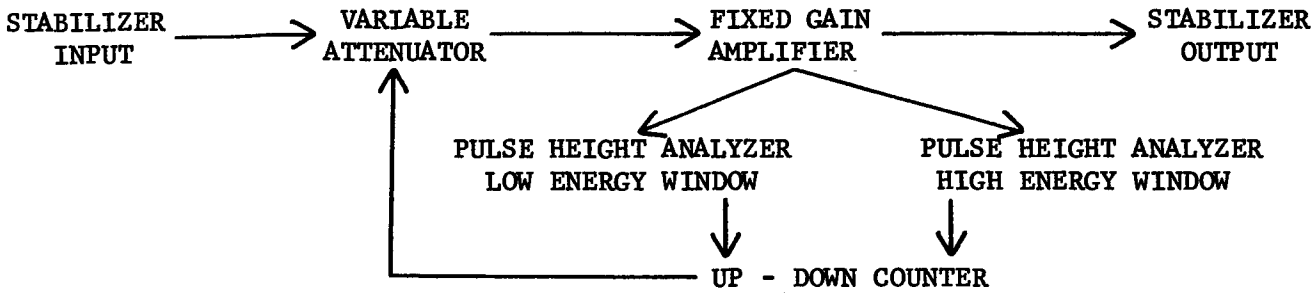

Figure 1: Diagram of X-ray Stabilizer

into two internal pulse height analyzers, the windows of which are placed symmetrically on the sides of the energy peak using front panel controls to set the nominal pulse amplitude, the width of the analyzers windows, and the spacing between the two windows. Pulses passing through the windows are fed into an up-down counter which controls the variable attenuator. A pulse passing into the low energy window causes the counter to count "up" which results in a decrease in the attenuation; a pulse passing into the high energy window causes the counter to count "down" which results in an increase in the attenuation. At equilibrium, the number of pulses passing into the two windows will be the same and no net change in the counter or the attenuator will occur. A change in the input pulse amplitude will cause one window to pass more pulses than the other window and this will result in the counter varying the attenuator in the appropriate direction until the count rate in the two windows is again balanced.

The stabilizer will compensate for input amplitudes of ½ to 2 times the nominal amplitude and the system gain is held constant to 0.2%. At an overall stabilizer gain of 1, the correction step size is 0.05% of the nominal pulse amplitude; one correction step is made for each pulse into the up-down counter and hence the correction rate is dependent on the pulse rate through the windows of the two internal analyzers. As the overall gain of the stabilizer is changed from unity, the size of the correction step is decreased.

The X-ray stabilizer may be used in electron microprobe, X-ray fluorescence, and X-ray diffraction systems. The stabilizer is particularly useful in microprobe analysis as in this technique very large changes in counting rate may occur between sample and standard, resulting in substantial changes in pulse amplitude. The use of the stabilizer permits the setting of a narrower window on the main pulse height analyzer than heretofore, thus leading to improved peak-to-background ratios. It is still necessary to set the main pulse height analyzer at the high count rate as the unit does not compensate for the increased width of the energy peak at the high count rate.

The unit has been used on an ARL microprobe and in Figure 2 typical results are

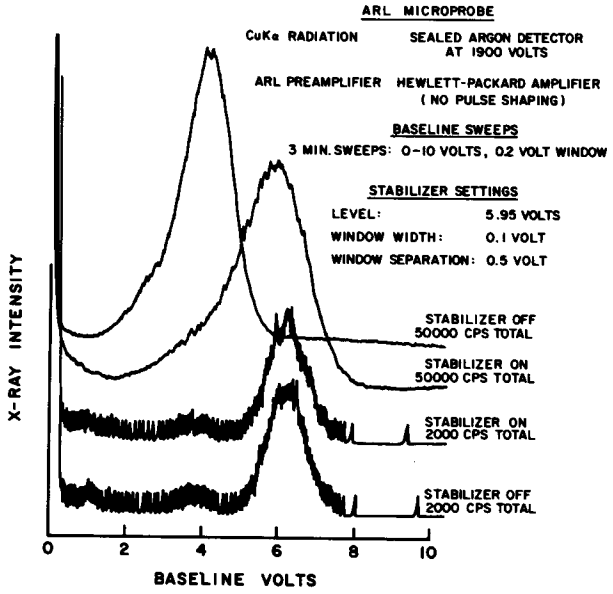

Figure 2: Baseline Sweeps on the ARL Microprobe

shown. Pulse height analyzer baseline sweeps were made at 2000 cps (total counts incident on detector) and at 50,000 cps with the stabilizer on and again with the stabilizer off. It can be seen that the use of the stabilizer at the high count rate reduces the shift in energy to a negligible amount. The stabilizer has also been used with Siemens and Norelco fluorescence units and with a Picker diffractometer. It is very easy to use with the Siemens fluorescence unit (which incorporates a sine amplifier) and with the diffractometer because the output of the linear amplifier has, apart from the intensity dependent shift, a constant pulse amplitude. With the ARL microprobe and the Norelco fluorescence unit it is necessary to either reset the stabilizer or to adjust the linear amplifier gain or the detector high voltage supply when there are substantial changes in the linear amplifier output due to changes in the wavelength of the X-rays incident on the detector.

We would like to express our thanks to Dr. W. T. Kane of Corning Glass Works, Corning, New York, who suggested to us the possible use of this technique for pulse amplitude compensation.

QUANTITATIVE ANALYSIS OF ELECTRON PROBE IMAGES

C.Fisher and D.W.Gibbard

Image Analysing Computers Ltd., Melbourn, Royston, Hertfordshire, England.

Quantitative image analysis techniques which were developed for optical microscope images have since been applied to many other fields[1]. One of the most recent applications has been in the field of Electron Probe images[2]. At the same time, new techniques have been introduced which permit methods of feature classification to be performed which are not possible for other types of image producing devices. Thus the electron probe makes the best use of the I-A techniques whilst the converse is also true since the techniques allow simultaneous processing rates may be up to 1000 times faster than the usual photon limits suggest.

Before any sort of analysis can begin, the image must be converted into a form understandable by a machine. This is the 'detection' process in which those areas of interest are extracted from the image and converted into a digital signal. The amount of data storage required for processing the image may be considerably reduced at this stage by firstly defining the "grey" level of interest, thus avoiding having to remember the grey level at each point in the image, and secondly by performing real-time analysis in a special purpose computer, so that storage is only needed for continuously updated local regions and not the whole frame.

One important recent innovation in feature counting is the separation of the signal which defines the outline of the feature from the signal which defines the parameters by which it is to be classified[3]. These signals may be derived from one video signal, e.g. cells whose outline is defined by a detected grey level, and characterised by the area of their nuclei defined by another grey level. With an electron probe, the two signals may be derived from two video signals which are obtained from a specimen simultaneously. Typical parameters which may be used for classification are area, perimeter, height and width. They may be used either in themselves, e.g. for a size distribution in terms of feature area, or in combination as form factors, e.g. Area/(Perimeter)^2 for segregating different shapes. Another parameter which may be used for feature classification is volume, or a derivative of it, density, (volume/area) where the third dimension is a grey scale representing thickness in the absorption mode. A very important development of density classification is for X-ray signals on SEM's and micro-analysers where the third dimension is the number of X-ray pulses per picture point and the classifying parameter is X-ray density. The signal defining the feature outline is a video signal obtained simultaneously, e.g. a specimen current signal. By this method features may be classified according to their composition identified by characteristic X-radiation at speeds up to 1000 times higher than those normally associated with X-ray images.

These feature specific measurements give a powerful pattern recognition capability not possible with simple lineal methods of analysis.

Data from a single field of view is rarely meaningful since it represents a very small proportion of the specimen. Many fields from each specimen must usually be examined and a range of image analysis equipment is not complete without automatic means of handling specimens, controlling a program of analysis and of storing and displaying results or performing more processing on them, e.g. with on-line digital

computers. In spite of the increasing use of automation, a human operator is likely to remain an important part of the system and a significant improvement in the man/machine interaction will be the use of a light pen for feature identification. It is doubtful whether it will ever be possible to put specimens on an image analysis machine and get sensible results without some setting up procedure. It is considered essential to have a display of the image and facilities for super-imposing detected signals and computed functions, which is a facility not found in simple lineal analysis methods.

Image analysis will in future be increasingly used in new fields, e.g. application to on-line process control, requiring special input and output devices and the techniques themselves will become more powerful and faster. There will be more interaction with conventional digital computers, using such techniques as described here to give real-time results when used "on-line"; steps will be taken towards more automation in the detection process and automatic specimen handling will become available in fields other than optical microscopy and will become more accurate and versatile, e.g. automatic focussing and rotation controls.

Acknowledgements

The authors wish to thank Cambridge Scientific Instruments Co., and Philips for their co-operation on these projects.

References

1. Fisher C. "The New Quantimet 720". The Microscope. Vol.19 Jan.1971. 1-20.

2. Braggins D.W., Gibbard D.W., & Gardner G.M. "The Application of Image Analysis Techniques to Scanning Electron Microscopy." SEM/1971. Proc. 4th Annual SEM Symposium, I.I.T.Research Inst. 1971.

3. Gibbard D.W., Crawley J.A., Cowham M.J. "The Application of Image Analysis Techniques in Electron Microscopy." Electron Microscopy and Analysis Group, Inst. Physics & Physics Soc., Cambridge, U.K. 1971.

SIMPLE METHODS FOR AUTOMATIC QUANTITATIVE ANALYSIS OF SEM AND PROBE IMAGES

J. Lebiedzik and E. W. White
Materials Research Laboratory
The Pennsylvania State University
University Park, Pennsylvania 16802

Techniques for quantitative image evaluation range from sophisticated computer analyses such as by CESEMI[1,2] and dedicated image analyzing computers[3] to the tedious manual techniques. The purpose of this paper is to describe an intermediate approach that utilizes, to a great extent, the electronic readout systems associated with most microprobes and SEMs. In this study quantitative image analysis data are accumulated on conventional scalers or alternatively in a multichannel analyzer, and read out on teletype.

The range of signals providing the image contrast mechanisms in the probe/SEM include secondary electrons, electron backscatter, cathodoluminescence, characteristic x-ray, etc., from which one can make unambiguous phase identifications in most cases. For the purpose of this paper we consider porosity as a phase.

The method is based on an analog comparator for making decisions as to when the beam is on or off the selected phase. Figure 1 schematically illustrates the electronic logic. A scan-line monitor helps in the selecting of the critical level where, for example, everything above the critical level is considered to be on the selected phase and everything below is on background. The analog comparator switches a clock pulse train from the background counter to the phase counter depending on brightness level. The output from the analog comparator is either zero or logic one. Each time the output switches from zero (background) to logic one (on phase) the "Number of Chords Scaler" is triggered. The clock train pulse gating is shown in Figure 2.

Chord length to pulse height conversion is done by a DAC with storage register, counter and switching logic. The DAC with an output of 0 - 10 V per 8 bits has a conversion constant $\frac{10\ V}{256}$ volts per single pulse. The conversion consists of accumulations clock pulses in a binary counter, while the analog comparator shows logic one (see Figure 2). The information is transferred at the end of the chord to a DAC and the result is an analog output from the DAC proportional to the number of pulses stored in the binary counter. A time delay circuit (10 μs) resets the counter and the register to zero, thus the output of the DAC also goes to zero. The result of this entire conversion is a pulse of 10 μs duration and of a height corresponding to the chord length.

The ratio of on phase count to off phase count is the volume fraction or relative area occupied by the phase. The total "on count" divided by the number of chords is the average chord length. The chord length distribution (lineal analysis) is the output of multichannel analysis zero.

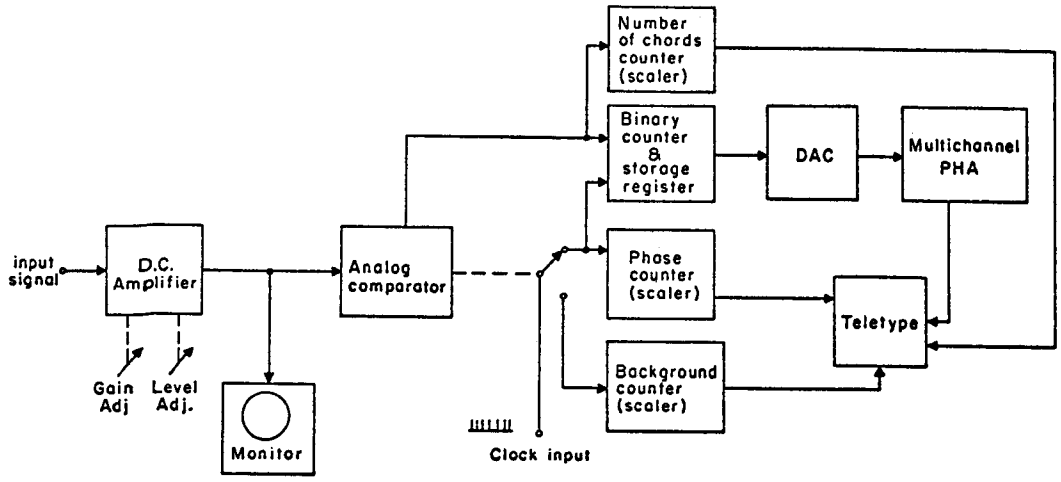

Figure 1. Block Diagram of Phase Integrator and Chord Length Analyzer.

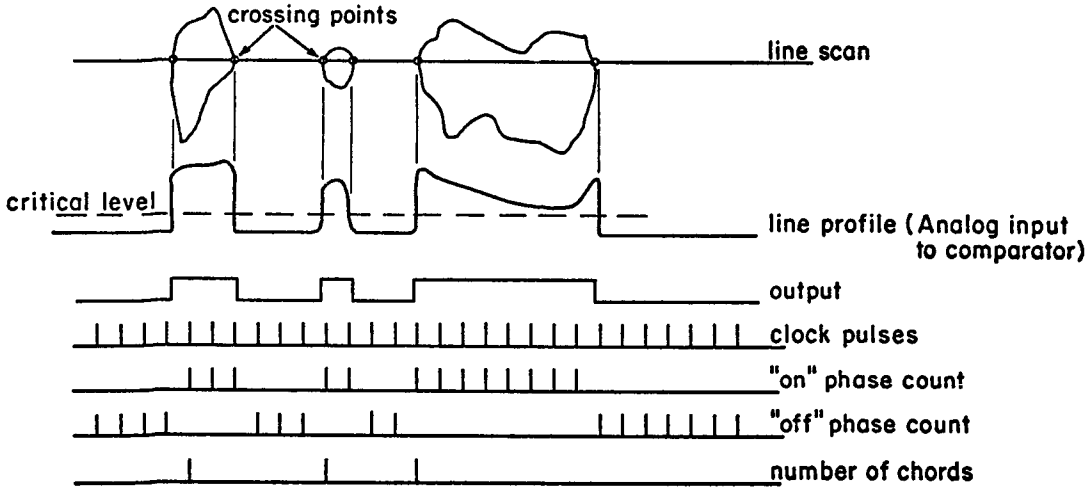

Figure 2. Timing Diagram for Phase Integrator.

Precision in the analyses mostly depends on the number of points per frame and the electronic stability and contamination rates in the SEM or probe. Analyses done on the SEM with a digitally controlled sweep system yielded a precision better than 1% for a matrix 256 x 256 points.

This instrumentation is being used in conjunction with both a Model JSM SEM and a Model EMX electron probe. For the SEM, a digital raster is routinely used but a problem exists when using the same electronics for the analog sweep of the EMX. In this latter case it is convenient to use a free-running clock whose repetition rate is set to $\frac{\text{number of analog raster lines}}{\text{time for scanning single line}}$ in order to achieve a square matrix of points.

Typical analyses performed to date include study of particle sizes and pore characteristics in polished sections of ceramic materials and quantitative petrography of rock and ceramic specimens. The advantages and limitations of this type of information will be discussed.

This work is being supported by the Department of Navy Contract No. N00014-67-A-0385-0007.

REFERENCES

1. Matson, W. L., H. A. McKinstry, G. G. Johnson, Jr., E. W. White and R. E. McMillan. "Computer Processing of SEM Images by Contour Analysis," Pattern Recognition, 2, 303-312, Pergamon Press 1970.

2. White, E. W., H. Görz, G. G. Johnson, Jr. and R. E. McMillan. "Particle Size Distribution of Particulate Aluminas from Computer-Processed SEM Images," Proc. 3rd Annual Scanning Electron Microscopy Symp., IITRI (1970).

3. Braggins, D. W., D. W. Gibbard and G. M. Gardner. "The Application of Image Analysis Techniques to Scanning Electron Microscopy," Proc. 4th Annual Scanning Electron Microscopy Symp., IITRI (1971).

DETECTION OF BACKSCATTERED ELECTRONS WITH SILICON SOLAR CELLS

J. C. Potosky
Department of Electrical Engineering
University of Southern California
Los Angeles, California 90007

I. INTRODUCTION

Interest in backscattered electrons as signal information in scanning electron beam instruments has increased recently because crystal structure information[1] as well as topographic information can be obtained. In previous work detection of the BSE signal has primarily been done using a scintillator-photomultiplier combination[2], or a solid-state detector[3,4].

Inexpensive silicon solar cells have been tried and their performance found acceptable under certain limitations. The criteria for a BSE detection system is first discussed. The properties of a silicon solar cell are described followed by results obtained using such a cell as a BSE detector.

II. COMPARISON OF DETECTORS

A useful detection system for backscattered electrons depends on five factors. These are (1) cost, (2) complexity, (3) collection efficiency, (4) frequency response, and (5) reliability.

Scintillator-photomultiplier combinations are expensive due to the complexity of the system brought about by the need of bias and PM tube power supplies. Collection efficiency is low because of the small solid angle subtended by the detector. Frequency response, and energy discrimination needed to enhance crystallographic contrast[3], is good. However, most plastic scintillators decay with time and require replacement.

Commercial solid-state detectors do not require extensive peripheral equipment when used for BSE detection but still cost several hundred dollars. Their collection efficiency is quite high. Frequency response is adequate, and excellent energy discrimination is obtained with a high degree of reliability.

Silicon solar cells are simple in that they require no peripheral equipment. Energy discrimination is provided and high reliability is obtained. Frequency response is limited but collection efficiency is as high as a commercial solid-state detector. The cells also show a high degree of immunity to noise, and environmental conditions. The low cost of the cells is advantageous for experimental setups, especially if several cells are required or there is a chance of damaging the cells.

III. PROPERTIES OF SOLAR CELLS

Commercial solar cells depend on a shallow junction and a large surface area for light collection and photon to electron-hole pair conversion. When the cells are used as BSE detectors the large surface provides high collection efficiency and

the shallow junction allows lower energy electrons to be detected. Energy discrimination is automatically provided by the mechanism of producing electron-hole pairs from the energy in the incident electron. Additional energy discrimination is provided by the heavily doped surface layer of the cell.

The efficiency of collecting an electron-hole pair before recombination in the cell is a measure of the performance of the device and is found to be a function of the energy of the incident electron producing the electron-hole pairs. The expected short circuit current produced by an electron beam interacting with the cell is:

$$I_{exp} = \frac{E}{\varepsilon} I_B (1 - \tfrac{1}{2}N)$$

where E is the energy of the incident beam in eV, ε is the average energy required to produce an electron hole pair in Si 3.6 eV[5], and $\frac{1}{2}N$ is approximately the fraction of incident energy that is carried away by backscattered electrons. The efficiency of the cell defined as the ratio of measured cell current to expected cell current is shown in Fig. 1.

The frequency response of a cell is limited by the inherently high junction capacitance of the device. Fig. 2 shows the c-v characteristics of the cell. The linear $(1/c^2)$ plot indicates an abrupt junction. From this data the resistivity of the n type substrate is found to be 100 Ωcm. A cell of higher resistivity substrate would have a lower junction capacitance, but commercial cells fabricated with higher resistivity material may be difficult to find. Also, reverse biasing the cell will not lower the capacitance sufficiently to be advantageous over an unbiased cell.

The frequency response can be improved by connecting two or more cells in series or shunting the cells with a resistor, which drops the detectors signal output level, or combination of these two methods. A slower scan sweep rate may also be necessary. For a 1000 x 1000 line raster, 10^6 picture elements must be resolved. If the raster is scanned out in 4.0 seconds a time constant of less than 4×10^{-5} seconds is needed and a shunting resistor of 100 is required for one cell. A logarithmic response is predicted if the cell is used as an open circuit voltage source, the voltage appearing at the cell terminals being given by:

$$V = \frac{kT}{q} \ln \left(1 + \frac{I_L}{I_o}\right)$$

where I_L is the current when the cell is illuminated. However, the low frequency response of this arrangement precludes its use.

IV. SURFACE INHOMOGENEITIES

A cell was scanned with an electron beam to illustrate surface variations. Little variation was noticed over large areas of the cell, but smaller irregularities were seen. Fig. 3 illustrates surface inhomogeneities. It is interesting to note the change in the scanned image as the beam voltage is changed.

These images do not show the regular dislocation patterns observed by other authors on shallow diffused junctions. Perhaps this is because of the very heavy doping of the surface layer or the unprepared surface.

V. EXPERIMENTAL CONDITION AND RESULTS

The cells used to obtain the following results were made by HOFFMAN (El Monte, California) #120CLVC. They measure (2.0 cm x 1.0 cm x .25 cm). A metallic backing serves as one contact with a thin metallic strip as the other. The cells originally came with a laquer coating which was removed by soaking them in acetone for several days. Fig. 4 shows schematically the mounting arrangement and sample holder. The set of scanning coils in the top of the holder was used in a double deflection system which made angle scans of selected areas possible. Using the cells as BSE detectors the angle scanning pattern shown in Fig. 5 was obtained from a cleaved surface of silicon. The series cell connection tends to suppress differences between the cells and is therefore advantageous for angle scanning image. The experimental work for this paper was performed using an ARL EMX-SM.

REFERENCES

1. Coates, D. G., Phil. Mag. 16, 1179-1184 (1967).

2. Everhart, T. E. and Thornley, R. F. M., "Wide Band Detector for Micro-Microampere Low-Energy Electron Currents", J. Sci. Instrum., 37, 246-248 (1960).

3. Wolf, E. D. and Everhart, T. E., "Electron Beam Channeling in Single Crystal Silicon by SEM", Appl. Phys. Letters, 14, 299-300 (1969).

4. Gonzoles, A. J., Semiconductor Secondary Electron Detector, 4th Annual Symp. on E, I, and L Beam Tech. (1967).

5. C. A. Klein, Proc. of the International Conf. on the Phys. of Semiconductors p. 307, Kyoto, (1966).

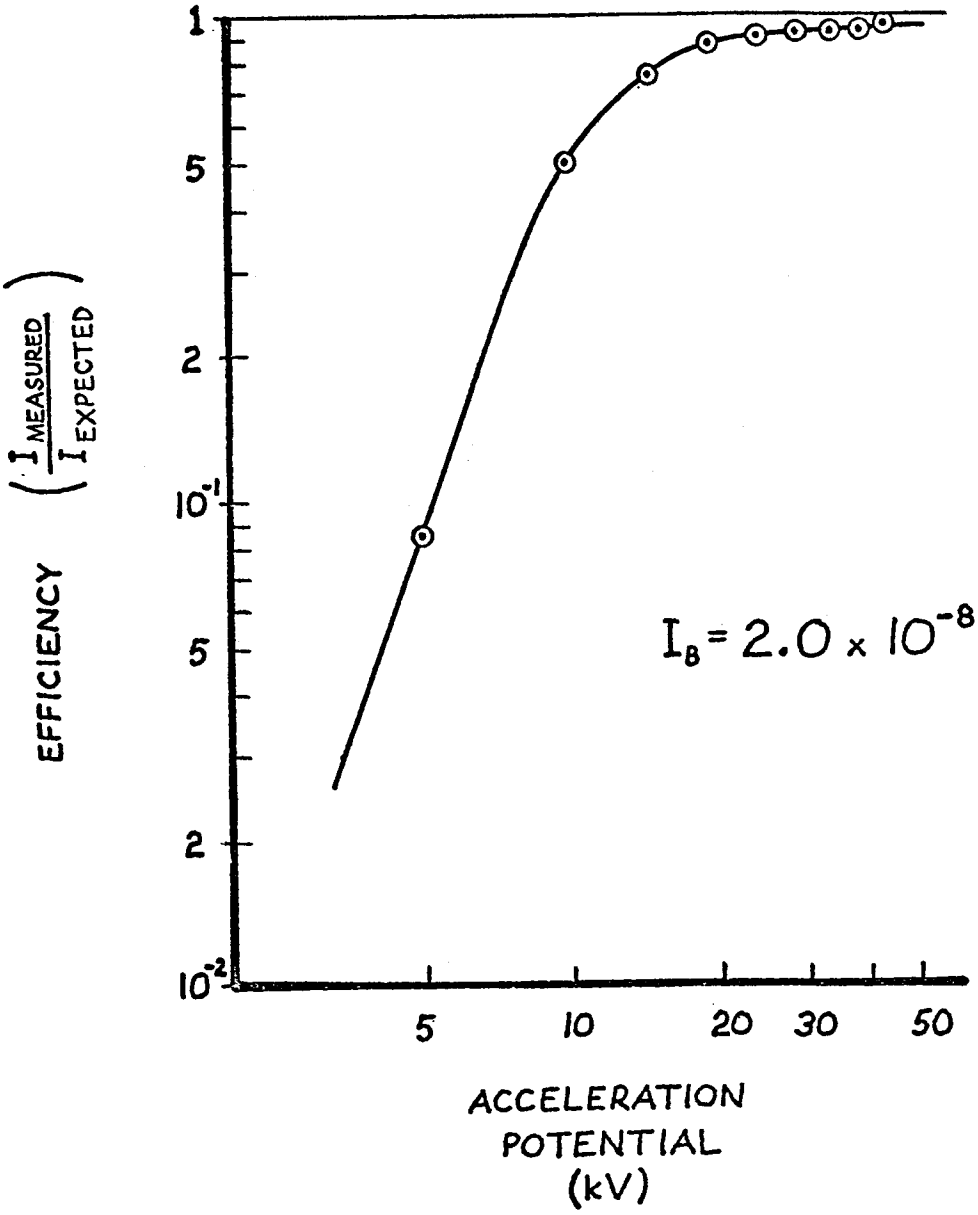
EFFICIENCY $\left(\frac{I_{MEASURED}}{I_{EXPECTED}}\right)$
1
5
2
10^{-1}
5
2
10^{-2}
$I_B = 2.0 \times 10^{-8}$
5
10
20
30
50
ACCELERATION POTENTIAL (kV)

fig. 1

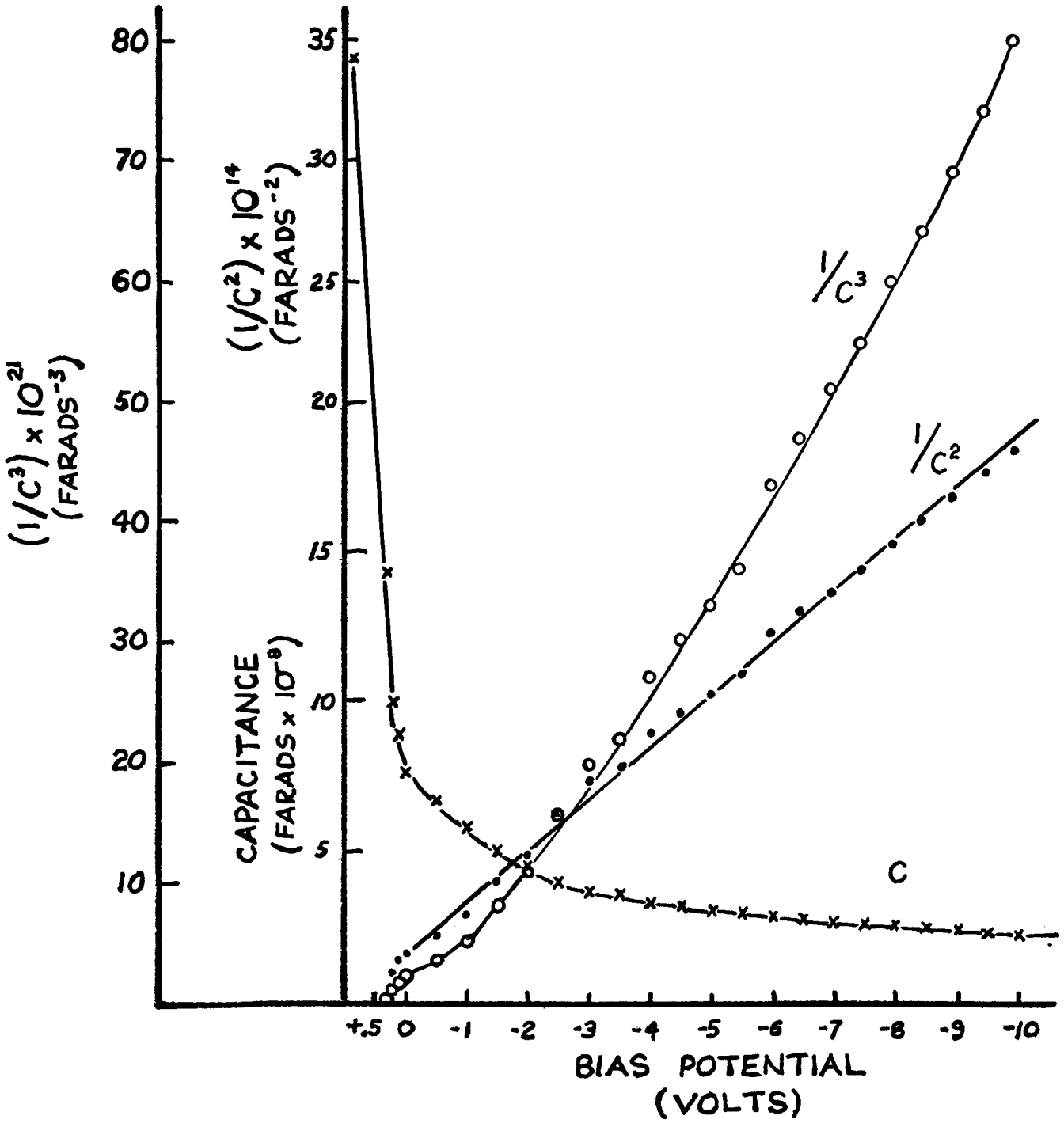
80
70
60
50
40
30
20
10
35
30
25
20
15
10
5
$(1/C^3) \times 10^{21}$ (FARADS^{-3})
$(1/C^2) \times 10^{14}$ (FARADS^{-2})
CAPACITANCE (FARADS $\times 10^{-9}$)
$1/C^3$
$1/C^2$
C
+.5 0 -1 -2 -3 -4 -5 -6 -7 -8 -9 -10
BIAS POTENTIAL (VOLTS)

fig.2

a

b

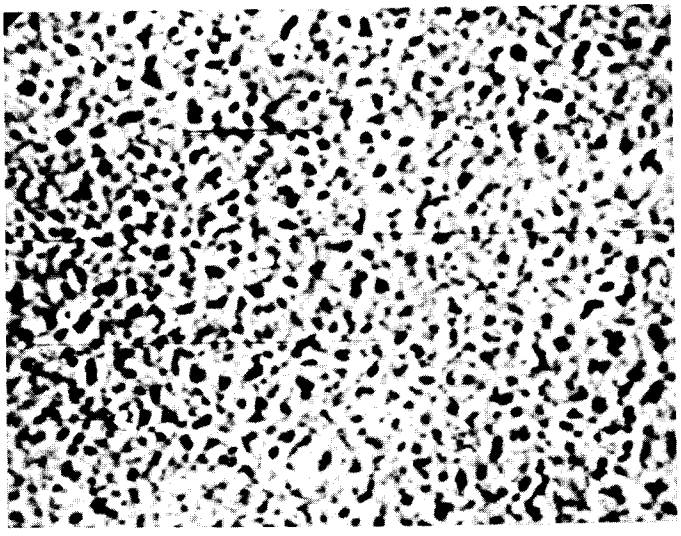

c

fig.3

Surface of silicon solar cell at 500x

a) 5 kV $I_b = 2.0 \times 10^{-7}$ a

b) 18 kV $I_b = 5.5 \times 10^{-8}$ a

c) 45 kV $I_b = 3.0 \times 10^{-8}$ a

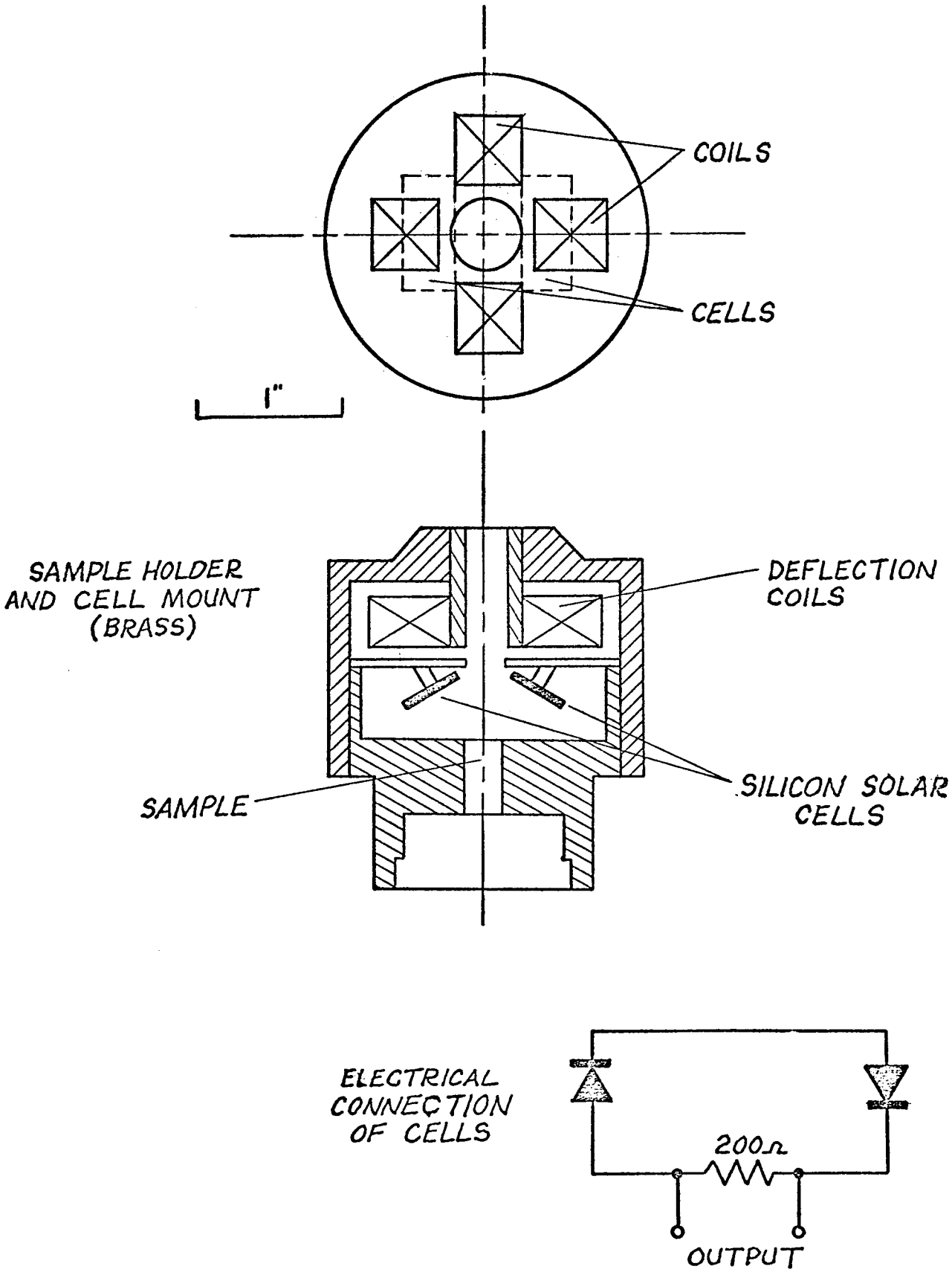
COILS
CELLS
1"
SAMPLE HOLDER AND CELL MOUNT (BRASS)
DEFLECTION COILS
SILICON SOLAR CELLS
SAMPLE
ELECTRICAL CONNECTION OF CELLS
200Ω
OUTPUT

fig.4

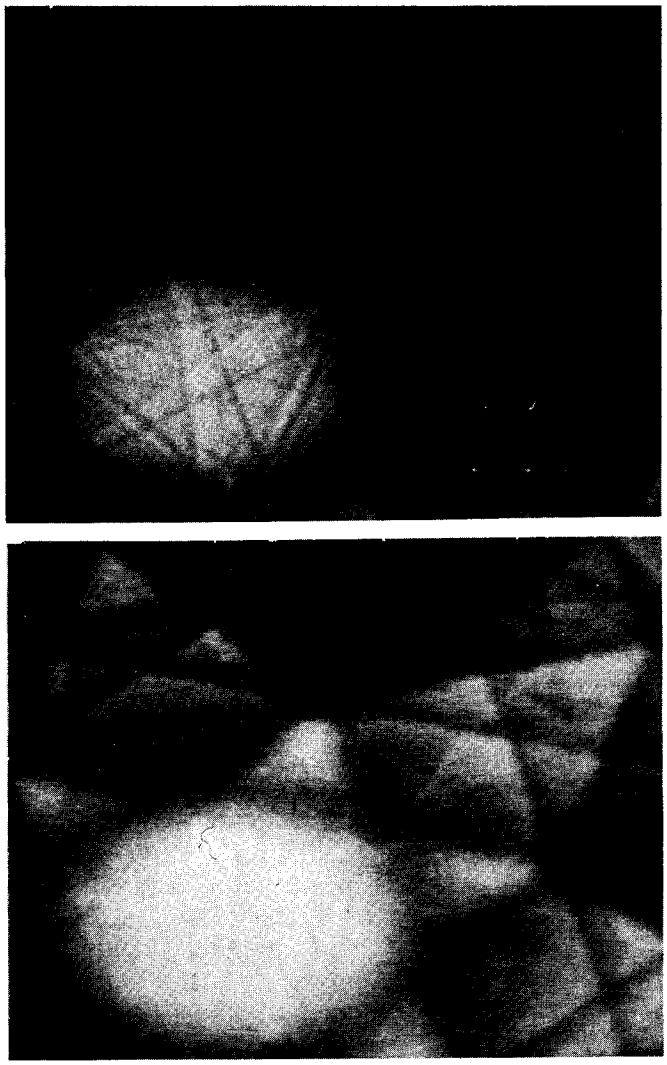

COATES PATTERNS

35 kV $I_b = 4.5 \times 10^{-7}$ a

fig.5

A PRACTICAL CONVOLUTION TECHNIQUE FOR INTERPRETING ELECTRON PROBE RESULTS

J. B. Gilmour, G. R. Purdy and J.S. Kirkaldy
Department of Metallurgy
and Materials Science,
McMaster University,
Hamilton, Ontario,
Canada.

When steep concentration profiles or localized concentration changes are analysed with the electron probe, the true concentration profile is smeared due to the finite mass of material from which X-rays are emitted. If this smearing can be mathematically resolved, a significant improvement in effective spatial resolution should result.

Theory

The observed X-ray intensity distribution from a specimen is the mathematical convolution of the true concentration profile with what will be called the probe function. This latter function is a rather nebulous concept physically although it is well defined mathematically. It may be thought of as the spatial intensity distribution of the emitted characteristic X-ray time being investigated, suitably normalized such that it is concentration independent. If one can determine this function under known conditions which closely approximate the analytical one* then it becomes mathematically possible to deconvolute the experimentally determined profile and obtain the true concentration curve. However, in practice we have found it more profitable to perform the "forward" calculation. The probe function is convoluted with a theoretical concentration profile and the calculated curve compared with the experimental result. Convolutions of this type may be readily carried out using numerical methods and machine computation. Perhaps the simplest technique is to represent both functions by their ordinates at some small interval (0.2μ in this study) and then to multiply the ordinates together as if they were the coefficients of a very high order polynomial.

Experimental

The probe function may be experimentally determined by passing the beam over a known concentration step made by clamping 2 alloys (similar to the material to be analysed) together, sectioning at right angles to the interface and polishing. In the present study we have used an iron-iron 3.5% manganese couple. Figure 1 shows the result of a step scan across such a sample. A simple timing device allowed the sample to be moved small reproducible distances (1/3 micron).

If it is assumed that the probe function is gaussian, then the probe trace should be an error function. It may be shown that the particular gaussian can be obtained

* This requirement places rather severe restrictions on the type of system which can be successfully treated using this method.

from an error function by measuring only the parameter "d" shown in Figure 1. The gaussian is then

$$g(x) = \frac{1}{d} \exp - \frac{\pi}{4} \left[\frac{x}{d}\right]^2$$

If the polynomial multiplication method is used for carrying out the convolution then the gaussian is normalized such that the sum of its ordinates at the interval decided upon is unity.

Figure 1 also shows the result of the calculation of the expected probe result for this step function and it may be seen that the assumption that the probe function is gaussian appears justified.

Once the probe function has been determined it may be used with theoretical or predicted concentration profiles to calculate the expected probe result and this may be compared with experiment. A typical result is shown in Figure 2 for the redistribution of manganese during the growth of proeutectoid ferrite in a 2.09 Atomic % Mn 1.11 Atomic % C steel transformed for 5 days at 728°C. The predicted profile was determined from the solution to the diffusion equations assuming a local equilibrium interface (1). This predicted concentration curve was convoluted with the probe function, (determined just before the analysis of the sample) and the result compared with the experimental points. The curve (predicted microprobe result and experimental points) have been positioned laterally to give a visual best fit.

In determining all experimental points, the samples were positioned such that the grain boundary was parallel to the direction of the spectromer take off. In addition, profiles which showed greater than expected width and decreased height were discarded on the assumption that these represented grain boundaries which intersected the surface at an angle.

Conclusion

The relatively simple method described, when properly carried out, allows a significant improvement in the effective spatial resolution of the microprobe. This should be of assistance to others studying similar topics.

Reference

1. G. R. Purdy, D. H. Weichert and J. S. Kirkaldy: Trans. Met. Soc. AIME, Vol. 230, p. 1025, 1964.

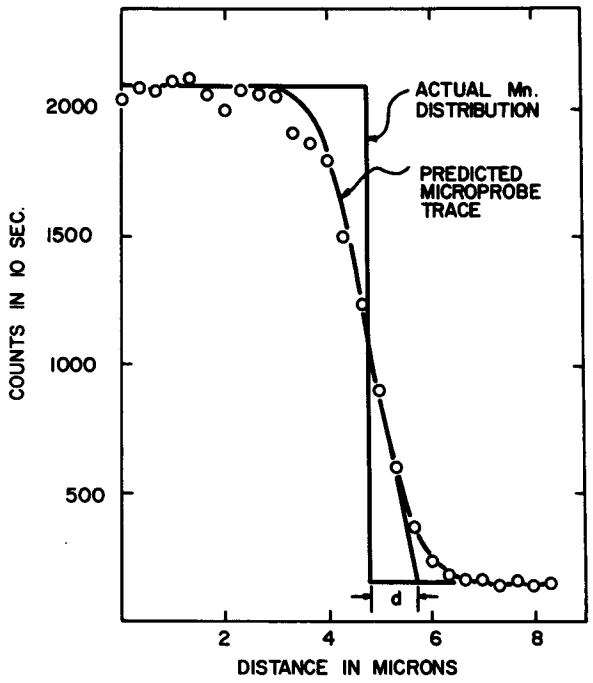

Figure 1: Electron probe microanalysis of a manganese concentration step. Predicted line is assuming a gaussian probe function with d = 0.9μ.

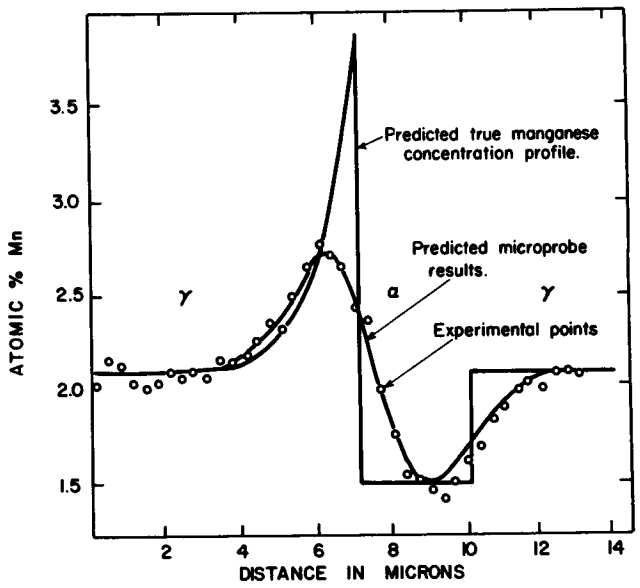

Figure 2: Microprobe analysis of a 2.09 Atom % Mn, 1.11 Atom % C alloy transformed for 5 days at 728°C.

THE LOCATION OF TRAPPED CHARGE INTRODUCED INTO THE SILICON DIOXIDE PASSIVATION LAYER OF AN INTEGRATED CIRCUIT DURING ELECTRON BEAM MICROANALYSIS

John J. Bart
John R. Haberer

Reliability Physics Section
Reliability Branch
Rome Air Development Center
Griffiss AFB, New York

INTRODUCTION

One of the important questions that arises during electron beam studies on solid state electronic devices is what type of damage is introduced after bombarding them with electrons. Early work in this area[1] reported degradation of such electrical parameters as reverse leakage current and current gain on integrated circuits which had undergone electron beam microanalysis. These studies indicated that electrons trapped within the thin silicon dioxide layer used to passivate the active regions of the integrated circuit were responsible for the observed parameter changes.

One of the factors which remained unknown was how these trapped charges were spatially distributed within the oxide layers. The microprobe was not an effective method of performing this type of a study because the electron beam would disturb or completely mask the previously established charge distribution.

The purpose of this paper is to present the initial results of mapping the location of trapped electrons using a nonperturbing method of analysis.

APPROACH

A previously reported[2] photoscanning technique was used to perform this investigation. As shown in Figure 1, a beam of light approximately 10 microns in diameter is scanned over the surface of a silicon device. Light absorbed within the silicon generates hole-electron pairs. Those carriers generated near or within the depletion region of a p-n junction result in current flow through the external circuitry. This current then is sensed as a photovoltage (Vp) developed across a high impedance load.

The sample studied was a commercially available linear operational amplifier integrated circuit. Figure 2 is a cross-sectional diagram of the resistor structure of this device which exhibited an inversion of the n-type silicon after electron bombardment in a microprobe. The electrons trapped within the oxide layer induced a change of surface conductivity which results in a continuous layer of p-type silicon connecting the various segments of the diffused p-type resistor material. Since the light beam is absorbed very close to the silicon-silicon dioxide interface, a photovoltage is generated which shows the location of these lateral induced p-n junctions. The photovoltage signal is measured between the metal contacts to the p and n-type silicon.

Another feature of this structure is the presence of a double layer of passivating silicon dioxide. This results in a discontinuity between the pyrolytically deposited and thermally grown oxide layers.

RESULTS

The photovoltage micrographs shown in Figure 3 are obtained by scanning the light beam in a raster over the surface of a device resistor structure and amplifying the generated photovoltage signal to intensity modulate a display oscilloscope.

Figure 3a is the response from a device which failed due to a high resistor-to-substrate leakage current. In addition to the normal response along the entire length of the diffused resistor, a bright diffuse region is seen near the upper left corner. This is the location of an inversion layer formed between the resistor and substrate due to negative ion contamination.

Figure 3b shows a typical response after irradiating a small portion of a similar noncontaminated resistor structure in the microprobe. A five kilovolt electron beam was scanned over the area bounded by the bright square response for five minutes. The beam current was four microamps.

The absence of a photovoltage response from the area under electron bombardment indicates that the oxide was made sufficiently conducting by the beam to remove most of the trapped electrons. The region around the scan indicates the presence of the trapped electrons which can cause surface inversion. It is suspected that the electrons are trapped very near or at the interface of the deposited and thermal oxides primarily because of the ease by which the induced inversion is eliminated at elevated temperature. Figure 3c shows the irradiated device after a 10 minute bake at 125°C, indicating the annealing characteristics of these trapped electrons.

Using this technique we observed reproducible effects of the electron beam not only on the same circuit after several irradiation-temperature cure cycles, but also on different devices with identical construction.

CONCLUSION

Results of mapping the spatial distribution of electrons introduced during electron beam analysis of integrated circuits indicate the major contribution to device surface inversion and electrical parameter degradation comes from a region adjacent to the area struck by the electron beam and not from within the scanned area itself.

REFERENCES

1. C. C. Nealey and C. W. Laakso, "Physics of Failure in Electronics," pp. 142-171, Vol. 3, 1965.

2. J. R. Haberer, "Physics of Failure in Electronics," pp. 51-82, Vol. 5, 1967.

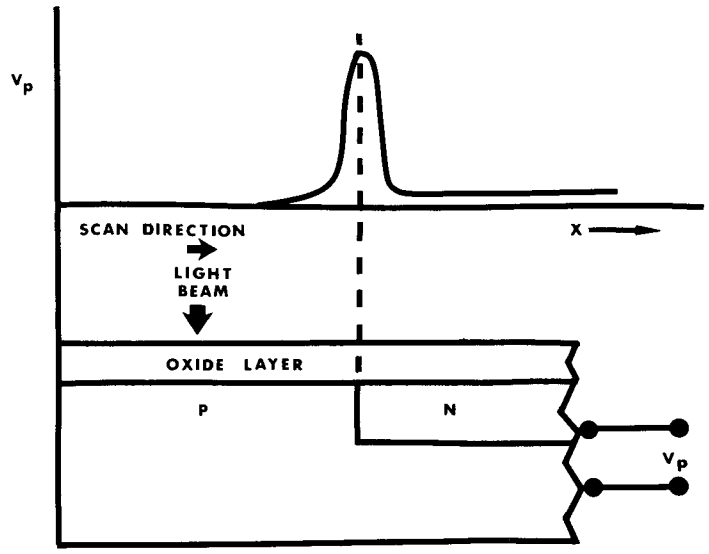

FIGURE 1
Photovoltage Response of a P-N Junction

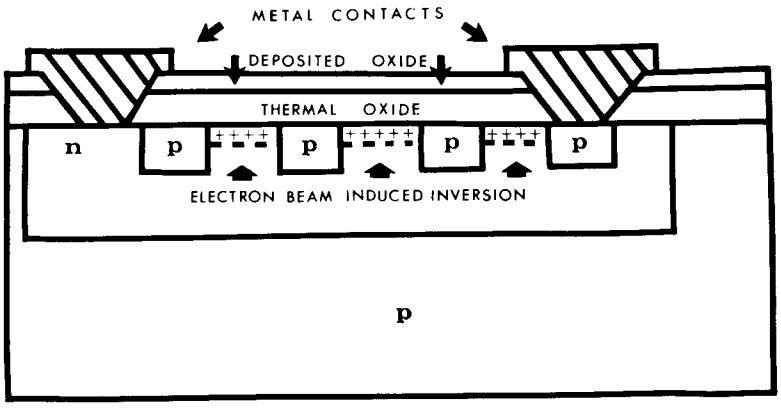

FIGURE 2
IC Diffused Resistor Structure with an
Electron Beam Induced Inversion Layer

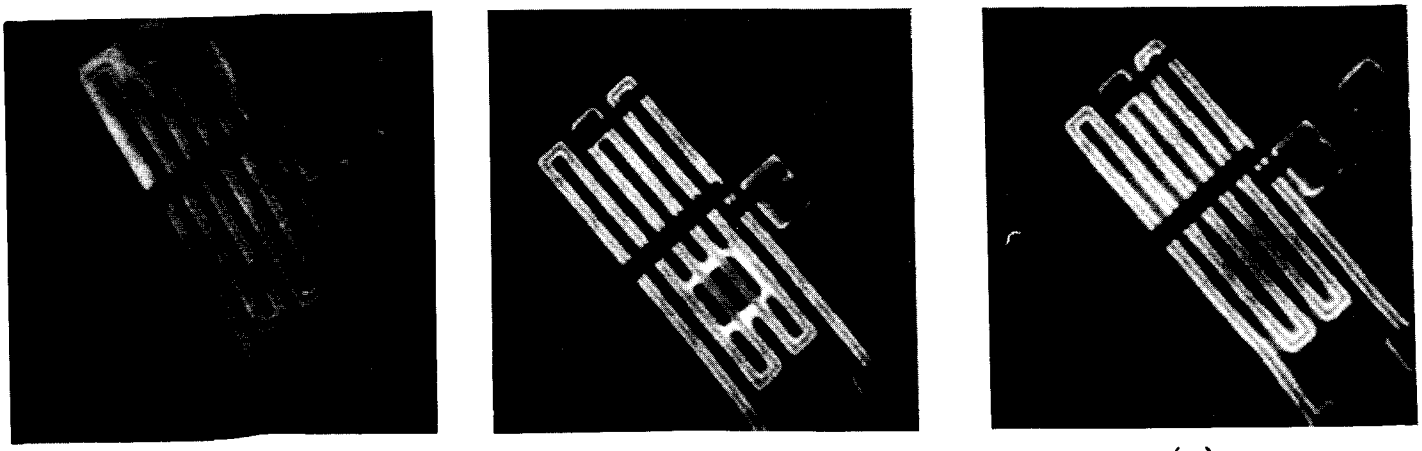

(a) (b) (c)

FIGURE 3
Photovoltage Micrographs of an IC Diffused Resistor Structure

A SIMPLIFIED ELECTRON MICROPROBE

Michael A. Bayard
Walter C. McCrone Associates, Inc.
449-493 East 31st Street
Chicago, Illinois 60616

The electron microprobe has always been a large, complex analytical tool. However, for many types of analyses the refinements available on the microprobe are simply not used. Accordingly, a very much simplified electron probe device has been developed. It will perform qualitative and semi-qualitative analyses on sample areas of about 5 μm diameter. The elemental range covered is from magnesium on up using a solid state detector.

The mini-probe consists of a focusing electron gun and an aperturing system to form the electron spot. The spot size is between 5 and 10 μm. An optical microscope is provided to view the area of the sample being analyzed. Like the optical arrangements of the microprobe, this microscope is a compromise between performance and working distance. A magnification of 180X and resolution of 1.7 μm is used. A mechanical stage with x, y and z motions is available.

The major advantage of this instrument is simplicity of operation. Sample change can usually be accomplished in less than one minute. Set up of the electron beam involves only three controls. Beam stability is good and beam wander minimal due to close aperture to sample distance. In general, a person able to use an optical microscope can be trained to use the mini-probe in a matter of a few hours.

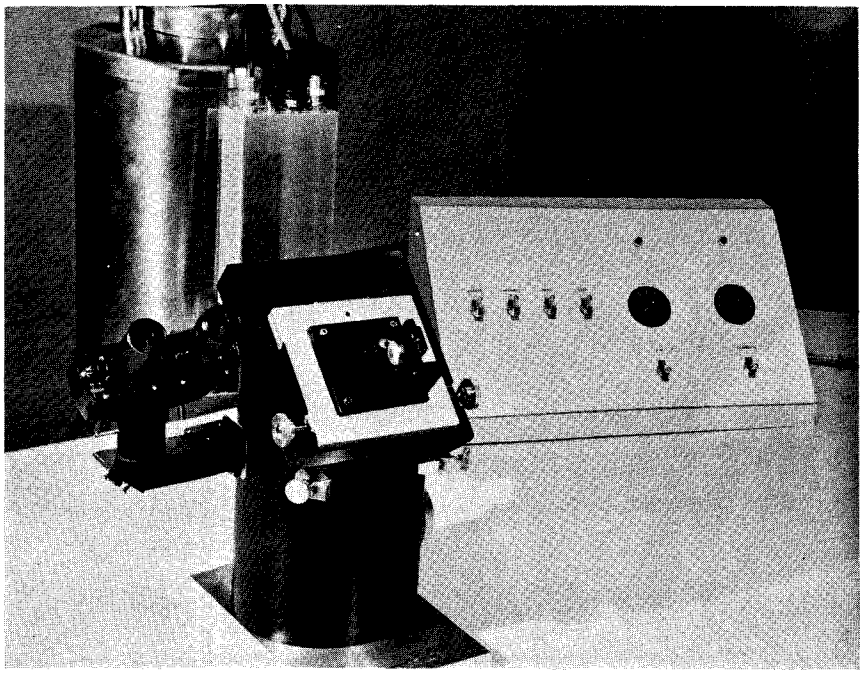

Fig. 1. Overall view of probe-forming unit. The electron gun is in the lower part of the cylindrical housing. The sample mounts on the top plate which is hinged for sample removal. The non-dispersive cryostat is located immediately behind the probe.

UNIVERSAL X-RAY DETECTOR: A FLOW PROPORTIONAL COUNTER FOR ANALYSIS OF ALL ELEMENTS FROM BERYLLIUM TO URANIUM*

by

A. J. Tousimis and J. A. Nicolino
brc-LABORATORIES and brc-INSTRUMENTS
Biodynamics Research Corporation
Rockville, MD. 20852

Flow proportional counter tubes have many advantages over the solid state detectors (for example lithium drifted silicon or germanium diodes coupled with low noise amplifiers). The solid state detectors are practical for very rapid qualitative analysis of the sample preferably for elements with atomic numbers higher than 13. These windowless solid state detectors are very useful in electron probe analysis when they are used in conjunction with the multichannel analyzer since they can present the entire detectable elemental spectrum for example in a 50th to a 100th of the time required for the same presentation using a standard X-ray spectrometer. Unfortunately, the solid state detectors have very poor signal-to-noise ratios ranging from 7 to 25 for calcium and chromium, respectively, as compared to over 1,000 for the same elements in the case of flow proportional counters when used in the spectrometer. Both types of detectors are not useful for the detection of low atomic elements such as nitrogen or oxygen since the resolution of the solid state detector is more than 150 volts and the flow proportional counters are affected by the poor transmission of the thin film windows.

A new window material, high in nitrogen content, showing at least ten times improvement in transmission of characteristic lines for Nitrogen $K\alpha$ has been developed. The detector with this new window is shown in Figure 1. Characteristic X-ray line percent transmission properties of this material versus the standard thin window material used in other commercially available detectors are listed on the following page.

*We are indebted to Dr. C. M. Taylor, Mr. R. Mattson, Mrs. K. Hoag, and Mrs. P. Monti for their cooperation during the developmental stages of this project.

X-RAY PERCENT TRANSMISSION OF
DETECTOR THIN WINDOW MATERIAL
IN THE 8.0Å to 70.0Å REGION

Window Type	% Transmission					
	B-Kα	CKα	NKα	OKα	FKα	NaKα
1/8 mil Mylar	1.1	19.0	0.5	2.0	1.9	26.7
Polypropylene	46.0	77.0	6.4	23	47.7	77.5
Nitrolucid™	87.0	91.0	69.0	85	91.2	94.0

TM-Trademark, applied U. S. Patent Office.

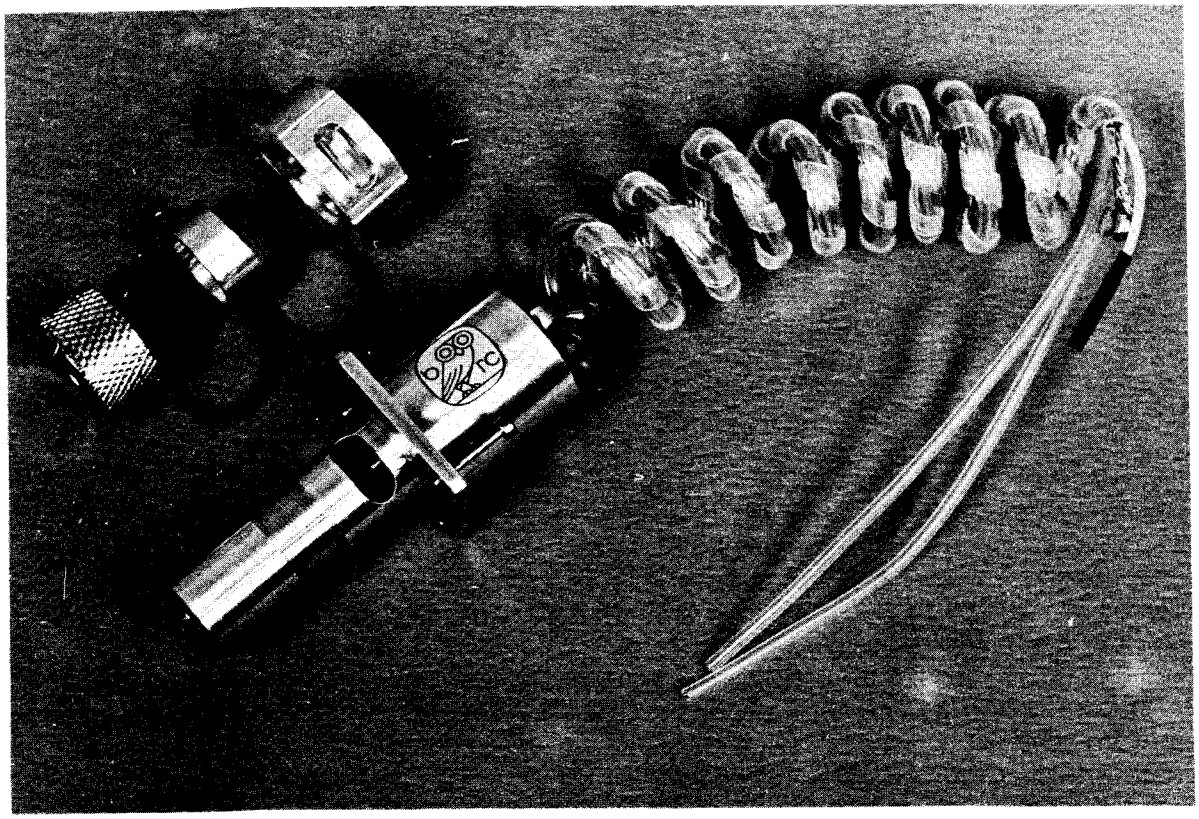

Figure 1. The Universal X-ray flow proportional counter with readily replaceable thin film window. The window ring is shown on the upper left. Size of the ring is less than 2.5 cm. in diameter.

With the new type of film and detector, the increase of transmission is evident for all wavelengths shown with the most dramatic improvement for nitrogen and oxygen. For this thin window detector, the optimum gas pressure was found to be approximately 200 mm-Hg, with gas mixtures containing higher percentage of methane (90%) than noble gases. An added advantage of the new detector is ease with which the window can be changed. The photograph of the new detector shows it with an extra window next to it. The window is replaced (Patent applied for-U. S. Patent Office) by simply removing the retaining ring. The gas feedthrough is also modified from that of now commercially available detectors. The combination of these improvements has resulted in a superior-performing detector for the analysis of specimens containing elements from Be to U with the electron probe x-ray microanalyzer.

A NOVEL SAMPLE SPINNER FOR UNIFORM FILM COATING OF NON-CONDUCTING SAMPLES FOR ELECTRON ANALYSIS AND SCANNING ELECTRON MICROSCOPY*

by

A.J. Tousimis and J.A. Nicolino
brc-Laboratories and brc-Instruments
Biodynamics Research Corporation
Rockville, MD. 20852

When a solid surface is bombarded with an electron beam of sufficient voltage, electrons with energies ranging in value from that of the impinging electrons down to less than 10 eV are emitted (backscattered) from the solid. This phenomenon was recorded in 1902 by Austin and Starke (1). The backscattered electrons are composed of the "true" secondaries (electrons with energies less than 50 eV), the elastically scattered (electrons with energy equal to that of the original electron beam) and the inelastically scattered (electrons that have lost their initial energy or those removed from the solid itself). The physicochemical nature of the bombarded surface of the specimen influences greatly the relative yield of the reflected electrons. Any of these backscattered electrons could be measured, provided suitable detecting systems are employed. Very simple devices are used to measure the intensity of the backscattered electrons, especially in scanning electron probe analysis while a combination of postacceleration, scintillation pipes and photomultipliers are employed for the detection of secondary electrons in scanning electron microscopy. Consequently, since specimens of various surface topography, elemental composition and electrical conductance are examined by SEM, a uniform and complete cover by layer of a high yield true secondary electron emitter is desirable. Heavy elements such as Pt, Pd, Au and others that can be evaporated onto the surface of the specimen are commonly used. A uniform layer of these heavy metals on the surface of the specimen not only contributes to better quality scanning electron micrographs but also will avoid any charging effects from portions of a non-conducting specimen which was not coated.

An apparatus meeting all of the above requirements has been developed and is in use in our laboratories for the past several years. The principle is illustrated in figures 1 and 2. The specimen to be coated is placed exactly in the center of a rotating holder about axis A while the entire assembly rotates about axis B. As a result of this movement, the sample is tilted from 0° to 90° with reference

---

* We wish to acknowledge the cooperation and assistance of Mr. T.R. Padden, Dr. Erik Pattola and Mr. R.A. Mattson during the development of this apparatus.

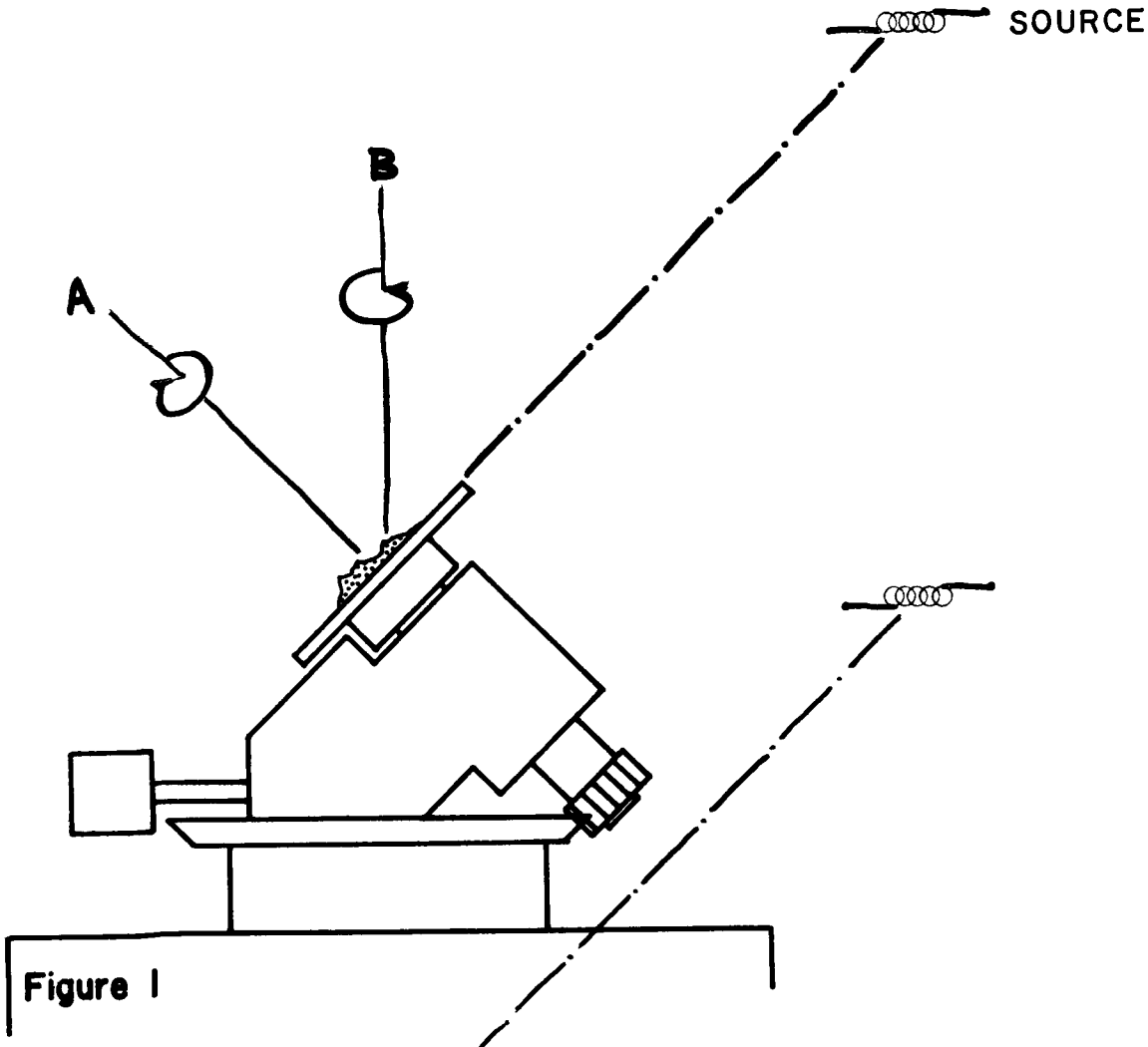

Figure 1

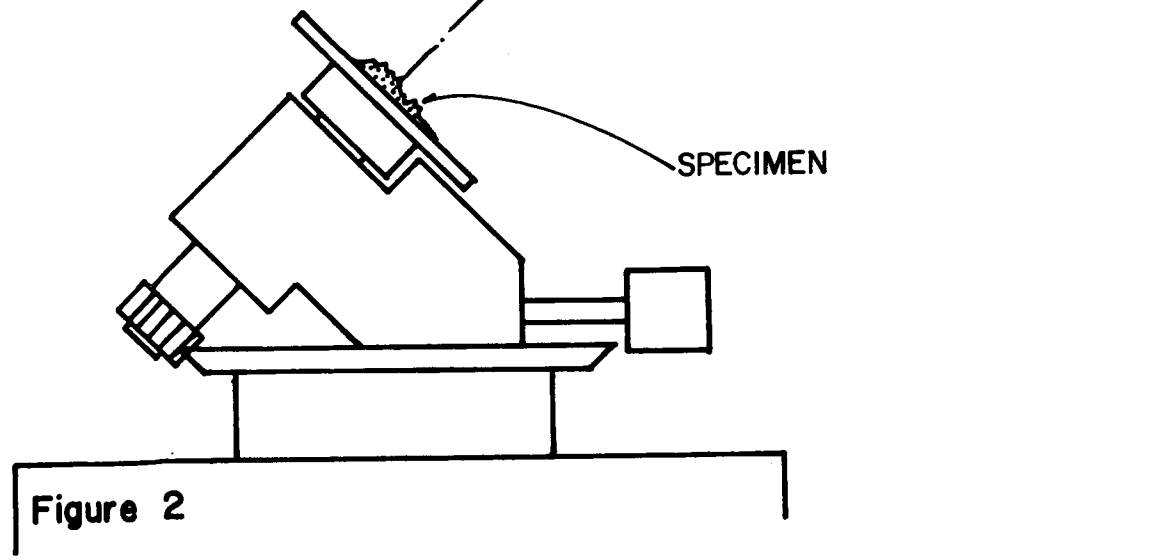

Figure 2

Figures 1 and 2. Schematic illustration of the SAMSPIN(TM) principle.

Figure 3. Photograph showing the sample spinner for uniform coating of specimens for SEM, EPA and TEM replicas.

to the metal source during evaporation of the metal alloy or carbon on the specimen. Figure 3 shows a photograph of this apparatus. The uniformity of coating of specimens of various shapes has been tested by producing carbon replicas of objects such as red blood cells and microsporidia (2) and sectioning of Pd-Au coated intestinal villi.

REFERENCES

(1) AUSTIN, L. and H. STARKE, Ann. Physik, 9, 271 (1902).
(2) TOUSIMIS, A.J. and T.R. PADDEN, Proc. 27th Annual EMSA Meeting, p. 44 (1969).

PRESENT STATUS OF MICROANALYSIS IN JAPAN

Gunji Shinoda
Japan Women's University
8-1, Meji Rodai 2 Chome
Bunkyo-Ku, Tokyo, Japan

This paper will include the following topics:

1. Further development of Shimizu Monte Carlo calculation, especially on light alloys.

2. Toyota Central Laboratory's newly published "Quantitative Analysis Chart" and its related fields.

3. Recent works of SEM group.

4. Ion microanalyzer and its applications of Hitachi group and Osaka University group.

5. Present status of auger electron spectroscopy.

THE DEPENDENCE OF ANALYTICAL ACCURACY UPON X-RAY SPECTROMETER GEOMETRY

P.J. KILLINGWORTH; CAMBRIDGE SCIENTIFIC INSTRUMENTS LTD., CAMBRIDGE. ENGLAND

Historically it has been maintained that the accuracy of quantitative analysis is governed principally by the reliability of data available for X-ray intensity correction. Increasing accuracy of coefficients and improvements in correction theory, combined with the use of computer programmes for iterative correction now invalidate this assumption for many elemental systems and necessitate a re-examination of the contribution of instrument/operator errors to overall analytical accuracy in routine analysis.

In theory, a wavelength dispersive x-ray spectrometer possesses a very simple geometry, which should contribute little to experimental errors; in practice, the versatility demanded of a microprobe, particularly beam scanning facilities, necessitates the incorporation of features requiring precise adjustment for accurate analysis, with consequent liability to error.

Given sufficient time, and a sufficiently careful operator, almost any assembly of electron and x-ray optics will yield an accurate experimental point analysis of a specimen, but careful consideration of spectrometer geometry and orientation is required if this accuracy is to be achieved on a routine basis. As a basic premise, let us assume that each measurement of x-ray intensity is required to be accurate to 1%, error will then be of the same order of magnitude as can be anticipated for subsequent correction procedures (1) There are then three causes of such error for which the spectrometer may be considered as the prime source:

Basic repeatability of the spectrometer mechanism
Movement of the x-ray source away from the Rowland circle
X-ray absorption within the specimen, which varies with take-off angle

The average point analysis may be taken to involve a volume of material approximately 2μm in diameter. Thus, if the material is inhomogeneous on the micro-scale, it becomes impractical to traverse from specimen to reference standard and hope to return to the same spot to within 1%. It therefore follows that either sufficient spectrometers must be available to permit simultaneous analysis of all constituents - which is both expensive, and seldom possible from an engineering viewpoint - or it must be possible to translate the spectrometers from one angle to another and return with the required precision. If a spectral scan is generated by scanning the spectrometer, it will be found that 1% fall-off in peak intensity occurs at approximately $\pm$ 7½ seconds of arc from the Bragg angle. Considering now spectrometer geometry, crystal and counter can be maintained on the Rowland circle with relative ease; this should be achieved by mechanical design rather than operator adjustment, if a further

source of error is not to be introduced. Repeatabilities of $\pm 7\frac{1}{2}$ seconds can then be consistently achieved, provided no limitation is inherent in the mode of angular setting. One simple way of overcoming manual setting errors is by use of servo-control; this permits the required angular settings to be stored and called up as required, and hence eliminates operator adjustment. Some similar method is almost essential, since tuning by ratemeter signal will not give the required accuracy, and use of the scalers for this purpose is generally too time-consuming to be considered for routine use.

Movement of the x-ray source away from the Rowland circle may be caused by one of two effects, shift of the electron beam over the surface of the specimen, or variation in specimen height. The first of these is not generally applicable in quantitative analysis, provided that the specimen itself can be traversed under the electron beam with sufficient accuracy to permit positioning of the area of interest; but height variation can be significant in two respects. It has been shown (2) that relatively small slopes on the surface of the specimen can give rise to appreciable errors in absorption correction, requiring, for example, an alignment of better than 1^{o} if the required accuracy is to obtained for a 20^{o} take-off angle. Secondly, although by means of an optical microscope, specimen height can be relatively accurately set for a static analysis, this is not practical for analysis either continuously or by automatic stepping, along a line generated by motor-driving the specimen stage. The geometry of a spectrometer is such that small shifts in source position in the direction of take-off of the x-ray beam, or in a direction perpendicular to the plane of the Rowland circle have only a secondary effect upon the x-ray intensity detected, butshift in a direction across the curvature of the crystal is, to a first approximation analagous to scanning through the x-ray peak. It is thus important that height variation should have a minimum component in this direction. For any height change, the locus of x-ray source movement will lie along the path of the electron beam, this means that the spectrometer should be oriented so that either the plane of the Rowland circle is perpendicular to the electron beam or the source-crystal direction is as closely aligned to the electron beam as possible. The former of these is only possible in conjunction with a tilted specimen, but gives exceptional insensitivity to height change, measurement on the Cambridge Stereoscan shows that the specimen height may be changed by 8mm for a 5% variation in detected intensity. Alignment close to the electron beam presents certain engineering problems, but by taking the x-rays back through the bore of the objective lens, a 15^{o} angle to the beam can be achieved, giving a 75^{o} take-off angle for a specimen normal to the electron beam. The angle subtended at the crystal by a given height change is a function of the source-crystal distance, 1; for a linear spectrometer, this varies with Rowland circle radius, R, and Bragg angle, θ according to the formula

$$1 = 2R \sin \theta$$

height sensitivity can therefore be reduced by increasing R; and for any given geometry will be maximum at low angles. Then, for 1% accuracy, i.e. $7\frac{1}{2}$ seconds of arc angular variation, the permitted height variation h is given by

$$h = \frac{1.\sin(7\frac{1}{2}\text{secs})}{\cos \phi}$$ where ϕ is the take-off angle.

and for R = 250mm, $\phi = 75^{o}$ and $\theta = 15^{o}$

$h = 18\mu m$

Such a geometry can therefore tolerate a specimen height change of $\pm$ 18 μm during the course of a line scan. It will be noted that h is inversely proportional to cos Ø, and consequently that this height tolerance diminishes rapidly for lower take-off angles, becoming, for example approximately $\pm$ 6 μm at 40° take-off angle.

The third significant source of error is the absorption of x-rays prior to emission from the specimen, the effect of path length upon this parameter has been well documented, showing that the absorption correction diminishes with increasing take-off angle, but the fluorescence correction increases. Where analysis aims at 1% accuracy, the fluorescence correction is generally negligible, being of this order of magnitude for many systems, and hence the influence of even a 10% error in the correction will not generally be significant. Absorption, alternatively, may reduce the detected intensity by a factor of 2 , consequently errors in its calculation are as significant as those in measured intensities. Absorption is a function of the cosecant of the take-off angle, and hence is again reduced at high angles.

Thus, to obtain consistent accuracy in quantitative analysis, which is substantially independent of operator error it is important to have spectrometers of large Rowland circle and high mechanical repeatability, positioned to give a high x-ray take-off angle. In general some means of resetting these spectrometers other than be reference to a ratemeter signal is required. This geometry must then be combined with a specimen stage whose traverses are precisely aligned to the plane of the specimen, and a further source of error is eliminated if reference standards lie in the same plane within the tollerance of the spectrometer geometry.

References.

1. K.F.J. Heinrich & H. Yakowitz: 5th Congress on X-ray Optics and Microanalysis Springer-Verlag 1969.

2. T.R. Sweatman & J.V.P. Long: J. Petrology Vol 10 No. 2. 1969. pp 332-379

INDEX OF AUTHORS AND THEIR AFFILIATIONS

		Paper Number
Conley, D. K.	Western Electric Company, 555 Union Boulevard, Allentown, Pennsylvania, 18103	9
Crewe, A. V.	Enrico Fermi Institute, University of Chicago, Chicago, Illinois, 60637	7
DiGiacomo, G.	IBM Corporation, East Fishkill Facility, Hopewell Junction, New York, 12533	16
Fischer, D. W.	Air Force Materials Laboratory, Wright-Patterson Air Force Base, Ohio, 45433	51
Fisher, C.	Image Analyzing Computers Limited, Melbourn, Royston, Hertfordshire, England	54
Galle, P.	Laboratoire de Biophysique, de la Faculte de Medecine de Creteil, France	34
Gedcke, D. A.	ORTEC, Incorporated, P. O. Box C, Oak Ridge, Tennessee, 37830	5
Gilmour, J. B.	McMaster University, Department of Metallurgy and Materials Science, Hamilton, Ontario, Canada	57
Goff, R. F.	3M Company, Central Research Laboratories, St. Paul, Minnesota, 55101	10
Heidel, R. H.	U. S. Geological Survey, Rocky Mountain Mineral Resources Branch, Federal Center, Denver, Colorado, 80225	25
Heinrich, K. F. J.	National Bureau of Standards, Washington, D. C., 20234	29
Herfert, R. E.	Northrop Corporation, Aircraft Division, 3901 W. Broadway, Hawthorne, California, 90250	32
Holliday, J. E.	Edgar C. Bain Laboratory for Fundamental Research, U. S. Steel Corporation, Monroeville, Pennsylvania, 15146	50
Hurley, R. G.	Pennsylvania State University, Materials Research Laboratory, University Park, Pennsylvania, 16802	44
Ingram, E.	University of Iowa, Department of Physiology and Biophysics, Iowa City, Iowa, 52240	37
Jackson, M. R.	Lehigh University, Department of Metallurgy and Materials Science, Bethlehem, Pennsylvania, 18015	22

		Paper Number
Jaklevic, J. M.	Lawrence Radiation Laboratory, University of California, Berkeley, California, 94720	1
Jones, W. K.	Massachusetts Institute of Technology, 77 Massachusetts Avenue, Cambridge, Massachusetts, 02139	31
Kelly, C. J.	Ford Motor Company, Scientific Research Staff, P. O. Box 2053, Dearborn, Michigan, 48121	53
Kirkendall, T. D.	COMSAT Laboratories, Box 115, Clarksburg, Maryland, 20734	19
Knox, B. E.	Pennsylvania State University, Materials Research Laboratory, University Park, Pennsylvania, 16802	11
Kunz, F.	Ford Motor Company, Scientific Research Staff, P. O. Box 2053, Dearborn, Michigan, 48121	18, 20
Lannin, T. E.	General Electric Company, Ballecitos Nuclear Center, Pleasanton, California, 94566	24
Lauchli, A.	Texas A & M University, College Station, Texas, 77843	35
Lebiedzik, J.	Pennsylvania State University, Materials Research Laboratory, University Park, Pennsylvania, 16802	55
McFarlane, A. A.	United Kindgom Atomic Energy Authority, Risley Engineering and Materials Laboratory, Risley, Warrington, Lancashire, England	49
Morgan, R. S.	Pennsylvania State University, Biophysics Department, University Park, Pennsylvania, 16802	39
Myklebust, R. L.	National Bureau of Standards, Washington, D. C., 20234	23
Nagel, D. J.	Naval Research Laboratory, X-ray Optics Branch, Washington, D. C., 20390	52
Potosky, J. C.	University of Southern California, Materials Science Department, Los Angeles, California, 90007	56
Sabol, G. P.	Westinghouse Electric Corporation, Research and Development Center, Pittsburgh, Pennsylvania, 15235	6

		Paper Number
Savanick, G. A.	Bureau of Mines, Twin Cities Mining Research Center, Minneapolis, Minnesota, 55111	46, 47
Sheble, A. M.	Hi-Rel Laboratories, 2116 Huntington Drive, San Marino, California, 91108	40
Short, J. M.	Xerox Corporation, Xerox Square W-114, Rochester, New York, 14603	4
Solomon, J. S.	University of Dayton Research Institute, Dayton, Ohio, 45409	43
Steele, W. J.	Lawrence Radiation Laboratory, University of California, Livermore, California, 94550	14
Sternglass, E. J.	University of Pittsburgh, Radiation Center, Pittsburgh, Pennsylvania, 15213	13
Taylor, C. M.	Biodynamics Research Corporation, 6010 Executive Boulevard, Rockville, Maryland, 20852	33
Tousimis, A. J.	Biodynamics Research Corporation, 6010 Executive Boulevard, Rockville, Maryland, 20852	36, 38 41, 60, 61
Warner, R.	University of Rochester, School of Medicine and Dentistry, Rochester, New York, 14620	42
Wells, O. C.	IBM Corporation, Thomas J. Watson Research Center, P. O. Box 218, Yorktown Heights, New York, 10958	30

THE ELECTRON PROBE ANALYSIS SOCIETY OF AMERICA

MEMBERSHIP LIST

****

Mr. Ronald A. Abelman
Applied Research Labs.
P.O. Box 129
Sunland, Calif. 91040

Mr. Jerry D. Adey
Univ. of Oregon Dental School
611 S.W. Campus Drive
Portland, Oregon 97201

Mr. Arden Albee
Deivision of Geological Sciences
California Institute of Technology
Pasadena, California 91109

Mr. Leslie O. Albin
4501 Valerie
Bellaire, Texas 77401

Mr. Carmelo F. Aliotta
6 Chiarpardi Place
Beacon, New York 12508

Mr. Charles H. Anderson
9545 Wentworth Street
Sunland, California 91040

Mr. Chris A. Anderson
2402 Janin Way
Solvang, California

Dr. D.H. Anderson
Director, Industrial Laboratory
Eastman Kodak Company
343 State Street
Rochester, N.Y. 14650

Mr. Charles W. Andrews
1926 Woodward Avenue
Cleveland, Ohio 44118

Dr. Kamal Asgar
1011 N. University
110 Dental School
Ann Arbor, Michigan 48104

Mr. Clarence W. Austin, Jr.
404 Hillmont Circle N.W.
Huntsville, Alabama 35805

Mr. Donald L. Bagnoli
R.D. Horace Rd.
Oak Ridge, N.J. 07438

Mr. Alexander K. Baird
Department of Geology
Pomona College
Claremont, Calif. 91711

Mr. Joseph D. Balser
5677 N. 94th Street
Milwaukee, Wisc. 53222

Mr. R.W. Barnard
Bell Telephone Labs
Res. & Dev. Unit
Mountain Ave.
Murray Hill, N.J. 07974

Mr. John J. Bart
R.D. #2, Dix Road
Rome, New York 13440

Mr. Ahron Batt
1001 Main St. West
Apt. 419
Hamilton, Ontario
Canada

Mr. William L. Baun
7418 N. Dakar Drive
Dayton, Ohio 45431

Dr. D.R. Beaman
2210 Burlington
Midland, Michigan 48640

Mr. Albert H. Beebe, III
29 Eichelberger Drive
Coraopolis, Pa. 15108

Mr. Melvin H. Beeson
664 Tamarack Drive
Union City, Calif. 94587

Mr. Leonard J. Bench
1200 Irene Lane
Pittsburgh, Pennsylvania 15236

Mr. Ralph F. Benck
316 Bynum Ridge Road
Forest Hill, Maryland 21050

Mr. Carl Berkley
Medical Research Technology
Great Notch, New Jersey 07424

Mr. Eugene P. Bertin
Room E-120
RCA Laboratories
Princeton, New Jersey 08540

Mr. Deane I. Biehler
Caterpillar Tractor Co.
Research Dept., Tech. Center E
Peoria, Illinois 61602

Professor Wilbur C. Bigelow
Dept. of Chemistry & Met. Engng.
University of Michigan
Ann Arbor, Michigan 48104

Mr. William D. Bingle
591 Wack Drive
Rochester, Pennsylvania 15074

Mr. L.S. Birks
Code 7680
Naval Research Laboratory
Washington, D.C.

Mr. Herbert L. Black
Universal-Cyclops, Spec. Steel Div.
Res. & Dev. Dept.
Mayer Street
Bridgeveille, Pa. 15017

Mr. John W. Blaise
Research and Technology Division
Chromalloy American Corp.
Blaisedell Road
Orangeburg, New York 10962

Mr. Roger B. Bolon
R.D. #2, Lake Road
Ballston, New York

Mr. Matthew J. Boris
Senior Research Chemist
American Steel Foundries
3761 Canal Street
East Chicago. Indiana 46312

Janice F. Bower
Smithsonian Astrophysical
60 Garden Street /Observatory
Cambridge, Massachusetts 02138

Mr. David E. Boyd
613 Salisbury Road
Waverly, Ohio 45661

Mr. Edward J. Brooks
U.S. Naval Research Laboratory
Washington, D.C. 20390

Mr. Dennis B. Brown
Code 7987
U.S. Naval Research Laboratory
Washington, D.C. 20390

Dr. James D. Brown
Faculty of Engineering Science
The Univ. of Western Ontario
London 72, Ontario
Canada

Mr. Laurence C. Brown
Department of Metallurgy
University of British Columbia
Vancouver 8, B.C.
Canada

Mr. Gary G. Brumbaugh
3808 Arnell Place
LaCrescenta, California 91214

Mr. G. Brumbaugh, EPASA Rep.
Consolidated Electrodynamics Corp.
Analytical Instruments Division
1500 South Shamrock Avenue
Monrovia, California 91017

James R. Buckmelter
Hq. Air Force Cambridge Research Labs
L.G. Hanscom Field
Bedford, Mass. 01730

Mr. W.C. Budke
303 North 31st Ave.
Yakima, Washington

Mr. Garrett A. Busch
Grumman Aerospace Co.
Research Dept. PET 26
Bethpage, New York 11714

Mr. J.W. Butler
Argonne National Laboratory
9700 South Cass Avenue
Argonne, Illinois 60439

Mr. Vincent E. Caldwell
Armco Steel Corporation
Research Center
Curtis Street
Middletown, Ohio 45042

Mr. William J. Campbell
U.S. Bureau of Mines
College Park, Maryland

Mr. Kenneth G. Carroll
29 Bowdoin Street
Cambridge, Massachusetts

Mr. Michel P. Cescas
Faculty of Agriculture
Laval University
Quebec 10, P.Q.
Canada

Mr. William F. Chambers
Sandia Corporation, Org. 1122
P.O. Box 5800
Albuquerque, New Mexico 87115

Mr. Wei H. Chang
180 Prospect St., Apt. F-5
East Orange, New Jersey

Mr. Eric J. Chatfield
Department of Physics
Ontario Research Foundation
Sheridan Park, Ontario
Canada

Mr. William T. Chester
Denton Vacuum, Inc.
Cherry Hill Ind. Ctr.
Cherry Hill, N.J. 08034

Dr. Arthur A. Chodos
California Institute of Tech.
Division of Geological Sciences
1201 E. California Street
Pasadena, Calif. 91109

Mr. William C. Clinton
5-A Cryton Apts.
Rolla, Missouri 65401

Mr. J.W. Colby
3125 Linda Lane
Allentown, Pennsylvania

Mr. James R. Coleman
Dept. of Radiation Biology & Biophysics
University of Rochester Med. Ctr.
Rochester, New York

Mr. Donald K. Conley
410 Hill Drive
Allentown, Pa. 18103

Mr. George A. Conrad
Dept. of Geology
Univ. of New Mexico
Albuquerque, New Mexico 87116

Mr. Paul D. Coulter
Union Carbide Corp.
Parma Technical Center
P.O. Box 6116
Cleveland, Ohio 44101

Mr. Arthur Cox
Dominion Foundries & Steel, Ltd.
Box 460
Hamilton, Ontario
Canada

Mr. Joseph F. Cox
1032 Winne Road
Schenectady, New York 12309

Ramon Coy-yll
Ecole Polytechnique
2500 Marie Guyard Avenue
Montreal, Quebec
Canada

Mr. Robert T. Craig
370 Maple Street
Danvers, Mass. 01923

Maria Luisa Crawford
Dept. of Geology
Bryn Mawr College
Bryn Mawr, Penna. 19010

Mr. John W. Criss
6686 Naval Research Lab
Washington, D.C. 20390

Mr. Robert S. Crouse
851 West Outer Drive
Oak Ridge, Tennessee 37830

Mr. Robert F. Cunningham
12841 Ranchwood Road
Santa Ana, Calif. 92705

Mr. James M. Dahl
1600 Huron Pkwy
Ann Arbor, Michigan 48106

Mr. Philip N. Dangel
11000 Cedar Road
Chase Brass & Copper
Cleveland, Ohio 44106

Mr. Andrew W. Danko
33 Buena Vista Drive
Delmont, Pa. 15626

Mr. Ernest Davidson
843 Amherst Drive
Burbank, Calif. 91504

Prof. Mysore A. Dayananda
School of Materials Science
& Metallurgical Engineering
Purdue University
Lafayette, Indiana

Mr. Robert De Beer
803 Amherst Drive
Burbank, Calif. 91504

Hillery S. De Ben
P.O. Box 900
Princeton, New Jersey 08540

Dr. D.K. De Grinberg
Gricina 113
Mexico 21, D.F.

Mr. George A. Desborough
2164 Zang Street
Golden, Colorado 80401

Mr. Giulio DiGiacomo
IBM Component Div.
Bldg. 585, Dept. 60A
East Fishkill, N.Y.

Mr. William D. Donnelly
Materials Science Dept.
San Jose State College
San Jose, Calif. 95114

Mr. Frank B. Drogosz
444 S. Osceola
Orlando, Florida 32801

Mr. Harris W. Dunn
P.O. Box 827
Kingston, Tennessee 37763

Mr. Leland B. Eminhizer
318 MS Bldg.
University Park
Pennsylvania, 16802

Mr. Bernard W. Evans
Dept. of Geologica Sciences
University of Washington
Seattle, Washington 98105

Mr. Donald J. Evins, EPASA Rep.
Materials Analysis Company
1060 East Meadow Circle
Palo Alto, Calif. 94313

Mr. James E. Ferguson
157 Athens Road
Oak Ridge, Tenn. 37830

Mr. James F. Ficca
1221 McKennons Church Road
Sherwood Park
Wilmington, Delaware

Mr. Kier M. Finlayson
Radio Crop. of America
Lancaster, Pa. 17601

Mary C. Finn
Lincoln Laboratory
244 Wood Street
Lexington, Mass. 02173

Mr. Charles E. Fiori
National Bureau of Standards
Building 222, Room A-132
Washington, D.C. 20234

Mr. Mark Firth
Dept. of Metallurgical Engng.
McGill University
Montreal, Quebec
Canada

Mr. J.J. Fischer
5 Larch Court
Suffern, New York

Mr. Gordon L. Fisher
Paul D. Merica Research Lab.
International Nickel Co., Inc.
Suffern, New York 10901

Mr. Mario M. Fornoff
Walcutt Drive
R.R. #1, Box 212A
Basking Ridge, N.J. 07920

Mr. Theodore F. Fox
OCAMA/MAGCM
Tinker AFB
Okla. 73145

Mr. Kurt Frederiksson
Smithsonian Institution
Washington, D.C.

Mr. William G. Fricke, Jr.
Alcoa Research Labs.
Box 772
New Kinsington, Pa. 15068

Mr. Oscar H. Fritzsche
4603 Moore Road
Middletown, Ohio 45042

Mr. Nobukatsu Fujino
Central Research Labs.
Sumitomo Metal Industries, 3
1-Chome Nichinagasu
Amagaski, Japan

Mr. Amalendu Ganguli
717 Bendix Drive
The Bendix Corporation
South Bend, Indiana 46620

Elvira Gasparrini
Dept. of Geology
University of Toronto
Toronto 5, Ontario
Canada

Mr. Donald C. Gaubtz
10033 Hillcrest Road
Cupertino, Calif. 95014

Mr. William E. Gawthrop
Battelle Memorial Institute
505 King Avenue
Columbus, Ohio 43201

Dr. E.D. Ghent
Geology Department
University of Calgary
Calgary 44
Canada

Mary M. Giles
810 Prospect Avenue
Bethlehem, Pa. 18018

Mr. Philip M. Giles
Homer Research Labs
Bethlehem Steel Corp.
Bethlehem, Pa. 18018

Mr. John V. Gilfrich
Code 7680
U.S. Naval Research Lab.
Washington, D.C. 20390

Mr. John T. Gilmore
Chevron Research Co.
576 Standard Ave.
Richmond, California

Mr. J.I. Goldstein
Dept. of Met. & Mat. Sc.
Whitaker Lab.
Lehigh University
Bethlehem, Pa. 18015

Mr. Jozef Graczyk
97 Poplar Avenue
Hackensack, N.J. 07601

Dr. Raymond T. Greer
Dept. of Nuclear Engng.
Iowa State University
Ames, Iowa 50010

Mr. Harold E. Guina
36853 Sunnydale
Livonia, Michigan 48154

Mr. Klaus P. Gumz
Maiden Lane
Durham, Conn. 06422

Mr. K.P. Gupta
Dept. of Metallurgy
Case Western Reserve Univ.
Cleveland, Ohio 44106

Mr. Ralph G. Gutmacher
Lawrence Radiation Lab.
L-404 University of Calif.
Livermore, California 94526

Mr. E. Arnold Hakkila
P.O. Box 125
Los Almos, N. Mex. 87544

Mr. Monte R. Hall
Graduate House West
Room 1031
West Lafayette, Indiana 47906

Mr. George Hallerman
Inland Steel Research Labs
East Chicago, Indiana 46312

Mr. Barry L. Hammond
4002 Winfield Court
Bowie, Maryland 20715

Mr. Bryce I. Hanna
20200 W. Outer Drive
Dearborn, Mich. 48124

Dr. H.F. Harnsberger
Chevron Research Company
Richmond, Calif. 94802

Mr. Andrew B. Harris
1314 N. Institute Place
Peoria, Illinois

Mr. Carl E. Harris
TRW Equipment Labs
23555 Euclid Avenue
Cleveland, Ohio 44117

Dr. Donald C. Harris
1435 Morisset Avenue
Ottawa, Ontario
Canada

Mr. Malcolm R. Harvey
3385 Martin Drive
Boulder, Colorado 80302

Mr. Robert H. Heidel
U.S. Dept. of Interior
Geological Survey
Bldg. 25, Rm. 2435
Denver Federal Center
Denver, Colorado 80225

Mr. Kurt F. Heinrich
804 Blossom Drive
Rockville, Maryland 20850

Mr. Peter J. Heinzer
2927 Jeanne Drive
Parma, Ohio 44134

Mr. Paul I. Henderson
J & L Steel Res. Lab
900 Agnew Road
Pittsburgh, Pa. 15230

Mr. Robert J. Henry
1539 Lois Lane
Bethlehem, Pennsylvania 18018

Mr. Tom Henson
R.R. #2
Westwood Estates
Clinton, Teneessee

Mr. Wayne D. Hepfer
6411 Columbine Dr.
Indianapolis, Indiana 46224

Mr. James R. Hinthorne
Applied Res. Lab.
Hasler Research Center
95 La Patera Lane
Goleta, Calif. 93017

Mr. Edward W. Holmes
17 W 034 - 69yh Street
Clarendon Hills, Ill. 60514

Mr. C.R. Hedgens
6135 Teagarden Circle
Dayton, Ohio 45449

Mr. RObert T. Huebner
D/314-6, Bldg. 6-M-00
P.O. Box 6
Endicott, N.Y. 13760

Mr. Fred M. Hurwich
P.O. Box 282
Montrose, Calif. 91020

Mrs. Gudrun A. Hutchins
Barber Pond Road
Pownal, Vermont 05261

Mr. Richard M. Ingersoll
P.O. Box 747
Waterbury, Connecticut

Mr. Sidney I. Ingrey
237 Bradford Street
Ottawa 14, Ontario
Canada K2B 525

Mr. Jose A. Isasi
2506 Damman Drive
Apt. 104
Midland, Michigan

Mr. F. Duane Ingram
1110 Cottonwood
Iowa City, Iowa 52240

Mrs. Marie Jefferys
Research & Technology Div.
Chromalloy American Corp.
Blaisdell Road
Orangeburg, New York 10962

Mr. William J. Jeitner
7 Sunset Drive
Cherry Hill, N.J. 08034

Mr. C.E. Johnson
Argonne National Lab.
9700 S. Cass Avenue
Argonne, Illinois

Mr. James W. Hohnson
1353 Carolyn Drive
Atlanta, Georgia 30329

Mr. Richard Jones
3712 Kimberly Lane
Fort Worth, Texas 76133

Mr. Robert Jones
1602 N. Oak Drive
Topanga, California 90290

Petrus Jongenburger (Prof.)
Lab. voor Metaalkunde
T.H. Delft
Rottendamseweg 137
Delft, the Netherlands

Mr. Gary Judd
Materials Department
Rensselaer Polytechnic
Troy, New York 12181

Mr. Thomas G. Jurcich
4723 W. Braddock Road
Apt. 200
Alexandria, Va. 22311

Mr. W.T. Kane
Corning Glass Works
Sullivan Research Park
Painted Post, New York

Mr. Thomas Kartelias, Jr.
18 MacArthur Drive
Edison, New Jersey 08817

Miriam Kastner
Harvard University
Dept. of Geological Sciences
Cambridge, Massachusetts

Mr. Y. Bruce Katayama
2125 Hudson
Richland, Wash. 99352

Dr. Klaus Keil
Dept. of Geology & Institute
of Meteoritics
The University of New Mexico
Albuquerque, New Mexico 87106

Mr. Edward G. Kelso
2509 Libson Avenue
Alexandria, Va. 22306

Mr. August S. Klein
931 Terminal Way
San CArlos, Calif. 94070

Mr. Richard N. Kniseley
Ames Laboratory
Iowa State University
Ames, Iowa

Mr. Lawrence Kobren
5705 Fieldview Ct.
Baltimore, Maryland 21207

Mr. Arnold Kolb
1010 Willard Street
Midland, Michigan 48648

Mr. Donald J. Kovach
energy Controls Division
The Bendix Corporation
717 Bendix Drive
South Bend, Indiana 46620

Miss Rose Kozak
Gould Inc.
Gould Laboratories
540 E. 105th Street
Cleveland, Ohio 44108

Mr. Frank W. Kunz
Scientific Research Staff
Ford Motor Co.
P.O. Box 2053
Dearborn, Michigan 48121

Mr. John D. Kuptsis
OVerhill Road, R.D. #5
Mahopac, New York 10541

Mr. David F. Kyser
1258 Pampas Drive
San Jose, Calif. 95120

Mr. Francis Laabs
33 Crestview
Ames, Iowa 50010

Mr. Tracy Lamanec
Box 292, Crawford Road, RD#3
Schenctady, New York

Mr. F. Parks Landis
2177 Story Avenue
Schenectady, New York 12309

Mr. D.K. Landstrom
698 S. Fifth St.
German Village
Columbus, Ohio 43206

Mr. Arthur M. Langer
Environmental Sciences Lab
Mt. Sinai School of Medicine
100th Street and Fifth Avenue
New York, New York 10029

Mr. T.E. Lannin
General Electric Co.
Vallecitos Nuclear Center
Vallecitos Road
Pleasantown, Calif. 94566

Elma Lanterman
Research Center
Borg-Warner Corp.
Des Plaines, Illinois 60018

Mr. Richard R. Larson
7310-24th Avenue
Hyattsville, Maryland 20783

Mr. Wayne A. Lasch
2913 Huntington Road
Shaker Heights, Ohio 44120

Dr. A. Lauchli
Dept. of Soils & Plant Nutri.
University of California
Davis, Calif. 95616

Mr. Claude P. Lechene
195 Bryant
Sherbrooke, Quebec
Canada

Mr. John W. Lenke
American Dental Association
Research Institute
211 E. Chicago Avenue
Chicago, Illinois 60611

Mr. John Leys
3-M Center Street
St. Paul, Minnesota 55101

Mr. Cesar Mario Libanati
Alvear 800
Martinez, Argentina

Mr. Paul Lublin
General Telephone & Electronics Labs
208-20 Willets Point Blvd.
Bayside, New York

Mr. Harvey W. Lyon
American Dental Association
211 E. Chicago Avenue
Chicago, Illinois 60611

Mr. H.R. MacQueen
Apt. 4A, Bickford Lane
Pleasantdale Estates
Troy, N.Y. 12182

Mr. Charles E. Makepeace
2413 Elmira Drive
Ottawa, Ontario
Canada

Dr. Victor J. Malasauskas
Caterpillar Tractor Co.
Res. Dept. Tech. Ctr. Bldg.
Peoria, Ill. 61602

Mrs. Lolly Marie Marchant
202 E. Hinckley Avenue
Ridley Park, Pa. 19078

Mr. Vincent C. Marcotte
Kuchler Drive, RD #1
La Grangeville, New York 12540

Dr. L.L. Marton
Museum of History & Technology
Room 5025
Smithsonian Institution
Washington, D.C. 20560

Mr. G.W. Matheus
27 Prince Charles Drive
Toronto 19, Ontario
Canada

Mr. Richard K. Matta
Radiation Center
Scaife Hall
PGH., Pa. 15213

Mr. James L. McCall
505 King Avenue
Columbus, Ohio 43201

Mr. Michael J. McGuire
Applied Research Labs
905 W. Hillgrove Ave.
La Grange, Ill. 60525

Mr. T.D. McKinley
E.I. du Pont de Nemours & Co.
Pigments Department
Experimental Station
Wilmington, Delaware 19898

Mr. William R. McMillan
3407 Bradford Road
Cleveland Heights, Ohio 44118

Mr. Robert W. Merchant
8 Melody Lane
Schenectady, N.Y. 12309

Mr. Arthur B. Meukle
2498 Crestline Road
Pleasanton, Calif. 94566

Mr. Emmett L. Miller
13914 Bora Bora Way
Apt. 216-D
Marina Del Rey, Calif. 90291

Mr. John L. Miller, Jr.
133 Nebraska Ave.
Oak Ridge, Tennessee 37830

Mr. Harold E. Mishmash
1755 Louise Avenue
St. Paul, Minn. 55106

Mr. William G. Morris
General Electric Res. & Dev. Ctr.
P.O. Box 8
Schenectady, New York 12301

Mr. John E. Mulhern, Jr.
Dept. of Physics
Univ. of New Hampshire
DeMeritt Hall, UNH
Durham, New Hampshire 03824

Mr. Norman A. Mulvenon
515 N. Highview Ave., Apt. 104
Addison, Illinois 60101

Mr. Anthony J. Murawski
20513 W. Outer Drive
Dearborn, Michigan 48124

Mr. A.P. Murphy
Procter and Gamble Company
Miami Valley Labs
P.O. Box 39175
Cincinnati, Ohio 45239

Mr. Karl E. Muszar, Jr.
7820 Scarborough Blvd.E.Dr.
Indianopolis, Indiana 46256

Mrs. Margaret Ryan Myers
Dept. of Geological Sciences
Univ. of Illinois at Chicago
Circle, Box 4348
Chicago, Illinois 60680

Mr. Robert L. Myklebust
Route 1
Frederic, Md. 21701

Mr. David J. Nagel
Code 7685, Naval Res. Lab
X-Ray Optics Branch
Washington, D.C. 20390

Mr. Samuel K. Nash
238 S. Third Street
Philadelphia, Pennsylvania

Mr. Hermann Neuhaus
280 Waverly Street, #6
Menlo Park, California 94025

Mr. Livingston A. Newberg
21 W. 518 Thorndale
Medinah, Illinois 60157

Mr. Robert F. Nickerson
P.O. Box 808
Livermore, California

Mr. James A. Nicolino
brc - Instruments
6010 Executive Boulevard
Rockville, Md. 20852

Mr. Henry Nikkel
28 Neff Drive
Canfield, Ohio 44406

Mr. Henry J. Noebels
32 Avenue Frontenex
Geneva, Switzerland

Mr. Robert L. Novak
229 Parkside Avenue
Pittsburgh, Pennsylvania

Mr. Charles R. Obermeyer
The Smithsonian Institute
Tenth and Constitution Avenue
MNH E-425
Washington, D.C. 20560

Mr. Robert E. Ogilvie
Metallurgy Department
Massachusetts Institute of
Technology
Room 13-4009
Cambridge, Massachusetts 02139

Mr. John R. Ogren
4782 Amerwood Avenue
La Palma, California 90620

Mr. Ray H. Olsen
113 S.W. 207th Street
Seattle, Washington

Mr. Poen Sing Ong
Philip Lab
345 Scarborough Road
Briar Cliff Manor, N.Y.

Mr. Joseph Ordonez
41 Hagen Drive
Poughkeepsie, New York 12603

Mr. John A. O'Rourke
2557 - 45th Street
Los Alamos, New Mexico

Mr. Bernard Ostrofsky
670 N. Tippecanoe Street
Gary, Indiana

Mr. Rodney (Rod) Harry Packwood
19 Lakeview Terrace
Ottawa, Ontario
Canada K1S 3H3

Mr. George N. Panagis
National Steel Corporation
Weirton, Virginia 26062

Mr. William Parrish
Dept. K05, IBM Res. Lab.
Monterey & Cottle Road
San Jose, Calif. 95114

Mr. John M. Parsons
PPG Industries Inc.
Glass Research Center
Box 11472
Pittsburgh, Pa. 15238

Mr. Bisweswar Patnaik
#5 Wenliss Terrace
Wappingers Falls, New York 12590

Mr. John E. Pearson
4075 - 52nd St. N.
St. Petersburg, Florida 33709

Mr. Edward Peters
A.D. Little
Acorn Park
Cambridge, Massachusetts 02140

Frances D. Pidgeon
24510-H Clareshire Drive
North Almsted, Ohio 44070

Mr. Pierre Jean-Louis Pinard
184, Avenue Berthelot
69 - Lyon
France

Mr. Stephen D. Piner
Canberra Industries
45 Gracey Avenue
Meriden, Conn. 06450

Mr. A.G. Plant
601 Booth Street
Ottawa, Ontario, Canada

Mr. Larry E. Plew
R. R. # 2
Linton, Ind. 47441

Mr. Fred W. Postma, Jr.
105 Mowhawk Road
Oak Ridge, Tennessee 37830

Mr. Robert F. Quirk
I.B.M. Dept. 877
Bldg. 300-84
Route # 52
Hopewell Junction,
New York 12533

Mr. Dennis Radcliffe
Department of Geology
University of Georgia
Athens, Georgia 30601

Mr. John N. Ramsey
I.B.M., Dept. 286
Bldg. 300-97
Hopewell Junction,
New York 12533

Mr. Stanley D. Rasberry
A-125 Chemistry
National Bureau of Standards
Washington, D.C. 20234

Mr. Madison William Reed, Jr.
3748 Hill Top Road
Fort Worth, Texas 76109

		Paper Number
Savanick, G. A.	Bureau of Mines, Twin Cities Mining Research Center, Minneapolis, Minnesota, 55111	46, 47
Sheble, A. M.	Hi-Rel Laboratories, 2116 Huntington Drive, San Marino, California, 91108	40
Short, J. M.	Xerox Corporation, Xerox Square W-114, Rochester, New York, 14603	4
Solomon, J. S.	University of Dayton Research Institute, Dayton, Ohio, 45409	43
Steele, W. J.	Lawrence Radiation Laboratory, University of California, Livermore, California, 94550	14
Sternglass, E. J.	University of Pittsburgh, Radiation Center, Pittsburgh, Pennsylvania, 15213	13
Taylor, C. M.	Biodynamics Research Corporation, 6010 Executive Boulevard, Rockville, Maryland, 20852	33
Tousimis, A. J.	Biodynamics Research Corporation, 6010 Executive Boulevard, Rockville, Maryland, 20852	36, 38 41, 60, 61
Warner, R.	University of Rochester, School of Medicine and Dentistry, Rochester, New York, 14620	42
Wells, O. C.	IBM Corporation, Thomas J. Watson Research Center, P. O. Box 218, Yorktown Heights, New York, 10958	30

THE ELECTRON PROBE ANALYSIS SOCIETY OF AMERICA

MEMBERSHIP LIST

****

Mr. Ronald A. Abelman
Applied Research Labs.
P.O. Box 129
Sunland, Calif. 91040

Mr. Jerry D. Adey
Univ. of Oregon Dental School
611 S.W. Campus Drive
Portland, Oregon 97201

Mr. Arden Albee
Deivision of Geological Sciences
California Institute of Technology
Pasadena, California 91109

Mr. Leslie O. Albin
4501 Valerie
Bellaire, Texas 77401

Mr. Carmelo F. Aliotta
6 Chiarpardi Place
Beacon, New York 12508

Mr. Charles H. Anderson
9545 Wentworth Street
Sunland, California 91040

Mr. Chris A. Anderson
2402 Janin Way
Solvang, California

Dr. D.H. Anderson
Director, Industrial Laboratory
Eastman Kodak Company
343 State Street
Rochester, N.Y. 14650

Mr. Charles W. Andrews
1926 Woodward Avenue
Cleveland, Ohio 44118

Dr. Kamal Asgar
1011 N. University
110 Dental School
Ann Arbor, Michigan 48104

Mr. Clarence W. Austin, Jr.
404 Hillmont Circle N.W.
Huntsville, Alabama 35805

Mr. Donald L. Bagnoli
R.D. Horace Rd.
Oak Ridge, N.J. 07438

Mr. Alexander K. Baird
Department of Geology
Pomona College
Claremont, Calif. 91711

Mr. Joseph D. Balser
5677 N. 94th Street
Milwaukee, Wisc. 53222

Mr. R.W. Barnard
Bell Telephone Labs
Res. & Dev. Unit
Mountain Ave.
Murray Hill, N.J. 07974

Mr. John J. Bart
R.D. #2, Dix Road
Rome, New York 13440

Mr. Ahron Batt
1001 Main St. West
Apt. 419
Hamilton, Ontario
Canada

Mr. William L. Baun
7418 N. Dakar Drive
Dayton, Ohio 45431

Dr. D.R. Beaman
2210 Burlington
Midland, Michigan 48640

Mr. Albert H. Beebe, III
29 Eichelberger Drive
Coraopolis, Pa. 15108

Mr. Melvin H. Beeson
664 Tamarack Drive
Union City, Calif. 94587

Mr. Leonard J. Bench
1200 Irene Lane
Pittsburgh, Pennsylvania 15236

Mr. Ralph F. Benck
316 Bynum Ridge Road
Forest Hill, Maryland 21050

Mr. Carl Berkley
Medical Research Technology
Great Notch, New Jersey 07424

Mr. Eugene P. Bertin
Room E-120
RCA Laboratories
Princeton, New Jersey 08540

Mr. Deane I. Biehler
Caterpillar Tractor Co.
Research Dept., Tech. Center E
Peoria, Illinois 61602

Professor Wilbur C. Bigelow
Dept. of Chemistry & Met. Engng.
University of Michigan
Ann Arbor, Michigan 48104

Mr. William D. Bingle
591 Wack Drive
Rochester, Pennsylvania 15074

Mr. L.S. Birks
Code 7680
Naval Research Laboratory
Washington, D.C.

Mr. Herbert L. Black
Universal-Cyclops, Spec. Steel Div.
Res. & Dev. Dept.
Mayer Street
Bridgeveille, Pa. 15017

Mr. John W. Blaise
Research and Technology Division
Chromalloy American Corp.
Blaisedell Road
Orangeburg, New York 10962

Mr. Roger B. Bolon
R.D. #2, Lake Road
Ballston, New York

Mr. Matthew J. Boris
Senior Research Chemist
American Steel Foundries
3761 Canal Street
East Chicago. Indiana 46312

Janice F. Bower
Smithsonian Astrophysical
60 Garden Street /Observatory
Cambridge, Massachusetts 02138

Mr. David E. Boyd
613 Salisbury Road
Waverly, Ohio 45661

Mr. Edward J. Brooks
U.S. Naval Research Laboratory
Washington, D.C. 20390

Mr. Dennis B. Brown
Code 7987
U.S. Naval Research Laboratory
Washington, D.C. 20390

Dr. James D. Brown
Faculty of Engineering Science
The Univ. of Western Ontario
London 72, Ontario
Canada

Mr. Laurence C. Brown
Department of Metallurgy
University of British Columbia
Vancouver 8, B.C.
Canada

Mr. Gary G. Brumbaugh
3808 Arnell Place
LaCrescenta, California 91214

Mr. G. Brumbaugh, EPASA Rep.
Consolidated Electrodynamics Corp.
Analytical Instruments Division
1500 South Shamrock Avenue
Monrovia, California 91017

James R. Buckmelter
Hq. Air Force Cambridge Research Labs
L.G. Hanscom Field
Bedford, Mass. 01730

Mr. W.C. Budke
303 North 31st Ave.
Yakima, Washington

Mr. Garrett A. Busch
Grumman Aerospace Co.
Research Dept. PET 26
Bethpage, New York 11714

Mr. J.W. Butler
Argonne National Laboratory
9700 South Cass Avenue
Argonne, Illinois 60439

Mr. Vincent E. Caldwell
Armco Steel Corporation
Research Center
Curtis Street
Middletown, Ohio 45042

Mr. William J. Campbell
U.S. Bureau of Mines
College Park, Maryland

Mr. Kenneth G. Carroll
29 Bowdoin Street
Cambridge, Massachusetts

Mr. Michel P. Cescas
Faculty of Agriculture
Laval University
Quebec 10, P.Q.
Canada

Mr. William F. Chambers
Sandia Corporation, Org. 1122
P.O. Box 5800
Albuquerque, New Mexico 87115

Mr. Wei H. Chang
180 Prospect St., Apt. F-5
East Orange, New Jersey

Mr. Eric J. Chatfield
Department of Physics
Ontario Research Foundation
Sheridan Park, Ontario
Canada

Mr. William T. Chester
Denton Vacuum, Inc.
Cherry Hill Ind. Ctr.
Cherry Hill, N.J. 08034

Dr. Arthur A. Chodos
California Institute of Tech.
Division of Geological Sciences
1201 E. California Street
Pasadena, Calif. 91109

Mr. William C. Clinton
5-A Cryton Apts.
Rolla, Missouri 65401

Mr. J.W. Colby
3125 Linda Lane
Allentown, Pennsylvania

Mr. James R. Coleman
Dept. of Radiation Biology & Biophysics
University of Rochester Med. Ctr.
Rochester, New York

Mr. Donald K. Conley
410 Hill Drive
Allentown, Pa. 18103

Mr. George A. Conrad
Dept. of Geology
Univ. of New Mexico
Albuquerque, New Mexico 87116

Mr. Paul D. Coulter
Union Carbide Corp.
Parma Technical Center
P.O. Box 6116
Cleveland, Ohio 44101

Mr. Arthur Cox
Dominion Foundries & Steel, Ltd.
Box 460
Hamilton, Ontario
Canada

Mr. Joseph F. Cox
1032 Winne Road
Schenectady, New York 12309

Ramon Coy-yll
Ecole Polytechnique
2500 Marie Guyard Avenue
Montreal, Quebec
Canada

Mr. Robert T. Craig
370 Maple Street
Danvers, Mass. 01923

Maria Luisa Crawford
Dept. of Geology
Bryn Mawr College
Bryn Mawr, Penna. 19010

Mr. John W. Criss
6686 Naval Research Lab
Washington, D.C. 20390

Mr. Robert S. Crouse
851 West Outer Drive
Oak Ridge, Tennessee 37830

Mr. Robert F. Cunningham
12841 Ranchwood Road
Santa Ana, Calif. 92705

Mr. James M. Dahl
1600 Huron Pkwy
Ann Arbor, Michigan 48106

Mr. Philip N. Dangel
11000 Cedar Road
Chase Brass & Copper
Cleveland, Ohio 44106

Mr. Andrew W. Danko
33 Buena Vista Drive
Delmont, Pa. 15626

Mr. Ernest Davidson
843 Amherst Drive
Burbank, Calif. 91504

Prof. Mysore A. Dayananda
School of Materials Science
& Metallurgical Engineering
Purdue University
Lafayette, Indiana

Mr. Robert De Beer
803 Amherst Drive
Burbank, Calif. 91504

Hillery S. De Ben
P.O. Box 900
Princeton, New Jersey 08540

Dr. D.K. De Grinberg
Gricina 113
Mexico 21, D.F.

Mr. George A. Desborough
2164 Zang Street
Golden, Colorado 80401

Mr. Giulio DiGiacomo
IBM Component Div.
Bldg. 585, Dept. 60A
East Fishkill, N.Y.

Mr. William D. Donnelly
Materials Science Dept.
San Jose State College
San Jose, Calif. 95114

Mr. Frank B. Drogosz
444 S. Osceola
Orlando, Florida 32801

Mr. Harris W. Dunn
P.O. Box 827
Kingston, Tennessee 37763

Mr. Leland B. Eminhizer
318 MS Bldg.
University Park
Pennsylvania, 16802

Mr. Bernard W. Evans
Dept. of Geologica Sciences
University of Washington
Seattle, Washington 98105

Mr. Donald J. Evins, EPASA Rep.
Materials Analysis Company
1060 East Meadow Circle
Palo Alto, Calif. 94313

Mr. James E. Ferguson
157 Athens Road
Oak Ridge, Tenn. 37830

Mr. James F. Ficca
1221 McKennons Church Road
Sherwood Park
Wilmington, Delaware

Mr. Kier M. Finlayson
Radio Crop. of America
Lancaster, Pa. 17601

Mary C. Finn
Lincoln Laboratory
244 Wood Street
Lexington, Mass. 02173

Mr. Charles E. Fiori
National Bureau of Standards
Building 222, Room A-132
Washington, D.C. 20234

Mr. Mark Firth
Dept. of Metallurgical Engng.
McGill University
Montreal, Quebec
Canada

Mr. J.J. Fischer
5 Larch Court
Suffern, New York

Mr. Gordon L. Fisher
Paul D. Merica Research Lab.
International Nickel Co., Inc.
Suffern, New York 10901

Mr. Mario M. Fornoff
Walcutt Drive
R.R. #1, Box 212A
Basking Ridge, N.J. 07920

Mr. Theodore F. Fox
OCAMA/MAGCM
Tinker AFB
Okla. 73145

Mr. Kurt Frederiksson
Smithsonian Institution
Washington, D.C.

Mr. William G. Fricke, Jr.
Alcoa Research Labs.
Box 772
New Kinsington, Pa. 15068

Mr. Oscar H. Fritzsche
4603 Moore Road
Middletown, Ohio 45042

Mr. Nobukatsu Fujino
Central Research Labs.
Sumitomo Metal Industries, 3
1-Chome Nichinagasu
Amagaski, Japan

Mr. Amalendu Ganguli
717 Bendix Drive
The Bendix Corporation
South Bend, Indiana 46620

Elvira Gasparrini
Dept. of Geology
University of Toronto
Toronto 5, Ontario
Canada

Mr. Donald C. Gaubtz
10033 Hillcrest Road
Cupertino, Calif. 95014

Mr. William E. Gawthrop
Battelle Memorial Institute
505 King Avenue
Columbus, Ohio 43201

Dr. E.D. Ghent
Geology Department
University of Calgary
Calgary 44
Canada

Mary M. Giles
810 Prospect Avenue
Bethlehem, Pa. 18018

Mr. Philip M. Giles
Homer Research Labs
Bethlehem Steel Corp.
Bethlehem, Pa. 18018

Mr. John V. Gilfrich
Code 7680
U.S. Naval Research Lab.
Washington, D.C. 20390

Mr. John T. Gilmore
Chevron Research Co.
576 Standard Ave.
Richmond, California

Mr. J.I. Goldstein
Dept. of Met. & Mat. Sc.
Whitaker Lab.
Lehigh University
Bethlehem, Pa. 18015

Mr. Jozef Graczyk
97 Poplar Avenue
Hackensack, N.J. 07601

Dr. Raymond T. Greer
Dept. of Nuclear Engng.
Iowa State University
Ames, Iowa 50010

Mr. Harold E. Guina
36853 Sunnydale
Livonia, Michigan 48154

Mr. Klaus P. Gumz
Maiden Lane
Durham, Conn. 06422

Mr. K.P. Gupta
Dept. of Metallurgy
Case Western Reserve Univ.
Cleveland, Ohio 44106

Mr. Ralph G. Gutmacher
Lawrence Radiation Lab.
L-404 University of Calif.
Livermore, California 94526

Mr. E. Arnold Hakkila
P.O. Box 125
Los Almos, N. Mex. 87544

Mr. Monte R. Hall
Graduate House West
Room 1031
West Lafayette, Indiana 47906

Mr. George Hallerman
Inland Steel Research Labs
East Chicago, Indiana 46312

Mr. Barry L. Hammond
4002 Winfield Court
Bowie, Maryland 20715

Mr. Bryce I. Hanna
20200 W. Outer Drive
Dearborn, Mich. 48124

Dr. H.F. Harnsberger
Chevron Research Company
Richmond, Calif. 94802

Mr. Andrew B. Harris
1314 N. Institute Place
Peoria, Illinois

Mr. Carl E. Harris
TRW Equipment Labs
23555 Euclid Avenue
Cleveland, Ohio 44117

Dr. Donald C. Harris
1435 Morisset Avenue
Ottawa, Ontario
Canada

Mr. Malcolm R. Harvey
3385 Martin Drive
Boulder, Colorado 80302

Mr. Robert H. Heidel
U.S. Dept. of Interior
Geological Survey
Bldg. 25, Rm. 2435
Denver Federal Center
Denver, Colorado 80225

Mr. Kurt F. Heinrich
804 Blossom Drive
Rockville, Maryland 20850

Mr. Peter J. Heinzer
2927 Jeanne Drive
Parma, Ohio 44134

Mr. Paul I. Henderson
J & L Steel Res. Lab
900 Agnew Road
Pittsburgh, Pa. 15230

Mr. Robert J. Henry
1539 Lois Lane
Bethlehem, Pennsylvania 18018

Mr. Tom Henson
R.R. #2
Westwood Estates
Clinton, Teneessee

Mr. Wayne D. Hepfer
6411 Columbine Dr.
Indianapolis, Indiana 46224

Mr. James R. Hinthorne
Applied Res. Lab.
Hasler Research Center
95 La Patera Lane
Goleta, Calif. 93017

Mr. Edward W. Holmes
17 W 034 - 69yh Street
Clarendon Hills, Ill. 60514

Mr. C.R. Hedgens
6135 Teagarden Circle
Dayton, Ohio 45449

Mr. RObert T. Huebner
D/314-6, Bldg. 6-M-00
P.O. Box 6
Endicott, N.Y. 13760

Mr. Fred M. Hurwich
P.O. Box 282
Montrose, Calif. 91020

Mrs. Gudrun A. Hutchins
Barber Pond Road
Pownal, Vermont 05261

Mr. Richard M. Ingersoll
P.O. Box 747
Waterbury, Connecticut

Mr. Sidney I. Ingrey
237 Bradford Street
Ottawa 14, Ontario
Canada K2B 525

Mr. Jose A. Isasi
2506 Damman Drive
Apt. 104
Midland, Michigan

Mr. F. Duane Ingram
1110 Cottonwood
Iowa City, Iowa 52240

Mrs. Marie Jefferys
Research & Technology Div.
Chromalloy American Corp.
Blaisdell Road
Orangeburg, New York 10962

Mr. William J. Jeitner
7 Sunset Drive
Cherry Hill, N.J. 08034

Mr. C.E. Johnson
Argonne National Lab.
9700 S. Cass Avenue
Argonne, Illinois

Mr. James W. Hohnson
1353 Carolyn Drive
Atlanta, Georgia 30329

Mr. Richard Jones
3712 Kimberly Lane
Fort Worth, Texas 76133

Mr. Robert Jones
1602 N. Oak Drive
Topanga, California 90290

Petrus Jongenburger (Prof.)
Lab. voor Metaalkunde
T.H. Delft
Rottendamseweg 137
Delft, the Netherlands

Mr. Gary Judd
Materials Department
Rensselaer Polytechnic
Troy, New York 12181

Mr. Thomas G. Jurcich
4723 W. Braddock Road
Apt. 200
Alexandria, Va. 22311

Mr. W.T. Kane
Corning Glass Works
Sullivan Research Park
Painted Post, New York

Mr. Thomas Kartelias, Jr.
18 MacArthur Drive
Edison, New Jersey 08817

Miriam Kastner
Harvard University
Dept. of Geological Sciences
Cambridge, Massachusetts

Mr. Y. Bruce Katayama
2125 Hudson
Richland, Wash. 99352

Dr. Klaus Keil
Dept. of Geology & Institute
of Meteoritics
The University of New Mexico
Albuquerque, New Mexico 87106

Mr. Edward G. Kelso
2509 Libson Avenue
Alexandria, Va. 22306

Mr. August S. Klein
931 Terminal Way
San CArlos, Calif. 94070

Mr. Richard N. Kniseley
Ames Laboratory
Iowa State University
Ames, Iowa

Mr. Lawrence Kobren
5705 Fieldview Ct.
Baltimore, Maryland 21207

Mr. Arnold Kolb
1010 Willard Street
Midland, Michigan 48648

Mr. Donald J. Kovach
energy Controls Division
The Bendix Corporation
717 Bendix Drive
South Bend, Indiana 46620

Miss Rose Kozak
Gould Inc.
Gould Laboratories
540 E. 105th Street
Cleveland, Ohio 44108

Mr. Frank W. Kunz
Scientific Research Staff
Ford Motor Co.
P.O. Box 2053
Dearborn, Michigan 48121

Mr. John D. Kuptsis
OVerhill Road, R.D. #5
Mahopac, New York 10541

Mr. David F. Kyser
1258 Pampas Drive
San Jose, Calif. 95120

Mr. Francis Laabs
33 Crestview
Ames, Iowa 50010

Mr. Tracy Lamanec
Box 292, Crawford Road, RD#3
Schenctady, New York

Mr. F. Parks Landis
2177 Story Avenue
Schenectady, New York 12309

Mr. D.K. Landstrom
698 S. Fifth St.
German Village
Columbus, Ohio 43206

Mr. Arthur M. Langer
Environmental Sciences Lab
Mt. Sinai School of Medicine
100th Street and Fifth Avenue
New York, New York 10029

Mr. T.E. Lannin
General Electric Co.
Vallecitos Nuclear Center
Vallecitos Road
Pleasantown, Calif. 94566

Elma Lanterman
Research Center
Borg-Warner Corp.
Des Plaines, Illinois 60018

Mr. Richard R. Larson
7310-24th Avenue
Hyattsville, Maryland 20783

Mr. Wayne A. Lasch
2913 Huntington Road
Shaker Heights, Ohio 44120

Dr. A. Lauchli
Dept. of Soils & Plant Nutri.
University of California
Davis, Calif. 95616

Mr. Claude P. Lechene
195 Bryant
Sherbrooke, Quebec
Canada

Mr. John W. Lenke
American Dental Association
Research Institute
211 E. Chicago Avenue
Chicago, Illinois 60611

Mr. John Leys
3-M Center Street
St. Paul, Minnesota 55101

Mr. Cesar Mario Libanati
Alvear 800
Martinez, Argentina

Mr. Paul Lublin
General Telephone & Electronics Labs
208-20 Willets Point Blvd.
Bayside, New York

Mr. Harvey W. Lyon
American Dental Association
211 E. Chicago Avenue
Chicago, Illinois 60611

Mr. H.R. MacQueen
Apt. 4A, Bickford Lane
Pleasantdale Estates
Troy, N.Y. 12182

Mr. Charles E. Makepeace
2413 Elmira Drive
Ottawa, Ontario
Canada

Dr. Victor J. Malasauskas
Caterpillar Tractor Co.
Res. Dept. Tech. Ctr. Bldg.
Peoria, Ill. 61602

Mrs. Lolly Marie Marchant
202 E. Hinckley Avenue
Ridley Park, Pa. 19078

Mr. Vincent C. Marcotte
Kuchler Drive, RD #1
La Grangeville, New York 12540

Dr. L.L. Marton
Museum of History & Technology
Room 5025
Smithsonian Institution
Washington, D.C. 20560

Mr. G.W. Matheus
27 Prince Charles Drive
Toronto 19, Ontario
Canada

Mr. Richard K. Matta
Radiation Center
Scaife Hall
PGH., Pa. 15213

Mr. James L. McCall
505 King Avenue
Columbus, Ohio 43201

Mr. Michael J. McGuire
Applied Research Labs
905 W. Hillgrove Ave.
La Grange, Ill. 60525

Mr. T.D. McKinley
E.I. du Pont de Nemours & Co.
Pigments Department
Experimental Station
Wilmington, Delaware 19898

Mr. William R. McMillan
3407 Bradford Road
Cleveland Heights, Ohio 44118

Mr. Robert W. Merchant
8 Melody Lane
Schenectady, N.Y. 12309

Mr. Arthur B. Meukle
2498 Crestline Road
Pleasanton, Calif. 94566

Mr. Emmett L. Miller
13914 Bora Bora Way
Apt. 216-D
Marina Del Rey, Calif. 90291

Mr. John L. Miller, Jr.
133 Nebraska Ave.
Oak Ridge, Tennessee 37830

Mr. Harold E. Mishmash
1755 Louise Avenue
St. Paul, Minn. 55106

Mr. William G. Morris
General Electric Res. & Dev. Ctr.
P.O. Box 8
Schenectady, New York 12301

Mr. John E. Mulhern, Jr.
Dept. of Physics
Univ. of New Hampshire
DeMeritt Hall, UNH
Durham, New Hampshire 03824

Mr. Norman A. Mulvenon
515 N. Highview Ave., Apt. 104
Addison, Illinois 60101

Mr. Anthony J. Murawski
20513 W. Outer Drive
Dearborn, Michigan 48124

Mr. A.P. Murphy
Procter and Gamble Company
Miami Valley Labs
P.O. Box 39175
Cincinnati, Ohio 45239

Mr. Karl E. Muszar, Jr.
7820 Scarborough Blvd.E.Dr.
Indianopolis, Indiana 46256

Mrs. Margaret Ryan Myers
Dept. of Geological Sciences
Univ. of Illinois at Chicago
Circle, Box 4348
Chicago, Illinois 60680

Mr. Robert L. Myklebust
Route 1
Frederic, Md. 21701

Mr. David J. Nagel
Code 7685, Naval Res. Lab
X-Ray Optics Branch
Washington, D.C. 20390

Mr. Samuel K. Nash
238 S. Third Street
Philadelphia, Pennsylvania

Mr. Hermann Neuhaus
280 Waverly Street, #6
Menlo Park, California 94025

Mr. Livingston A. Newberg
21 W. 518 Thorndale
Medinah, Illinois 60157

Mr. Robert F. Nickerson
P.O. Box 808
Livermore, California

Mr. James A. Nicolino
brc - Instruments
6010 Executive Boulevard
Rockville, Md. 20852

Mr. Henry Nikkel
28 Neff Drive
Canfield, Ohio 44406

Mr. Henry J. Noebels
32 Avenue Frontenex
Geneva, Switzerland

Mr. Robert L. Novak
229 Parkside Avenue
Pittsburgh, Pennsylvania

Mr. Charles R. Obermeyer
The Smithsonian Institute
Tenth and Constitution Avenue
MNH E-425
Washington, D.C. 20560

Mr. Robert E. Ogilvie
Metallurgy Department
Massachusetts Institute of
Technology
Room 13-4009
Cambridge, Massachusetts 02139

Mr. John R. Ogren
4782 Amerwood Avenue
La Palma, California 90620

Mr. Ray H. Olsen
113 S.W. 207th Street
Seattle, Washington

Mr. Poen Sing Ong
Philip Lab
345 Scarborough Road
Briar Cliff Manor, N.Y.

Mr. Joseph Ordonez
41 Hagen Drive
Poughkeepsie, New York 12603

Mr. John A. O'Rourke
2557 - 45th Street
Los Alamos, New Mexico

Mr. Bernard Ostrofsky
670 N. Tippecanoe Street
Gary, Indiana

Mr. Rodney (Rod) Harry Packwood
19 Lakeview Terrace
Ottawa, Ontario
Canada K1S 3H3

Mr. George N. Panagis
National Steel Corporation
Weirton, Virginia 26062

Mr. William Parrish
Dept. K05, IBM Res. Lab.
Monterey & Cottle Road
San Jose, Calif. 95114

Mr. John M. Parsons
PPG Industries Inc.
Glass Research Center
Box 11472
Pittsburgh, Pa. 15238

Mr. Bisweswar Patnaik
#5 Wenliss Terrace
Wappingers Falls, New York 12590

Mr. John E. Pearson
4075 - 52nd St. N.
St. Petersburg, Florida 33709

Mr. Edward Peters
A.D. Little
Acorn Park
Cambridge, Massachusetts 02140

Frances D. Pidgeon
24510-H Clareshire Drive
North Almsted, Ohio 44070

Mr. Pierre Jean-Louis Pinard
184, Avenue Berthelot
69 - Lyon
France

Mr. Stephen D. Piner
Canberra Industries
45 Gracey Avenue
Meriden, Conn. 06450

Mr. A.G. Plant
601 Booth Street
Ottawa, Ontario, Canada

Mr. Larry E. Plew
R. R. # 2
Linton, Ind. 47441

Mr. Fred W. Postma, Jr.
105 Mowhawk Road
Oak Ridge, Tennessee 37830

Mr. Robert F. Quirk
I.B.M. Dept. 877
Bldg. 300-84
Route # 52
Hopewell Junction,
New York 12533

Mr. Dennis Radcliffe
Department of Geology
University of Georgia
Athens, Georgia 30601

Mr. John N. Ramsey
I.B.M., Dept. 286
Bldg. 300-97
Hopewell Junction,
New York 12533

Mr. Stanley D. Rasberry
A-125 Chemistry
National Bureau of Standards
Washington, D.C. 20234

Mr. Madison William Reed, Jr.
3748 Hill Top Road
Fort Worth, Texas 76109

Mr. Guy Remond
B.R.G.M. Laboratorire
de Microsonde
BP 818 Orleans
France

Mr. Theodore S. Renzema
S.U.N.Y. at Albany
Physics Department
1400 Washington Avenue
Albany, New York 12203

Mr. Wilhad Reuter
I.B.M. Research
P.O. Box 218
Yorktown, New York

Mr. Paul H. Ribbe
Department of Geology Science
Virginia Polytechnic Institute
Blacksburg, Virginia 24061

Caterina Bianca Ricci Bitti
Castel Romano
Roma, Italy 00129

Mr. Neil A. Richard
Battelle Memorial Institute
505 King Avenue
Columbus, Ohio 43201

Mr. David H. Riefenberg
Dow Chemical Company
Rocky Flats Division
Box #880
Golden, Colorado

Mr. Henry J. Roden
875 Perry Court
Santa Barbara, California 93105

Mr. Peter A. Romans
U.S. Bureau of Mines
Albany, Oregon 97321

Mr. Elmer A. Rosauer
Iowa State University (EM-Lab.)
120 Engineering Annex
Ames, Iowa 50010

Mr. Mark Rosenblum
1730 Manor Place
Dayton, Ohio 45406

Mr. A.P. Von Rosenstiel
v.d. Lelystraat 55
Delft, Holland/Netherlands

Mr. John Rucklidge
Department of Geology
University of Toronto
Toronto 5, Canada

Mr. William J. Runkle
6411 Carrollton Avenue
Indianapolis, Indiana

Mr. Robert J. Ruscica
Materials Analysis Co.
1060 E. Meadow E.
Palo Alto, California 94303

Mr. Malcolm J. Rutherford
Brown University
Dept. of Geological Sciences
Providence, R.I. 02912

Mr. William E. Rutherford
R.R. #2, Box 225
Russiaville, Indiana 46979

Mr. Edward J. Saller
708 W. St. Gertrude Place
Santa Ana, California 92707

Mr. A. Sawatzky
5 Tupper
Pinawa, Manitoba, Canada

Mr. Stephen Sawruk
Mobil Oil Corporation
Research Department
Paulsboro, New Jersey 08066

Mr. William H. Scheub
Attn: Research Library
The Timken Company
Canton, Ohio 44706

Mr. Richard E. Schmunk
814 Raymond Drive
Idaho Falls, Idaho 83401

Mr. Thomas P. Schreiber
22918 Sunnyside
St. Clair Shores, Michigan
48080

Mr. David L. Schroeder
729 Harden Drive
Pittsburgh, Pa. 15229

Mr. Robert Seibert
Perkin-Elmer Corp.
Ultek Division
3911 Stoney Brook Drive
Houston, Texas 77042

Ursula Setz
35 Aubrey Street,
Summit, N.J. 07901

Mr. John W. Shaffer
Western Electric
Dept. 5150
555 Union Blvd.
Allentown, Pa. 18103

Mr. Thomas P. Sheehy
American Smelting & Refining Co.
Park Ave. & Oak Tree Road
So. Plainfield, N.J. 07080

Toshio Shiraiwa
3, 1-chome, Nishinagasu Hondori
Amagasaki-city,
Japan

Mr. M.A. Short
Scientific Research Staff
Ford Motor Co.
P.O. Box 2053
Dearborn, Michigan 48121

Mr. John E. Shott, Jr.
Gulf Research & Development Co.
P.O. Box 2038
Pittsburgh, Pa. 15230

Mr. Lester A. Siegel
American Cyanamid Co.
1937 West Main Street
Stamford, Connecticut 06904

Mr. Sylvester F. Simchick
1518 La Crosse Avenue
Reading, Pennsylvania 19607

Mr. Warren Singer
Bell & Howell
345 Boulevard
Hasbrouck Heights, N.J. 07604

Mr. Charles B. Slack
1500 Allen Avenue
Glendale, California

Mr. Robert Smid
Westinghouse/Bettis Atomic Power
P.O. Box 79
West Mifflin, Pa. 15122

Mr. D.G.W. Smith
Department of Geology
University of Alberta
Edmonton, Alberta
Canada

Mr. Joseph V. Smith
University of Chicago
Dept. of Geophysical Sciences
Chicago, Illinois 60637

Mr. Robert E. Smith
3815 Ansley Road
Birmingham, Alabama

Mr. Todd N. Solberg
924 N. Rosevere
Dearborn, Michigan 48128

Mr. James S. Solomon
1031 Dellwood
Troy, Ohio 45373

Mr. Joel L. Solomon
IBM/CD
Dept. MX3, 1401 Research Dr.
Rockville, Md. 20850

Mr. Charles J. Spengler
168 Paree Drive
Pittsburgh, Pennsylvania 15239

Mr. Gunter Springer
P.O. Box 900
Thornhill, Ontario, Canada

Mr. Lawrence S. Staikoff
Case Western Reserve University
10900 Euclid Avenue
Cleveland, Ohio 44106

Mr. Jeffrey J. Stepek
606 Old Leechburg Road
Pittsburgh, Pa. 15239

Mr. Richard E. Stevens
Ernest F. Fullam, Inc.
P.O. Box 444
Schenectady, N.Y. 12301

Mr. Joseph H. Stewart, Jr.
171 North Seneca Road
Oak Ridge, Tenn. 37830

Mr. George R. Strabel
5632 Norcross Road
Columbus, Ohio 43224

Mr. Bernard M. Strauss
P.O. Drawer 2038
Pittsburgh, Pa. 15230

Mr. Selby E. Summers
Ernest F. Fullam, Inc.
P.O. Box 444
Schenectady, N.Y. 12301

Mr. Walter J. Sutkowski
IBM E. Fishkill Faculty
RT. 52
Hopewell Junction, N.Y. 12533

Mr. B. Swaroop
Kelsey-Hayes Res. & Dev. Ctr.
2500 Green Road
Ann Arbor, Michigan 48105

Mr. Jack Tabock
19185 Mendota
Detroit, Michigan 48221

Mr. Charles M. Taylor
P.O. Box 7087
Stanford, California 94305

Mr. Anastasious J. Tousimis
Biodynamics Research Corp.
6010 Executive Blvd.
Rockville, Maryland 20852

Mr. R.J. Traill
Geological Survey of Canada
601 Booth Street
Ottawa, Canada

Mr. Lucien F. Trueb
Denver Research Institute
University Park
Denver, Colorado 80210

Mr. Thomas P. Turnbull
939 Northumberland Drive
Niskayana
Schenectady, N.Y. 12309

Mr. R.G. Vadimsky
Bell Telephone Laboratories
Mountain Avenue
Murray Hill, N.J. 07974

Mr. Joseph Vallone
Esso Research and Engineering Co.
P.O. Box 101
Florham Park, N.J. 07960

Mr. Lawrence A. Vassamillet
4400 Fifth Avenue
Pittsburgh, Pa. 15213

Mr. Jack Wagman
4504 Pamlico Drive
Raleigh, N.C. 27609

Mr. Paul J. Walitsky
45 Mountain Avenue
Bloomfield, N.J. 07003

Mr. Gilbert H. Walker
Star Route Box 60
Gloucester Point, Va. 23062

Mr. Charlie M. Wall
3600 Duncanville Road
Dallas, Texas

Mr. Norman M. Walter
The Boeing Co.
Vertol Division, Boeing Center
P.O. Box 16858
Philadelphia, Pa. 19142

Mr. Stephen Hon Yin Wei
Department of Pedodontics
College of Dentistry
University of Iowa
Iowa City, Iowa 52240

Mr. Oliver Craig Wells
1324 Leland Drive
Yorktown Hts, N.Y. 10598

Mr. Thomas H. West, Jr.
Gulf General Atomic
P.O. Box 608
San Diego, California 92122

Mr. Norman E. Weston
Engineering Materials Labs.
DuPont Experimental Station
Wilmington, Delaware 19898

Mr. Eugene W. White
1119 Houserville Road
State College, Pa. 16801

Marion R. Wiemann, Jr.
P.O. Box 386
Chesterton, Indiana 46304

Mr. J.Paul Williams
Corning Glass Works
Research and Development
Corning, New York 14830

Mr. Timothy Williams
Chromalloy American Corp.
R & T Division
Orangeburg, N.Y. 10962

Mr. Donald E. Wilson
106 Rocky Road
Shelton, Connecticut 06484

Mr. Arlo Lewis Wingirt
5212 S.W. Charleston
Seattle, Washington 98116

Mr. Walter N. Wise
2776 River Road
Hamilton, Ohio 45015

Mr. George J. Wolfe
P.O. Box 102
Norvelt, Pa. 15674

Mr. John B. Woodhouse
Materials Research Lab.
University of Illinois
Urbana, Illinois

Mr. Harvey Yakowitz
Rm B114, Materials Bldg., NBS
Washington, D.C. 20234

Mr. G. Robert Zechman, Jr.
Department of Geophysical Sciences
University of Chicago, 39-F
1101 E. 58th Street
Chicago, Illinois 60637

Mr. William F. Zelezny
1694 Juniper Drive
Idaho Falls, Idaho

Mr. Thomas O. Ziebold
9701 Fields Road, Apt. # 600
Gaithersburg, Md. 20760

STUDENT

Nicholas Carl Barbi
S-4 Edgehill Terrace
Troy, New York 12180

Richard H. Barkalow
270 Shafer Avenue
Phillipsburg, N.J. 08865

Yves C. Bienvenu
Mellon Institute
Metal Physics Group
4400 Fifth Avenue
Pittsburgh, Pa. 15213

Kuang-Yi Chiu
Dept. of Materials Sciences
University of Souther Calif.
Los Angeles, Calif. 90007

J. Stephen Duerr
Massachusetts Institute of Technology
Room 13-4022
Cambridge, Mass. 02139

Robert Earl Gauldin
6619 Easton Street
Los Angeles, Calif. 90022

Kedar P. Gupta
Materials Science Dept.
Suny
Stony Brook, N.Y. 11790

Jay I. Herman
P.O. Box 279
MIT Branch
Cambridge, Mass. 02139

Ronald G. Hurley
159 Eng. Sc. Bldg.
Penn State University
University Park, Pa. 16802

Melvin R. Jackson
232 Parson Street
Easton, Pa. 18042

Jozef Lebiedzik
Materials Res. Lab
University Park, Pa. 16802

Wen N. Lin
3730 McClintock Avenue
Apt. 433
Los Angeles, Calif. 90007

Charles E. Lyman
Room 13-4006
Mass. Institute of Technology
Cambridge, Mass. 02139

Gregory S. Maurer
Oberlin College
Oberlin, Ohio 44074

Thomas J. Nichol
6-4 Nott Drive
Troy, New York 12180

Philip A. Stine
139-2 Airport Road
West Lafayette, Indiana 47906

Lubomir Parobek
16 Christie Street
London 11, Ontario
Canada

Paul A. Sullivan
508 N. Wilton Place
Los Angeles, Calif. 90004

John C. Potosky
6602 Picovista Road
Pico Rivera, Calif. 90660

Michael W. Vannier
8805 Westport Road
Louisville, Kentucky 40222

Theodore E. Sargent, Jr.
96 South Main Street
Mansfield, Mass. 02048

Raymond E.F. Weaver
8 Sterrett Street
Pittsburgh, Pa. 15205